Antarctic Meteorites XXV

Papers presented to the Twentyfifth Symposium on Antarctic Meteorites

June 21-23, 2000

NATIONAL INSTITUTE OF POLAR RESEARCH, TOKYO

国立極地研究所

Wednesday, June 21, 2000

0900 – 1200	Registration	Auditorium (6th Floor)
0925 – 0930	Opening Address	**Takeo Hirasawa** Director-General National Institute of Polar Research

*Speaker

Chairs: Kimura M. and Tsuchiyama A. **Page**

1200 – 1300 Lunch Time

Chairs: Nakamura T. and Hiyagon H. **Page**

1700 – 1900 Reception Lecture room (2F)

Thursday, June 22, 2000

Special Session: Kobe Meteorite

Chairs: Nakamura N. and Matsuda J.

Chairs: Misawa K. and Mikouchi T.

1200 – 1300 Lunch Time

-- Special Talk (I) --

Chair: Nakamura N.

Friday, June 23, 2000

Special Session: Antarctic Micrometeorites

Chairs: Noguchi T. and Terada K. **Page**

1145 – 1245 Lunch Time

Poster Session **Page**

Abstract only

ABSTRACTS

NEW INSTRUMENT ASSEMBLAGES FOR PLANETARY GEOLOGY ON THE HUNVEYOR-1 & -2: EXPERIMENTAL UNIVERSITY LANDERS IN HUNGARY: OF THE EÖTVÖS (BUDAPEST) AND JANUS PANNONIUS (PÉCS) UNIVERSITIES

T. Diósy[1], F. Roskó[1], S. Hegyi[2], M. Keresztesi[2], B. Kovács[2], K. Gránicz[1], B. Drommer[1], Sz. Tóth[1], V. Cech[1], Cs. Z. Béres[2], L. Gimesi[2], J. Herbert[3], Gy. Imrek[2], P. Lengyel[2], A. Fabriczy[4], Sz. Bérczi[1,5],

[1]Eötvös University, Faculty of Science, Dept. G. Technology, Cosmic Materials Space Research Group, H-1117, Budapest, Pázmány Péter sétány 1/a, Hungary, (bercziszani@ludens.elte.hu)

[2]Janus Pannonius (Pécs) University, Faculty of Science, Deptartment of Informatics and G. Tecnology, and Department of Physical Chemistry, H-7625 Pécs, Ifjúság u. 6., Hungary, (hegyis@ttk.jpte.hu)

[3]Angster József Szakközépiskola, H-7624 Pécs, Rét u. 41., Hungary

[4]Eötvös University, Teachers Training College, H-1126, Budapest, Kiss J. altb. u. 42., Hungary

[5]Eötvös University, Dept. Petrology/Geochemistry, H-1088, Budapest, Múzeum krt. 4/a, Hungary

ABSTRACT

Two Hungarian universities uses a planetary lander type robot in planetary geology education. Eötvös University and Pécs University construct Hunveyor-1 & -2 (**H**ungarian **UN**iversity **SURVEYOR**) and develop new instrument-assemblages on them. Both groups built new instrumentations, of which we report some as follows: a) spectrometer, thermometer, drill unit on the Hunveyor-1, b) opto-chemical sensor unit on the Hunveyor-2, c) rover unit of the Hunveyor-2, c) Hunveyor-1 Martian desert geomorphology.

INTRODUCTION

Construction of the **Hunveyor** experimental university minimal probe was first reported on the 1998 LPSC [1] by the Eötvös University, Budapest, (Dept. G. Technology) group. Next year the same Eötvös University group prepared a rover and internet availability [2]. Also in 1999 we made a planetary geology park around Hunveyor-1 [3], and the JPTE Pécs group also begin to build his Hunveyor-2. Since that time the following new developments were carried out: a) soil analyzer measuring unit, (Hunveyor-1), b) opto-chemical sensor unit, (Hunveyor-2), c) Martian desert landscape studies and realization surrounding Hunveyor-1. We work together with JPTE Pécs University group, in competition who develop more original instrumental assemblages. In the last months two new colleges began this work (Berzsenyi Dániel College, Szombathely, West Hungary University, Székesfehérvár).

SOIL ANALYZER ASSEMBLAGE (HUNVEYOR-1.)

The soil analyser unit consists of three new instruments. The increasing number of instruments needed the development of the PC based control system of the lander. This was served by a new I/O card, which connect through control buses to the units by data and address.

Spectrometer: It consists of five photodiodes emitting light in 5 different wavelengths. They begin to emit in a sequential arrangement, the reflected light advances through a phototransistor and an A/D converter to be analysed by the computer on board of Hunveyor. The measurements are in real time processed the result of the analysis appears on the screen.

Temperature measuring sensors: We intend to measure to things. First the temperature of the atmosphere, second the temperature of the soil. To measure the air a sensor is placed on the end of the robotic arm. To measure the soil we placed a sensor into the drill. The sensors send the data through an A/D converter to the computer, which again analyses the data and send it to the control computer.

Drilling to the planetary surface: First it was intended to drill on the NASA Deep Space 2 Mission. There the plan was to drill some 10 centimeters deep into the soil in order to see stratification of the soil. Our Hunveyor drill has a similar aim, but we placed the drill onto the skeleton to be more stable and fixed position. Similarly to the Mars Microprobe the drill of the Hunveyor penetrates some 10 centimetres into the loose soil of Mars desert. The drill measures two things: a) the conductivity of the soil, b) the temperature of the soil. Another unit of the Pécs Group builds the chemical sensor unit to measure aqueous and gaseous components in the soil.

OPTICAL CHEMICAL SENSORS (HUNVEYOR-2.)

For medical applications - such as blood gas analysis - sensitive optical chemical sensor devices have been developed [6, 7]. They also can be used for environmental monitoring of dissolved gases, ions or other chemical substances. Fibre optic chemical sensors have small mass, low energy consumption, great variability, therefore multiple number of specific sensors can be mounted on a rover. We focus on gases: carbon-dioxide (CO_2), ammonia (NH_3), oxygen (O_2), sulphur-dioxide (SO_2) or hydrogen-sulphide (H_2S). These compounds are present in the recent atmosphere, some of them may indicate remnants of living tissues [4-6].

The fibre optic chemical sensor device consist of 1) a selective sensing layer placed on one end of an optical fibre and 2) of a small instrument, which measures the changes of the optical property of the sensing layer at a given wavelength. Among the variety of optical properties (and methods) available for the detection, the measurement of the reflection or fluorescence of the sensing layer is fairly simple and therefore frequently used. The sensing layer of the sensor contains carrier and dye molecules. The carrier molecule catches selectively the compound of interest, while the dye molecule acts as a transducer: it converts the chemical signal (the presence of the analyte) to optically detectable information (e.g. its colour or fluorescence will be changed).

FIBER OPTIC MEASUREMENTS

The construction of a fibre optic photo/fluorometer can be made very simple (Fig. 3). The light source can be a light emitting diode or a laser diode (LD). The incident beam passes through a splitter (M) and is coupled into the optical fibre (OF) via lenses (L). The light reaches the sensing layer (SL) at the sensor head (SH) through the fibre and is partially absorbed by the dye molecules. In reflection mode the reflected light comes back to the same way and is reflected to the primary silicon detector (D). A second detector is used to monitor the energy of the light source. In fluorescence mode the beam splitter is replaced by a dichroic mirror and a filter is placed between the detector and the mirror for complete separation of the exciting and fluorescent light.

ROVERS AROUND THE FIXED STATION (HUNVEYOR-2)

CHASSIS FOR ROVER: 3 WHEEL PAIRS, LOCAL TURNING AROUND

We began our rover developing work first formulating the requirements: 1. Be able to go on sand, 2. Can cross over a decimeter sized trench, 3. Be able to turn around its vertical axis in the plane of the wheels, 4. Hold instrument platform in a level, 5. Work with solar panel energy, 6. Communicate with the fix station. For the requirements Martian conditions were imagined: the size distribution of the rocks, low average slope. For spatial arrangement and design we studied the great number of pictures of the NASA JPL homepage. We selected one with 3 pair of wheels. Detailed design of the driving of the three wheel pairs (individually driven wheels) was a planning task for students. Making a moving model was the second step.

STRATEGY: DIFFERENT SPECIAL ROVERS AROUND THE STATION

Events on planetary missions with rovers left open the question: how specific problems and measurements can be realized with not only one, but greater number of different smaller rover units. If they have specific tasks they may have smaller mass, they may be more mobile, with better maneuver ability. From smaller units multiple copies can be transported to the planetary surface. They should have common supply of camera and communication. We focused on this strategy and tried to plan the program for 3 rover solution. Therefore we began to develop the specific instrumentation of them. The main task we agreed was to find martian life traces if there exist. In order to this goal we supported the rovers with optical chemical sensors.

BENEFITS OF HUNVEYOR: ROBOTICS AND PLANETARY SCIENCE IN HIGH SCHOOLS

Hunveyor experimental lander was also an enthusiastic tool to teach any kind of robotics and measurements on a landscape. Therefore we begin to use it in high school education, to make movements in imagination by robotics in students. The frame of Hunveyor was made in the Angster József High School, Pécs. Teachers and students together developed the two minimal experiments (arm

and TV) onto the Hunveyor. They attached classical elementary measurements of temperature, magnetism, and wind marker meteorological instruments to make joyful activities on their imagined space probe, yet in terrestrial station. (International Space Camp program was so realized in the high school education, too [12]).

MARS DESERT MORPHOLOGY (MICROLANDSCAPE AROUND HUNVEYOR-1)

Last year we arranged Hunveyor as if it were landed on a planetary surface and arranged around it the most important rock types from the Solar System rocky bodies. The list of rocks were given in [2]

Not only the rock types may serve real planetary environment studies on the hypothetical landing site of Hunveyor. This year we arranged desert sand morphology according to the observations and result of Pathfinder. (Results were reported on LPSC XXX and XXXI.) The following surface characteristics were considered: 1) the main wind system above the landing site determines the orientation of the wind-tails [7], 2) the strength of the wind can be deciphered from the deposition of deflation style of the lee-forms [8], 3) the large scale relief was formed both by fluvial and aeolian effects; a larger dune-system was seen both on panorama and orbiter MGS MOC pictures [9], 4) the elongated pits, ventifacts, flutes are the products of the sand transported with earlier strong winds, they also give paleowind orientations [10], 5) impact pits on rocks and broken fresh surfaces of the rocks in the Pathfinder and its rover vicinity witness a kind of erosion modifying the rocky desert landscape [11]. Building these observations into the desert geomorphology around Hunveyor makes the landscape realistic. All these landscape forms may appear in the arctic snowy-deserts in Antarctic geomorphology.

SUMMARY

We continued developing instrument assemblages supporting our planetary lander type robots Hunveyor -1 & -2. [14-16]. Our program not only develops experimental practice with instruments and robotics but makes enthusiastic planetary geology education of students and makes possible studying a simulated planetary terrain. [7-11]. Over these benefits our program in the future may: a) help to design new instrumentation, trigger initiatives, make the possibility to realize ideas, b) help in keeping fresh the enthusiasm, constructive activity of students in natural sciences, c) help selection of new constructional units and measurements, e) help forming international university community working together on planetary science [13].

ACKNOWLEDGMENTS:

Partly supported by T 026660 OTKA and OMFB-MEC-02265/1999.

REFERENCES:

[1] Bérczi Sz., Cech V., Hegyi S., Borbola T., Diósy T., Köllő Z., Tóth Sz. (1998): LPSC XXIX, #1267; [2] Drommer B., Blénessy G., Hanczár G., Gránicz K., Diósy T., Tóth Sz., Bodó E. (1999): LPSC XXX, #1606; [3] Bérczi Sz., Drommer B., Cech V., Hegyi S., Herbert J., Tóth Sz., Diósy T., Roskó F., Borbola T. (1999): LPSC XXX. #1332, [4] Mohr, G.J., Werner, T., Oehme, I., Preininger, C., Klimant, I., Kovács B., Wolfbeis, O.S. (1997) *Advanced Materials*, **9**, No. 14. 1108. [5] Wolfbeis, O.S., Kovács B., Goswami K., Klainer, S.M. (1998) *Mikrochim. Acta,* **129**, 181-188. [6] Bérczi Sz., Lukács B. (1997) LPSC XXVIII, 97-98. (#1591); [7] Kuzmin R.O. & Greeley R. (1999): LPSC XXX, #1415; [8] Greeley R. (1999): LPSC XXX, #1300; [9] Golombek M.P. (1999): LPSC XXX, #1387; [10] Bridges N.T. & Parker T.J., Kramer G.M. (1999): LPSC XXX, #1907; [11] Hörz F. & Cintala M.J. (1999): LPSC XXX, #1443, [12] Blackwell T. L. (1993): Teachers Program. NASA MSFC, Huntsville, [13] Bérczi Sz., Kabai S., Hegyi S., Cech V., Drommer B., Földi T., Fröhlich A., Gévay G. (1999): LPSC XXX, #1037; [14] S. Hegyi, B. Kovács, M. Keresztesi, I. Béres, Gimesi, Imrek, Lengyel, J. Herbert (2000): Experiments on the planetary lander station and on its rover units of the Janus Pannonius University, Pécs, Hungary. LPSC XXXI, #1103, Houston, [15] T. Diósy, F. Roskó, K. Gránicz, B. Drommer, S. Hegyi, J. Herbert, M. Keresztesi, B. Kovács, A. Fabriczy, Sz. Bérczi (2000): New instrument assemblages on the Hunveyor-1 and -2 experimental university lander of Budapest and Pécs. LPSC XXXI, #1153, Houston, [16] F. Roskó, T. Diósy, Sz. Bérczi, A. Fabriczy, V. Cech, S. Hegyi (2000): Spectrometry of the NASA Lunar Sample Educational Set. LPSC XXXI, #1572, Houston

MAGNETIC SPHERULES FROM THE DEVONIAN-CARBONIFEROUS BOUNDARY (MONTAGNE NOIRE, FRANCE) — A PRELIMINARY REPORT

Don Gy. - Detre Cs. H.

Geological Institute of Hungary

H-1143 Budapest, Stefánia u. 14.

In August 1998 we carried out sampling in the stratotype area of the Devonian-Carboniferous boundary (La Serre, Montagne Noire, France), guided by Catherine Girard, Raimund Feist, and Francois Marini, as well as in the Puech de la Suque section of similar position. From the latter five samples were collected as follows:

PS-1 - Hangenberg shale (Upper Devonian); PS-2 - Light grey limestone, (Uppermost Devonian); PS-3 - Light grey limestone, (Lowermost Carboniferous); PS-4 - Grey shale (clay)(Lower Carboniferous), ; PS-5 - Light grey limestone, (Lower Carboniferous).

Applying 10% hydrochloric acid to the 100 g samples the insoluble residue was separated to two fraction : <0.063 mm and >0.063 mm. The magnetic fraction was extracted through magnetic separation. As a result, magnetic spherules have been revealed in two samples. In the PS-3 140, 5-50 micron spherules of black bright and mat surface was discovered, whereas the PS-5 sample yielded 16, 10-30 micron spherules of black mat surface. The spherule-bearing pelagic limestone of compact texture lies exactly above the Devonian-Carboniferous boundary, in the lowermost Carboniferous. Spherules are abundant in the PS-3 sample directly above the D-C boundary, whereas they occur only sporidically in the PS-5 sample upward the profile.

On the basis of the results we can suppose two possibilities of the origin of spherules : (1) meteoritic origin, (2) volcanic origin.

Further investigations can help for more exact genetic conclusions.

The figure 1 shows the stratigraphic position of the spherules.

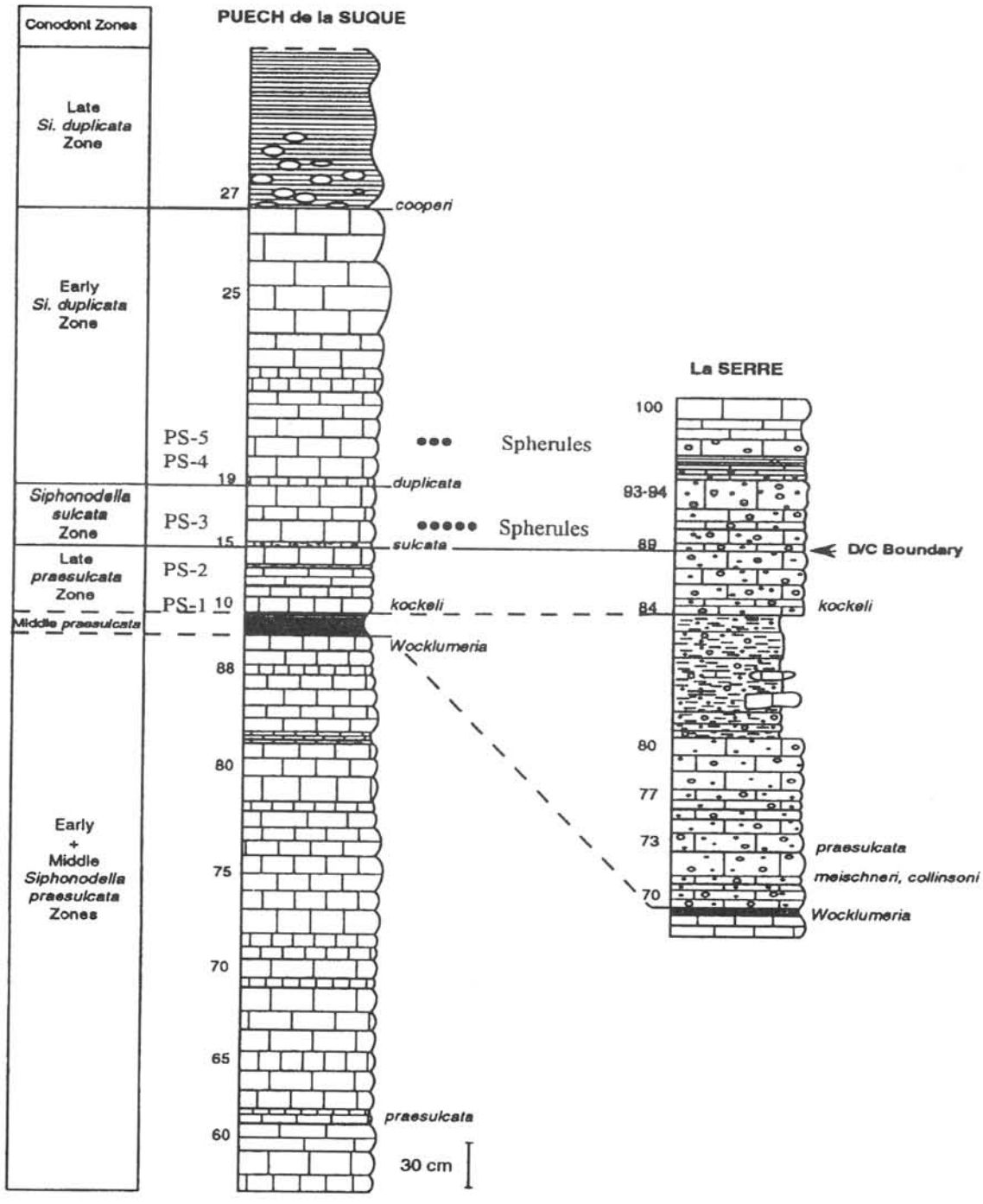

Fig. 1 Stratigraphical position of the Puech de la Suque spherules

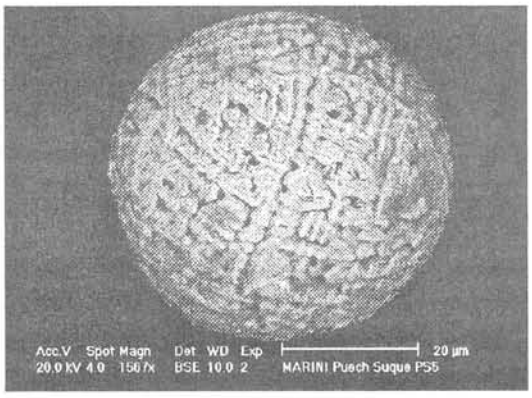

Fig. 2
BSE image of the PS 5 spherule
(Francois Marini)

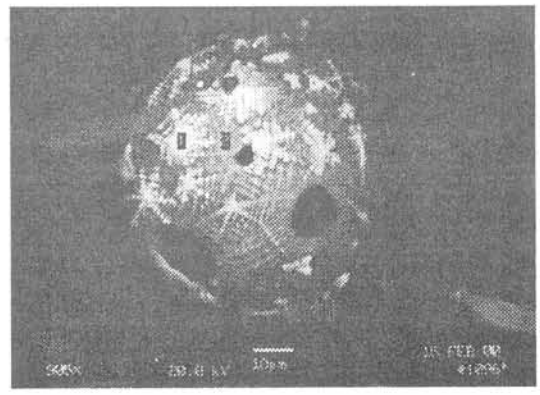

Fig. 3
BSE image of the PS 3 spherule
(Kamilla Gál-Solymos)

Chemical composition of the spherules (Fig. 3) :
(EDS analysis)

1. Fe (magnetite)
2. Al 24.25 (wt%)
   Si 44.37
   K 0.68
   Ca 2.54
   Ti 1.27
   Fe 26.88

References

Girard, Catherine (1994) : Conodont Biofacies and Event stratigraphy across the D/C Boundary in the stratotype area (Montagne Noire, France) – *CFS-Courier 168, pp.299-309*

Yamakoshi, Kazuo (1994) : Extraterrestrial Dust - Laboratory Studies on Interplanetary Dust, Terra Tokyo, 213p.

Acknowledgement :
These investigations were supported by the OTKA Grant no. T-25641 and Cooperation Scientifique Franco-Hongroise „Balaton".

Chemical behavior of phosphorus in primitive ordinary chondrites

M. Ebihara[1] and N. Sugiura[2]
[1]Graduate School of Science, Tokyo metropolitan University, Hachioji, Tokyo 192-0397
[2]Graduate School of Science, University of Tokyo, Hongo, Bunkyo-ku, Tokyo 103-0033

Phosphorus is ubiquitously present in meteorites. Condensation calculation predicts that phosphorus condenses in Fe-Ni alloy with making solid-solution at 1151 K (for 50% condensation) at 10^{-4} atm from the gas of solar composition [1]. Thus, phosphorus behaves as a siderophile element at the early stage of the solar system. Indeed, phosphorus is a significant constituent of iron meteorites, where much of the phosphorus is known to be present as schreibersite. Such a distribution of phosphorus in schreibersite and Fe-Ni phases is also found in enstatite chondrites. In ordinary chondrites, phosphorus is present as phosphates (chlorapatite, $Ca_5(PO_4)_3Cl$ and merrillite, $Ca_9MgNa(PO_4)_7$ (or $Ca_3(PO_4)_2$)) rather than phosphides like schreibersite; schreibersite is absent or present only in traces. These chemical formulae imply that phosphorus is no longer siderophile in ordinary chondrites, where phosphorus behaves as a lithophile element instead. Apparently, the distribution of phosphorus in meteorites is controlled by the oxidation state at which meteoritic materials were formed (or metamorphosed).

Ca-phosphates are know as host minerals of REE and actinoids like Th and U (and Pu) in ordinary chondrites [2]. Distribution of these elements were observed to be related with the petrologic type of ordinary chondrites. The higher the petrologic type, the higher the concentration of these elements. The distribution of REE (especially, light REE) considerably changes among unequilibrated ordinary chondrites (UOCs) [3]. During metamorphic change from low petrologic type UOCs to high petrologic type UOCs, REE are migrated among constituent minerals of chondrites, probably from glassy mesostasis to Ca-phosphates [4].

In this study, we investigated the distribution of phosphorus in Antarctic UOCs, ALH 76004, ALH 77214 and ALH81024, by using SEM and SIMS. For reference, St Severin was also studied. From the SEM observation, the morphological distribution of phosphorus was studied. Phosphates observed are all Ca-phosphates (possibly, merrillite) and morphologically classified into three groups. Most phosphates are closely located with metal (and sulfide). In ALH 77214, phosphates were observed to be present as a rim, surrounding a chondrule. Phosphorus contents in metal phases in ALH 77214 and ALH 76004 were determined by SIMS. St Severin was also studied for comparison. In iron meteorites, phosphorus is more abundant in α-phase (kamacite) than in γ-phase (taenite) [5]. In UOC (ALH 76004), a similar distribution was observed, suggesting that the distribution of phosphorus in UOC is simply controlled by diffusion of phosphorus between α- and γ-irons. In contrast, α-irons in St. Severin is highly depleted in phosphorus (less than 1ppb) whereas the phosphorus content in γ-iron is in the same range as that for UOCs. We have been trying to find an reasonable explanation for such a distinct difference in the distribution of phosphorus between α- and γ-irons between UOCs and EOCs, but not come to a conclusion so far.

References [1] Wasson J. T. (1985) *Meteorites*, Freeman. [2] Ebihar M. and Honda M. (1984) *Meteoritics* 19, 69-77. [3] Shinotsuka K (1997) Ph. D. dissertation, Tokyo Metropolitan University. [4] Ebihara M., Hirano K. and Ozaki H. (1992) *Geochem. J.* 26, 425-434. [5] Doan A. S., Jr. and Goldstein J. I. (1969) in *Meteorite Research.* p. 763-779, D. Reidel.

1990-2000: Ten years of Antarctic meteorite search by the Italian PNRA

L. Folco and M. Mellini
Museo Nazionale Antartide, Università, Via Laterina 8, I-53100 Siena, Italy
correspondence: folco@unisi.it

The Italian Programma Nazionale delle Ricerche in Antartide (PNRA) has been involved in Antarctic meteorite research since 1990. Efforts have been devoted to three main activities: search for meteorites in northern Victoria Land, curation, classification and distribution of samples to the scientific community, and study of the meteorite concentration mechanism. From 1990 to 1993 part of these activities were carried out under the auspices of a joint programme with EUROMET.

Search for meteorites. Five meteorite collection expeditions have been undertaken in 1990, 1993, 1995, 1997 and 1999 in the Rennick Glacier region (northern Victoria Land). Logistic support was provided by the Italian base Terra Nova Bay Stn.. Systematic searches at the Frontier Mountain blue ice field have yielded 438 meteorite fragments for a total mass of about 11 kg. If one also considers the previous recovery of 34 fragments by the German GANOVEX IV field party in 1984, to date a total of 472 specimens have been recovered from Frontier Mountain.

Reconnaissance field campaigns were carried out in several blue ice fields of the Rennick Glacier region to assess their potential in yielding high meteorite concentrations. The Lichen Hills, Caudal Hills, Sequence Hills, Johannessen Nunatak, Miller Butte, Roberts Butte, Mount Bower, Mount Weihaupt, Derbyshire Peak, Oona Cliff, Welcome Mountain, Mount Phelan and Schroeder Spur blue ice fields were explored for time periods of up to a few days by two to four searchers. No meteorites were found during the reconnaissance campaigns and none of these areas proved suitable for systematic searches.

Curation. The Frontier Mountain meteorites collected by the PNRA are maintained by the Earth Sciences Section of the Museo Nazionale dell'Anatartide in Siena (MNA-SI). Established in 1996 within the framework of the PNRA, the museum curates the geological specimens collected during the Italian Antarctic expeditions and organises the distribution of samples to the scientific community. The MNA-SI collection also includes an Antarctic meteorite recovered from the Allan Hills main ice field (Victoria Land) by a PNRA geological party in January 2000, and over 300 meteorite specimens from various locations worldwide which were acquired for research purposes. The catalogue of the MNA-SI is available on-line at http://www.mna.unisi.it. MNA-SI has also created an electronic data-base for the whole MNA-SI collection and a GIS for the Frontier Mountain meteorites to facilitate and keep record of research activity. Samples are available for study; so far, the MNA-SI has allocated several tens of samples to various laboratories worldwide for research. For sample request guidelines contact: mna@unisi.it. Type specimens and thin sections of the 1990, 1993 and 1995 Frontier Mountain collections are also held at the Planetary Sciences Research Institute of the Open University (UK).

Several laboratories operating within the framework of PNRA (Siena, Roma, Padova) have contributed to the classification of the meteorites recovered from Frontier Mountain in a joint effort with European Institutions of the EUROMET consortium. Their classification is regularly reported in the Meteoritical Bulletin (see the Meteoritical Bulletin No. 72, 73, 74, 75, 77, 81, 82, 83 and the forthcoming issue No. 84).

As shown in Table 1, the Frontier Mountain collection is characterised by a high frequency (96%) of ordinary chondrites and a very high H-/L-class frequency ratio of 3.4. The latter ratio is higher than that observed in other Antarctic populations and more than 3 times that of the observed falls; it may be due to the presence of large shower falls within the Frontier Mountain H-class population. In addition, the Frontier Mountain collection lacks irons, stony-irons and enstatite chondrites, in keeping with the low frequency trend common to other Antarctic populations. The statistics for the Frontier Mountain meteorites illustrated in Table 1 are similar to those outlined by Grady (1999), but are more representative since they are based on a larger number of samples, including the recently recovered 1997 and 1999 meteorites (99 specimens). The Frontier Mountain collection includes many ordinary chondrites and some remarkable findings such as 8 ureilites, 3 lodranites, 1 acapulcoite, two eucrites, two CO3 and two CV3.

Study of the Frontier Mountain meteorite trap. In 1993 PNRA initiated a detailed glaciological study of the Frontier Mountain meteorite stranding surface to provide qualitative and quantitative data for understanding the concentration mechanism. The study has focused on:
1) determination of the regional drainage system through the interpretation of satellite images;

2) determination of the ice flow pattern within the blue ice area through the mapping of ice structures such as crevasses and tephra layers;
3) determination of the horizontal component of the ice flow and ablation rates at a local scale through a six-years monitoring of a strain net network of 24 stations;
4) reconstruction of the bedrock topography through Radar Echo Sounding surveys;
5) evaluation of the effectiveness of wind action in re-distributing meteorite fragments on bare ice through the monitoring of 'rock races'.

On the basis of the data from these surveys and of field descriptions of the recovery sites we conclude the following:

1) Contrary to what can been observed from surface morphology, meteorite concentration at Frontier Mountain develops in a blue ice field upstream of an absolute and subice barrier. The ice field is characterised by mean ablation rates of 6 cm/a and horizontal speeds decreasing from >100 to <10 cm/a on approaching the obstacle.
2) Wind action moves stones of up to 170 g lying on bare ice at speeds >m/a; it thus plays an important role in re-distributing the small masses of the Frontier Mountain meteorites (min. 0.15 g, max 1667.8 g, avg. 25.3 g, median 5.6 g, mode 1.9 g; statistics based on 465 specimens).
3) The meteorite accumulation model can be described as 'stagnant ice or slow-moving ice against an absolute and a subice barriers', according to the descriptive scheme proposed by Cassidy et al. (1992).

References

CASSIDY W., HARVEY R., SCHUTT J., DELISLE G. AND YANAI K. (1992). The meteorite collection sites of Antarctica. *Meteoritics* **27**, 490-525.

GRADY M. M. (2000) Meteorites from cold and hot deserts: How many, how big, and what sort? In *Workshop on extraterrestrial materials from cold and hot deserts* (Schultz L., Franchi I., Reid A. and Zolensky M. eds.). LPI Contribution No. **997**, 36-40

Table 1. Occurrence frequency (%) of meteorite types from Frontier Mountain compared to other Antarctic populations and falls. Data for all Antarctic meteorite populations has not been corrected for pairing.

	Iron	St.-Iron	Achond	H	L	LL	E	C	Other*
Frontier Mt.[1]	0.0	0.0	3.5	73.3	21.6	1.2	0.0	0.9	0.0
Yamato[2]	0.2	0.1	6.4	52.5	29.9	5.2	1.2	4.0	0.5
Asuka[2]	0.0	2.2	18.3	23.7	28.0	11.8	1.1	14.0	1.1
ANSMET[2]	0.8	0.4	2.8	41.3	45.0	5.0	1.0	3.4	0.3
Fall[2]	5.0	1.3	8.1	34.1	37.9	7.6	1.5	3.9	0.5

* Includes K-type, R and ungrouped meteorites.
[1] Statistics from 430 classified meteorites
[2] Data from Grady (2000)

Instrumental neutron activation analysis of individual Antarctic micrometeorites collected by the 39th Japan Antarctic Research Expedition

Takaaki Fukuoka[1], Yuji Tazawa[2], Ken-ichi Nogami[3], Yuko Saito[4], Takaaki Noguchi[5], and Toru Yada[6]

[1] Dept. of Environmental Systems, Fac. of Geo-Environmental Sci., Rissho Univ., 1700 Magechi, Kumagaya, Saitama 360-0194, Japan, [2] Dept. of Phys., Fac. of Sci., Kyoto Univ., Sakyo, Kyoto 606-8502, Japan, [3] Dept. of Phys., Dokkyo Univ., School of Medicine, Mibu, Tochigi 321-0293, Japan, [4] College of Sci. and Eng., Aoyama Gakuin Univ., 6-16-1 Chitosedai, Setagaya, Tokyo 157-8572, Japan, [5] Dept. of Materials and Biological Sci., Ibaraki Univ., Bunkyo 2-1-1, Mito, Ibaraki 310-8512, Japan, [6] Dept. of Earth and Planet. Sci., Fac. of Sci., Kyushu Univ., Hakozaki, Fukuoka 812-8581 Japan

9 Antarctic micrometeorite (AMMs) samples were provided as a part of consortium study for initial investigations. These were collected from Minami-Yamato 3 site by the 39th Japan Antarctic Research Expedition team. Their size range is 100-238 μm. They were also examined by SEM-EDS without a conductive coating, after observation under stereomicroscope.

The samples were heat sealed in synthetic quartz tube individually, after weigh by a Mettler UMT2 balance. Samples in quarts tubes were activated with thermal neutron for 100 hrs at 35 MW (1 x 10^{14}n/cm^{2}s) at JRR-3M reactor of the Japan Atomic Energy Research Institute (JAERI) for measurement of long-lived radionuclides. Before γ-ray spectrometry, samples were heat sealed in tiny pure polyethylene film bag (3 x 3 mm size) individually for quick handling on pneumatic irradiation, after removal of quartz tubes. Then, the samples with pure polyethylene film were reactivated with thermal neutron for 10 min at 35MW (1.9 x 10^{13}n/cm^2·s) at JRR-3M reactor of the JAERI for measurement of short-lived radionuclides. The γ-ray spectrometry for the samples were carried out by the Aoyama-gakuin Univ. and JAERI counting systems. Glass chips with made from G. S. J standard.rock JB-1, alloys of Al and Au, and Ni, Os, Ir, and Au were also activated as standard and/or control samples.

Two spherule samples were missed during process of weigh and heat sealing. One spherule could not take out from a quarts tube, because it was just fitted in bottom of quartz tube. Normally, on INAA, first irradiation of thermal neutron is carried out for short-lived radionuclides and second irradiation is for long-lived radionuclides. However in this study, first irradiation was done for long-lived radionuclide. This technique has great advantage for protection from mechanical damage of samples when individual sample is taken from polyethylene film. However, on Ti γ-ray spectrometry for 320 KeV, γ-ray peak of ^{51}Ti was suffered from interference of remaining 320 keV peak of long-lived ^{51}Cr. Therefore Ti values were not get in this study.

The preliminary results of INAA are shown in Table 1. Siderophiles, such as Ir and Au, which are typical extraterrestrial elements were found in all 6 samples. The most of lithophiles include REE with some exclusions are chondritic. These means all 6 AMMs in this study are extraterrestrial origin. The analytical results of all elements for IB004 are chondritic. This sample is partially melted micrometeorite (MM) by observation under stereomicroscope. IB006 is porous MM. The analytical results of all elements are also chondritic. These two MMs were primitive, and not influenced of the thermal effect. IB007 shows high Fe content with low lithophiles. This indicates IB007 is typical Iron type spherule. IB001, 002 and 005 spherules show low-Na contents. This suggests that Na were lost by heat during entry into earth atmosphere from space.

Table 1. Preliminary INAA results for individual Antarctic micrometeorites collected by the 39th Japan Antarctic Research Expedition team

Sample* (Y98M03)		IB001	IB002	IB004	IB005	IB006	IB007	JB-1	Error** %
Wt	μg	21.3	4.6	3.3	5.8	1.7	9.4	21.8	
Al_2O_3	%	3.2	2.5	3.1	3.1	5.6	0.07	=14.53	1-7
FeO[1)]	%	27.8	32.5	34.0	35.2	8.5	114	=8.11	1-2
MgO	%	30.1	13.9	18.5	19.0	5.0	-	=7.74	4-22
CaO	%	3.3	2.0	1.4	3.2	-	-	=9.24	8-31
Na_2O	%	0.003	0.003	0.56	0.007	0.11	0.003	=2.80	1-11
MnO	%	0.25	0.23	0.55	0.26	0.09	0.01	=0.15	1-15
Cr	ppm	1350	3600	4980	3800	1680	2800	=414	1-2
V	ppm	71	60	68	80	56	2.4	=207	4-22
Sc	ppm	10.2	7.44	7.78	8.64	3.03	0.17	=28.9	1-25
La	ppm	0.41	0.27	0.25	0.22	-	-	=38.8	7-24
Sm	ppm	0.28	0.20	0.20	0.20	0.076	-	=5.02	3-12
Yb	ppm	0.39	0.23	0.26	0.32	0.17	-	=2.4	18-33
Lu	ppm	0.06	0.04	0.07	0.03	0.02	-	=0.37	18-43
Co	ppm	61	547	435	255	95	150	=39.1	4-5
Ir	ppb	6	92	640	308	160	34	-	3-90
Au	ppb	2	5	202	15	64	33	-	5-73

* Samples were all collected from the Minamiyamato 3 region.

** Errors for INAA are due to counting statistics.

1) Total iron as FeO

FORMATION AND EARLY EVOLUTION OF THE SOLAR SYSTEM: METEORITIC CONSTRAINTS. J. N. Goswami[1,2], [1]Max-Planck-Institut für Chemie, 55128 Mainz, Germany; [2]Physical Research Laboratory, Ahmedabad 380009, India.

The formation of the solar system was initiated by the gravitational collapse of a dense molecular cloud fragment that led to the formation of a central star, the Sun, and a rotating gas and dust disk around it. Gradual evolution of the disk material finally led to the formation of the planets and their satellites and other minor objects such as the asteroids and the comets. This scenario for a coupled evolution of the Sun and the solar system objects is supported by recent astronomical observations that provide evidence for the presence of rotating gas and dust disk around newborn star as well as discovery of planets around a large number of young solar type stars. A quantitative understanding of the formation and early evolution of the solar system, however, requires a knowledge of the time scales of the various processes involved, e.g., collapse of the prtotosolar molecular cloud fragment to form the Sun, formation of the first solar system solids, aggregation of solids leading to the formation of planetesimals, accumulation of planetesimals to form planets and differentiation of the planetesimals and the planetary objects. Isotopic records in meteorites, particularly those produced by now-extinct radionuclide, have provided some crucial input in this regard and have led to some significant changes in our ideas about the formation and early evolution of the solar system.

Meteorite studies have provided evidence for the presence of a host of now-extinct radionuclide with half-life ranging from ~10^5 years (^{41}Ca) to ~82 Ma (^{244}Pu) in the early solar system. Even though a stellar origin for these nuclides is generally favored, there are suggestions that some of the shorter-lived nuclides, such as, ^{41}Ca, ^{26}Al, and ^{53}Mn could have been produced by energetic particles from an active early Sun interacting with nebular gas and dust. If the short-lived nuclides, particularly, ^{41}Ca and ^{26}Al (half-life ~$7x10^5$ years), are indeed freshly synthesized stellar products that were injected into the collapsing protosolar molecular cloud, their presence in early solar system solids would require that the time scale of cloud collapse leading to the formation of the proto-Sun has to be less than a million years. Since the time scale of unassisted collapse to form a solar mass star is estimated to be ~5-10 Ma, the inferred short collapse time scale for the protosolar cloud argues for an assisted or triggered origin of the solar system. It has been conjectured that the stellar event that synthesized the short-lived nuclides and injected them into the protosolar cloud could itself act as the trigger. Recent numerical simulation studies of induced cloud collapse processes appear to confirm the dynamical feasibility of a triggered origin of the solar system within the time constraint placed by the meteorite data.

A stellar origin for the short-lived nuclides also constrains the time scale for the formation of some of the first solar system solids, the so-called CAIs (Ca-Al-rich Inclusions), which almost exclusively contain records of the two shorter-lived nuclides, ^{41}Ca and ^{26}Al, to less than a million years. Analytical studies that consider stellar nucleosythetic yields of several short-lived nuclides (^{41}Ca, ^{36}Cl, ^{26}Al, ^{60}Fe, ^{53}Mn, and ^{107}Pd) and their eventual injection into the protosolar cloud also require such a short time scale to match the observed initial abundances of these nuclides in CAIs as well as in bulk samples of undifferentiated and differentiated meteorites.

The relatively rare CAIs, found predominantly in carbonaceous chondrites, and the ubiquitous chondrules, present in chondritic meteorites, are generally considered to be nebular products formed during transient high temperature events. Records of the short-lived

nuclide ^{26}Al found in these two sets of objects appear to suggest that nebular processes were operative for a relatively longer time scale of a few million years. Such an extended duration of nebular processing appears to be in conflict with our present understanding of the dynamical evolution of small objects in the solar nebula under the influence of gravitational and gas-drag forces. This remains an open question at present, even though several suggestions have been put forward to resolve this problem.

Isotopic records of the short-lived nuclides ^{53}Mn (half-life ~3.7 Ma), ^{107}Pd (half-life ~6.5 Ma), and ^{182}Hf (half-life ~9 Ma), observed in differentiated meteorites suggest a time scale of 5-15 Ma, within which accretion, heating, melting and silicate/metal fractionation in plenatesimal-sized objects representing the parent bodies of the differentiated meteorites, took place. A significant result obtained recently is the observation of fossil records of the short-lived nuclide ^{26}Al in a differentiated meteorite, the eucrite Piplia Kalan that could be a fragment of the asteroid 4 Vesta. This observation confirms the suggestion that ^{26}Al was the heat source for the early melting of planetesimals and also indicates that differentiation and crust formation on the asteroid Vesta were complete within five million years of the formation of the solar system. This time scale is consistent with the observed systematics of the short-lived nuclide ^{53}Mn in eucrites. Further, the time scales of accretion, differentiation and crust formation for asteroid 4 Vesta, inferred from theoretical studies of ^{26}Al heating and differentiation of this asteroid, also appear to be consistent with the isotopic data.

A major problem inherent in the study of extinct radionuclide records in meteorites is the fact that it is neither possible to look for fossil records of the whole suite of extinct nuclides in a given meteorite sample nor it is possible to look for records of a given extinct nuclide in samples of all the different meteorite types. Even when this has been achieved in a limited scale (e.g. observation of ^{26}Al, ^{41}Ca, and ^{53}Mn in CAIs, of ^{26}Al and ^{53}Mn in CAIs, chondrules, and differentiated meteorites, and of ^{53}Mn, ^{107}Pd, and ^{182}Hf in differentiated meteorites), the combined data sets do not always yield self-consistent solution. An attempt will be made to summarize our present state of understanding in this area and possible future directions in research that may resolve some of the existing problems.

[Note: The pertinent references are too numerous to include in the text. Most of them can be found in: Goswami, J. N. and Vanhalla, H. A. T. (2000) in *Protostars and Planets IV* (eds. V. Mannings, S. Russell, and A. Boss), Tucson, Arizona Univ. Press (in press)].

POSSIBLE METEORITE ANALOGS FOR ASTEROID 1989ML — TARGET OF MUSES-C ASTEROID SAMPLE RETURN MISSION —

TAKAHIRO HIROI[1], MICHAEL E. ZOLENSKY[2], AND MICHAEL E. LIPSCHUTZ[3].

[1]*Department of Geological Sciences, Brown University, Providence, RI 02912, USA*
[2]*SN2, NASA Johnson Space Center, Houston, TX 77058, USA*
[3]*Department of Chemistry, Purdue University, West Lafayette, IN 47907, USA.*

Introduction

Asteroid 1989ML, the current target of MUSES-C mission, does not show any strong signature of Fe^{2+} absorption bands of silicates, and its surface properties such as composition and presence of regolith are not well known. Therefore, spectroscopic measurements of the surface objects of 1989ML have to take all the possible physical and compositional properties into account in planning the experiment. As an advantage unique for MUSES-C mission, not only it can map the entire asteroid surface with high spatial and NIR spectral resolution but also its microrover can measure optical properties of individual rock or mineral grains. Smart combination of Visible-NIR spectrometers on-board the satellite and those on the microrover should give us clues to the surface physical condition and mineral composition of 1989ML. The microrover experiments will be an ideal link between satellite/telescopic observations of the asteroid surface and laboratory measurements of meteorites and other candidate materials for the surface composition of 1989ML. In order to make those returned data used most effectively, we will have to accumulate more reflectance spectra of various kinds of meteorite analogs under various physical conditions (fine powder, coarse powder, and rock chip) and viewing geometries. In this paper, possible meteorite analogs for 1989ML are studied using the telescopic spectral measurements and laboratory measurements of about 100 meteorites.

Data Acquisition

An ECAS-JHK reflectance spectrum of 1989ML was measured by Dave Tholen (personal communication). Reflectance spectra of about 100 samples of meteorites were taken from the RELAB database. Among them, bidirectional reflectances were measured at RELAB, and directional-hemispherical reflectance spectra of some E chondrites were measured by [1]. Heating experiments of samples of Abee (E4) and Murchison (CM2) were done by [2].

Meteorite Analogs for 1989ML

Shown in Fig. 1 is comparison of reflectance spectra of 1989ML with about 100 meteorite samples grouped according to the meteorite classification scheme. All spectra are normalized to 1.0 at 701 nm, and spectra of different meteorite classes are offset from one another for clarity. It is admittedly difficult to see which ones are close fits with 1989ML in black/white print, close examination reveals that Abee (E) sample heated at 500 C°, Tajera dark chondrite, Ivuna (CI) sample heated at 400 C°, and possibly a certain combination of heated Murchison (CM) samples are the best matches as shown expanded in Fig. 2.

The cases of heated Abee, Tajera, and Ivuna give albedos of 5.6 %, 8.5 %, and 1.8 %, respectively. The question will be whether the observed albedo of 1989ML falls within the reasonable range of these meteorite analogs. If not, either the composition or physical properties of surface of 1989ML should be different from these samples. The fact that many experimentally-heated samples came to the best analog candidates suggests that the asteroid may have gone through internal heating, external collisional heating, or space weathering.

Acknowledgments: RELAB a multiuser facility supported by NASA grant NAG5-3871. Authors thank Drs. Dave Tholen and Dan Britt for permission to use their data. Antarctic mateorite samples were loaned from Meteorite Working Group at NASA Johnson Space Center and National Institute of Polar Research.

References: [1] Gaffey M. J. (1976) *J. Geophys. Res.* **81**, 905-920. [2] Ikramuddin et al. (1976) Geochim Cosmochim Acta **40**, 133-142; Biswas *et al.* (1980) Geochim Cosmochim Acta **44**, 2097-2110

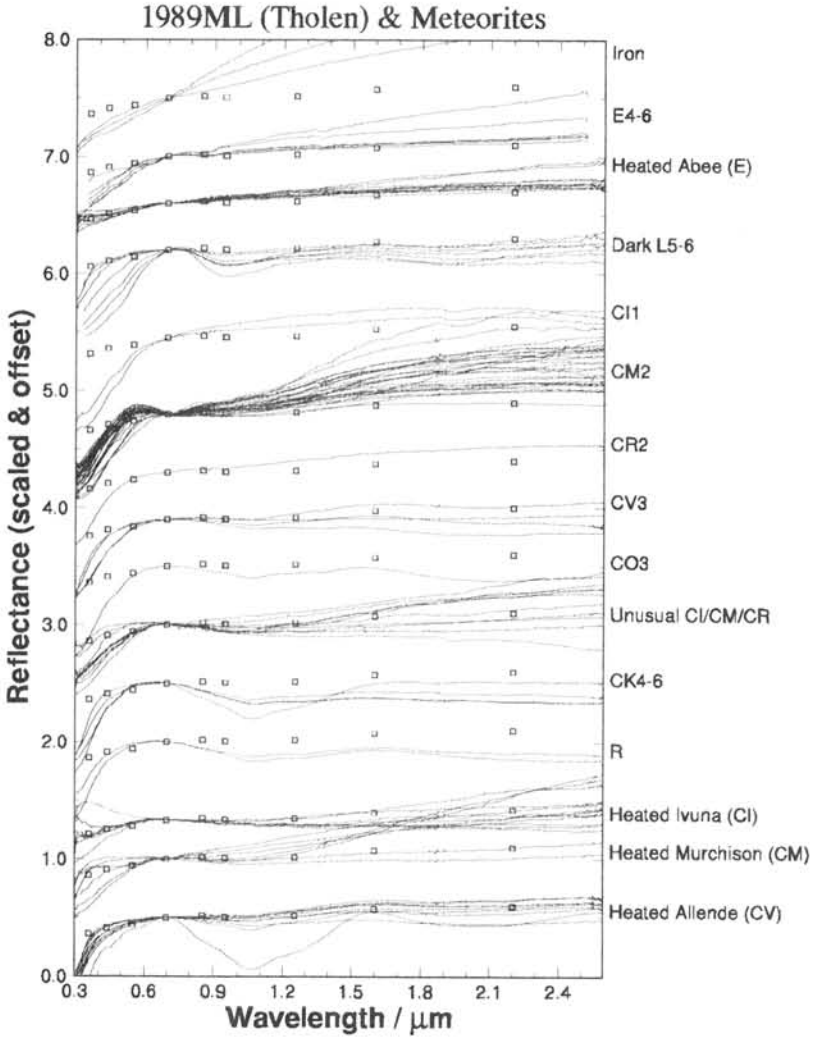

Fig. 1. Comparison of the ECAS-JHK spectrum of 1989ML (D. Tholen) and laboratory reflectance spectra meteorite samples.

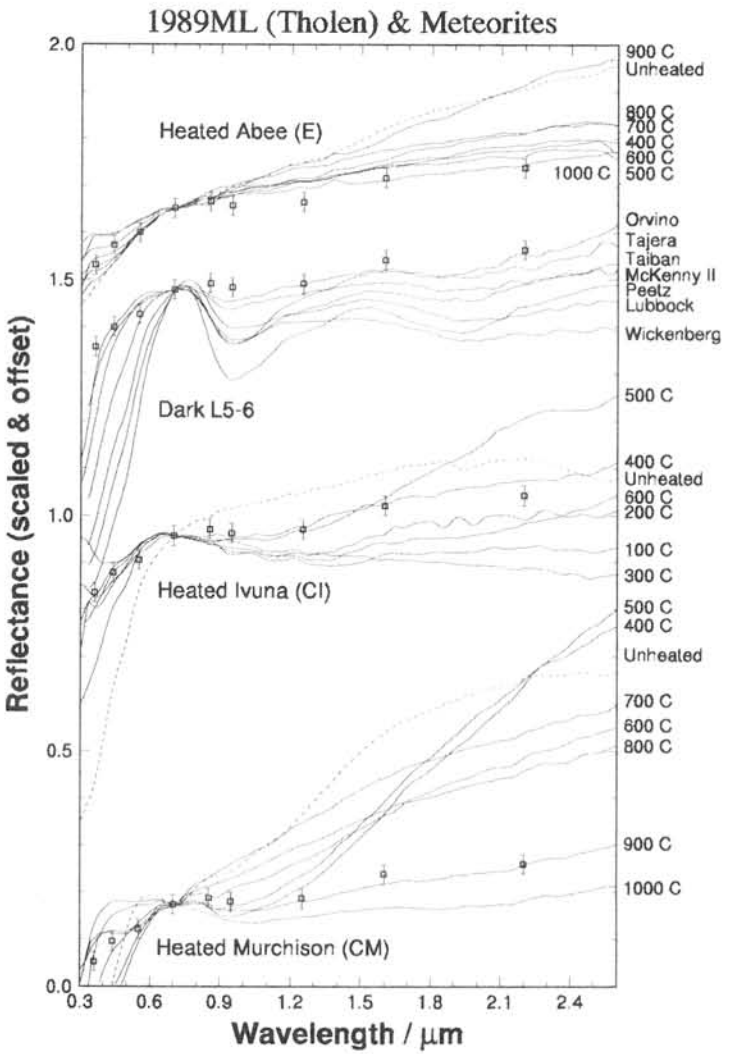

Fig. 2. Expanded view of spectra of groups that contain best spectral matches with 1989ML.

AN ANOMALOUS REE COMPONENT IN THE KOBE METEORITE

Yusuke HIROTA[1], Noboru NAKAMURA[1,2], Hiroshi ONOUE[2], Keiji MISAWA[3], Katsuyuki YAMASHITA[2] and Daode WANG[4]

[1]Graduate School of Science and Technology, Kobe University; [2]Department of Earth & Planetary Sciences, Faculty of Science, Kobe University, Nada, Kobe 657-8501; [3]National Institute of Polar Research, 9-10 Kaga 1, Itabashi, Tokyo 173-8515, [4]Inst. Geochem. Academia Shinica Guiyang, P. R. China

Introduction

The Kobe meteorite fell on September 26th, 1999. Two fragments (C and E) are on loan from the meteorite owner to N. Nakamura. Based on petrographical, chemical and oxygen-isotopic measurements, Kobe is tentatively classified as CK4 [1]. In order to compositionally characterize the Kobe meteorite and compare it with other CK group meteorites, we report here the results of isotope dilution analyses (IDMS) of trace elements including rare earth elements (REEs) for two specimens from Kobe, along with the results for Ningqaing (CK3). Kallemeyn et al. (1991) [2] reported trace element abundance data obtained by INAA for CK group meteorites, but details of REE features have not been well known.

Sample and Analytical Procedures

Aliquots (44 and 66mg) of powdered specimens prepared from chips of Kobe C-3 (0.92g) and E-2,3 (1.42g) [3] were analyzed in present study. Alkalis were analyzed by direct loading IDMS, and REEs were analyzed by conventional IDMS [4]. Aliquots of specimens C has also been analyzed for rare gases at Osaka University and cosmogenic nuclides at University of California, and specimen E has been used for wet-chemical analyses at NIPR and activation analyses at Tokyo Metropolitan University.

Results and Discussion

In Fig. 1, CI-normalized trace element abundance patterns for Kobe C and E are compared with those of Ningqiang and CK mean [2]. Except for Kobe E, the abundance patterns for Kobe C and CK mean are similar. Ningqaing shows a flat REE pattern with small negative anomalies of Ce and Eu. Kobe C shows basically flat REE pattern, which is similar to the CK mean. It is noted that middle REEs (Gd, Dy) in Kobe C are somewhat higher than other REE.

The abundances of La, Nd, Gd and Dy in Kobe E are 1.5-2 times higher than other REE (Fig. 1). On the other hand, relative abundances of Eu, Yb and Lu in Kobe E are consistent with those of mean CK. To our knowledge, such an irregular pattern has not been reported for bulk chondrites. As mentioned above, Kobe C also indicates similar REE trend to that of Kobe E. It is considered that some unknown component(s), which have anomalous REE abundances, were included in the Kobe E sample analyzed by us, although Kobe E specimen was originally thought as most "representative" for Kobe and thus used for wet-chemical

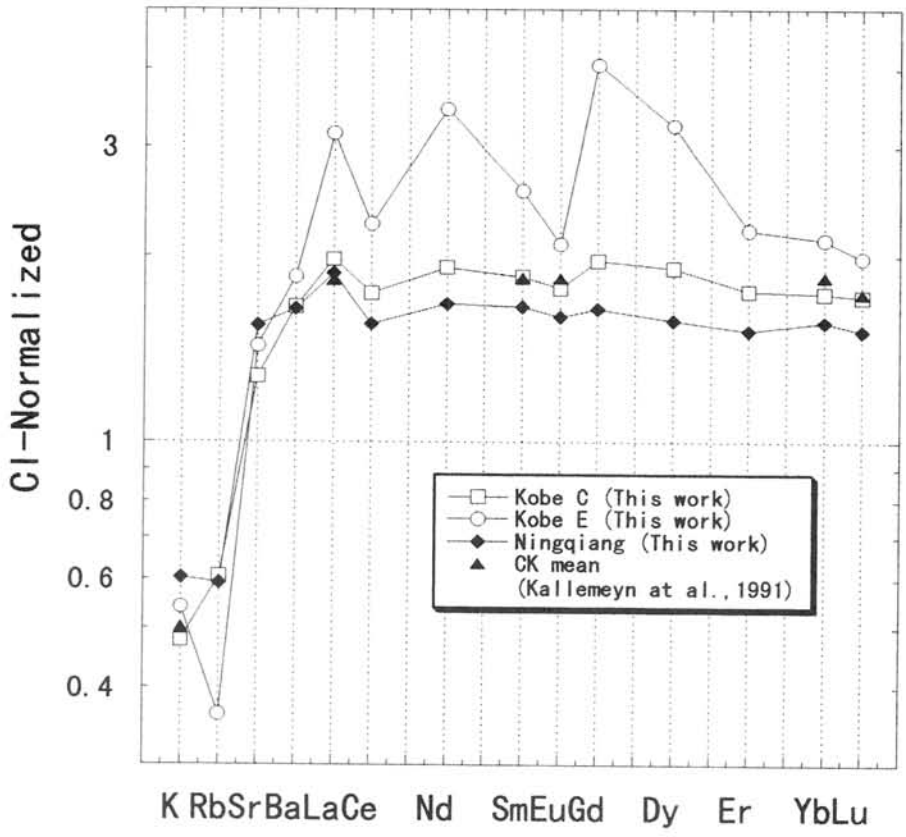

Fig. 1 CI-normalized trace element patterns for Kobe C and E, compare with other CK meteorites.

analyses of major elements as well as activation analyses [3]. In order to estimate REE abundances in this component, we made a model calculation using a mass balance equation; Kobe E = X(component) + (1-X)(matrix), where X represents mass fraction of unknown component.

In Fig. 2, CI-normalized (and re-normalized to La) REE patterns estimated for the unknown component are shown as function of X. Note that the estimated REE patterns are almost independent of the parameter X (and also of absolute REE abundnaces in matrix). The REE pattern has now more exaggerated features; enriched in ultrarefractory REEs (i.e., Gd and Dy). This REE pattern appears to be complementary to Group II REE and is quite similar to those of some type of hibonite grains in Murchison spinel-hibonite inclusions (e.g. SBIB 13-60) which have, in general, fractionated Mg, Ca and Ti isotopes and $^{26}Al/^{27}Al$ ratio of $5x10^{-5}$ [5] and also to that of Allende chondrule R-11 which carries a relict CAI grain [6].

Generally, refractory inclusions, typical of CAIs, are considered as carriers that have unique REE characteristics caused by vapor fractionations. It is also pointed out that some type of ferromagnesian chondrules carries vapor-fractionated REE [7]. Kobe contains significant amounts of chondrules (35Vol.%) [8], but no refractory inclusions have been identified so far. Therefore it is unlikely that the observed anomalous REE feature is due to refractory inclusions but more likely that some specific types of chondrules carry anomalous REE. It is also possible that this is only a remnant memory of refractory precursor materials

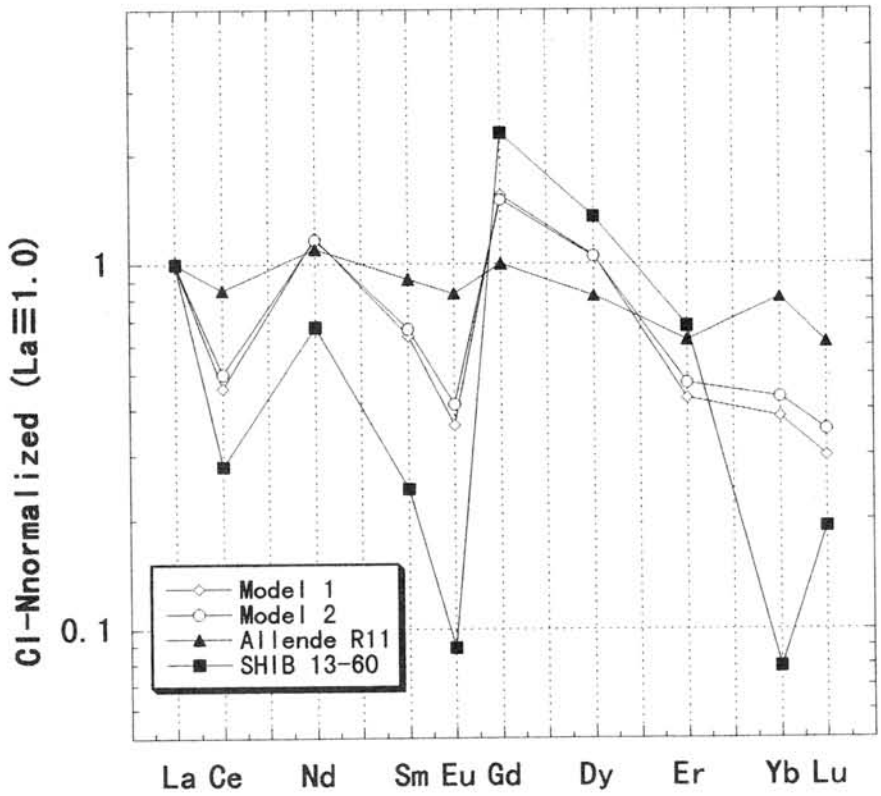

Fig. 2 Calculated REE patterns for unknown component in Kobe E (model 1: matrix REE=1.5xCI, X=0.01; model 2: matrix REE=1.5xCI, X=0.1). They are compared with those of a hibonite gain (SHIB 13-60) from Murchison spinel-hibonite inclusion [5] and of Allende chondrule R-11 [6].

of Kobe which had been destroyed and redistributed heteorogeneously during the later thermal events such as chondrule-forming melting. If this is the case, actual REE carriers will not be found. On the other hand, however, if any specific REE carrier is identified in future works, it is interesting to see whether this carrier also has presolar isotopic signatures. Such consideration will be tested by IDMS/isotopic analyses of individual chondrules and other components and/or by in-situ analyses by SIMS. Therefore, further detailed studies of Kobe are required to clarify this problem.

We are indebted to Mr. Ryoichi Hirata for providing N. Nakamura with the Kobe meteorite samples for consortium studies.

Reference

[1] Nakamura N. et al. (2000) Lunar Planet Sci. 31, 1234 (abstr.); [2] Kallemeyn, G. W., Rubin, A. E. and Wasson, J. T. (1991) GCA 55, 881-892; [3] Nakamura N. et al. (2000) Antarctic Meteorites XXV (this volume); [4] Nakamura, N. et al. (1989) Anal. Chem. 61, 755-762; [5] Trevor, R. Ireland (1990) GCA 54, 3219-3237; [6] Misawa, K. and Nakamura, N. (1996) "Origin of Refractory Precursor Components of Chondrules from Carbonaceous Chondrites", In *Chondrules and the Protoplanetary Disk* pp99-105; [7] Misawa K. & Nakamura N. (1988) Nature 334, 47-50; [8] Tomeoka, K. et al. (2000); Antarctic Meteorites XXV(this volume).

AN ION MICROPROBE STUDY OF OXYGEN ISOTOPES IN SOME INCLUSIONS IN KAINSAZ AND Y-81020 CO3 CHONDRITES.

Hajime Hiyagon

Department of Earth and Planetary Science, University of Tokyo, Bunkyo-ku, Tokyo 113-0033, Japan.

1. Introduction

Refractory inclusions or CAIs (calcium-aluminium-rich inclusions) are known to have large oxygen isotopic anomalies with $\delta^{17}O \sim \delta^{18}O \sim -40‰$ relative to SMOW (standard mean ocean water) [1,2]. The origin of the oxygen isotopic anomaly, however, is still under debate [3]. In the present study, *in situ* ion microprobe analyses have been performed for two refractory inclusions in Yamato-81020 (CO3) chondrite and an amoeboid olivine aggregate (AOA) incorporated in a chondrule in Kainsaz (CO3) chondrite.

2. Samples and experimental procedures

Yamato-81020

Inclusion #1 is ~550 μm x ~700 μm in size; a half of this inclusion (A) consists mostly of melilite with small amount of spinel, fassaite, anorthite and perovskite, and surrounded by relatively thin (≤50μm) Wark-Lovering rim layers of spinel and diopside, while the other half (B) consists of abundant fassaite and anorthite with small amount of spinel and perovskite surrounded by rather thick (up to 100μm) W-L rim layers of spinel and diopside. Melilite and fassaite in the melilite-rich part (A) and fassaite, anorthite, a spinel-rich phase (containing some anorthite and diopside) and diopside (in W-L rim) in the other part (B) were analyzed.

Inclusion #54 consists mostly of melilite interspersed with samll spinel grains. The total size of this inclusion is about 500μm x 500μm, but it shows a highly irregular shape and is separated into 3 or 4 "islands" in the thin section. It has no visible Wark-Lovering rim layers. A melilite-rich part was analyzed, but it contained two small (≤2μm) spinel grains.

Kainsaz

Chondrule #130 is a type 2 (Fe-rich) porphiritic olivine chondrule with ~300μm x 400μm in size. It contains relatively large olivine phenocrysts (up to ~100μm in diameter). The fayalite content (Fa) of the olivine phenocrysts are from Fa~20 in the center to Fa~40 in the margin, and smaller grains show almost homogeneous composition of Fa~40. Interestingly, this chondrule contains an amoeboid olivine aggregate (AOA) near its center. The AOA is ~120μm x ~140μm in size and consists of smaller (1-10μm) but more Fe-poor (Fa down to ~6.5) olivine grains. This suggests that the AOA experienced a much shorter heating episode under Fe-rich environment compared with that for the chondrule itself. Judging from the highly disequilibrium character of the AOA and the chondrule, the

AOA must have been separated from the chondrule (or the chondrule precursor material) until the last moment of the chondrule formation, when the AOA became incorporated in the chondrule.

In situ analyses of oxygen isotopic compositions were performed using a CAMECA ims-6f ion microprobe in the University of Tokyo. A Cs^+ primary beam with an impact energy of 19.5kV was used for the analyses. The beam size was ~15μm in diameter with an intensity of ~0.4nA. Other analytical conditions were essentially the same as those described in [3] and [4]. The reproducibility of the analyses was ±2‰ for $\delta^{17}O$ and ±2.5‰ for $\delta^{18}O$, respectively.

3. Results

The results are summarized in Figs.1 and 2. Error bars shown is the figures are 2σ. Also shown in the figure are the TF (terrestrial fractionation) line and the CCAM (carbonaceous chondrite anhydrous minerals) line.

The distribution of oxygen isotopes among different minerals in inclusion #1 of Y-81020 chondrite is consistent with the previous observation [5], that is, spinel and fassaite show high ^{16}O excesses but melilite and anorthite show much smaller ^{16}O excesses. Anorthite in this inclusion, however, shows rather high anomalies with $\delta^{18}O$ down to ~-20‰ On the other hand, melilite in inclusion #54 shows a very high excess ^{16}O with $\delta^{17}O \sim\delta^{18}O \sim$-40‰. This suggests that the event(s) which erased the oxygen isotopic anomaly in melilite in inclusion #1 is *not* the parent body process(es) *but* most likely the nebular process(es).

It was found that the oxygen isotopic compositions of the chondrule #130 in Kainsaz chondrite and the AOA inside this chondrule are highly disequilibrium with each other, that is, the AOA shows $\delta^{17}O \sim\delta^{18}O \sim$-40‰, which is the typical values for AOAs and OIs [3,6], while olivine phenocrysts in the chondrule show $\delta^{17}O$ and $\delta^{18}O$ close to 0‰. The AOA apparently retains its original oxygen isotope signature. The present observation suggests that the AOA must have been separated and "preserved" in an environment different from that of the chondrule formation region and was later incorporated into the chondrule at the time of the chondrule formation. The exact meaning of this observation is not clear at present. However, this would give an important constraints on the formation mechanisms of the (type 2) chondrules and the amoeboid olivine aggregates.

References: [1] Clayton R. N., Grosmann L. and Mayeda T. K. (1973) *Science* **182**, 485-488. [2] Clayton R. N. (1993) *Ann. Rev. Earth Planet. Sci.* **21**, 115-149. [3] Hiyagon H. and Hashimoto A., *Science* **283**, 828-831, 1999. [4] Hiyagon H., Mizutani S., Noguchi T., Nakamura T. and Yada T. (2000), this volume. [5] Clayton R. N., Onuma N., Grosmann L. and Mayeda T. K. (1977) *Earth Planet. Sci. Lett.* **34**, 209-224. [6] Hiyagon H. and Hashimoto A. (1999) *Lunar Planet. Sci.* **XXX**, Abstr.#1320 (CD-ROM).

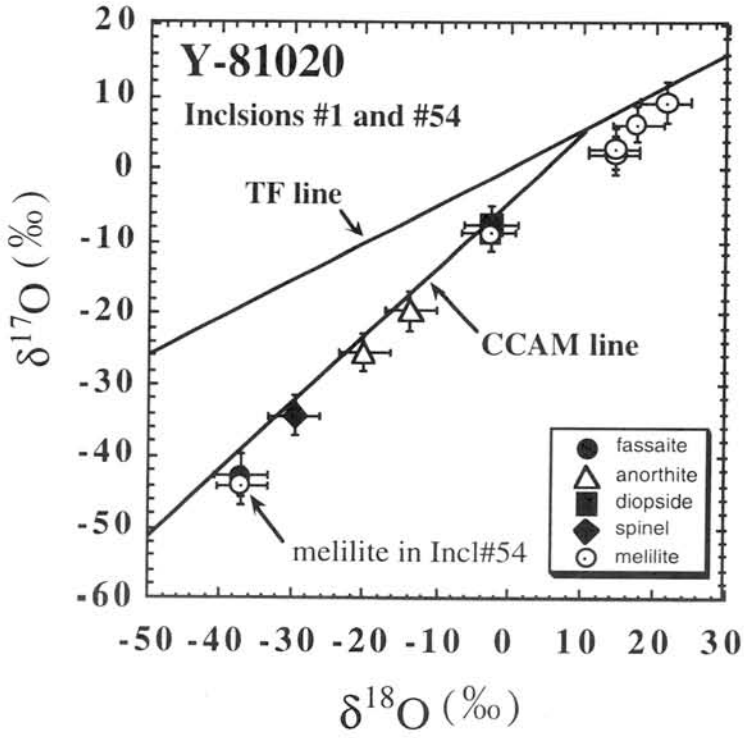

Fig. 1 Oxygen isotopic compositions of different phases in two refractory inclusions in Y-81020 (CO3) chondrite.

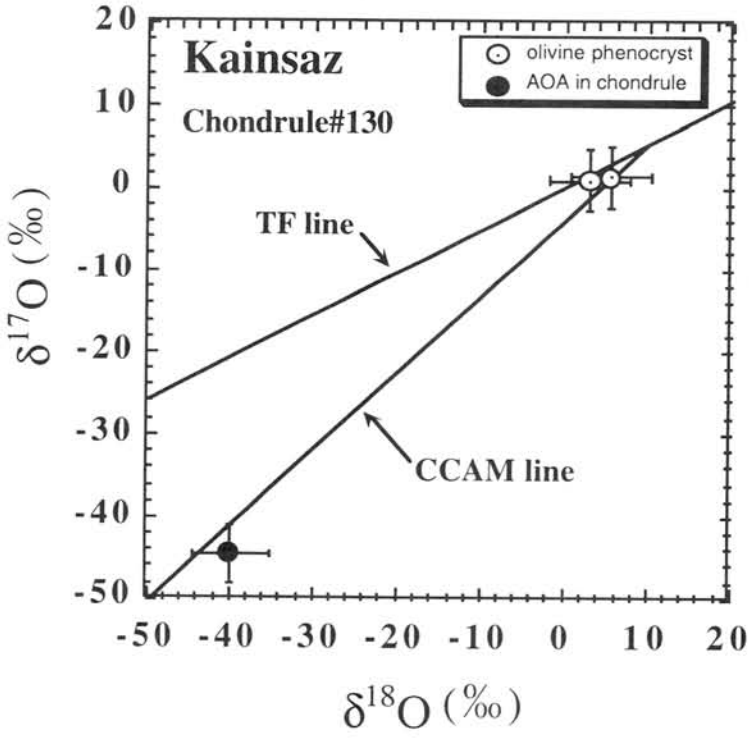

Fig. 2 Oxygen isotopic compositions of olivine phenocrysts in a type 2 (Fe-rich) chondrule and olivine in an AOA incorporated in this chondrule.

A PRELIMINARY STUDY OF OXYGEN ISOTOPES IN ANTARCTIC MICROMETEORITES USING AN ION MICROPROBE.

[1)]Hajime Hiyagon, [1)]Sadahiro Mizutani, [2)]Takaaki Noguchi, [3)]Tomoki Nakamura and [3)]Toru Yada.

1) Department of Earth and Planetary Science, University of Tokyo, Bunkyo-ku, Tokyo 113-0033, Japan.; 2) Department of Materials and Biological Science, Ibaraki University, Bunkyo 2-1-1, Mito 310-8512, Japan.; 3) Department of Earth and Planetary Sciences, Kyushu University, Hakozaki Fukuoka 812-8581, Japan.

1. Introduction

Micrometeorites may represent a population of the extraterrestrial material which may be different from those represented by conventional meteorite collections [1]. Some of them are only partially melted upon entry to the Earth's atmosphere, and hence, may retain their original extra-terrestrial signatures. It is well established that oxygen isotopic compositions of bulk meteorites are heterogeneous among different meteorite groups [2,3], and for this reason, oxygen isotopic composition is widely used to classify meteorites. In order to understand the origin of micrometeorites, it is important to analyze their oxygen isotopic compositions and to compare them with those of known meteorite groups. In the present study, we have performed *in situ* oxygen isotope analyses on Antarctic Micrometeorites (AMMs) using an ion microprobe.

2. Samples and experimental procedures

The AMMs used in the present study were recovered from the unprocessed samples (bottle of 971127-1) collected at the Dome Fuji Station in 1997 [4]. Each AMM was hand-picked under an optical microscope from the Fraction G3 (magnetic fraction with grain size <155μm), examined with SEM-EDS, and only the grains showing chondritic compositions (i.e., showing strong Mg, Fe and Si peaks) were selected for the ion microprobe study. Each AMM was fixed on a slide glass (5mm x 5mm in size) using resin, polished, carbon coated and re-examined with SEM-EDS. Five AMMs were selected and loaded in a sample holder for the CAMECA ims-6f ion microprobe in the University of Tokyo. A Cs^+ primary beam with an impact energy of 19.5kV was used for the analyses. The beam size was 15-20μm in diameter with an intensity of ~0.2nA. An electron flood gun was used for charge compensation. Negative secondary ions of $^{16}O^-$, $^{17}O^-$ $^{16}O^1H^-$ and $^{18}O^-$ were accelerated at -9.5kV and analyzed at a mass resolution of ~5000. The beam intensity of $^{16}O^-$ ion was measured with a Faraday Cup (FC) and those of the other three ions were measured with an electron multiplier (EM)-based ion counting system. Mass 15.9, where no ion peak existed, was also measured with the FC for the correction of the back ground level of the FC. San Carlos olivine standard of known composition was repeatedly analyzed before and after the period of the sample analyses

and all the results were normalized to the average of the standard values. The reproducibility of the analysis was ~±3.4‰ and ~±2.4‰ (2σ) for $\delta^{17}O$ and $\delta^{18}O$, respectively, but larger instrumental mass fractionation may be expected because the sample surface was not perfectly flat. The analytical procedure was essentially the same as described in [5].

Four out of five samples (F97AT006, 008, 011 and 013) were successfully analyzed. F97AT006 is porous, ~70 μm in diameter and consists mostly of clinopyroxene. F97AT008 is ~100 μm in diameter and shows a texture similar to that of a porphiritic olivine chondrule. Analyzed phases were an olivine phenocryst and a mixture of olivine and glass. F97AT011 is ~60x110 μm in size and consists of matrix-like material with a large (25x40 μm) orthopyroxene crystal on one end. Both the opx crystal and matrix-like material were analyzed. F97AT013 is ~60x80 μm in size and consists mostly of matrix-like material with a few crystal grains (e.g., pyroxene).

3. Results

The results are summarized in a three-isotope diagram of oxygen isotopes in Fig.1. Also shown in the figure are the TF (terrestrial fractionation) line and the CCAM (carbonaceous chondrite anhydrous minerals) line, which was defined by CAI minerals from the Allende meteorites. Because the surface of the sample was not perfectly flat, there could be some instrumental mass fractionation effect in the present results, and hence, the present results must be considered rather preliminary. However, an interesting observation of the present results is that all the data points fall *below* the TF line. Note that an instrumental mass fractionation effect, if existed, would move the data points only along the slope ~0.5 line in the figure, so that it would not change this conclusion. This suggests that AMMs are more closely related to the carbonaceous chondrite groups rather than ordinary chondrite groups. Another interesting observation is that the analyzed compositions of the matrix-ilke portions fall upper right portion of the diagram, while those of the crystals fall lower left portion of the diagram. This is more or less consistent with the results by Clayton and Mayeda [6]. The present results as a whole are very consistent with recent results by Engrand et al. [7]. However, the number of analyses for AMMs is still limited and there may be some bias in the selection of the samples. Further studies are required to better understand the origin of micrometeorites and to draw new information from their analyses.

References: [1] Engrand C. and Maurette M. (1998) *Meteoritics Planet. Sci.* **33**, 565-580. [2] Clayton R. N., Onuma N. and Mayeda T. K. (1976) *Earth Planet. Sci. Lett.* **30**, 10-18. [3] Clayton R. N. (1993) *Ann. Rev. Earth Planet. Sci.* **21**, 115-149. [4] Nakamura T. et al. (1998) *Antarctic Meteorites* **XXIII** (abstr.), 104-106. [5] Hiyagon H. and Hashimoto A., *Science* **283**, 828-831, 1999. [6] Clayton R. N., and Mayeda T. K., *Geochim. Cosmochim. Acta* **63**, 2089-2104, 1999. [7] Engrand C., McKeegan K. D. and Leshin L. A., *Geochim. Cosmochim. Acta* **63**, 2623-2636, 1999.

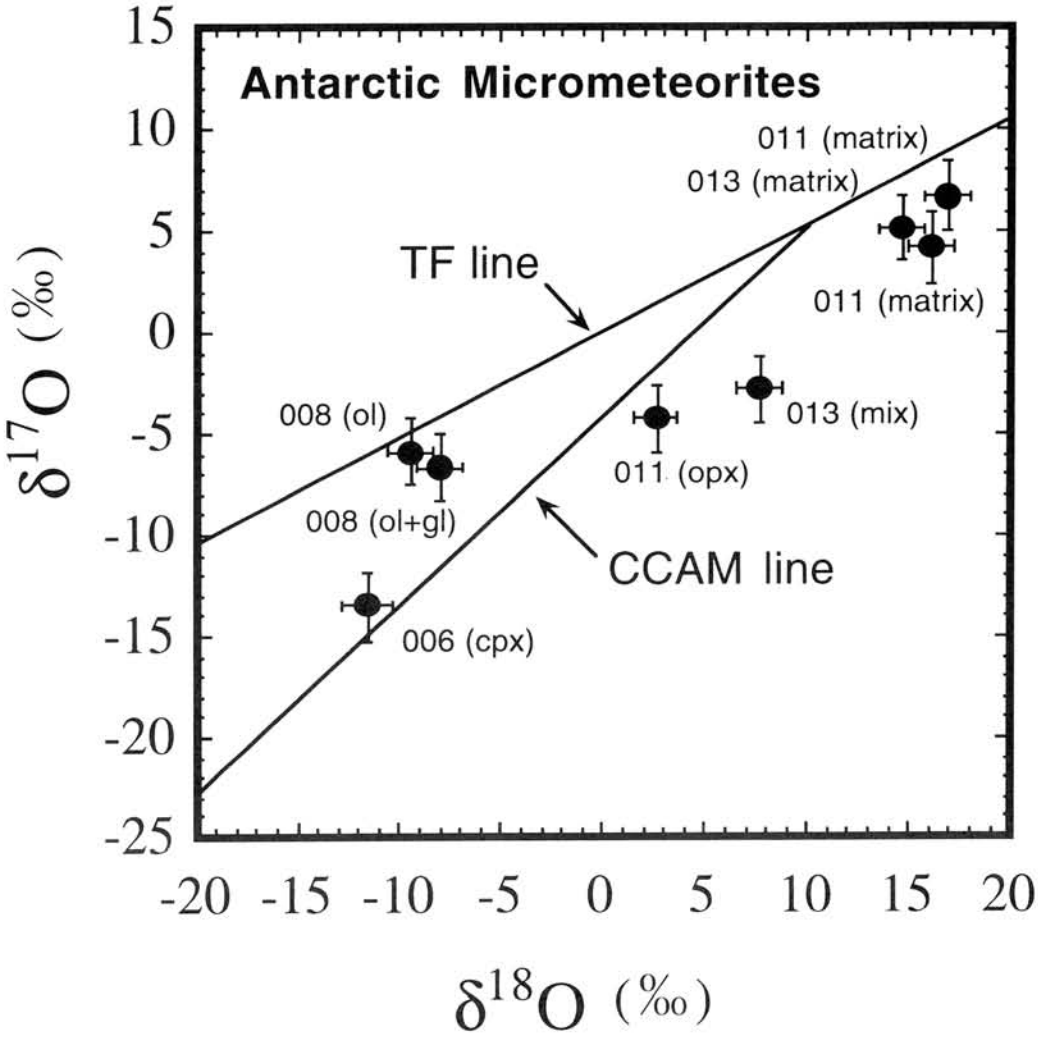

Fig. 1 Oxygen isotopic compositions of AMMs. Note that all the data fall *below* the TF line, suggesting that they are more closely related to carbonaceous chondrites than ordinary chondrites. Error bars are 1σ, but larger instrumental mass fractionation may be expected (see text).

Phyllosilicate-bearing Dark Clasts in the Polymict Ureilites

Yukio Ikeda[1] and Martin Prinz[2]
[1]Dept. Material & Biol. Sci., Ibaraki University, Mito 310, Japan
[2]Dept. Earth & Planet. Sci., Am. Museum Nat. Hist., New York, NY 10024, USA

Four polymict ureilites were studied -Dar Al Gani (DAG) 319, Nilpena, North Haig and Elephant Moraine (EET) 83309 - and they consist mainly of lithic and mineral clasts [1,2,3]. These clasts vary in texture and mineralogy and seem to have different origins from one another. They are classified into several groups in Table 1. Among them, what we call the dark clasts are a common lithology and they have a similar appearance to dark inclusions which occur in some carbonaceous chondrites. However, the dark clasts in polymict ureilites contain no chondrules but do contain exotic anhydrous minerals, indicating they differ from dark inclusions in the carbonaceous chondrites. Brearley and Prinz [4] concluded that the phyllosilicate-bearing dark clasts in Nilpena are most similar to CI chondrites, rather than CM chondrites, but differ from the CI chondrites in detail. Phyllosilicate-bearing dark clasts in polymict ureilites are a few hundred microns to a few mm across in size and are friable. They are mostly breccia and sometimes show a breccia-in-breccia structure. They are classified into two types, fayalite(Fa)-free and Fa-bearing (Table 1).

[Fa-free Type] Fa-free dark clasts consist mainly of phyllosilicate-rich matrix with variable amounts of phyllosilicate nodules, opaque-mineral aggregates, sometimes with framboidal magnetite, and carbonate fragments (Fig. 1a). In addition to phyllosilicates, the matrix contains small grains of euhedral to subhedral pyrrhotite, subrounded magnetite, tiny phosphate, etc. Phyllosilicate veins occur (Fig. 1b) in some Fa-free dark clasts, and a narrow vein cuts a broad vein in one dark clast. Phyllosilicates occur as veins, nodules (or fragments), and matrix in the Fa-free dark clasts, and they are plotted in Fig. 2. They are mainly serpentine (or chlorite) with minor smectite. The matrices contain tiny grains of Fe-bearing phases such as magnetite, sulfide or ferrihydrite, and they plot toward the Fe end-member. The Al_2O_3 contents of the phyllosilicates range mainly from 1-6 wt%; phyllosilicates with low Al_2O_3 [LA] have less than 3.5 wt% and are predominant in the Fa-free type. Those with high Al_2O_3 [HA] have more than 3.5 wt% and are minor. LA and HA phyllosilicates are probably serpentine and smectite (or chlorite), respectively.

[Fa-bearing Type] This type consists mainly of fayalitic olivine (Fo<40), phyllosilicates, magnetite, sulfide, etc. However, the matrix is more porous than that of the Fa-free type, suggesting that crystallinity of the Fa-bearing matrix is lower. The degree of hydration of the Fa-bearing type is probably lower than that of the Fa-free type. Phyllosilicates in the Fa-bearing matrix are plotted in Fig. 2. Matrix phyllosilicates in the Fa-bearing type are enriched in SiO_2 and Al_2O_3 in comparison to those in the Fa-free type, suggesting that the Fa-bearing matrices contain more abundant smectite component.

[Exotic Anhydrous Materials] Dark clasts also include exotic anhydrous materials set directly into the phyllosilicate-rich matrix. These exotic materials seem to differ between the Fa-free and Fa-bearing types. The Fa-free type contains olivine (Fo>50), pigeonite, enstatite, and rhyolitic glass, etc. The Fa-bearing type includes magnesian olivine, orthopyroxene, augite, and basaltic or ultramafic lithologies. The differences in the exotic materials found in the two types may be due to the differences in their formational stages. These exotic materials may have been incorporated into regolith breccias either during or after the hydration processes that took place near the surface of the UPB.

[Summary] The hydration that produced the dark clasts in the polymict ureilites may have taken place on a surficial veneer of the UPB. The degree of hydration for the Fa-bearing type was very weak and it may represent an early stage of hydration. The Fa-free type underwent moderate to intense hydration, resulting in the formation of framboidal magnetite or phyllosilicate veins. These findings are consistent with the conclusions of Brearley and Prinz [4].

References: [1] Jaques and Fitzgerald (1982) GCA ,46, 893-900; [2] Prinz et al. (1987) LPSC XVIII, 802-803; [3] Ikeda and Prinz (2000) AMR,13; [4] Brearley and Prinz (1992) GCA 56, 1373-1386.

Table 1. Classification of lithic and mineral clasts in polymict ureilites.

(A) Coarse-grained Mafic Lithic Clasts
(B) Fine-grained Mafic Lithic Clasts
(C) Felsic Lithic Clasts
(D) Dark Clasts
(D1) Fa-free type
(D2) Fa-bearing type
(E) Sulfide or Metal-rich Lithic Clasts
(F) Chondrule and Chondrite Fragments
(G) Isolated Mineral Clasts (mainly single crystals)

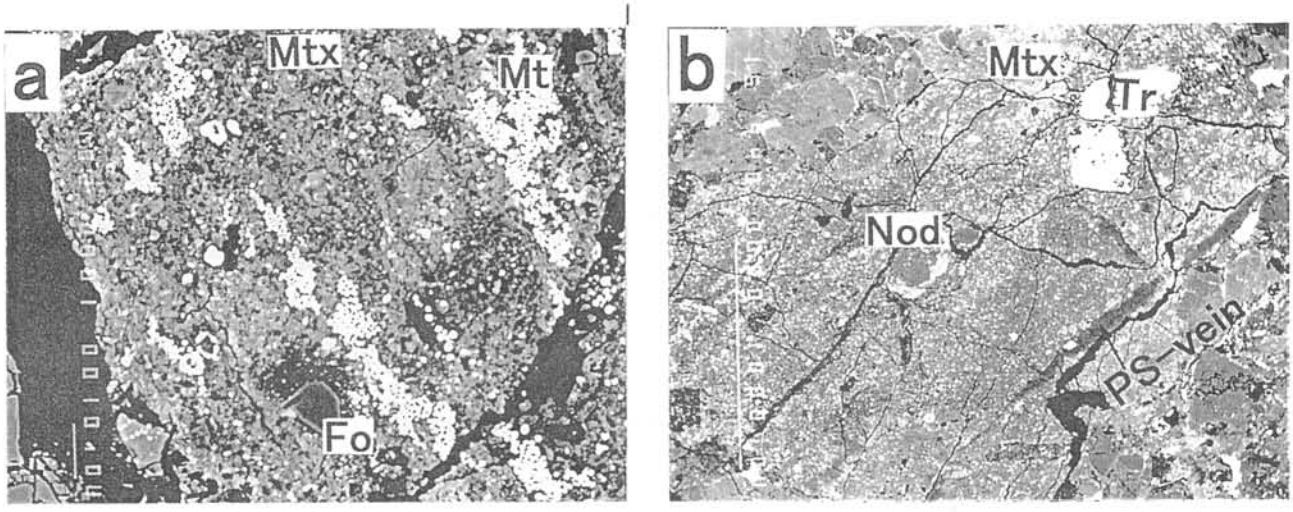

Figure 1. Back scattered electron images of Fa-free dark clasts. (a) A dark clast in Nilpena consists mainly of phyllosilicate-rich matrix (Mtx), magnetite aggregates (Mt), as well as exotic anhydrous forsterite (Fo). Width is about 120 microns. (b) A dark clast in DAG 319 containing large pyrrhotite grains (Tr), phyllosilicate nodules (Nod), and phyllosilicate veins (Ps-vein). Width about 2.7 mm.

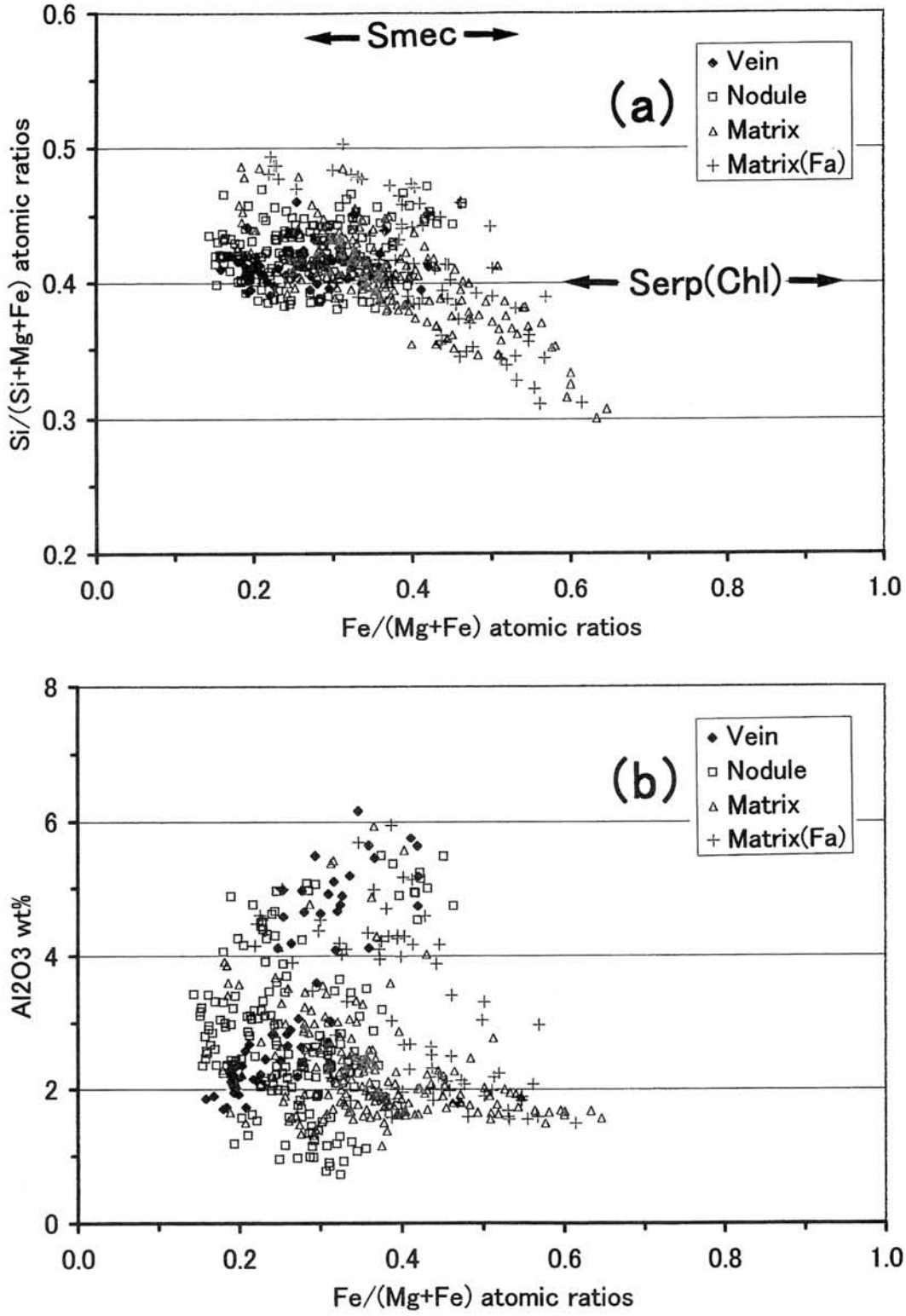

Fig. 2. Si/(Si+Mg+Fe) atomic ratios (a) and Al_2O_3 wt% (b) of vein phyllosilicates (Vein), nodule or fragmental phyllosilicates (Nodule), matrices (Matrix) in the Fa-free type, and matrices (Matrix(Fa)) in the Fa-bearing type are plotted against their Fe/(Mg+Fe) atomic ratios. Serpentine (or chlorite) solid solution and smectite solid solution are shown by Serp(Chl) and Smec, respectively.

Distribution of oxygen isotopes in an amoeboid olivine aggregate from the Allende meteorite

Hajime Imai and Hisayoshi Yurimoto
Department of Earth and Planetary Sciences, Tokyo Institute of Technology, Meguro, Tokyo 152-8551, Japan. (hajime@geo.titech.ac.jp)

1. Introduction

Amoeboid olivine aggregates (AOAs) predominantly consist of irregular shaped olivine and pyroxene. AOAs often contain Al-rich inclusions. The textures of AOAs show that they condensed directly from solar nebula and have been retaining information about early solar nebula since it condensed [1]. Several oxygen isotopic studies have been performed for AOAs from the Allende meteorite by [2, 3, 4].

In order to clarify the formation mechanism of AOAs and the environments around them, we have measured distribution of oxygen isotopes in a large amoeboid olivine aggregate (TTA1-02) from the Allende meteorite.

2. Experimental Procedure

The sample used was a polished thin section (TTA1) from the Allende meteorite. The sample surface was coated with 20 nm carbon film and then examined by scanning electron microscope, JEOL JSM-5310LV, equipped with energy dispersive X-ray spectroscopy, Oxford LINK ISIS.

After the petrological and mineralogical studies, the carbon film was removed and then gold film of 30nm thick was coated onto the sample surface. In-situ oxygen isotope analysis was performed by the TiTech CAMECA ims 1270 SIMS instrument. The primary ion beam was mass filtered positive $^{133}Cs^+$ ions accelerated to 20 keV and the beam spot size was ~ 5 μm in diameter. Negative secondary ions of the ^{16}O-tail, $^{16}O^-$, $^{17}O^-$, $^{16}OH^-$ and $^{18}O^-$ were analyzed at a mass resolution power of ~6000, sufficient to completely eliminate hydride interference. In order to correct instrumental mass fractionation, a Russian spinel with known O isotope ratios [5] was used for standardization.

3. Results and discussion

An AOA named TTA1-02 is irregular in shape and c.a. 5 x 3 mm in size on the thin section. Aggregates of fine olivine and fassaite grains (ol-fas aggregates) mainly comprise TTA1-02. Four Al-rich inclusions (#1, #2, #3, and #4) are embedded in the ol-fas aggregates. These characters resemble to those of AOA described in [1, 6, 7].

Typical olivine crystals in the ol-fas aggregates are c.a. 10 μm in diameter with c.a.

Fo_{90}. Typical oxygen isotopic compositions, ($\delta^{17}O$, $\delta^{18}O$), of the Mg-rich olivine and fassaite in the ol-fas aggregates are (-45‰, -45‰) and (-40‰, -40‰), respectively (Fig. 1). These results are consistent to previous study [3]. From texture, the original ol-fas aggregates directly condensed around Al-rich inclusions from solar nebula gas with $\delta^{17}O$, $\delta^{18}O$ values of -45 - -40‰.

Some fassaite grains in the ol-fas aggregates show fluffy and porous texture. The values of ($\delta^{17}O$, $\delta^{18}O$) of porous fassaites are plotted along the slope 1/2 line, which parallels with the terrestrial fractionation line, through the point (-40‰, -40‰) (Fig. 2). This fractionation is thought to be results of evaporation of ^{16}O-rich materials.

The Mg-rich olivine grains are often rimed by Fe-rich olivine grains. The composition between them changes abruptly, i.e., thickness of the boundary layer is less than 2 μm. Figure 2 shows the $\Delta^{17}O$ value ($\Delta^{17}O = \delta^{17}O - 0.52\delta^{18}O$) versus the forsterite content. The $\Delta^{17}O$ values of Fe-rich and Mg-rich olivines are c.a. –8‰ and -25‰, respectively. The texture and $\Delta^{17}O$ values between Fe-rich and Mg-rich olivine grains suggest that Fe-rich olivine have been produced after AOA formation in the ^{16}O-poor environment.

The Al-rich inclusions in TTA1-02 consist of core-rim layered structure. The core consists of aggregates of fine grains of spinel, fassaite, perovskite, anorthite, nepheline and phyllosilicate. The rim layer consists of fassaite. The texture of Al-rich inclusions resemble to those in [7]. Oxygen isotopic compositions of primary phases (spinel, perovskite, fassaite) in the Al-rich inclusions are (-40‰, –40‰) (Fig. 2). These results are consistent to previous study [3]. Oxygen isotopic compositions of secondary phases (anorthite, nepheline, phyllosilicate) in the Al-rich inclusions are (~0‰, ~0‰) (Fig. 2). Because Al-rich inclusions consist of fine-grain minerals, it is thought that original Al-rich inclusions directly condensed from solar nebula gas with $\delta^{17}O$, $\delta^{18}O$ values of -40‰ and then secondary phases were produced after AOA formation in ^{16}O-poor environment.

Oxygen isotopic distribution, CAI size, petrology and mineralogy of the Al-rich inclusions in TTA1-02 are similar to those of fine-grained CAIs in the Murchison meteorire [8]. Those similarities indicate that Al-rich inclusions in AOAs and fine-grained CAIs in the Murchison meteorite were formed at the same environment in the solar nebula.

It is thought that TTA1-02 was produced by following processes. As temperature dropped, Al-rich inclusions condensed from ^{16}O-rich nebula gas and then the ol-fas aggregates sequentially condensed surrounding them. After condensation of the ol-fas aggregates, ol-fas aggregates have experienced evaporation probably by reheating event. After the AOA formation, Fe-rich olivine and secondary phases in Al-rich inclusions were produced in ^{16}O-poor environment.

References

[1] Grossman, L. and Steele, I. M. (1976) *Geochim. Cosmochim. Acta* **40**: p. 149-155. [2] Clayton, R. N. et al. (1977) *Earth Planet. Sci. Lett.* **34**: p. 209-224. [3] Hiyagon, H. and Hashimoto, A. (1998) *Antarctic Meteorites* **XXIII**: p. 33-35. [4] Kobatake, H. et al. (1999) *Antarctic Meteorites* **XXIV**: p. 78-80. [5] Yurimoto, H. et al., (1994) *Earth and Planet. Sci. Let.* **128**: p. 47-53. [6] McSween, H. Y. (1977) *Geochim. Cosmochim. Acta* **41**: p. 1777-1790. [7] Hashimoto, A. and Grossman, L. (1987) *Geochim. Cosmochim. Acta* **51**: p. 1685-1704. [8] Sakai, T. and Yurimoto, H. (1999) *Lunar Planet. Sci.* XXX, #1528, CD-ROM.

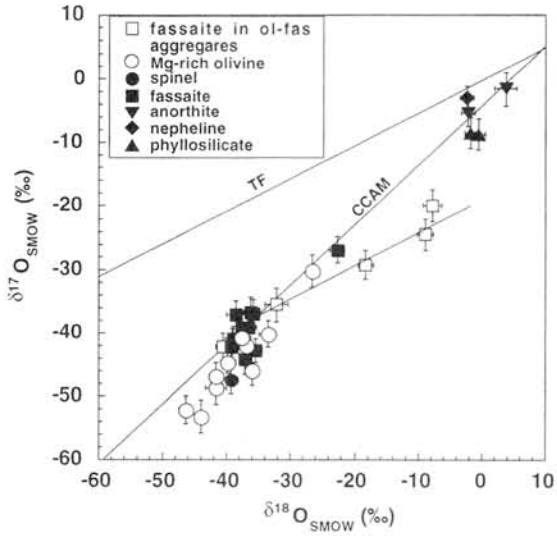

Fig. 1 Oxygen isotopic compositions of Al-rich inclusions and Mg-rich olivine and fassaite in ol-fas aggregates of TTA1-02. TF and CCAM represent terrestrial fractionation line and carbonaceous chondrite anhydrous mineral line, respectively.

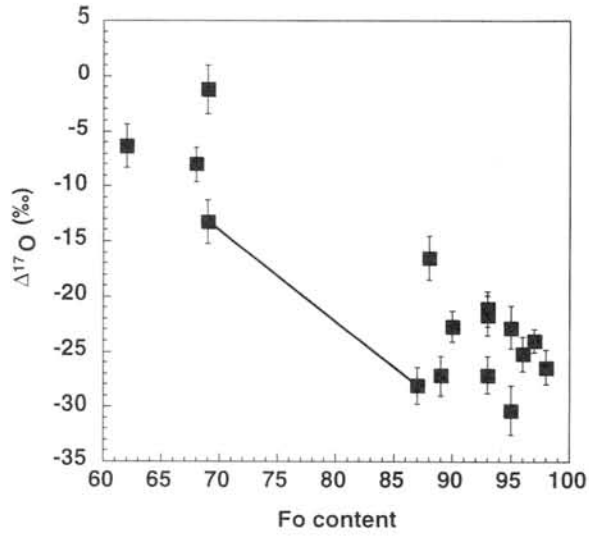

Fig. 2 Oxygen isotopic composition vs. Fo content. $\Delta^{17}O = \delta^{17}O - 0.52\delta^{18}O$. The symbols connected by tie line represent olivine crystals, which directly contact each other.

Oxygen isotopic compositions of spinel, olivine and pyroxene grains in Y-691 EH3 chondrite.

Shoichi Itoh[1], Hideyasu Kojima[2] and Hisayoshi Yurimoto[1]
[1] Department of Earth and Planetary Sciences, Tokyo Institute of Technology, Meguro, Tokyo 152-8551 Japan.
[2] National Institute of Polar Research, Kaga, Itabashi, Tokyo 173-8515 Japan

Introduction: Enstatite chondrites were formed under lower oxygen fugacities than other chondrites [1] and, thus, the inclusions in enstatite chondrites indicate a region of solar nebula that was spatially or temporally distinct from the nebula regions where carbonaceous and ordinary chondrites originated [2]. Therefore, it may be constrained how high-temperature processing or times during evolution of the solar nebula to compare the textures and isotopic compositions of individual crystals from enstatite chondrite with those from other groups. Previous studies of the descriptions of refractory inclusions in enstatite chondrites are a single Al-rich chondrule in Qingzhen [3] and a survey of 30 Al-rich objects [4]. This study presents the relationships between petrologic properties, chemical and oxygen isotopic compositions for individual crystals of Al-rich objects in Y-691 EH3 chondrite.

Analytical techniques: Polished thin section of Y-691,78-5 was used in this study. The thin section was examined with a petrographic microscope and with JEOL JSM-5310 LV scanning electron microscope equipped with Oxford LINK ISIS energy dispersive X-ray spectrometer.

Oxygen isotope ratios were measured by the TiTech Cameca ims 1270 SIMS instrument using a 20keV Cs^+ primary ion beam, focussed to a ~5μm spot, with a beam current of ~3pA. Oxygen isotopes was measured as negative secondary ions with M/ΔM of ~6000. Other analytical conditions and data calibration method have been described elsewhere [5].

Results and discussion: We found eight Ca-Al-rich objects in matrix of Y-691,78-5 thin section whose primary mineralogy is dominated by enstatite and the minor minerals are spinel, Al-rich diopside, periclase and calcic plagioclase and nepheline. Size distribution of most Ca-Al-rich objects ranges in across from 20 to 500 μm. We identified that some (#1, 7, 8) of the Ca-Al rich objects in Y-691 belong to Al-rich chondrule in the texture and mineralogy. Y-691-8 consists of barred Al-rich diopside and spinel grains dominated by enstatite(Fig.1). The remaining objects are isolated mineral grains and a corundum-graphite spherule.

The chemical compositions of individual minerals in Ca-Al-rich objects are shown in Table.1. Spinels in Y-691 are almost free from FeO components and always contain Cr_2O_3 components (<18wt%).

O-isotopic compositions of all individual crystals in Ca-Al-rich objects from Y-691 are shown in Fig.2. Except for corundum grains, all of phases (spinel, diopside, albite, olivine and periclase) in the objects are not enriched in ^{16}O as CAI minerals. The O isotopic compositions consist with bulk O isotopic composition of enstatite chondrite [6]. The O isotopic compositions in this study are different from those of CAIs in enstatite chondrites[7, 8].

O isotope ratios of corundum ($\delta^{17}O$=~ -3‰, $\delta^{18}O$=~ -18‰) in the corundum-graphite spherule is plotted on the left hand side of the bulk O isotopic composition. The isotopic composition shows that isotopic fractionation process occurred on the corundum formation. Although the plot is slightly upward from the terrestrial (or enstatite chondritic) fractionation line, the discrepancy may be due to the analytical error of rough surface condition of the object.

Table.1. Representative chemical compositions of minerals in Y-691,78-5.

object #	#1		#2	#3	#4
type	PPC			POC	
mineral	ab	cpx	sp	ol	cor
Na2O	9.30	-	-	-	0.10
MgO	-	21.4	23.1	49.3	0.70
Al2O3	17.5	4.90	50.7	-	71.8
SiO2	63.5	48.5	3.7	39.2	0.10
SO3	1.30	-	-	-	1.10
K2O	0.40	-	-	-	-
CaO	0.30	11.0	0.7	-	-
Cr2O3	-	-	16.9	-	-
TiO2	-	-	-	-	-
FeO	2.10	9.30	4.00	4.50	0.70
total	94.4	95.1	99.1	93.0	74.5
Na	0.83	-	-	-	0.00
Mg	-	1.22	0.88	1.89	0.02
Al	0.96	0.22	1.54	-	1.93
Si	2.95	1.86	0.10	1.01	0.00
S	0.05	-	-	-	0.02
K	0.02	-	-	-	-
Ca	0.01	0.46	0.02	-	-
Cr	-	-	0.34	-	-
Ti	-	-	-	-	-
Fe	0.08	0.30	0.09	0.10	0.01
O	8.00	6.00	4.00	4.00	3.00
total	4.90	4.06	2.97	2.99	1.99

object #	#7	#8		
type	PPC		BPC	
mineral	sp	sp	Al-di	en
Na2O	-	-	-	-
MgO	27.5	26.3	13.8	38.4
Al2O3	69.1	68.8	12.2	-
SiO2	-	-	43.1	61.9
SO3	-	-	-	-
K2O	-	-	-	-
CaO	-	0.30	21.6	-
Cr2O3	1.70	1.10	-	-
TiO2	-	-	1.30	-
FeO	-	-	3.50	-
total	98.2	96.6	95.5	100
Na	-	-	-	-
Mg	0.99	0.97	0.79	0.95
Al	1.97	2.00	0.55	-
Si	-	-	1.65	1.03
S	-	-	-	-
K	-	-	-	-
Ca	-	0.01	0.89	-
Cr	0.03	0.02	-	-
Ti	-	-	0.04	-
Fe	-	-	0.11	-
O	4.00	4.00	6.00	3.00
total	3.00	2.99	4.03	1.97

* PPC: porphyritic pyroxene chondrule, POC: porphyritic olivine chondrule, BPC: barred-pyroxene chondrule. ab: albite, cpx: pyroxene, sp: spinel, ol: olivine, en: enstatite, Al-di: Al-rich diopside, cor: corundum.

References: [1] Keil K. (1969) *Earth Planet. Sci. lett.* **7**, 243-248. [2] Kallemeyn G. W. and Wasson J. T. (1986) *GCA* **50**, 2153-2164. [3] Rambaldi, E. R. et al.(1984) *Lunar & Planet. Sci.*, **XV**, 661-662. [4] Bischoff et al. (1985) Chem. Erde, **44**,97-106. [5] Yurimoto H., Ito M., Nagasawa H. (1998) *Science*, **282**, 1874-1877. [6] Clayton, R. N (1993) *Annu. Rev. Earth Planet. Sci*, **21**, 115-149. [7] Fagan, T. J. et al. (2000) *Lunar & Planet. Sci.*, **XXXI**, #1592. [8] Guan Y. et al. (2000) *Lunar & Planet. Sci.*, **XXXI**, #1744.

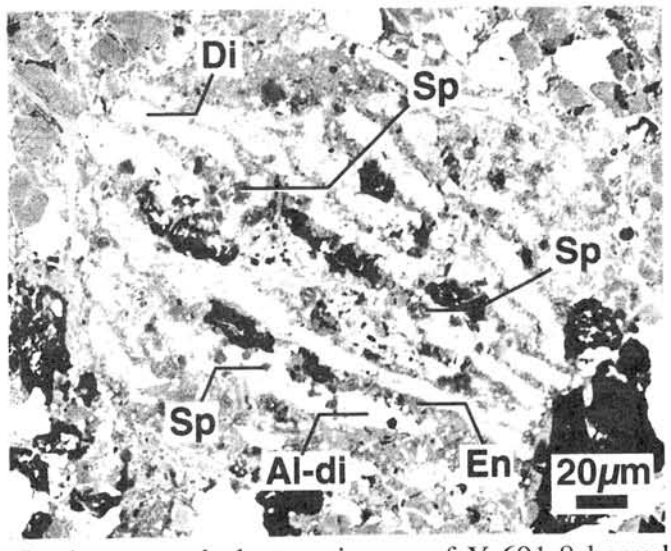

Fig.1. Back-scattered electron image of Y-691-8 barred-pyroxene chondrule in the Y691 enstatite chondrite. This chondrule mainly consists of enstatite(En), Al-diopside(Al-di), spinel(Sp).

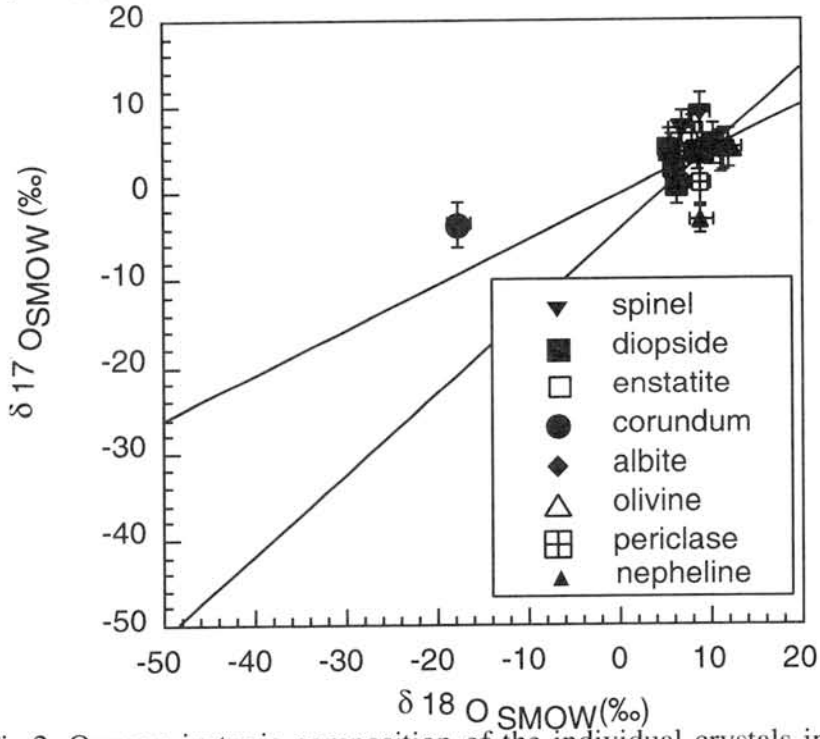

Fig.2. Oxygen isotopic composition of the individual crystals in Ca-Al-rich objects of Y-691. Error bars are ± 1 σ_{mean}.

Isotope Systematics of SNC Meteorites.

E. Jagoutz and G. Dreibus

Max Planck Institut fuer Chemie
55122Mainz Saarstrasse 23 Germany
(< jagoutz@mpch-mainz.mpg.de>< dreibus@mpch-mainz.mpg.de>)

SNC meteorites are a group of 13 volatile rich achondrites, which radiometric dating has shown to have a complicated polymetamorphic history. Their young internal mineral ages (< 1.3 Ga) have been taken as evidence that these meteorites were derived from Mars on the basis of that planet's presumed continuing magmatic activity. Some other, age-independent similarities, such as a match in Xe/Kr with that obtained from the Mars Lander mission, seem to support a Martian origin. However, some isotopic evidences exist that could be used to argue against a Martian origin. Further isotopic analysis of the SNC meteorites is therefore essential in order to unravel their complex evolutionary history.

In this presentation Nd, Sr and Pb isotopic data on SNC meteorites are summarized, followed by a special case study . New isotope data on Nakhla are presented in the special case study, on which this abstract will focus on. This new data are compared to the isotopic results obtained on earlier studies on the SNC meteorites Dag (Dar al Gani 476) and Que (Que 94201).

Igneous minerals from Dag form a linear array on a Sm-Nd isochron plot, suggesting an age of around 800 Ma. The whole rock and leach analyses from Dag, however, plotted above the trend of the igneous minerals a feature common to several of the SNC meteorites. Because it is evident that Dag suffered considerable terrestrial alteration, 3 whole rock samples were prepared to assess the effects of such alteration on the isotopic systematics. A coarse-grained, a fine-grained, and a finely powdered whole rock sample were leached in warm 2.5 N HCl, and the leaches and residues were analyzed. On an isochron plot the residue and leach fractions define separate mixing lines between endmember components, which are taken to be 'indigenous' whitlockite and terrestrially contaminated silicate minerals. The proportion of contamination in the leaches decreases with increasing grain size, and the isotopic composition of the alteration-free whitlockite is then determined by extrapolating to the intersection of the two mixing lines.

For this study we handpicked a clinopyroxene and an olivine separate from Nakhla. The clinopyroxene separate was judged to be 100% pure while the olivine separate contained some small inclusions (possible melt inclusions). The surfaces of the mineral separates were extensively cleaned with diluted HF and HCl in an ultrasonic bath. In addition, two finely powdered whole rock samples were leached in warm 2.5 N HCl. The cleaned clinopyroxene and olivine, the two leaches, and one of the residues were analyzed, and the results are shown on a Sm-Nd isochron plot in fig 1.

The data points clearly are not all colinear within analytical uncertainty. While the leach and residue points alone align along a 1.38 Ga isochron, a least square fit to all the data gives a distinctly younger age of 1.29 Ga. Nonetheless, these ages are in the range of other published internal mineral ages on SNC meteorites. In particular, the Nd isotope data from Governador Valadares (Shih et al, 1999) and Lafayette (Jagoutz, unpubl. data) plot close to these data, and Chassigny (Jagoutz, unpubl. data) may also be derived from the same isotopic source.

Two other new observations that are shown in figs 2 and 3 also need to be taken into consideration. In fig 2 the combined leaches from Nakhla, Dag, and QUE94201 (Qe; (Jagoutz, unpubl. Data; Borg et al 1997) show a good linear relationship on a Sm-Nd isochron plot, suggesting an age of 1.2 Ga. Although, as mentioned above, the leaches of Dag might be

affected by terrestrial contamination, a 'clean' leach isotopic composition can be estimated by using a mixing calculation.

By contrast, in fig 3 the olivine and pyroxene from Nakhla and Dag as well as the Mg-pyroxene from Qe all presumed to be the first igneous minerals to crystallize in each of the three meteorites are shown to have an isochron age of 705 Ma. Although these minerals display a wide range in Sm/Nd, the isochron is of remarkably good quality and suggests that the mafic minerals of these meteorites come from the same source. We note that the plagioclase of Dag and Qe as well as the Fe-pyroxene from Qe do not plot on this isochron, possibly because the Fe-pyroxene is a late crystallizing phase and the plagioclase might be terrestrially contaminated. Interestingly, however, samples of whole rocks from Nakhla, Dag, and Qe do yield a combined isochron age of 1.13 Ga.

From these data we conclude that Nakhla, Governador Valadares, Lafayette, Chassigny, Dag, and Qe all originated from the same isotopic reservoir. This conclusion is also supported by other isotope data; i.e., these meteorites all have a positive 142Nd anomaly of between 70 and 80 ppm, and the Sr isotopic composition of all these meteorites is rather primitive. Furthermore, the noble gasses from these meteorites also indicate a common source.

Several possible scenarios can be constructed to explain these observations. The first scenario is that the three meteorites represent rocks that were differentiated from a common source, and, consequently, they plot on a whole rock isochron. At a later time the minerals in each of these rocks were internally reset (producing individual leach-residue isochrons). While the whole rocks remain closed systems on the original isochron, the reset whitlockites (low Sm/Nd) and mafic silicate minerals (high Sm/Nd) will now plot to the left and right side, respectively, of the original isochron. However, neither the whitlockites (leaches) nor mafic minerals (residues) from the different, chemically distinct meteorites would themselves form isochrons by such process, and, therefore, this scenario can be excluded.

In the second scenario magma from a LREE-depleted reservoir crystallizes as a differentiated sequence of very LREE-depleted rocks. These rocks are then invaded and contaminated by a trace element-enriched (similar to KREEP on the Moon) fluid having a more radiogenic Nd than the magmatic rocks. Isotopic equilibration is not achieved, however, and a mixing line with positive slope between the trace element-enriched and indigenous Nd is thereby established. As the system subsequently ages, this mixing line will rotate 'ahead' of the true magmatic isochron and does not carry with it any age significance. Because of the somewhat contrived chemical and isotopic conditions required by this scenario, we also hesitate to pursue it further.

The third, and favored, scenario attributes the observed isotopic patterns to mixing processes accompanying the impacting of a heterogeneous regolith. Using a mixing calculation, the observed major and trace element contents of the SNC meteorites can be explained in terms of three endmember (mafic, felsic, and trace element-enriched) components. Thus, olivine and pyroxene are contributed by the mafic component; elements having a constant ratio to Al, such as P, Ti, HREE, etc., are controlled by the felsic component; and Rb, Sr, LREE, K, etc., are derived dominantly from the trace element component. In this scenario the three isochrons (fig 2, fig 3, and the whole rock isochron) cannot all have age significance, and at least two of these lines must be mixing lines. The existing data already strongly suggest that the whitlockite and the igneous mafic minerals are not in equilibrium in these rocks. Previous Sr isotopic studies of SNC meteorites have also shown that whitlockite and plagioclase are isotopically distinct, and neither mineral contains sufficient Rb to explain this difference by in situ decay. A Sr isotopic investigation of Nakhla currently underway will be very helpful in deciding which of the isochons has an age significance. Regardless, the most important conclusion based on these new Sm-Nd data is that Chassigny, Nakhla, Governador, Valadares, Lafayette, Dag, and Qe derive from the same

source despite their very different exposure ages. This conclusion also seems to be supported by existing Rb-Sr data, which show all these meteorites to have unradiogenic Sr isotopes. Furthermore, these meteorites all share a Chassignytype rare gas composition and a similar 142Nd excess.

References: Shih et al.(1999), Meteoritics 34 647-655; Borg et al (1997) GCA 61 4915-4931.

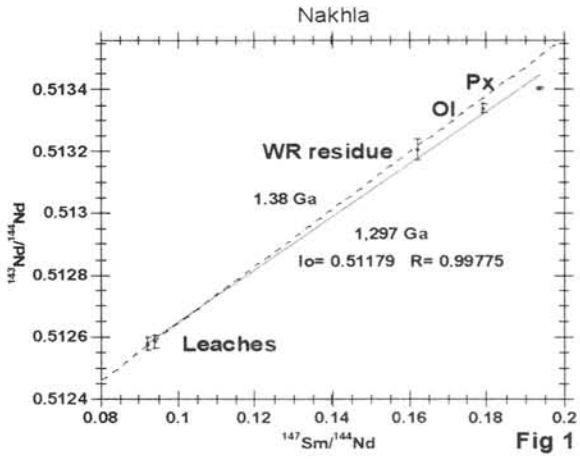

Fig 1

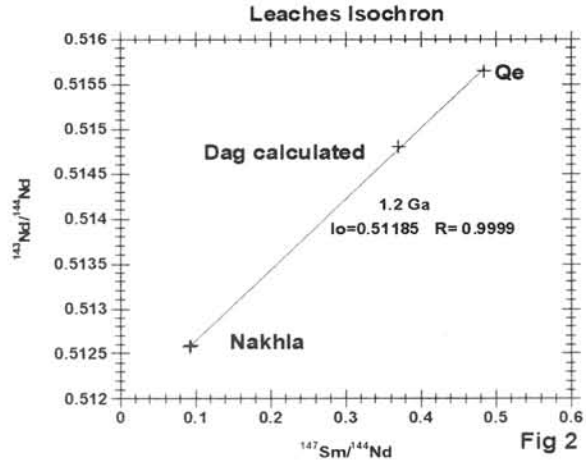

Fig 2

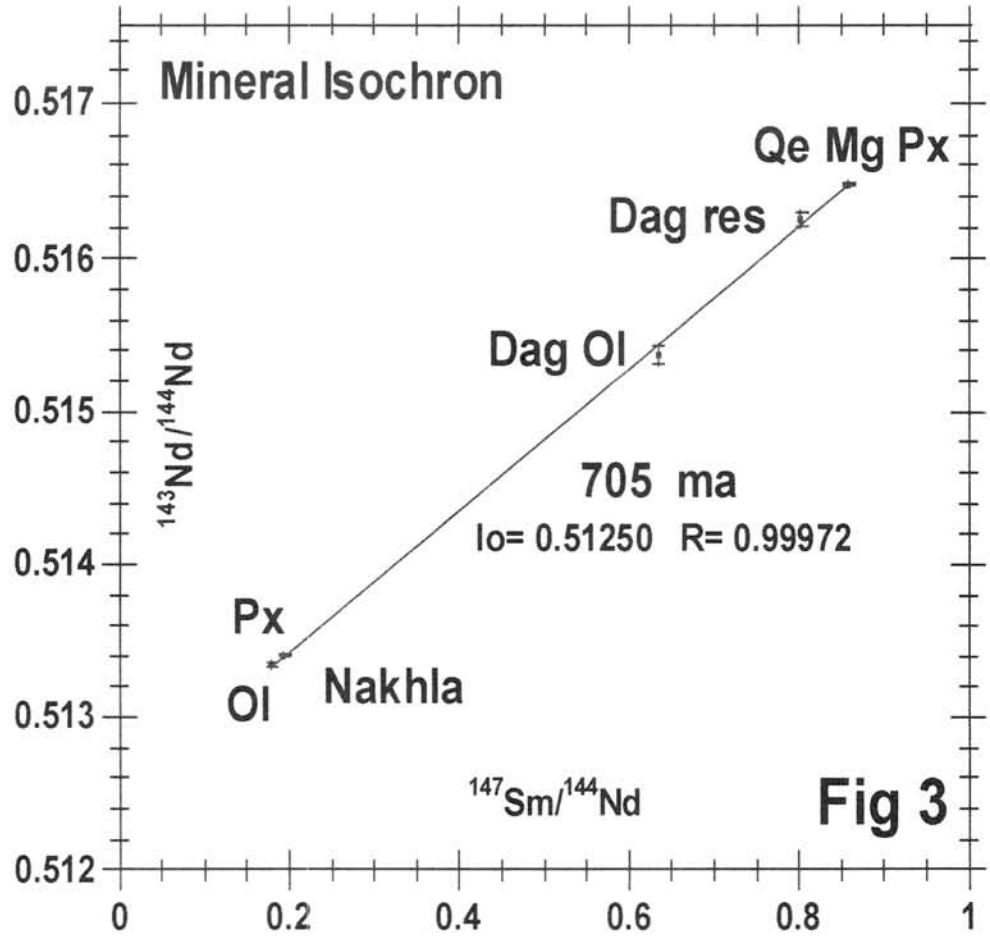

Fig 3

Anomalous H-chondrites, Y-792947, Y-793408 and Y-82038, with high abundance of refractory inclusions and very low metamorphic grade. M. Kimura[1], H. Hiyagon[2], H. Palme[3], B. Spettel[4], D. Wolf[3], R.N. Clayton[5], T.K. Mayeda[5], T. Sato[1] and H. Kojima[6]. [1]Faculty of Science, Ibaraki University, Mito 310-8512, Japan, [2]Dept. Earth and Planet. Science, University of Tokyo, Tokyo 113-0033, Japan, [3]Universität zu Köln, Institut für Mineralogie und Geochemie, 50674 Köln, Germany, [4]Max-Planck-Institut für Chemie, 55020 Mainz, Germany, [5]Enrico Fermi Institute, University of Chicago, Chicago, IL 60637, USA, [6]National Institute of Polar Research, Tokyo 173-8515, Japan.

Introduction

Y-793408, Y-792947 and Y-82038 were tentatively classified as L3 or H3 chondrites, and they show some unusual features, such as higher concentrations of Al and Ca, and smaller chondrule size than those of typical ordinary (O) chondrites [1,2]. Kimura *et al.* [3] discovered abundant refractory inclusions in the three chondrites, and temporarily classified these chondrites into an unusual chondrite grouplet. Here we report petrography, bulk chemistry and oxygen isotopic compositions of these chondrites to explore their classification.

Petrography and mineralogy

The three chondrites are similar in texture and constituents to each other. They show typical chondritic texture mainly consisting of chondrules, isolated minerals and matrix. Chondrules and isolated silicate minerals occupy 70-77 vol.% of these chondrites. The modal compositions of the matrix and opaque minerals (Fe-Ni metal > troilite) are 12-17% and 8-13%, respectively. These chondrites are assigned to shock stage S1.

Chondrules (0.32mm in apparent average size) contain abundant clean glassy groundmass. The abundance of porphyritic and non-porphyritic (radial and barred) chondrules is 80 and 20%, resectively. Olivine and low-Ca pyroxene (mainly clinoenstatite) show wide compositional ranges, $Fa_{0.3\text{-}59}$ (average Fa_{15} and PMD = 72) and $Fs_{0.3\text{-}53}$, respectively.

We found 43 refractory inclusions and their fragments in 5 thin sections (2.67 cm^2 in total), corresponding to an abundance of 0.5-0.7vol%. The inclusions (30-230μm) consist mainly of spinel with olivine, high-Ca pyroxene (diopside to fassaite), nepheline, sodalite, hibonite, ilmenite, perovskite and rutile. Most spinels are enriched in FeO (10.5-23.6%) and ZnO (1.0-3.1%). These inclusions were heavily subjected to secondary alteration, like those in carbonaceous (C) chondrites.

Chemical and oxygen isotopic compositions

Two ~100 mg samples of each meteorite were analyzed by INAA and two 120 mg splits by XRF. Some of the results are shown in Table 1. The three chondrites are remarkably similar in their chemical compositions confirming petrological evidence.

The oxygen isotopic compositions of acid-washed whole rock samples of Y-792947, Y-793408 and Y-82038 are $\delta^{18}O$ = +3.95, +3.87 and +3.98‰, and $\delta^{17}O$ = +2.61, +2.52 and +2.69‰, respectively.

We preliminarily measured the oxygen isotopic compositions of olivines in refracory inclusions, chondrules and isolated minerals, using a CAMECA ims-6f ion microprobe. An olivine grain in an inclusion plots on the CCAM line ($\delta^{18}O$ = -30.3 and $\delta^{17}O$ = -31.7‰). Olivines in chondrules and isolated minerals are distributed around the whole rock oxygen isotopic compositions. The isotopic compositions of these olivines seem not to be correlated with their fayalite contents, which coincides with the observation in C-chondrites [4, 5].

Discussion

The oxygen isotopic compositions of the whole rock samples of Y-792947 and others are all close to the mean values for H-chondrites. This is supported by the chemical composition of these chondrites. They are chemically very similar to H-chondrites. They have exactly the same Mg/Si ratios, and the same depletion in refractory elements (Al/Si and Ca/Si ratios). They have identical Mn/Mg ratios as H-chondrites which distinguishes them from C-chondrites. One of the few differences of these chondrites to H-chondrites are the Na/Mg ratios which are lower than those of H-chondrites. Given the similarity in Fe/Mg ratios between these chondrites and the H-chondrites as well as the close match in siderophile elements in general, it is clear that only H-chondrites fit (Table 1). In addition, the similarity in Se-contents between H-chondrites and Y-792947 and others suggests the same amount of sulfide in these meteorites as in H-chondrites, as the S/Se ratio in chondritic meteorites is with 2500 fairly constant [6].

The modal compositions of chondrules, matrices and opaque minerals, and abundant non-porphyritic chondrules of Y-792947 and others are also typical of H-chondrites [7]. The small chondrule size distributions are within the ranges of both H and CO chondrites.

Chondrules in these chondrites are sharply defined, and olivine and pyroxene show wide ranges of compositions. These features indicate that they are of petrologic type 3, which is supported by abundant clinoenstatite and clean glass. Ninagawa *et al.* [8] also classified them into subtypes 3.1-3.3 from TL data.

All these data suggest that Y-792947 and others are members of H3.1-3.3(S1), although they could be paired with one another. The most primitive H-chondrite ever reported is Roosevelt County 075 (H3.2(S2)) [9], although it was subjected to heavily terrestrial weathering resulting in the loss of most Fe-Ni metal. Many trace element concentrations in this chondrite were disturbed by weathering. On the

other hand, Fe-Ni metals in Y-792947 and others escaped severe terrestrial weathering. These chondrites preserve most of the original chemical features of H-chondrites, except perhaps for some loss of Na and gain of Br. Therefore, they represent the most primitive H-chondrites known to date, hardly affected by thermal and shock metamorphism and terrestrial weathering.

On the other hand, the abundance of refractory inclusions in these chondrites are extraordinarily high in comparison with any known O-chondrites. Bischoff and Keil [10] found only 4 inclusions from 19 sections of 14 H-chondrite samples. Therefore, Y-792947 and others are probably members of an inclusion-rich very primitive subgroup of H-chondrite.

References: [1] Yanai K. and Kojima H. *Catalog of the Antarctic Meteorites*, 1995. [2] Nobuyoshi T. *et al. Antarct. Meteorite Res.*, **10**, 165-180, 1997. [3] Kimura M. *et al. MAPS*, **34**, A63, 1999. [4] Hiyagon H. and Hashimoto A. *Antarctic Meteorites* **XXIV**, 37-39 1999. [5] Leshin L.A. *et al. Lunar Planet. Sci.* **XXXI**, #1918, 2000. [6] Dreibus G. *et al. Meteoritics*, **30**, 439-445, 1995, [7] Grossman J.N. *et al. Meteorites and the Early Solar System*, 660-679, 1988. [8] Ninagawa K. *et al. Papers 17th Symp. Antarc. Meteorites*, 239-240, 1992. [9] McCoy T.J. *et al. Meteoritics*, **28** 681-691, 1993 [10] Bischoff A. and Keil K. *GCA*, **48**, 693-709, 1984.

Table 1. Comparison of the chemical composition of Y-793408, Y-792947 and Y-82038 with the common classes of chondrites.

	Y-793408,96	**Y-792947,68**	**Y-82038,69**	CI	CV	H	L	EH
Mg %	**12.82**	**13.21**	**13.06**	9.61	14.5	*14.0*	14.9	10.6
Mg/Si	**0.82**	**0.82**	**0.83**	0.90	0.93	*0.83*	0.81	0.63
Al/Si	**0.064**	**0.066**	**0.064**	0.081	0.11	*0.067*	0.066	0.049
Ca/Si	**0.071**	**0.074**	**0.074**	0.089	0.122	*0.074*	0.071	0.051
Fe/Mg	**1.86**	**1.80**	**1.90**	1.90	1.62	*1.96*	1.44	2.74
Cr/Mg	**0.026**	**0.025**	**0.026**	0.028	0.025	*0.026*	0.026	0.030
Mn/Mg	**0.016**	**0.016**	**0.016**	0.020	0.010	*0.017*	0.017	0.021
Na/Mg	**0.037**	**0.035**	**0.036**	0.052	0.023	*0.046*	0.047	0.064
Se ppm	**7.63**	**7.95**	**7.75**	19.6	8.3	*7.7*	9.0	25.5
Ir ppb	**740**	**753**	**759**	460	760	*760*	490	565
Au ppb	**201**	**197**	**210**	144	144	*215*	162	330

ratios as weight ratios

The first discovery of high-pressure polymorphs, jadeite, hollandite, wadsleyite and majorite, from an H-chondrite, Y-75100.

Kimura M.[1], Suzuki A.[2], Kondo T.[2], Ohtani E.[2] and El Goresy A.[3], [1]Ibaraki University, Mito, Japan, [2]Tohoku University, Sendai, Japan, [3]Max-Planck-Institut für Chemie, 55128 Mainz, Germany.

1. Introduction

High-pressure minerals, such as ringwoodite, wadsleyite, akimotoite and $(Mg,Fe)SiO_3$-perovskite, majorite-pyrope garnet, magnesiowüstite, and hollandite, have been found in the shock melt veins of many L-chondrites, which indicated shock-induced melting and crystallization under the pressure and long duration of high-pressures and -temperatures [1, 2]. However, no high-pressure phases have been encountered in the shock veins of H-chondrites [3, 4]. Kimura *et al.* [4] suggested that the petrologic setting in the shocked H-chondrites is indicative of shock-melt after pressure release. Following our previous work [4], we conducted mineralogical study, with micro Raman investigations, of heavily shocked H-chondrites, Y-791524 (H4), ALH-78108 (H5), A-880993 (H6), Y-75100 (H6) and Y-75277 (H6), in comparison with shocked L-chondrites, Y-791384 (L6) and Y-74445 (L6). The purpose of this study is to explore the shock history of H-chondrites.

2. Petrography and mineralogy

All the H-chondrites studied here consist of chondritic hosts with shock-induced melt veins. The melt veins mainly comprise two lithologies: 1) coarse-grained rounded to irregular silicate grains (~10 to ~100μm), and 2) fine-grained (below ~5μm) silicate aggregate. Our Raman spectroscopic investigations indicate that the veins in all H-chondrites including three samples by Kimura *et al.* [4], except Y-75100, contain no any high-pressure polymorphs of silicate phases.

On the other hand, a vein in Y-75100 contains some high-pressure polymorphs both in two lithologies. Coarse-grains of Fa_{17-20} are mixture of wadsleyite and olivine. All coarse grains of plagioclase composition ($An_{13}Ab_{83}Or_4$) are evidently jadeite. This is the first occurrence of jadeite in H-chondrites, along with recent discovery of jadeite from an L-

chondrite [5]. We noticed the strongest line of hollandite in some spectra of jadeite-rich grains. Such spectra display no evidence for high-pressure polymorphs of silica. However, we can not exclude the possibility that the strongest line of coesite may overlap the line of jadeite at 520cm^{-1}. Coarse-grains with average composition of $En_{82}Fs_{16}Wo_2$ were identified as low-Ca pyroxene. On the other hand, fine-grained lithology in the vein of Y-75100 is a mixture of olivine, wadsleyite, low-Ca pyroxene and majorite.

L-chondrites studied here abundantly contain ringwoodite, majorite and hollandite, in the melt veins, like the other shocked L-chondrites [1, 2].

3. Implications

Survival of high-pressure phases in shocked L-chondrites indicates the veins were quenched under high-pressure [1]. On the other hand, H-chondrites hardly contain high-pressure phases. Therefore, the parent body of H-chondrites might have experienced different shock events from that of L-chondrites.

Jadeite may have been formed through retrograde transformation of hollandite under moderate post-shock pressure and high temperature conditions. The assemblage of wadsleyite plus majorite in the shock vein of Y-75100 constrains the pressure and temperature to be ~15 GPa and ~1800 °C, respectively [6, 7], which is much lower than the pressures estimated for the shocked L-chondrites [1, 2]. We assume that the duration of shock-induced high-pressure in the parent bodies of H-chondrite could be much shorter than that of L-chondrites.

References: [1] Chen M. *et al.* (1996) *Science*, **271**, 1570-1573. [2] Gillet P. *et al.* (2000) *Science*, **287**, 1633-1602. [3] Stöffler D. *et al.* (1991) *GCA*, **55**, 3845-3867. [4] Kimura M. *et al.* (1999) *Antarctic Meteorite* **XXIV**, 67-68. [5] El Goresy A. *et al*, MAPS. (2000), in press. [6] Zhang J. and Herzberg C. (1989) *JGR*, **99**, 17729-17742. [7] Agee C.B. *et al.* (1995) *JGR*, **100**, 17725-17740.

SHOCK METAMORPHIC EFFECTS OF THE ALLENDE CV CHONDRITE AT 20-50 GPa: AN EXPERIMENTAL STUDY

K. Kiriyama[1], K. Tomeoka[1] and T. Sekine[2]

[1] Department of Earth and Planetary Sciences, Faculty of Science, Kobe University, Nada, Kobe 657, Japan.
[2] National Institute for Research in Inorganic Materials, 1-1 Namiki, Tsukuba, Ibaraki 305, Japan.

INTRODUCTION

Carbonaceous chondrites are porous and volatile-rich, so they are expected to respond to shock compression differently from other types of meteorites. However, highly shocked carbonaceous chondrites are rare, and the shock effects on them have been poorly understood. The previous petrographic study by Scott et al. [1] showed that shock effects differ considerably even among the different types of carbonaceous chondrites. For example, almost all CM chondrites are shock stage S1 (virtually unshocked), whereas CV chondrites show a range of shock stages from S1 to S4 (shocked to 30-35 GPa). In order to better understand the shock history of the carbonaceous chondrites, we believe that experimental research is necessary. Recently, Tomeoka et al. [2] have reported the results of a series of shock-recovery experiments of the Murchison CM chondrite at pressures from 4 to 49 GPa and revealed a variety of shock effects that have never been observed in naturally shocked CM chondrites. Previously, Nakamura et al. [3] have attempted to shock the Allende CV chondrite and found that chondrules are flattened in the plane of the shock front by shock pressures from 10 to 20 GPa. We have carried out a series of shock-recovery experiments of Allende at pressures from 27 to 49. The main purposes of our work are to examine shock effects of Allende at pressures higher than 20 GPa, to compare the effects with those of Murchison, and to establish quantitative estimates of shock intensities in CV chondrites.

MATERIALS AND METHODS

The shock-recovery experiments were performed by using a single stage 30-mm bore propellant gun at National Institute for Research in Inorganic Materials. The targets were disks of Allende, 10 to 12 mm in diameter and 1.8 to 3 mm in thickness. The Allende samples were shocked in five experiments at peak pressures 27, 31, 37, 41 and 49 GPa. Details of the shock experimental procedures are described in Tomeoka et al. [2]. Polished thin sections or thick sections were made from each recovered sample by cutting along the shock compression axis. They were studied by using an optical microscope, a scanning electron microscope (JEOL JSM-5800) equipped with an energy dispersive X-ray spectrometer (EDS), and an electron probe microanalyzer (JEOL JXA-8900) equipped with wavelength-dispersive X-ray spectrometers (WDS).

RESULTS

Impact at 27 and 31 GPa

Chondrules are flattened roughly in the plane of the shock front, with mean aspect ratios of 2.14 (27 GPa) and 2.36 (31 GPa). Most coarse grains of olivine and pyroxene in chondrules are irregularly fractured to subgrains of ~10 μm in size. Wide (~10 μm), long (100-1000 μm) fractures form in matrix typically in directions oblique to the compression axis. Local melting occurs as melt veins preferentially along boundaries between chondrules and

matrix at 27 GPa. The melts contain numerous tiny spherules of Fe-Ni sulfides (1-10 μm in diameter) and vesicles (~1 μm). The melts are apparently produced from the matrix but are consistently enriched in Na, Ca and S relative to the matrix. The enrichment of Ca and S relative to the meteorite matrix was also observed in the melts produced in shocked Murchison [2]. No melting was observed at 31 GPa.

Impact at 37 and 41 GPa

Chondrules are flattened, with mean aspect ratios of 2.38 (37 GPa) and 2.39 (41 GPa). The degrees of chondrule flattening and preferred orientations are approximately the same as those in the sample shocked at 31 GPa. Most coarse grains of olivine and pyroxene in chondrules are irregularly fractured to subgrains of 1-10 μm in size; fracture density increases with increasing shock pressure. Density of wide (~10 μm), long (100-1000 μm) fractures in matrix also increases with increasing pressure. At 41 GPa, in addition to those wide fractures, narrow (1-10 μm), subparallel fractures form at high densities in matrix in directions roughly perpendicular to the compression axis. The texture closely resembles that produced in Murchison shocked at 25-30 GPa [2]. Local melting occurs as melt veins preferentially along chondrule/matrix boundaries at 37 GPa and as melt veins and pockets at 41 GPa. The volume fraction of melts in the sample shocked at 41 GPa is much larger than that in the sample shocked at 37 GPa.

Impact at 49 GPa

Most chondrules are disrupted. Some chondrules are flattened with a mean aspect ratio of 2.44 but show no preferred orientations. The matrix is almost totally melted. The melts contain much larger vesicles (1-100 μm in diameter) than those in the samples shocked at lower pressures. The overall texture is similar to that of Murchison shocked at 49 GPa.

DISCUSSION

Our experimental study reveals that chondrules are flattened in the plane of the shock front in Allende by shock pressures up to 41 GPa. Chondrules are flattened even at 49 GPa, but most are disrupted. Extensive comminution of matrix begins to occur at 41 GPa. Although local melting occurs at 27 GPa, pervasive melting in matrix does not occur even at 41 GPa. These results are distinctly different from those from the previous experimental study of Murchison [2]. In Murchison, chondrules are flattened at 4 to 30 GPa, but at pressures higher than 30 GPa, they are extensively disrupted. In Murchison, extensive comminution of matrix begins at 25 to 30 GPa, and pervasive melting of matrix begins at ~35 GPa. The results from these studies indicate that shock pressures to produce chondrule disruption, extensive comminution of matrix, and pervasive melting in Allende are approximately 10 to 15 GPa higher than in Murchison. This implies that the shock pressures to cause catastrophic disruption of CV chondrites would be 10 to 15 GPa higher than that of CM chondrites. These experimental results appear to be consistent with the previous petrographic observations that CV chondrites show a wide range of shock stages, from S1 to S4, while most CM chondrites are stage S1 [1].

REFERENCES

[1] Scott, E.R.D., Keil, K. and Stoffler, D. (1992) Geochim. Cosmochim. Acta 56, 4281-4293.

[2] Tomeoka, K., Yamahana, Y. and Sekine, T. (1999) Geochim. Cosmochim. Acta 63, 3683-3703.

[3] Nakamura, T., Tomeoka, K., Sekine, T and Takeda, H. (1995) Meteoritics 30, 344-347.

Thermal metamorphism of CM chondrites from the viewpoint of graphitization of chondritic carbonaceous macromolecular matter.

F. Kitajima, T. Nakamura, N. Takaoka, and T. Murae

Department of Earth and Planetary Sciences, Faculty of Sciences,
Kyushu University, Hakozaki, Fukuoka 812-8581, Japan.

CM chondrites are primitive meteorites that are thought to have been a part of water-bearing hydrated asteroids, formed outer and low-temperature (<500°C) regions in the early solar system. However, dehydration of phyllosilicates in CM chondrites were observed in some Antarctic meteorites (*e. g.* Akai 1988, Tomeoka et al. 1989), suggesting that thermal metamorphism occurred after aqueous alteration in their parent bodies. CM chondrites contain about 2% of carbon mainly as solvent unextractable macromolecular matter, like kerogen or poorly crystalline graphite (*e.g.* Simmonds et al. 1969, Hayatsu et al. 1977, Murae 1995). The interlayer spacing (d_{002}) can be related to the degree of graphitization of this matter (Rietmeijer and Mckinnon 1985). Pyrolysis-GC also can provide information on the degree of graphitization. Poorly graphitized carbon can generate larger amounts and variety of pyrolysis products than highly graphitized matter. In this study, the authors analyzed carbonaceous macromolecular matter of CM and the Allende CV3 chondrites by pyrolysis-GC and estimated their graphitization degrees.

Each powdered sample was wrapped with pyrohoil, and pyrolyzed at 740°C for 3 sec. using Curie-point pyrolyzer (JHP-3, Japan Analytical Industry). Stepwise pyrolysis at 333, 445 and 740 °C was also performed for several samples. The GC column was Neutrabond-5 (30m × 0.25mm i.d.). A-791198, Murray and Cold Vokkeveld are unheated chondrites, although Murray and Cold Vokkeveld were experienced aqueous alteration. A-881458 and Y-793321 were weakly heated, while A-881334, Y-86789, B-7904, Y-86695, and Y-82054 were strongly heated (Akai and Tari 1997, Nakamura et al. 2000). Allende, weakly heated at up to 400°C, was also analyzed for comparison.

Fig. 1 shows some pyrograms at 740°C of the CM chondrites. The observed pyrolyzates from strongly heated chondrites, Y-82054, Y-86695 and A-881334 were quite poor compared with the unheated chondrites (A-791198, Murray and Cold Vokkeveld). The two weakly heated chondrites, A-881458 and Y-793321, gave intermediate amounts of pyrolyzates. Naphthalene was the main product among the pyrolyzates whose retention times were later than 5min. in accord with the previous

reports (*e. g.* Murae et al. 1987, Kitajima and Masuda 1992).

The total peak area of pyrolyzates with a retention time later than 5 minutes (= "$S_{RT>5}$") *vs.* the ratio of peak area of naphthalene to "$S_{RT>5}$" (="$S_N/S_{RT>5}$") is plotted in Fig. 2. In this pyrolytic "graphitization" diagram, strongly heated, or highly graphitized sample will be plotted at the lower left-hand corner. To the contrary, unheated, primitive sample will be distributed over upper right-hand area. Pyrolyzates whose retention times are earlier than 5minutes are excluded, because this fraction can be easily influenced by terrestrial adsorbents on the sample surfaces.

As expectedly, highly graphitized samples; Y-82054, Y-86695 and A-881334 are plotted at the lower left-hand corner, and primitive samples, Y-791198, Murray and Cold Vokkeveld are distributed over upper right-hand area. Most samples were plotted on the curve from upper right-hand to lower left-hand suggesting evolutional graphitization lineage. The locations of almost samples are basically consistent with mineralogical and noble gas observations (Nakamura et al. 2000). The locations of Cold Vokkeveld and Allende in the diagram do not conflict with the estimated metamorphic temperature by Rietmeijer and Mckinnon based on d_{002} reflection (1985). B-7904, using a datum of single step pyrolysis, was plotted in the region of weakly heated samples, however, when the datum of stepwise pyrolysis at 740 °C was used, it was plotted at the consistent location with mineralogical observation. Based on this diagram, Y-82054 and Y-86695, both chondrites are strongly heated, were experienced as same metamorphic temperature as that of B-7904; 750-900°C, if differences of duration times and heating mechanisms can be neglected.

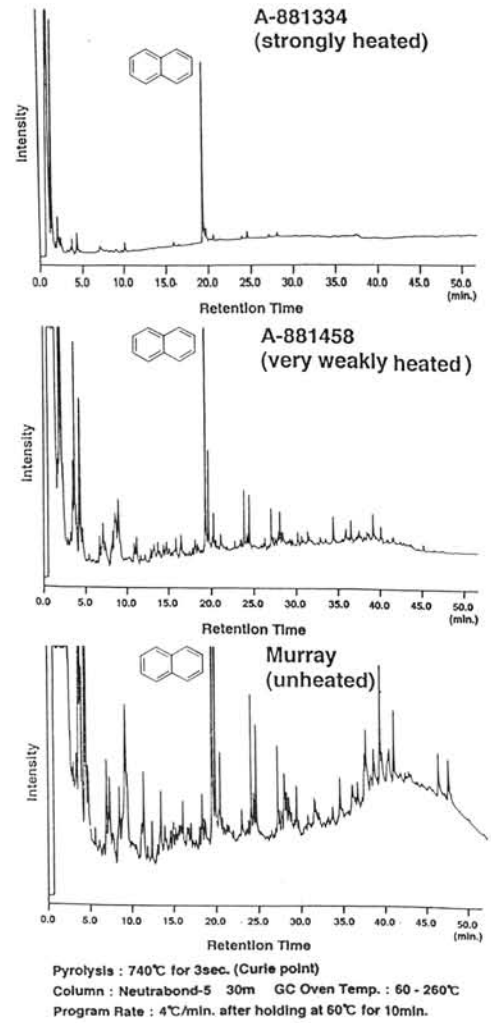

Fig. 1 The pyrograms of A-881334, A-881458 and Murray.

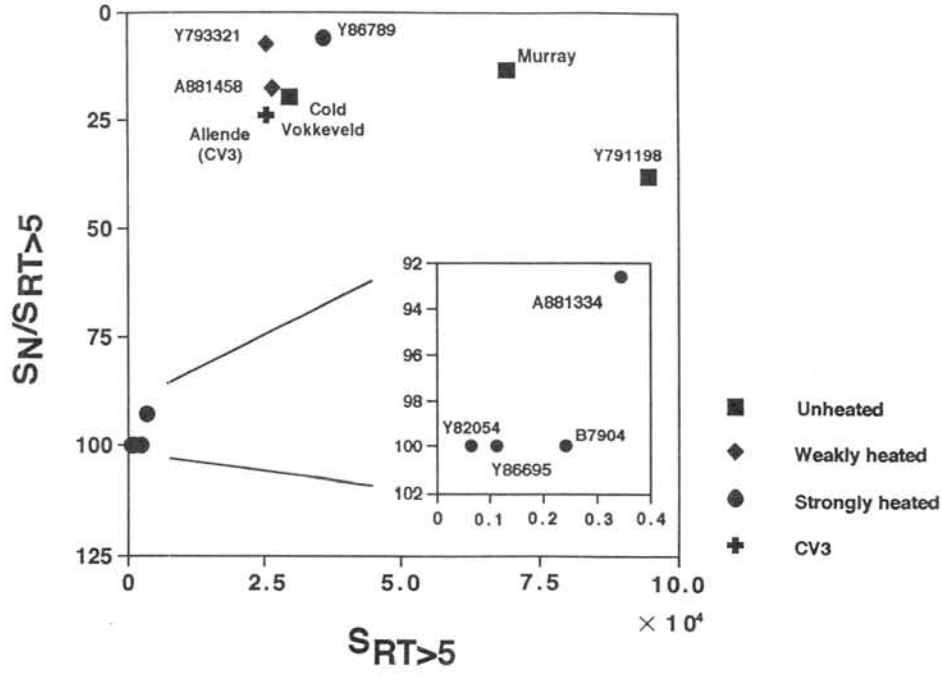

Fig. 2 Pyrolytic "graphitization" diagram.

*1 The data of pyrolysis at 740°C are plotted.
For B-7904 and Y-86789, the data of stepwise pyrolysis at 740°C are used.

*2 The datum of Allende was normalized as it contains 2.0% of carbon.

[References]

Akai J. (1988) *Geochim. Cosmochim. Acta*, **52** 1593-1599.

Akai J. and Tari S. (1997) *LPI Technical Report 97-02 Part I*, 1-2.

Hayatsu R., Matsuoka S., Scott R. G., Studier M. H., and Anders E. (1977) *Geochim. Cosmochim. Acta*, **41** 1325-1339.

Kitajima F. and Masuda A. (1992) *Papers presented on the 17th symposium on Antarctic meteorites*, 65-68.

Murae T. (1995) *J. Anal. Appl. Pyrolysis*, **32** 65-73.

Murae T., Masuda A., and Takahashi T. (1987) *Mem. Natl. Inst. Polar Res., Spec. Issue*, **46** 196-204.

Nakamura T., Kitajima F., and Takaoka N. (2000) *Papers presented on the 25th symposium on Antarctic meteorites.*

Rietmeijer F. J. M., and Mckinnon I. D. R. (1985) *Nature*, **315** 733-736.

Simmonds P. G., Bauman A. J., Bollin E. M., Gelpi E., and Oró J. (1969) *Proc. Nat. Acad. Sci. (USA)*, **64** 1027-1034.

Tomeoka K., Kojima, H., and Yanai, K. (1989) *Proc. NIPR symp. Antarct. Meteorites*, **2** 55-74.

Nitrogen and Rare Gases in CO Chondrites

Kaoru Kiyota, Naoji Sugiura and Shigeo Zashu
Department of Earth and Planetary Science, Univ. of Tokyo, Tokyo 113-0033, Japan

CO chondrites release isotopically light nitrogen [1]. The release profiles of N are similar to that of ALHA77214 by a stepped combustion method. ALHA77214 is a UOC and some UOCs also have similar release profiles of N, though some UOCs have different release profiles of N and ^{36}Ar[2].

We have measured N, Ne and Ar of bulk samples of four CO chondrites (Yamato 82094, Yamato791717, Yamato 790992 and ALH 77003) and one acid residue of CO chondrite (Yamato 791717) by a stepped combustion method. The temperature of combustion was from 200°C to 1200°C. The acid treatment was performed 7 days with 5N-HCl. The release profiles of N and trapped ^{36}Ar of Yamato791717 are shown in Fig. 1. Acid treatment removed about 80% of trapped ^{36}Ar and about 90% of light N of Yamato791717. The result is consistent with that of [3]. Therefore, the light N and trapped ^{36}Ar from the acid residue are possibly due to Q-phase and presolar diamond. The release profiles of N and ^{36}Ar of the bulk and the acid residue are similar to those of bulks and acid residues of ALHA77214 type UOCs. It can be concluded that carriers of light N and trapped ^{36}Ar in CO chondrites and ALHA77214 type UOCs are the same. The major carriers of light N are ambiguous because they are resolved by the acid. One candidate is solar component. Measurement of N isotopic ratio of lunar soil by SIMS has revealed light N component of solar wind [4]. A lunar rock sample releases light N bimodally by a stepped combustion [5]. Since solar wind is located at the thin surface layer, acid treatment removes the solar wind component easily. Detailed study is needed to identify the component of the acid soluble light N.

References

[1] Newton J. (1994) Doctor Thesis.
[2] Sugiura N., Kiyota K. and Hashizume K. (1998) Meteorit. Planet. Sci. **33**, 463-482.
[3] Taniguchi Y. and Hashizume K. (1997) Antarctic Meteorites XXII, 188-190.
[4] Hashizume K. Chaussidon M. and Marty B. (2000) LPS XXXI.
[5] Brilliant D. R. Franchi I. A. and Pillinger C. T. (1994) Meteoritics **29**, 718-723.

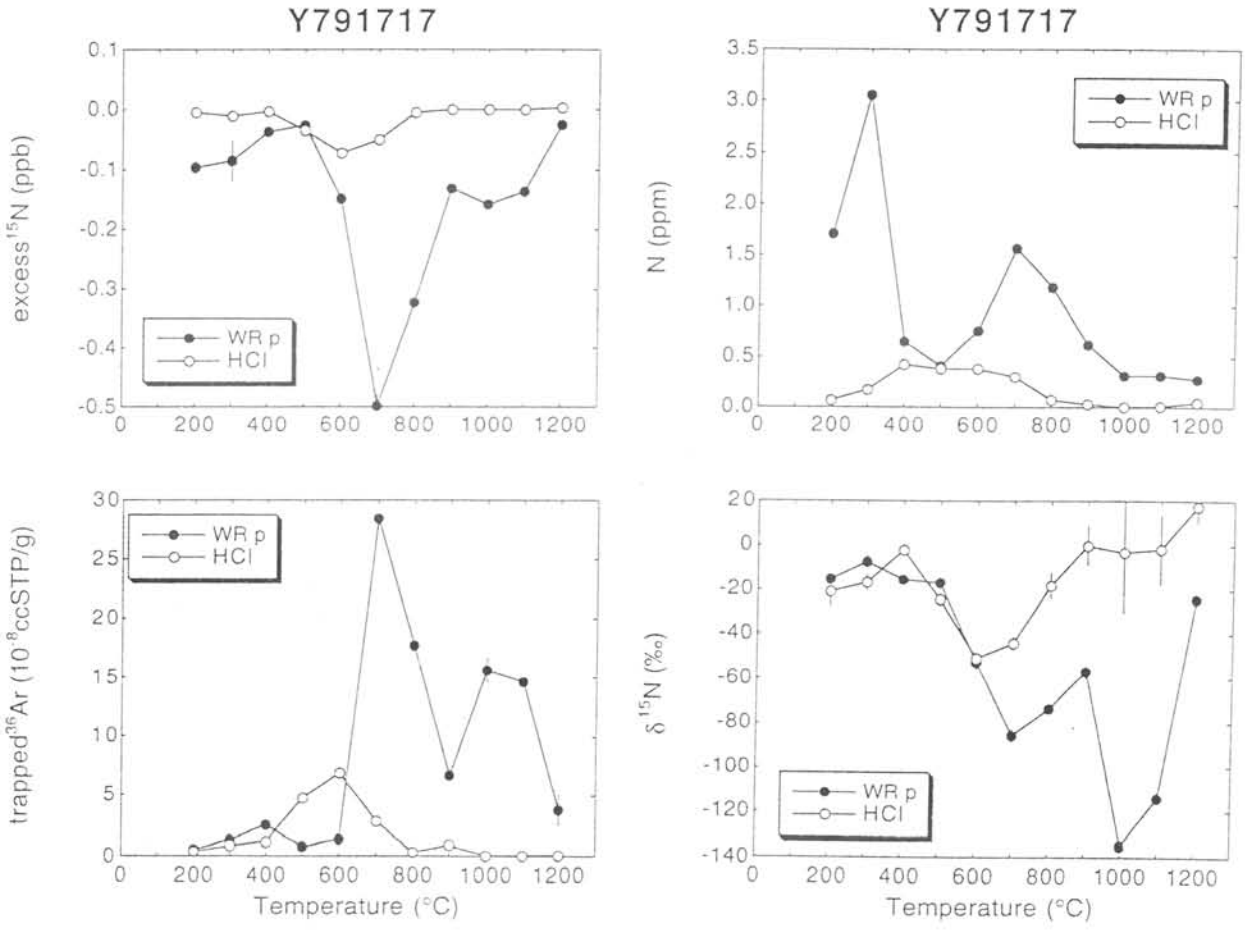

Fig. 1 Stepped combustion results of Yamato791717. The difinition of excess^{15}N is

excess^{15}N = d^{15}N x (^{15}N/^{14}N)air x [N]

where (^{15}N/^{14}N)air is N isotopic ratio of air and [N] is N abundance. Bulk sample releases light N and trapped ^{36}Ar bimodally and most of them are removed by the acid treatment.

Direct observation of evaporation and condensation from Silicate melts

Hidekazu Kobatake[1], Katsuo Tsukamoto[1], Hisayoshi Yurimoto[2], Chihiro Kaito[3] and Etsuro Yokoyama[4]

1) Tohoku Univ. 2) Tokyo Institute of technology 3) Ritsumeikan Univ.

4) Yamaguchi Univ.

1. Introduction

Although the kinetics of evaporation and condensation of cosmic materials in pre-solar nebular is the key to understand the dynamic environment during the formation of solar system, there are not so many experimental studies on this process. This is because of the difficulties in the measurement of parameters related to crystallization process of these cosmic materials in such an extreme condition. It was therefore aimed to visualize the evaporation process from high temperature melt and condensation of these gases to ultra-fine particles. This in situ experiment would become possible if we employed newly developed interferometry.

2. Experimental

Spheres of silica glass and forsterite glass with the diameter of few mm were held on a Ni holder. These spheres were heated by CO_2 laser (100W) to form melt droplets. Before and after the melting process, Mach-Zhender interferometry using He-Ne laser was applied to the environment around the melt sphere, so that one can visualize the difference of the refractive index, which can later be transformed to the concentration and the temperature distribution around the melt sphere.

Our advanced interferometry is capable of resolving the difference of 10^{-8} of refractive index, which corresponds to the concentration difference $10^{-7}g/cm^3$. The maximal frame rate in TV recording is 10,000 frame / sec.

Since this study was in a preliminary stage, experiments were done in normal atmosphere. In order to suppress both thermal and the concentration

convection, the experiments were done also in microgravity. This is because the convection plays an important role not only on the thermal environment but also on the nucleation kinetics as was reported before.

Since refractive index is a function of gas molecule density, the concentration of gas can be calculated from the measurement of the refractivity of the gas. Mach-Zhender interferometer was used for visualizing the thermal and concentration distribution around the gas-liquid interface.

In microgravity, the spheres were fixed by Pt wire and evaporated by CO_2 laser ablation. Condensation products from the evaporated gas were collected on a Cu mesh for TEM and compared with those condensed in gravity.

3. Result and discussion

Fo and SiO_2 glass were used for this experiment. Fig.1 shows an example of the Mach-Zehinder interferogram during heating. The displacement of the interference fringes to the neighboring fringes corresponds to the optical path of a half of wavelength of He-Ne laser (633nm). Fig.2 shows an image-processed image from the original interferograms recorded in a digital video recorder. The evaporation from the melt sphere can be visible, which indicates enough sensitivity of the interferogram to measure the concentration of the gas. It may be important to note that the same method can be applied also to measure the equilibrium gas concentration at various temperatures.

Condensation products of CAI and En composition materials from the evaporated gas were sampled with the help of a tiny vacuum tweezers. This sampling was done also in microgravity. The collected fine particles are shown in Fig.3, where the fine particles were directly sampled onto a copper mesh for transmission electron microscopy (TEM), which were followed by the characterization by TEM.

In microgravity, condensation products were enriched in Al_2O_3 and alumina-silicates and well crystallized, whereas those products in gravity were enriched in SiO_2 and amorphous. These differences can be discussed based on the difference of heat and mass transport between in gravity and in microgravity.

a) b)

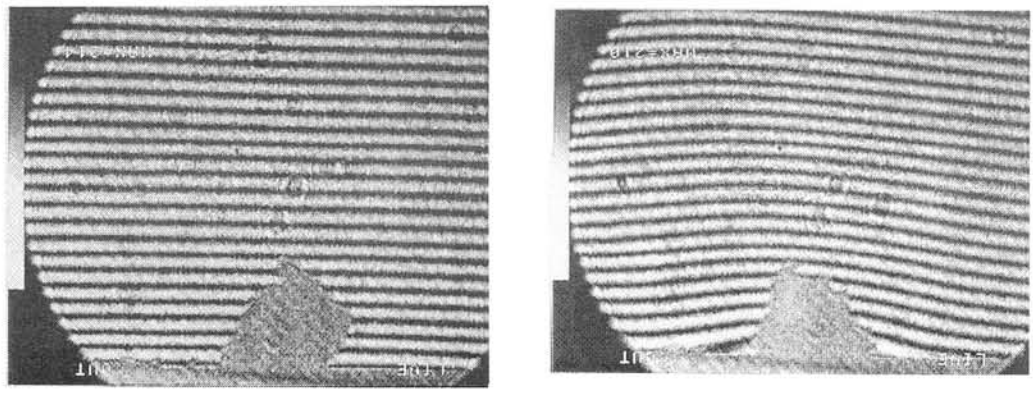

Fig.1 Mach-Zehinder interferogram of the gas around forsterite. a) The interferogram shows parallel straight line (fringe) before heating. Line. b) Forsterite was heated by CO_2 laser in the air. The fringe is deformed by the change of the refractive index of the gas surrounding the forsterite.

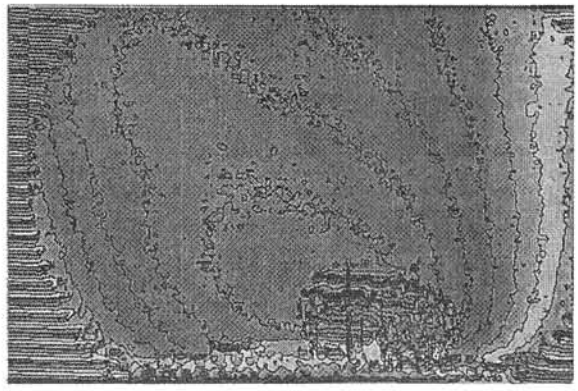

Fig.2 An image-processed image from the original interferograms recorded in a digital video recorder. The difference of refractive index is shown.

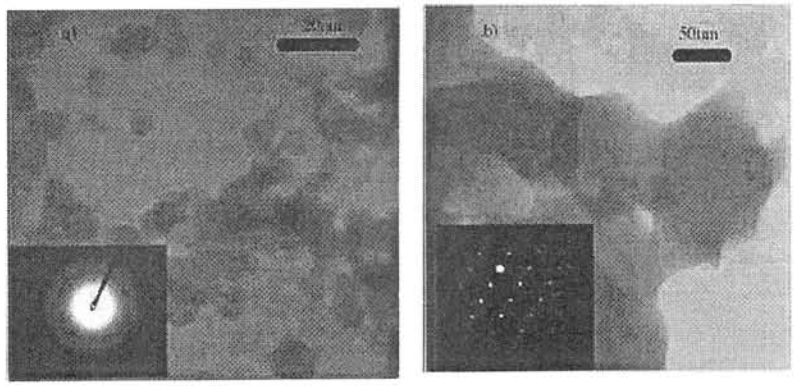

Fig.3 TEM images and diffraction patterns of condensed particles. a) These particles were condensed in microgravity. Each size of particle is about 100nm. These condensed particles are well crystallized. b) These particles are condensed in gravity. The size of particle is about 20 – 30 nm. These particles are amorphous

The mineral assemblage of symplectites in lunar meteorite Asuka-881757

[1]Yumiko Kobayashi and [2]Takanobu Oba

[1]ISO system Company, 942-0051 Joetsu, Japan

[2]Department of Geosciences, Joetsu University of Education, 943-8512 Joetsu, Japan

Abstract

Asuka-881757 is different from other known lunar meteorites. It retained the original diabase-gabbro textures. Most ilmenites, troitites and some Fe-Ni metals are surrounded by symplectite. Symplectite consists very fine-grained Fe-rich olivine (Fa: 93), Ca-poor pyroxene, plagioclase (An 90~An96) and silica phase. The coexisting fayalite and silica phase indicate that the pressure of crystalization of fayalite and silica phase is below 1.95 GPa at 1200°C.

Introduction

Yanai and Kojima (1991) reported that symplectite is one of the most characteristic features of the Asuka-31 (official name: Asuka-881757). They described that symplectite is composed mainly of very fine-grained olivine, pyroxene,apatite, plagioclase, Fe-Ni metal (?) and silica phase (quartz?). The olivine is Fe-rich, ranging from $Fa_{86.6}$ to $Fa_{94.6}$. We observed the coexisting silica phase and fayalite in the symplectite as reaction rim of troilite and pyroxene.

Bowen and Schairer (1935) reported that ferrosilite decomposed fayarite and quartz at low pressure. Lindsley et al. (1964) investigated that ferrosilite is stabe at temperatures between 1150°C and 1400°C and 18 and 45 kbar, respectively. Ferrosilite has been synthesized by Akimoto et al. (1964, 1965) under pressure-temperature conditions range from 12 to 73 kbar and 620°C to 1270°C. They decided the equation for the boundary curve of fayalite + quartz = ferrosilite.

Therefore, we attempt to estimate the presure limit of the reaction between fayalite and silica phase.

Petrography

Asuka-881757 is a coarse-grained and unbrecciated rock, consisting mainly of pyroxene (60%) and maskelynite plagioclase (30%) with small amounts of ilmenite and troilite, and traces of olivine, apatite, silica phase and Ni-Fe metal.

Pyroxene occurs as subhedral crystals showing wavy extinction. The chemical composition of the pyroxene is heterogeneous, ranging from $Wo_{20.2}En_{17.0}Fs_{62.8}$ to $Wo_{37.5}En_{13.5}Fs_{49.1}$. Yanai

and Kojima (1991) reported that the composition of the pyroxene is heteogeneous, ranging from $En_{7.8}$ to $En_{43.6}$, $Fs_{30.7}$ to $Fs_{68.2}$, $Wo_{11.6}$ to $Wo_{40.9}$. Plagioclase is completely maskelynitized, its composition is ranging from An_{90} to An_{96}. Symplectite is observed the boundary of pyroxene and troilite or Fe metal. Olivine, Ca-rich pyroxene and silica mineral crystallized by the reaction.

Discussion

Maskelynite and Pyroxene with wavy extinction suggest that the symplectite was formed under relatively extreme temperature and pressures such as the meteorite impacts. Ca-poor pyroxene has reacted with troilite to form the Fe-rich olivine (fayalite) - silica phase - Fe metal symplectite. The corresponding chemical reaction is given by the equation:

$$2Fe_2Si_2O_6 + 2FeS = 3Fe_2SiO_4 + SiO_2 + 2S.$$

Ferrosilite is not stable at low pressure, it is stable at high pressure. Lindsley et al. (1964) investigated in the experiment that ferrosilite is stabe at temperatures between 1150°C and 1400°C and 18 and 45 kbar, respectively. Akimoto et al. (1964, 1965) reported the boundary curve for the reaction: $1/2(Fe_2SiO_4) + 1/2SiO_2 = FeSiO_3$ under pressure-temperature conditions range from 12 to 73 kbar and 620°C to 1270°C. The equation for the curve is:

$$P_{kbars} = 2.7 + 0.014T(°C).$$

Troilite does not break down completely in Asuka-881757. This fact indicates that the maximum temperature is not over 1200°C (Kullerud, 1967). At 1200°C the pressure estimated by the equation (Akimoto et al. 1965) is 1.95 GPa. Stöffler et al. (1991) proposed that the peak pressure of the transformation of plagioclase grain to maskelynite is reached about 25 and 34 GPa. Pyroxene with wavy extinction also indicates the shock effects by the impact metamorphism.

In conclusion, the pressure estimated by the coexisting fayalite and silica is lower than that proposed by Stöffler et al. (1991).

Some unique achondrites in the Yamato 98 meteorites

Hideyasu Kojima

Antarctic Meteorite Research Center, National Institute of Polar Research, Kaga 1-chome, Itabashi-ku, Tokyo 173-8515, Japan

Approximately 4100 meteorites have been collected around the Yamato Mountains and the Belgica Mountains (Kojima et al., 1999). They were named and roughly classified after defreezing at NIPR. Total number of meteorites is 4180. 32 of them were named Belgica 98 meteorite and remaining 4148 are Yamato 98 meteorite. They include many kinds of rare meteorites. By the classification at the field, 2 lunar meteorites, 3 irons, 4 stony irons, 15 ureilites, 37 diogenites, 63 eucrites, 29 unclassified achondrites and 160 carbonaceous chondrites were distinguished.

Lunar meteorite: Yamato 981031 is classified into lunar meteorite. It is 185.8 g in weight and 6.9x4.6x3.8 cm in size. This rock has some thin, yellow-green fusion crust. This color of fusion crust is one of the features of the lunar highland rocks. A thin section (15 mm width) shows a polimict regolith breccia with feldspar rich lithic and mineral clasts set in a dark matrix. Glass spherules and glass fragments are also observed. Microprobe analyses show that the pyroxene ranges En63.1Fs30.4Wo6.5 to En18.7Fs55.1Wo26.2. Plagioclase composition is An97.4-85.4 with one albite rich one (Ab46.7). Olivine ranges Fo68.7-59.2. The FeO: MnO ratio of pyroxenes is high, 82.1-40.3 characteristic of lunar material. It was collected several km west of the Kurakake Nunatak of the Minami-Yamato Nunataks. Estimating from the field number, there is high possibility that Yamato-793274 lunar meteorite also collected near the Minami-Yamato Nunataks. Because meteorite search of JARE 20 has been done near the Minami-Yamato Nunataks on the day when the meteorite was collected. Following is bulk chemical compositions of both two meteorites.

	SiO2	TiO2	Al2O3	Fe2O3	FeO	MnO	MgO	CaO	Na2O	K2O	P2O5	Cr2O3	Total
Y981031	44.88	0.71	18.44	0.00	12.43	0.20	9.42	12.85	0.34	0.04	0.13	0.26	99.70
Y-793274	45.67	0.53	16.73	0.48	13.57	0.09	9.52	12.28	0.42	0.08	0.08	0.15	99.75

(analyzed by Haramura H.)

Two are very similar. The textures of two meteorites are also similar. So it is possible that Y981031 and Y-793274 are pair.

Cumulate eucrite: A thin section of Yamato 980318 shows that it consists of very coarse-grained pyroxene and plagioclase in a subhedral granular texture. This texture indicates that this is a coarse-grained cumulate eucrite. About 30 of this type eucrite were collected in relatively narrow area of southwest of Minami-Yamato Nunataks. These are pair.

MINERALOGY AND PETROGRAPHY OF AMOEBOID OLIVINE AGGREGATES FROM THE REDUCED CV CHONDRITES EFREMOVKA, LEOVILLE AND VIGARANO

Mutsumi Komatsu[1], Alexander N. Krot[1], Alexander A. Ulyanov[2],
Klaus Keil[1], and Masamichi Miyamoto[3]
[1]Hawai'i Institute of Geophysics & Planetology, School of Ocean & Earth Science & Technology, University of Hawai'i at Manoa, Honolulu, HI 96822, USA
[2]M. V. Lomonosov Moscow State University, Moscow 117999, Russia
[3]Department of Earth & Planetary Science, Graduate School of Science, University of Tokyo

Abstract

Amoeboid Olivine Aggregates (AOAs) in the reduced CV chondrites Leoville, Vigarano and Efremovka consist of fine-grained (1-10 μm) forsteritic olivine and abundant, small (<250 μm) Al-diopside-spinel-anorthite refractory inclusions. The AOAs experienced variable degrees of secondary alteration, which is generally much less extensive than that experienced by AOAs in the oxidized CV chondrites Allende and Mokoia. The alteration resulted only in partial replacement of anorthite by Na-bearing phases (nepheline and sodalite) and small enrichment of spinel and olivine in FeO. None of the AOAs studied shows mineralogical evidence for extensive melting, which suggests that they were absent in a chondrule-forming region(s). At the same time, AOAs and olivine-rich anorthite-bearing chondrules contain mineralogically very similar refractory inclusions possibly indicating a genetic relationship between these objects.

Introduction

Amoeboid olivine aggregates (AOAs) are irregularly shaped, mm to cm sized objects composed of olivine and primary refractory minerals such as spinel, Al-diopside, melilite, perovskite, and anorthite [1-6]. Mineralogical studies of AOAs from the oxidized CV chondrites Allende and Mokoia showed that these objects experienced variable degrees of late-stage alteration resulting in replacement of their primary minerals by secondary nepheline, sodalite, hedenbergitic pyroxenes, andradite, fayalitic olivine, and phyllosilicates [3, 4]. In order to characterize primary mineralogy of AOAs and understand their thermal and alteration history and possible relationship between AOAs, CAIs and Al-rich chondrules, we studied AOAs from the reduced CV chondrites (Efremovka, Leoville and Vigarano), which are less altered than the Allende-like CV chondrites [7].

Analytical Procedures

Polished thin sections of CV chondrites Efremovka *3-7-2*, *5-b*, *8-7-22*, Vigarano *UH-35*, *-65*, *USNM6295*, and Leoville *UH122*, *-2*, *-3* were studied in reflected and transmitted light using optical microscopy and X-ray mapped in Ca, Al, Mg, Ti and Na Kα with resolution of 5-10 μm (2 μm for individual AOAs) using the Cameca SX-50 electron microprobe at University of Hawai'i. Backscattered electron (BSE) images of 5-10 AOAs in each of the meteorites were obtained using the Zeiss DSM-962 scanning electron microscope (SEM) and Hitachi S-800 Field-Emission SEM. Mineral compositions were analyzed using SX-50.

Results

Amoeboid Olivine Aggregates (AOAs)

AOAs from the reduced CV chondrites consist of fine grained (5-20 μm) forsteric olivines and variable abundances of refractory inclusions (1-250 μm in apparent diameter) composed largely of spinel, Al-diopside and anorthite (Figs. 1, 2, 3). The olivines show smaller compositional variations (Fa_{1-10}) than those in the Allende AOAs (Fa_{1-35}) with peaks at ~Fa_{1-4} (Fig. 1), which is consistent with the more primitive nature of the reduced CVs [7]. Olivine grains in some of the AOAs form aggregates with 120° triple junctions possibly indicating an annealing episode. Most of the AOAs studied show no clear textural evidence for melting. However, in some AOAs, olivine grains are overgrown by Al-diopside, possibly suggesting small degree of melting.

Refractory inclusions in the AOAs are typically mineralogically zoned with cores composed of spinel, anorthite and Al-Ti-diopside and rims composed of Al-diopside (Fig. 2,4). The Al-diopsides show significant compositional variations (1-20 wt% Al_2O_3; 0.1-3.5 wt% TiO_2). Most spinel and anorthite grains are too fine-grained to be analyzed by EPMA. The inclusions show variable degrees of alteration, which largely affected anorthite and spinel and resulted in partial-to-complete replacement of anorthite

by Na-bearing phases, nepheline and sodalite, and enrichment of spinel in FeO. The degree of alteration appears to increase from Leoville to Vigarano to Efremovka. Hedenbergite, wollastonite, and phyllosilicates have not been observed in any of the AOAs studied.

Anorthite-rich chondrules (ARCs)

The reduced CV chondrites commonly contain magnesian chondrules with crystalline An-rich plagioclase. These chondrules are texturally and mineralogically similar to plagioclase olivine inclusions described by Sheng *el al.* [8] in Allende. The An-rich chondrules (ARCs) consist of relatively coarse-grained forsteritic olivine (Fa_{1-5}), igneously-zoned pyroxenes with low-Ca pyroxene ($Fs_{1-3}Wo_{1-2}$; 2-4 wt% Al_2O_3) cores and high-Ca pyroxene ($Fs_{1-2}Wo_{40}$; 1-3 wt% TiO_2, Al_2O_3) rims, lath-shaped anorthitic plagioclase (An_{80-90}) and rounded metal-sulfide nodules (Fig. 3). Plagioclase grains show variable degrees of replacement by nepheline. CAIs associated with these chondrules are mineralogically similar to those in the AOAs described above and consist of spinel, Al-diopside and anorthite (Figs. 3, 4).

Discussion

Our mineralogical observations indicate that AOAs in the reduced CV chondrites Efremovka, Leoville and Vigarano experienced significantly lower degrees of alteration than those in the oxidized CV chondrites Allende and Mokoia. It appears that Efremovka is the most altered, whereas Leoville is the least altered meteorite among the reduced CVs. Mineralogy and petrography of the AOAs are consistent with being aggregates of nebular condensates [1-6]. Although some of the studied AOAs may have experienced high-temperature annealing and small degree of melting, there is no clear mineralogical evidence for their extensive melting. We infer that these AOAs were largely absent from a chondrule-forming region(s); they were either removed prior to chondrule formation or formed in different regions. At the same time, the AOAs and ARCs contain mineralogically very similar refractory inclusions possibly indicating genetic relationship between these objects. In order to understand genetic relationship between AOAs, ARCs and associated with them CAIs, we are currently analyzing bulk compositions of these objects.

References: [1] Grossman L. and Steele I. M. (1976) *Geochim. Cosmochim Acta* **40**, 149-155; [2] Grossman et al. (1979) *Geochim. Cosmochim Acta* **43**, 817-829; [3] Hashimoto A. and Grossman L. (1987) *Geochim. Cosmochim Acta* **51**, 1685-1704; [4] Cohen et al. (1983) *Geochim. Cosmochim Acta* **47**, 1739-1757; [5] Rubin A. E. (1998) *Meteor. Planet. Sci.* **33**, 385-391; [6] Bar-Matthews et al. (1979) *Meteoritics* **14**, 342; [7] Krot et al. (1995) *Meteoritics* **30**, 748-775. [8] Sheng et al. (1991) *Geochim. Cosmochim Acta* **55**, 581-599.

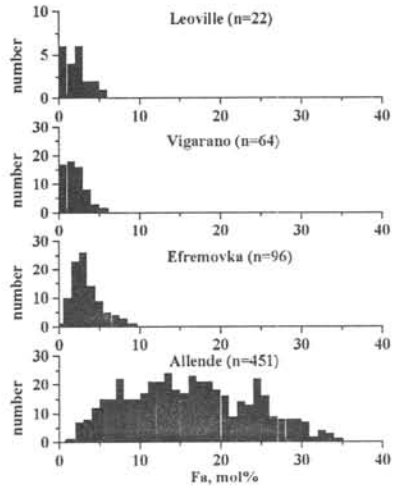

Fig. 1. Histograms of olivine compositions in amoeboid olivine aggregates from the reduced CV chondrites Efremovka, Leoville and Vigarano [this study] and oxidized CV chondrite Allende [1].

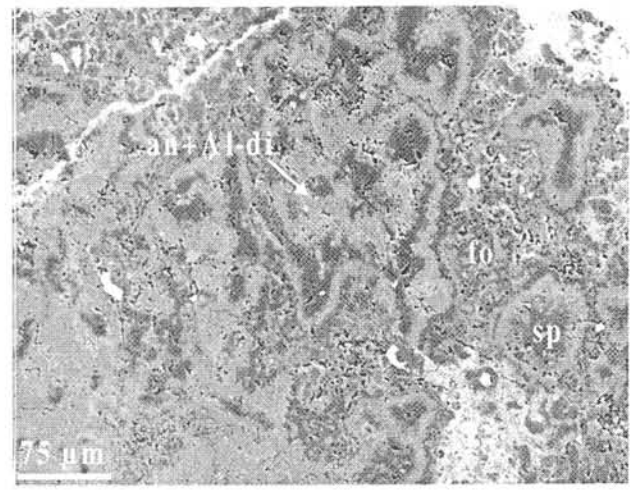

Fig.2. BSE image of an amoeboid olivine aggregate from Efremovka. It consists of forsteritic olivine (fo) and refractory inclusions composed of spinel (sp) cores surrounded by anorthite (an) and Al-diopside (Al-di).

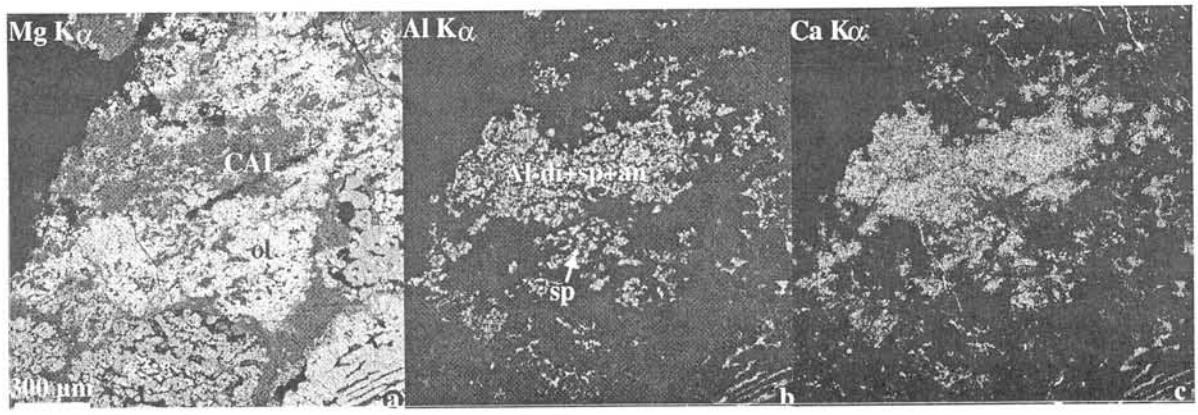

Fig. 3. X-ray elemental maps in Mg (a), Al (b) and Ca Kα (c) of an amoeboid olivine aggregate from Efremovka. The aggregate consists of forsteritic olivine (ol) and contains abundant CAIs composed of anorthite (an), Al-diopside (Al-di) and spinel (sp).

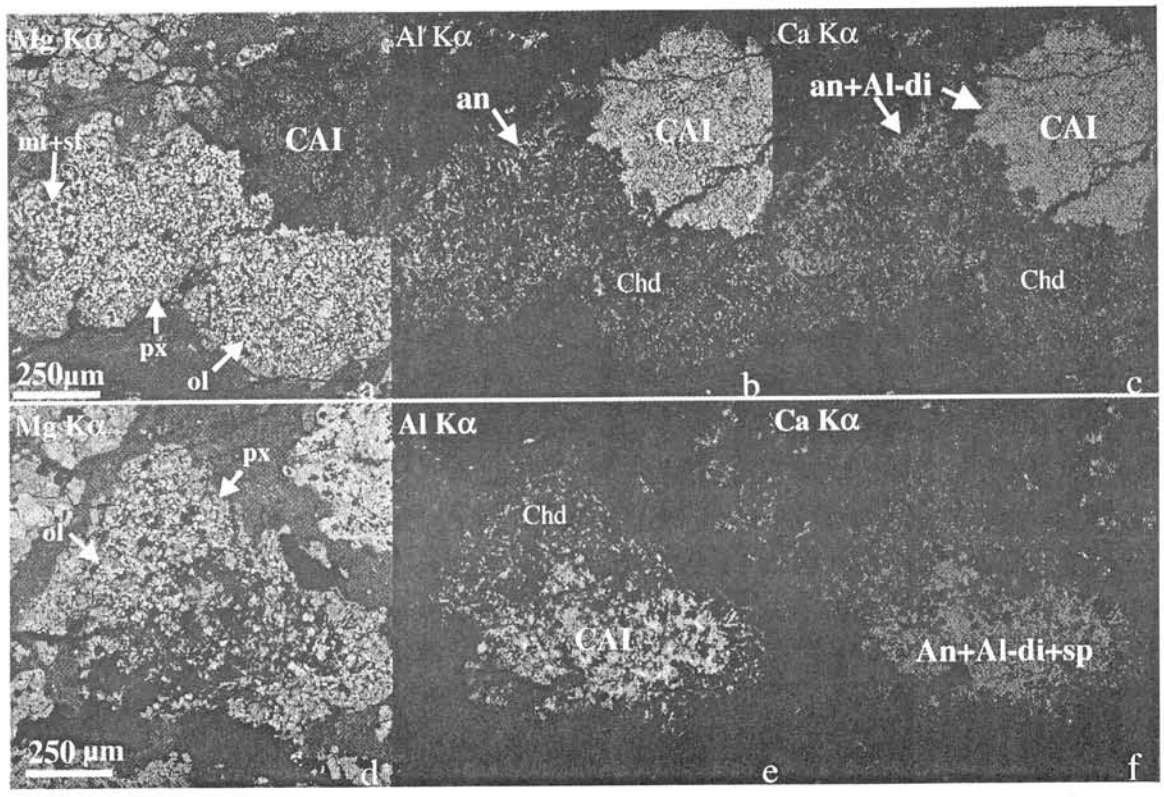

Fig. 4. X-ray elemental maps Mg (a,d), Al (b,e) and Ca (c, f) of the anorthite-rich chondrules (ARC) with spinel-anorthite-Al-diopside refractory inclusions from Leoville. The CAIs are mineralogically similar to those inside AOAs and consist of anothite (partly replaced by nepheline), spinel and Al-diopside. In contrast to AOAs, the chondrules contain igneously-zoned pyroxene grains with low-Ca pyroxene cores and high-Ca pyroxene rims, lath-shaped anorthite crystals and abundant metal-sulfide nodules suggesting crystallization from melts. an - anorthite, cpx - Al-diopside, px - low-Ca pyroxene, sp - spinel, ol - forsteritic olivine, mt - metal, sf - sulfide, chd - chondrule, CAI - Ca, Al-rich inclusion.

Cosmogenic Nuclides in Kobe Meteorite fell on Sep. 26th, 1999

Kazuhisa. KOMURA[*1], Mutsuo. INOUE[*1]and Noboru. NAKAMURA[*2]

[*1] Level Radioactivity Laboratory, Kanazawa University.,Wake, Tatsunokuchi, Ishikawa 923-1224, Japan

[*2]Faculty of Science, Kobe University, Rokko-dai, Nada, Kobe 657-0013, Japan

On September 26th (20:25 local time), 1999, a small meteorite fell into the room through roof tile of a house located in Kita-ku, Kobe, Hyogo Prefecture, Japan. More than 20 fragments were collected in the room. The meteorite samples were brought to Scientific Crime Institute of Hyogo Prefectural Police (SCI). Each fragments were photographed, weighed and some of large fragments were subjected to X-ray fluorescence analysis to determine bulk chemical composition. Immediately after the general inspection at SCI, largest fragment (62g) was brought to Ogoya Underground Laboratory locating some 200km NE direction from Kobe to measure radionuclides induced by cosmic-ray interaction with meteorite.

The meteorite sample was measured non-destructively by using low background Ge detector installed in a underground laboratory of Low Level Radioactivity Laboratory of Kanazawa University constructed in a tunnel (270mwe depth) of former Ogoya Copper. The detecor used is 93.5% coaxial type Ge with 93.5% of relative efficiency and 2.0 keV of resolution at 1.33 MeV. Gamma-ray measurement was started on 17:25 of Septermber 27th (21 hour after fall) and stopped on Oct. 1st 7:06. Gamma ray spectrum was recorded several times a day to search gamma-ray peaks from short lived radionuclides.

Gamma-ray spectra of region of interest are shown in Fig. 1. Despite rather short counting time (5090min), more than 20 cosmogenic nuclides such as Na-24 (T1/2=15h), Mg-28 (20.9h), K-43 (22.3h), Ni-57 (1.58d), Sc-48 (1.82d), Sc-44m (2,44d), Sc-47 (3.35d), Mn-52 (5.59d), Ni-56 (5.5d), V-48 (16.8d), Cr-51 (27.8d), Be-7 (53.3d), Co-58 (70.8d), Co-56 (77.3d), Sc-46 (83.8d), Co-57 (272d), Mn-54 (312d), Na-22 (2.60y), Co-60 (5.26y), Ti-44 (49y) and Al-26 (7.2×10^5y) were detected, though only a few counts were observed for some nuclides. Among these, detection of Mg-28, K-43, Ni-57, Sc-47 are considered to be first in meteorite. Very low Co-60 activity showed that pre-atmospheric size of the meteorite was small.

Concentrations of cosmogenic nuclides will be discussed with those of recently fallen meteorites [Neagari Meteorite (fell 18th Feb., 1995) and Tsukuba Meteorite (fell 8th Jan., 1996)] particularly emphasis on 11 year of solar cycle.

The authors express their deep thanks to R. Hirata who kindly lent us meteorite sample.

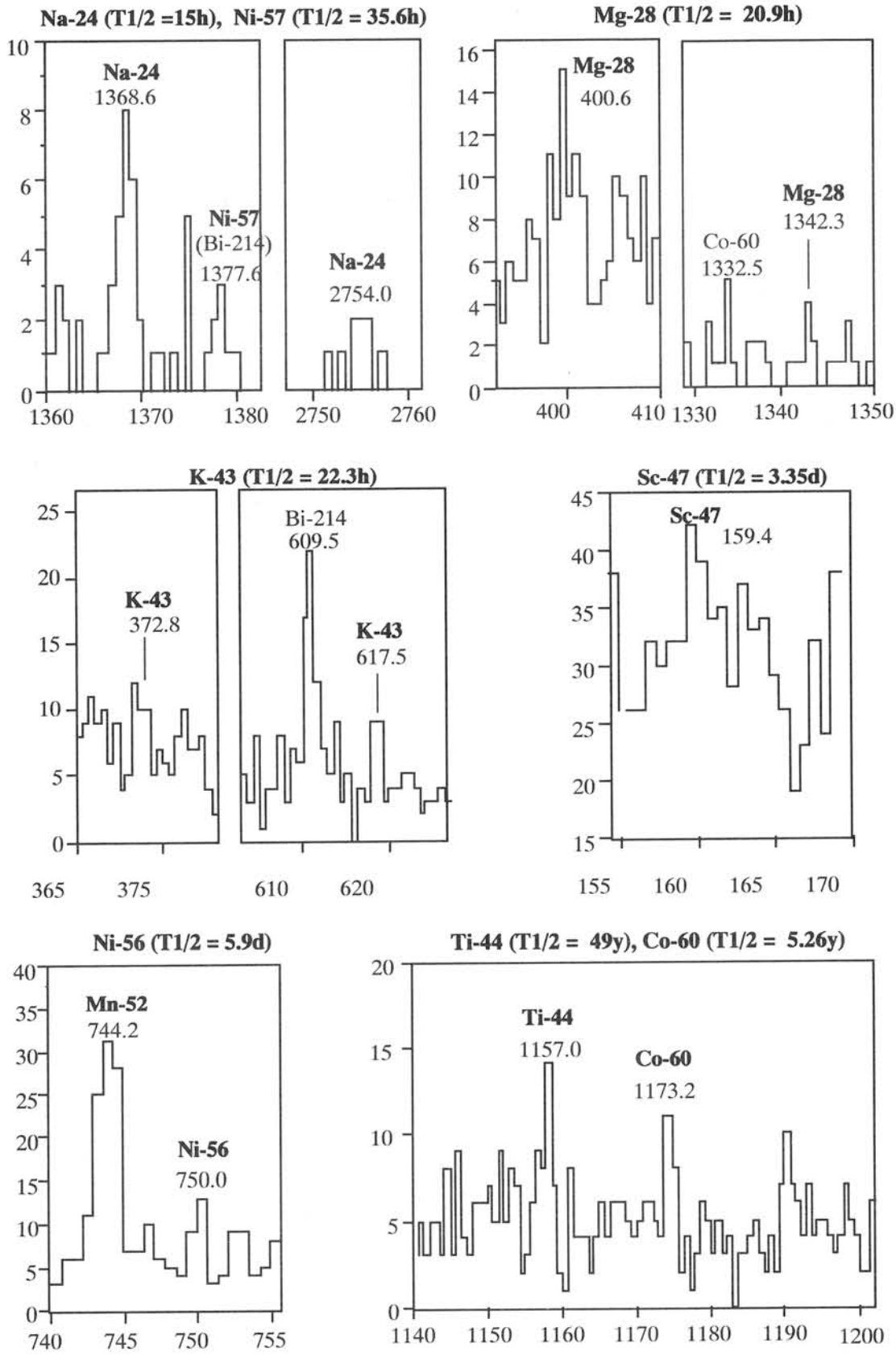

Fig 1 Region of interest in the spectrum of Kobe Meteorite

TWO STAGES OF ASTEROIDAL ALTERATION RECORDED IN RIMMED ALLENDE DARK INCLUSIONS: EVIDENCE FROM MINERALOGY AND OXYGEN ISOTOPE COMPOSITIONS

Alexander N. Krot[1], Hajime Hiyagon[2], Mikhail I. Petaev[3], Anders Meibom[4], and Klaus Keil[1] [1]Hawai'i Institute of Geophysics & Planetology, School of Ocean & Earth Science & Technology, University of Hawai'i at Manoa, Honolulu, HI 96822, USA; [2]University of Tokyo, Dept. of Geophysics & Planetary Physics, Tokyo, Japan; [3]Harvard-Smithsonian Center for Astrophysics, Cambridge MA 02138, USA; [4]Geological & Environmental Sciences, Stanford University, CA 94305, USA.

Introduction. Dark inclusions in the Allende meteorite are lithic chondritic clasts which are genetically related to the oxidized CV chondrites of the Allende-like subgroup; both have similar alteration features, chemical and oxygen-isotopic compositions [1-6]. The most heavily-altered inclusions, containing partially-to-completely pseudomorphed chondrules, are surrounded by Ca-Fe-silicate rims composed of salite-hedenbergite pyroxenes, wollastonite, andradite, and kirschsteinite [5]. These rims are texturally and mineralogically similar to the outermost Ca-Fe-rich rims around altered Allende CAIs [7]. Largely based on these similarities, it was concluded that Ca-Fe-rich rims around dark inclusions formed by direct condensation of the Ca-Fe-rich minerals from highly-oxidized nebular gas produced by evaporation of nebular regions with enhanced ($>10^4$ x solar) dust/gas ratio [2]. Kurat with coworkers [4] inferred that the rimmed Allende dark inclusion (All-AF) was broken off a larger piece of rock and that Ca-Fe-rich rim formed by reactions between the vapors from inside the inclusion with the hot ambient nebular gas. Contrary to the nebular models, other researchers [3, 5, 6, 8] suggested that Allende dark inclusions experienced relatively low temperature alteration in an asteroidal environment. In order to understand location (nebula *vs.* asteroid) and conditions (high-temperature *vs.* low-temperature) of the alteration, we studied mineralogy (SEM, EPMA) and oxygen-isotope compositions (ion microprobe) of five heavily-altered, rimmed Allende dark inclusions.

Mineralogy and Petrography. The Allende dark inclusions *3529, 4301-2, IV-1, 3b-1,* and *IVa* consist exclusively of secondary minerals: fayalitic olivine (Fa_{40-45}), salitic pyroxenes ($Fs_{10-30}Wo_{50}$), andradite, nepheline, sodalite, and Fe,Ni-sulfides. Chondrules in these inclusions are completely pseudomorphed by fayalitic olivine and nepheline; rare incompletely pseudomorphed chondrules and isolated olivine grains occur in *3529.* The chondrule pseudomorphs in *3529, 4301-2,* and *IVa* are surrounded by salitic pyroxene and Fe,Ni-sulfide rims, which are commonly interconnected (Figs. 1a,d). Matrices and chondrule pseudomorphs of these inclusions are crosscut by multiple veins which are composed of salitic pyroxenes and Fe,Ni-sulfides; the veins do not extend into the Allende host. There are progressive depletions in Ca of the inclusion matrices from *3529* to *4301-2* to *IV-1* to *3b-1* to *IVa* (Fig. 1).

All five inclusions are surrounded by continuous Ca-rich rims which have variable widths and show roughly symmetric mineralogic zoning (Fig. 2). The innermost zone consists of diopside-salitic pyroxenes (~$Fs_{10-15}Wo_{48-50}$). The central zone is composed of hedenbergite ($Fs_{48-50}Wo_{48-50}$), wollastonite, andradite, and rare kirschsteinite. The outermost zone consists of salite-hedenbergitic pyroxenes ($Fs_{15-35}Wo_{48-50}$). The rims are commonly intergrown with the Allende matrix olivines and enclose isolated forsteritic olivines, chondrule fragments and regions of fine-grained matrix which are texturally and mineralogically similar to those of the Allende matrix. Fayalitic olivines in the central portions of the dark inclusions on average are less Fe-rich ($Fa_{41\pm1}$, n=23) than those in their outer zones ($Fa_{44\pm1}$, n=19) and in the Allende matrix near Ca-rich rims ($Fa_{47\pm1}$, n=13). Abundant concentrically-zoned objects composed of andradite-wollastonite cores and salite-hedenbergitic pyroxene rims, are observed in the Allende matrix near the Ca-rich rims. These objects are commonly intergrown with chondrule fragments and fayalitic olivine of the Allende matrix.

Oxygen-isotopes. Oxygen-isotope compositions of Ca-Fe-rich silicates from two analyzed inclusions, *IV-1* and *3529,* are listed in Table 1 and plotted in Fig. 3. In *IV-1,* only rim andradite, wollastonite and salite-hedenbergitic pyroxenes were analyzed. In *3529,* only salite-hedenbergitic pyroxene-andradite objects in the matrix were analyzed. Calcium-iron-rich pyroxene-andradite objects in the *IV-1* matrix and the *3529* rim silicates are too porous and fine-grained for ion microprobe study. The *IV-1* rim silicates show relatively small range in $\delta^{18}O$ and plot near terrestrial fractionation (TF) line ($-3‰ < \Delta^{17}O < -1‰$; $1\sigma = \pm2‰$), to the left from both carbonaceous chondrite anhydrous mineral (CCAM) line [9] and "primary" ^{16}O-line [10]. The *3529* matrix pyroxene-andradite objects also plot near TF line ($-4‰ < \Delta^{17}O < -1‰$), but largely to the right from "pristine" ^{16}O-line (Fig. 3). Andradite cores of the matrix objects have compositions, which are systematically heavier than those of salite-hedenbergite rims around them (Table 1), possibly due to contamination by matrix olivines which are closely intergrown with rim pyroxenes.

Discussion. The presence of complete chondrule pseudomorphs surrounded by interconnected salitic pyroxene and sulfide rims and observed salitic pyroxene veins crosscutting the chondrule pseudomorphs and matrices of the dark inclusions suggest that the Allend dark inclusions experienced alteration after lithification and aggregation, i.e., as rocks. This alteration resulted in replacement of primary chondrule minerals by secondary fayalitic olivine, nepheline, sodalite, and Fe,Ni-sulfides. Calcium lost from the chondrules was re-deposited as salite-hedenbergitic pyroxene veins and rounded objects in the inclusion matrices, and as rims around chondrules. Following this alteration, the inclusions were excavated from their original location (most likely the CV asteroidal body) and incorporated into the host Allende. The second stage of alteration took place *in situ* and resulted in dissolution of Ca-Fe-rich pyroxenes in the dark inclusions and re-deposition of Ca-Fe-rich silicates as rims around inclusions and in the Allende matrix as well. The proposed mechanism of the rim growth involves diffusional exchange of Ca and Fe between the dark inclusions and Allende, driven by the compositional difference between their matrix olivines.

Because fractionation factors between high temperature gas and solids are small, the overall large range in $\delta^{18}O$ for Ca-Fe-rich silicates in the Allende dark inclusions (Fig. 3) is inconsistent with a condensation nebular origin of

andradite, Ca-Fe-rich pyroxenes and wollastonite proposed by [2]. However, this range can be explained by the two-stage alteration at relatively low temperatures (<330°C) in the presence of limited amount of aqueous solutions discussed above. We note that similar $\Delta^{17}O$ values have been previously reported for secondary fayalite and magnetite from the oxidized CV chondrites Kaba and Mokoia [11] and magnetite from Allende [12]. This indicates that oxygen-isotope composition of the oxidizing reservoir (most likely water) responsible for secondary mineralization in the Allende dark inclusions and oxidized CV chondrites was near the TF line.

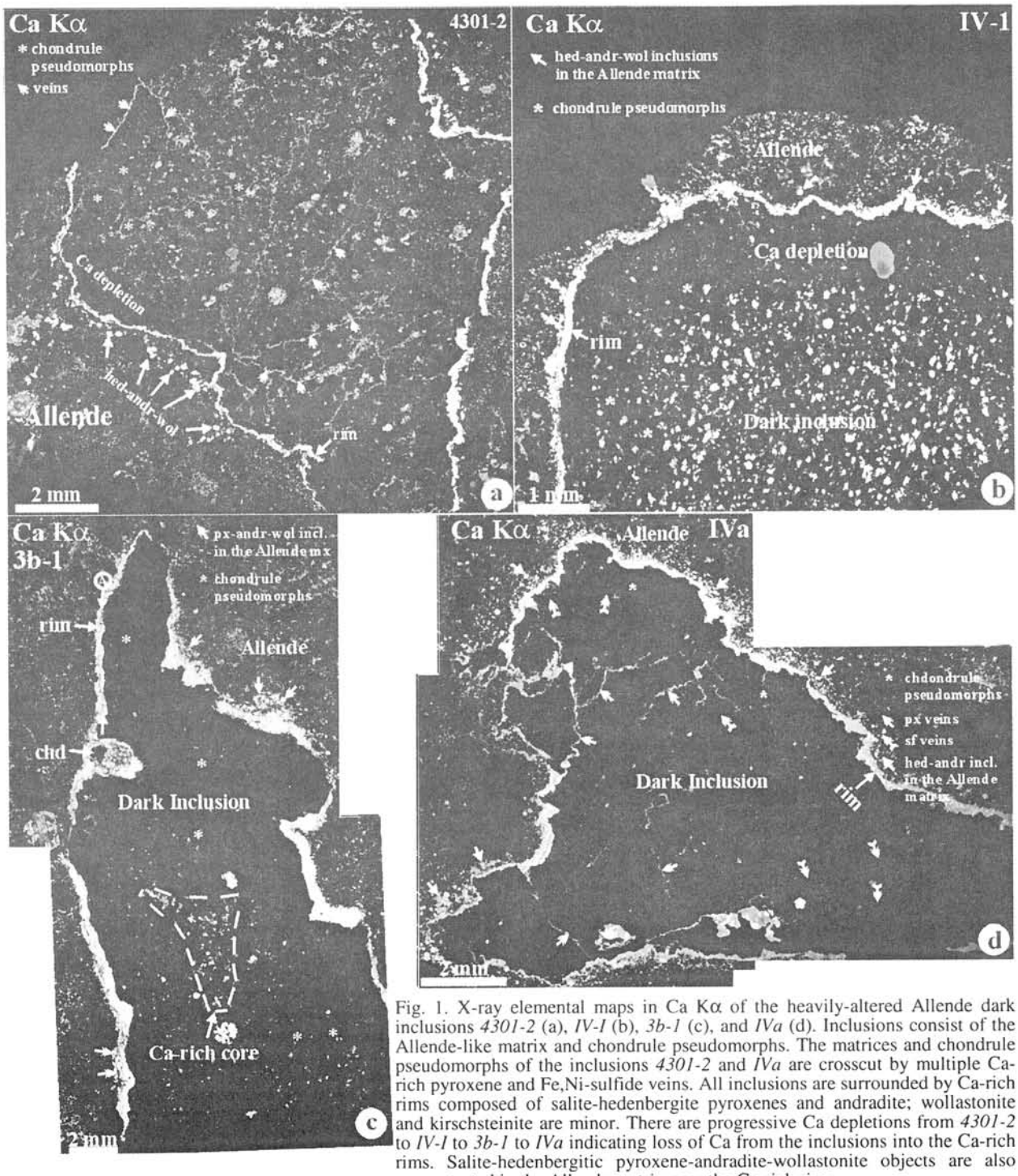

Fig. 1. X-ray elemental maps in Ca Kα of the heavily-altered Allende dark inclusions *4301-2* (a), *IV-1* (b), *3b-1* (c), and *IVa* (d). Inclusions consist of the Allende-like matrix and chondrule pseudomorphs. The matrices and chondrule pseudomorphs of the inclusions *4301-2* and *IVa* are crosscut by multiple Ca-rich pyroxene and Fe,Ni-sulfide veins. All inclusions are surrounded by Ca-rich rims composed of salite-hedenbergite pyroxenes and andradite; wollastonite and kirschsteinite are minor. There are progressive Ca depletions from *4301-2* to *IV-1* to *3b-1* to *IVa* indicating loss of Ca from the inclusions into the Ca-rich rims. Salite-hedenbergitic pyroxene-andradite-wollastonite objects are also concentrated in the Allende matrix near the Ca-rich rims.

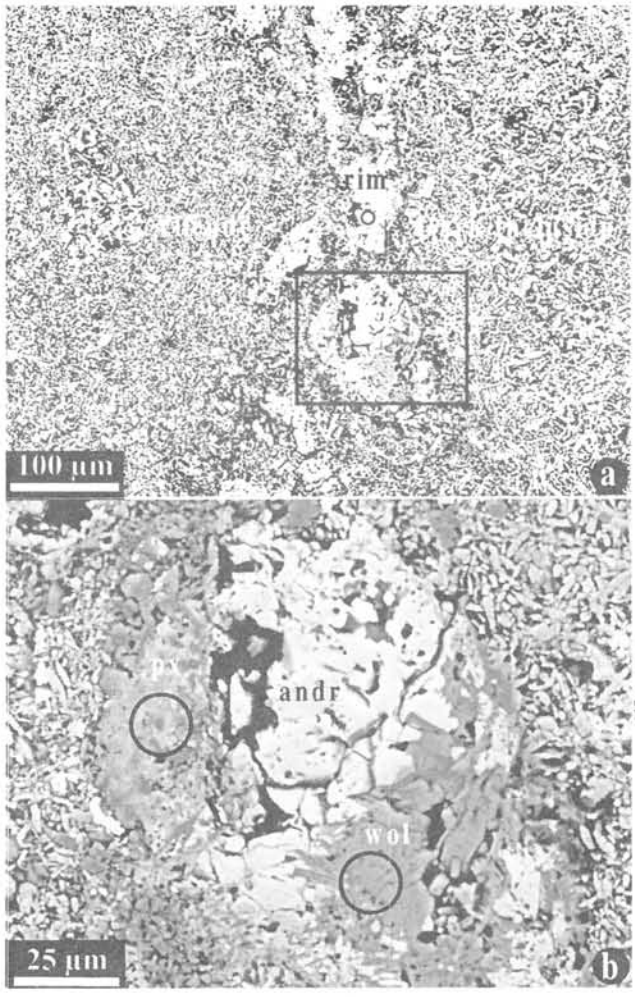

Fig. 2. Backscattered electron images of a Ca-rich rim around the Allende dark inclusion *IV-1*. The rim consists of salite-hedebergitic pyroxenes (px), andradite (andr) and wollastonite (wol). Region outlined in "a" is shown in detail in "b". Regions analyzed by ion probe for oxygen are indicated by circles in "a" and "b".

References: [1] Krot et al. (1998) *LPSC*, **29**, CD-ROM #1555; [2] Johnson et al. (1990) *GCA*, **54**, 819; [3] Kojima T. and Tomeoka K. (1996) *GCA*, **60**, 2651; [4] Kurat et al. (1989) *Z. Naturforsch.*, **44a**, 988; [5] Krot et al. (1998) *M&PS*, **33**, 623; [6] Buchanan et al. (1997) *GCA*, **61**, 1733; [7] MacPherson et al. (1981) *Proc. LPSC*, **12B**, 1079; [8] Krot et al. (1995) *Meteoritics*, **30**, 748; [9] Clayton et al. (1977) *EPSL*, **34**, 209; [10] Young E. D. and Russell S. S. (1998) *Science*, **282**, 452; [11] Choi et al. (1999) *M&PS*, submitted; [12] Choi et al. (1997) *EPSL*, **146**, 337.

Fig. 4. Oxygen isotopic compositions of secondary fayalite and magnetite from the oxidized CV chondrites Kaba and Mokoia [11] and magnetite from Allende [12].

Table 1. Oxygen isotopic compositions of secondary minerals from the Allende dark inclusions *3529* and *IV-1*.

mineral, location	$\delta^{17}O$ (‰)	$\delta^{18}O$ (‰)	$\Delta^{17}O$
IV-1 (rim)			
sa-hed px	-5.4 ± 2.6	-6.5 ± 2.9	-2.0 ± 2.1
sal-hed px	-7.2 ± 2.6	-11.3 ±2.9	-1.4 ± 2.1
andradite	-5.4 ± 2.6	-2.1 ± 2.9	-2.7 ± 2.1
wollastonite	-5.4 ± 2.6	-12.2 ± 3.0	-1.9 ± 2.1
sal-hed px	-5.4 ± 2.6	-5.4 ± 2.9	-1.7 ± 2.1
andradite+wol	-5.4 ± 2.6	-8.4 ± 2.9	-1.2 ± 2.1
3529 (matrix objects)			
olivine fragment	0.4 ± 2.7	1.1 ± 2.8	-2.0 ± 2.1
andradite, obj-1	3.4 ± 2.7	12.3 ± 2.8	-2.0 ± 2.1
sal-hed px, obj-1	1.5 ± 2.6	6.4 ± 2.9	-2.0 ± 2.1
sal-hed px, obj-1	3.1 ± 2.7	8.5 ± 2.9	-2.0 ± 2.1
andradite, obj-2	6.4 ± 2.7	19.6 ± 2.9	-2.0 ± 2.1
sal-hed px, obj-2	-4.2 ± 2.8	-3.6 ± 2.9	-2.0 ± 2.1
andradite, obj-3	-6.2 ± 2.7	17.9 ± 2.8	-2.0 ± 2.1
sal-hed px, obj-3	0.6 ± 2.7	3.8 ± 2.8	-2.0 ± 2.1

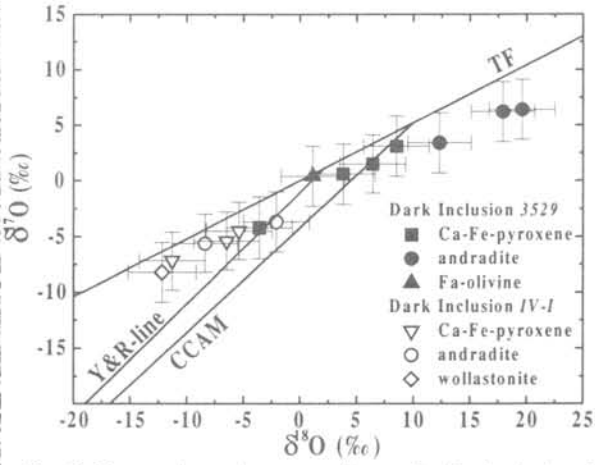

Fig. 3. Oxygen-isotopic compositions of salite-hedenbergitic pyroxenes, wollastonite, andradite and fayalitic olivine from the Allende dark inclusions *3529* and *IV-1*. CCAM - carbonaceous chondrite anhydrous mineral line [9]; Y&R-line - "pristine" ^{16}O-line defined by Young and Russell [10]. Error bars correspond 1σ.

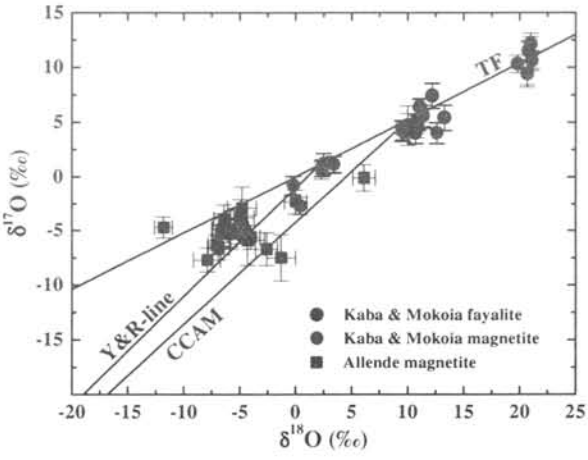

The reaction of forsterite with hydrogen - its apparent and real temperature dependences. Daisuke Kuroda and Akihiko Hashimoto, Graduate School of Earth and Planetary Sciences, Hokkaido University, Sapporo, Japan. dikuroda@ep.sci.hokudai.ac.jp. /akihiko@ep.sci.hokudai.ac.jp.

We have studied experimentally the reaction rate between solid forsterite and hydrogen gas, one of the most fundamental reactions in the solar nebula. Hashimoto (1998) concluded that it was atomic hydrogen that reacted with forsterite, from the result that the reaction rate was linearly proportional to the concentration of atomic hydrogen. In his experiment, however, a sintered, porous forsterite (porosity = 34.5±0.8%) was used; it was found that the reactive gas (*viz* hydrogen) pervaded the forsterite through the pores, and enhanced the reaction rate uniformly. This was equivalent to increasing the surface area which was calculated for the exposed exterior of sample. The present study has used a polished, polycrystalline forsterite with a much less porosity (7.2±0.2%) in order to have a better control on the surface area. We have carried out experiments at 1200, 1300, 1400, and 1500℃, and determined the reaction rate per unit surface area and unit time, and its activation energy.

Figure 1 is a conceptual illustration of the experimental system. Molecular hydrogen is controlled for its flow rate with a mass flow regulator, and is continuously fed into the reaction cell (made of Mo), which is set inside a high-temperature vacuum furnace. Figure 2 shows the inside of the reaction cell. Its upper 2/3 space is filled with fine-grained granules and foil strips of metallic tungsten as a catalyst. Hydrogen flows from the top through numerous narrow channels between the granules and strips, and undergoes many time collisions with the tungsten surface. By the time it flows into the sample room, a dissociation equilibrium is established: $1/2H_2 \Leftrightarrow H$; $P_H=K(T)\,P_{H2}^{1/2}$, where K(T) is the equilibrium constant and P's are partial pressures. The mixed (molecular and atomic) hydrogen reacts with sample, and the product vapor as well as unreacted hydrogen are exhausted into the vacuum chamber through a long tube. The chamber is kept in a high vacuum with a large capacity vacuum diffusion pump (3,000 liter/sec). The resistance the inside wall of the tube exerts on the gas flowing through it gives rise to the pressure increase in the sample room relative to the vacuum. When the pressure in the sample room P_1 at temperature T_1 is maintained by the flow rate f_0 of hydrogen which passes through the flow meter at pressure P_0 and temperature T_0, the conservation of mass leads to the following equation with U_k as the conductance of the evacuation tube.

$$\frac{f_0 P_0}{RT_0} = \frac{U_k(P_1 - P_2)}{RT_1} = \frac{U_k P_1}{RT_1} \quad ; \; U_k = \frac{d^3}{6L}\sqrt{\frac{2\pi RT_1}{M}} \qquad \text{-- (1)}$$

, where R is the gas constant, P_2 is the pressure at the tube outlet (taken ~0), and M is the mean molecular weight (~that of molecular hydrogen in the present experiment). P_0=1atm, T_0=293K, d=0.80cm, and L=5.40cm. If f_0=20cc/min and T_1=1773K(1500℃), then $P_1 \sim P_{H2} = 1.9 \times 10^{-4}$ atm and $P_H = 3.9 \times 10^{-6}$atm from the dissociation equilibrium.

The product vapor is not immediately evacuated from the reaction cell for the same reason described above. Naturally, some vapor molecules would change their direction and collide on the forsterite surface: a backward reaction should occur. Thus the value of Jexp measured in the experiment (as will be described below) is a 'net' reaction rate, which is the difference from the true reaction rate J_F after subtraction of a backward reaction rate J_B. J_B would be proportional to the pressure of the product vapor around the sample, which in turn be proportional to the sample surface area A and Jexp. Thus it is supposed that J_B is proportional to AJexp. If a tentative proportionality constant is expressed by χ, the equation becomes as follows.

$$J_{exp} = J_F - J_B = J_F - \chi A J_{exp} \qquad \text{-- (2)}$$

Our experiment determined Jexp for six types of forsterite sample having different surface areas (108.5, 72.7, 43.7, 25.0, 12.3, and 6.3 mm^2, respectively). All samples are cylindrical in

shape, with the top and bottom surfaces being polished before the experiments. Except for the largest and smallest samples, the four types are similar in shape with the top and bottom surface area combined accounting for 65% of the total surface area. All samples are left slightly uneven on the circumferential side due to a lack of polishing; however, a possible contribution of the unevenness to the effective surface area has not been taken into account. A hydrogen flow of 2cc/min was applied while raising the cell temperature at 10℃/min. The flow rate was changed to 20cc/min the moment the maximum temperature was reached; the same flow rate and temperature were maintained for a prescribed duration. When the cell temperature started falling, the flow was switched to 2cc/min again. The difference in sample weight before and after the experiment, the duration of heating at the maximum temperature, and the sample surface area averaged for before and after the experiment were combined to give J_{exp}, the net reaction rate of forsterite per unit time and unit surface area at temperature and hydrogen pressure. The experimental duration was chosen so as to minimize the weight change; typically 2~5% of the initial weight was lost by reaction. The weight change during the temperature ramps (rising and falling) was minimal and ignored.

Figure 3 shows the experimental results for 1500, 1400, and 1300℃. A linear correlation was obtained for each temperature as expected from Eq.(2). According to this equation the backward reaction rate reduces to zero at an infinitesimal A; in this limit the net reaction rate J_{exp} should be equal to the true reaction rate J_F. Thus J_F for each temperature was obtained from the y-intercept of the linear regression line for that temperature. The single experiment for 1200℃ did not allow such a procedure, but the J_{exp} value itself was taken as J_F because it used a sample with a small A. Figure 4 is an Arrhenius plot of the true reaction rate J_F *vs* temperature 1/T. The data (open circles) and the regression line labelled (a) denote original values of the y-intercepts from Fig.3. These plots, however, may not be suitable for the present purpose because the hydrogen pressure in the reaction cell at each temperature is slightly different from one another due to the different thermal expansion while the same flow rate (20 cc/min at 293K and 1 atm) was used for all the experiments. In order to compare data under the same pressure condition, data (a) are corrected for the pressure difference using the linear relationship of the reaction rate with $P_{H2}^{1/2}$ (Hashimoto, 1998, 1999). The result is data (b), where $P_{H2}=1.9\times10^{-4}$ atm (the actual P_{H2} at 1500℃) was chosen for reference. The regression line of data (b) gives the "apparent" activation energy for the reaction between hydrogen and forsterite, 93.7±3.6 kcal/mol. Because P_{H2} is approximately equal to the total pressure in the nebula, the (b) line represents the reaction (evaporation) rate of forsterite at the total pressure 1.9×10^{-4} atm, provided that the dissociation equilibrium is established between H_2 and H.

Because the degree of dissociation is dependent on temperature, the partial pressure of atomic hydrogen was not constant for the different experimental temperatures even if the partial pressure of molecular hydrogen was kept nearly constant. Since Hashimoto (1998,1999) has found that it was atomic hydrogen that actually reacted with forsterite, the 'real' temperature dependence of the reaction rate should be evaluated under the same pressure of atomic hydrogen. Again, in order to compare data under the same pressure condition, data (a) are corrected for the pressure difference using the linear relationship of the reaction rate with P_H (Hashimoto, 1998, 1999). The result is data (c), where $P_H=3.9\times10^{-6}$ atm (the actual P_H at 1500℃) was chosen for reference. Then, the real activation energy for the reaction between hydrogen and forsterite, determined by the regression, is 40.7±3.6 kcal/mol. From this, a general formula that gives the true reaction rate of forsterite with hydrogen follows:

$$\log(J_F/\mathrm{g\,cm^{-2}sec^{-1}}) = -40.7(\pm3.6)\times10^3/2.303RT + \log(P_H/\mathrm{atm}) + 5.03(\pm0.04).$$

This formula is valid *whether the dissociation equilibrium of hydrogen is achieved or not*, because it does not contain the dissociation constant.

[References] Hashimoto, A. (1998) Meteoritics & Planetary Science **33**, A65. Hashimoto, A. (1999) Yuseijin **8**, 266-282.

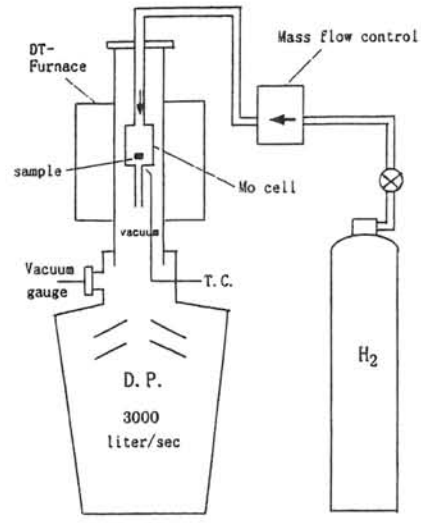

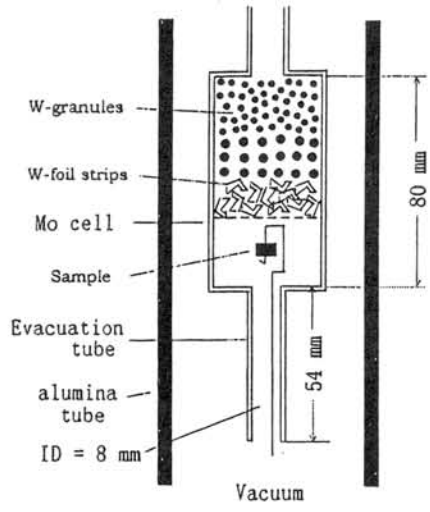

Fig. 1 Experimental system for the solid - hydrogen reaction. (left)

Fig. 2 Inside view of the reaction cell. (right)

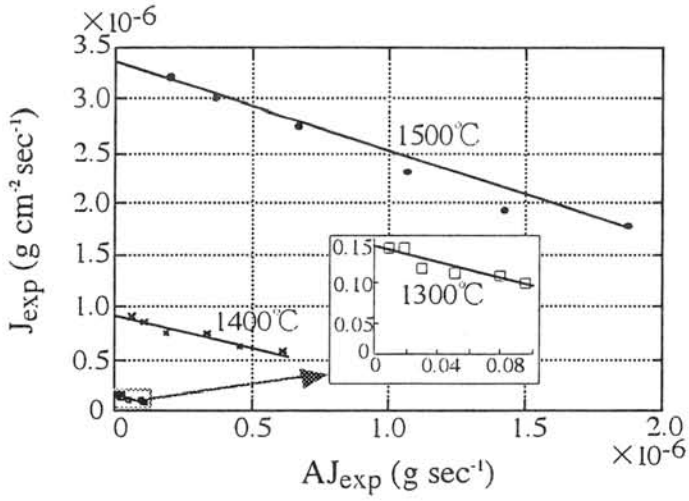

Fig. 3 Net reaction rates of forsterite with hydrogen (flow rate 20 cc/min) at three temperatures. Six data points for each temperature represent 6 experiments using different sample surface areas. The y-intercept of each regression line gives the true reaction rate at the temperature and the hydrogen flow rate.

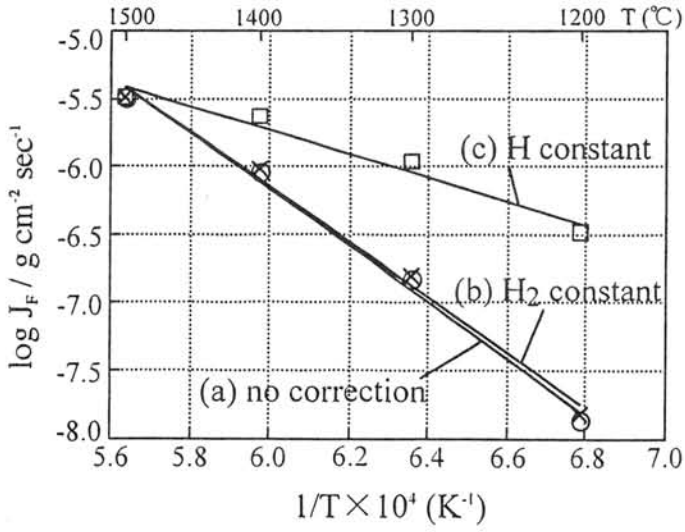

Fig. 4 Arrhenius plot of the true reaction rate determined for the forsterite - hydrogen reaction. Line (a) and open circles denote raw data from the y-intercepts in Fig.3. Line (b) and crosses denote the values corrected for the same H_2 pressure (1.9×10^{-4} atm). Line (c) and open squares denote the values corrected for the same H pressure (3.9×10^{-6} atm).

TWO METEORITE FALLS IN ZHUANGHE CITY, LIAONING PROVINCE, CHINA

Yangting Lin[1], Daode Wang[1], Jinyuan Liu[2], Makoto Kimura[3], and Ziyan Wang[2]

[1]Guangzhou Institute of Geochemistry, Chinese Academy of Sciences, Guangzhou 510640, China; [2]Dalian Museum of Natural History, Dalian 116023, China; [3]Astrophysics and Planetary Science, Faculty of Science, University of Ibaraki, Mito 310-8512, Japan

At 20:33 local time, August 18, 1976, a stone fell in Shishan village, Zhuanghe, Liaoning province, China (39°40'N, 122°59'E). It weights 2.90kg, and has lots of cracks on its surface formed by impacting into muddy earth. This meteorite was named Zhuanghe, but has not yet been studied. After 20 years later, at about 8 a.m., December 30, 1996, another stone fell in Guangmingshan village, Zhuanghe (39°48'15"N, 122°45'50"E), only about 20 km from the first fall site. It hit frozen earth of cropland on hill, and broke into three pieces. The stone was still hot when picked up by a local villager, Mr. Bingde Wang. This meteorite was named as Guangmingshan. Both meteorites are collected in Liaoning Museum of Natural History. In this abstract, we report the first petrography and mineral chemistry of them.

Zhuanghe: It contains plenty of chondrules with somewhat blurred outlines. Most of the chondrules show porphyritic or barred textures, and other less abundant types are radial and granular. They are 0.4-1.2 mm in diameter, except of three large barred olivine chondrules (1.6, 2.3, and 3.8mm). Silicate matrix of the meteorite is recrystallized, and size of the grains is > 10 μm. Most low-Ca pyroxene is orthorhombic, and plagioclase is 20-60 μm in size. Olivine and pyroxene are commonly fractured and show undulatory extinction. Several parallel shock-induced veins (<400 μm in width) were found across the polished thin section studied in this work. The veins consist mainly of silicate fragments with minor immiscible melts of metal-troilite and silicates. Bulk composition of the meteorite is (in vol%): 39.4% olivine, 35.7% low-Ca pyroxene, 4.3% diopside, 8.4% plagioclase, 0.4% phosphates (apatite and whitlockite), 7.2% kamacite, 0.7% taenite, 3.4% troilite and 0.5% chromite.

Olivine ($Fa_{18.3-20.7}$) is homogeneous (PMD of Fa: 3.1%), and CaO was not detected in the most grains. Low-Ca pyroxene has composition of bronzite ($Fs_{15.7-18.6}Wo_{0.8-1.7}$). Analyses of core and rim of a diopside grain show homogeneous composition ($Fs_{6.2-6.7}En_{47.3-47.8}Wo_{45.5-46.5}$) too, with minor TiO_2 (0.45-0.49wt%), Al_2O_3 (0.54wt%), Cr_2O_3 (0.82wt%) and Na_2O (0.54-0.56wt%). Plagioclase has composition of $An_{10.8-12.5}Or_{3.2-8.1}$. Kamacite contains 0.40-0.65wt% Co and 3.23-6.75wt% Ni. Electron probe profiles across three taenites embedded in kamacite reveal that two of them are relatively homogeneous possible tetrataenite (49.6-51.1, 52.0-53.1wt% Ni, respectively), and the other with Ni content increasing from the core (36.1wt%) to rims (40.0-45.8 wt%).

Guangmingshan: Chondrules contains no any glass and show similar textures as those in Zhuanghe. However, outlines of the chondrules are more readily delineated. 27 chondrules have diameters of 0.3-1.0 mm, and other 4 within range of 1.3-1.6 mm. Silicate matrix is recrystallized too, with grain sizes > 10 μm. Most low-Ca pyroxene is orthorhombic, but plagioclase is smaller (<20 μm). Most olivine and pyroxene are fractured, but only a few of them show undulatory extinction. Bulk modal composition is (in vol%): 41.2% olivine,

34.4% low-Ca pyroxene, 4.1% diopside, 7.0% plagioclase, 0.5% phosphates (apatite and whitlockite), 8.9% kamacite, 0.6% taenite, 2.9% troilite and 0.3% chromite.

Compositions of olivine ($Fa_{18.5-21.6}$, PMD of Fa: 2.3%), low-Ca pyroxene ($Fs_{16.4-18.7}Wo_{0.8-1.8}$), and diopside ($Fs_{4.8-8.8}En_{45.5-48.3}Wo_{45.7-47.7}$) are almost identical to those from the Zhuanghe meteorite. 26 analyses of plagioclase have compositions of $An_{10.2-13.5}Or_{2.0-5.6}$, one grain contains low CaO ($An_{8.7}Or_{5.7}$), and another is K_2O-rich ($An_{11.6-11.8}Or_{27.5-17.3}$). Co content of kamacite (0.39-0.55wt%) is within the range of Zhuanghe, but the Ni content is higher (5.35-7.10wt%). All five electron probe profiles across taenites show typical "M" type zoning, with Ni contents increasing from core to rim. Furthermore, the Ni contents of the core reversely correlate with distances from the edges.

Classification: The high metal abundances and kamacite/taenite ratios (10-15) of both Zhuanghe and Guangmingshan are typical of H group chondrites [1]. This is confirmed by their Fa contents of olivine, Fs contents of low-Ca pyroxene, and Co contents of kamacite [1,2]. The somewhat blurred outlines of chondrules, absence of glass, recrystallized matrix, readily visible plagioclase, and predominant orthorhombic low-Ca pyroxene suggest that both meteorites are highly equilibrated, and they can be classified as type 5 according to Van Schmus-Wood's criteria [3]. This is also supported by the homogeneous compositions of olivine and low-Ca pyroxene. Accordingly, the Zhuanghe and Guangmingshan meteorites are classified as H5.

Except of the above similaries, there are also significant differences between these two meteorites, e.g. more blurred outlines of chondrules and coarser-grained plagioclase in Zhuanghe than Guangmingshan, suggesting more severe thermal metamorphism of the former than the later. In addition, the lower Ni content of kamacite, but higher Ni content of taenite from Zhuanghe could be related to equilibrium between the metals at lower temperature, or in other words, Zhuanghe is more equilibrated than Guangmingshan. Other differences between these two meteorites are related to shock metamorphism. The common fracturing and undulose of silicates in Zhuanghe suggest a shock grade of S2 [4]. The occurrence of shock-induced veins in Zhuanghe, however, does not indicate a higher shock grade, because that these veins are very thin and consist predominantly of mechanical fragments of silicates. In comparison, Guangmingshan shows only fracturing and less common undulose of silicates, suggesting of a shock grade of S1.

References: [1] R. T. Dodd. Meteorites: A petrologic-chemical synthesis. 1981, pp368. [2] A. E. Rubin. *GCA*. 1990, **54**, 1217-1232. [3] W. R. Van Schmus & J. A. Wood. *GCA*. 1967, **31**, 747-765. [4] D. Stöffler, et al. *GCA*. 1991, **55**, 3845-3867.

Noble gases in the Kobe meteorite

Yoshiki Matsumoto[1], Takuya Matsumoto[1], Jun-ichi Matsuda[1] and Noboru Nakamura[2]

[1] Department of Earth and Space Science, Graduate School of Science, Osaka University

[2] Department of Earth and Planetary Sciences, Faculty of Science, Kobe University

INTRODUCTION

The Kobe meteorite fell on 26th, September, 1999, in northern part of Kobe-city, Japan. The meteorite penetrated a roof of the house and crushed into 20 pieces with their total mass of 136g. Soon after the falling, some pieces were subjected to preliminary chemical and mineralogical investigations which have revealed that the meteorite is the first 'fall' carbonaceous chondrite in Japan with a close affinity to the Karoonda group (i.e., CK chondrites) [1]. In order to further characterize this rare new meteorite, we have investigated elemental and isotopic compositions of noble gases (He, Ne, Ar, Kr and Xe) of the bulk meteorite.

EXPERIMENTAL PROCEDURE

As the first trial of the noble gas investigation on Kobe, we have analyzed elemental and isotopic compositions of all five noble gases on a bulk sample (C-3-1) of 27.79mg without chemical treatment. The sample was wrapped in Al-foil and loaded into ultrahigh vacuum gas extraction and purification line attached to a VG5400 mass spectrometer. After baking the sample at about 120℃ (total 29hrs), the gases were extracted from the sample by heating it at 1600℃ with a resistively-heated double-vacuum furnace. The sensitivity and mass discrimination corrections for the noble gases were calibrated by analyses of aliquots of known volume and isotopic compositions from standard air pipettes. Appropriate corrections for the procedural blank (and interference in case of neon) were made.

RESULTS

Character as the CK group

It was reported that the CK group is characterized by comparatively low abundances of trapped heavy noble gases (Kr and Xe) and high $^{129}Xe/^{132}Xe$ ratios (>1.5) [2]. As shown in Fig. 1, the noble gas elemental abundances of Kobe are in agreement with the range previously reported from the CK chondrites (Fig. 1). This and the observed large ^{129}Xe excess ($^{129}Xe/^{132}Xe = 6.5 \pm 0.2$) are both consistent with the notion that Kobe belongs to the CK group (Fig. 2). It is also possible to estimate the sample's petrologic type by using the amounts of trapped Kr and Xe [2]. This is shown in Fig. 3 where the amounts of Kr and Xe observed in various CK chondrites are plotted. As shown in Fig. 3, there is a clear positive correlation between those amounts and is a progressive increase in their Kr and Xe amounts from CK6 to CK3. The present results plot in the area defined by CK4 to CK5. Therefore, the present noble gas analyses on the bulk sample suggest that Kobe is indeed belonging to the CK group possibly with its petrologic type to be CK4-5, which is consistent with a notion (CK4) suggested independently from its chemical and mineralogical analyses [1].

Cosmic-ray exposure age

We assumed all observed ^{3}He and ^{21}Ne to be cosmogenic, because the observed $^{3}He/^{4}He$ ratio (0.042

± 0.002) is two orders of magnitude higher than the reported solar or planetary component and the observed $^{20}Ne/^{22}Ne$ and $^{21}Ne/^{22}Ne$ ratios (0.838 ± 0.004 and 0.92 ± 0.01, respectively) are agreed perfectly with the reported cosmogenic composition (0.85 and 0.92, respectively). Using the production rates given by Eugster [3] with an assumed chemical composition of CV as a target, the cosmic-ray exposure ages of Kobe were estimated to be 12Ma and 41Ma from the observed amount of cosmogenic ^{3}He and ^{21}Ne, respectively. The apparently shorter exposure age inferred from the cosmogenic ^{3}He in Kobe may be an indicative of a helium loss due to solar heating in space [4]. The obtained exposure age from ^{21}Ne may be somewhat longer than those reported for many CK chondrites, but is close to that reported for Karoonda (40 Ma; [2]).

SUMMARY

We have measured noble gas elemental and isotopic compositions of the recently fallen meteorite, Kobe. The results indicate that heavy noble gas in Kobe is consistent with the Karoonda group and that its petrologic type is suggested to be CK4-5. Isotopic compositions of He and Ne are predominantly of cosmogenic origin, and the apparent cosmic-ray exposure ages of 12 to 41Ma were suggested.

Acknowledgements: We thank Mr. R. Hirata for providing us with the Kobe meteorite.

REFERENCES

[1] Nakamura, N. *et al.* (2000) *Lunar Planet. Sci.* **31**, no. 1234.

[2] Scherer, P. and Schultz, L. (2000) *Meteorit. Planet. Sci.* **35**, 145-153.

[3] Eugster, O. (1988) *Geochim. Cosmochim. Acta* **52**, 1649-1662.

[4] Scherer, P. *et al.* (1998) *Meteorit. Planet. Sci.* **33**, 259-265

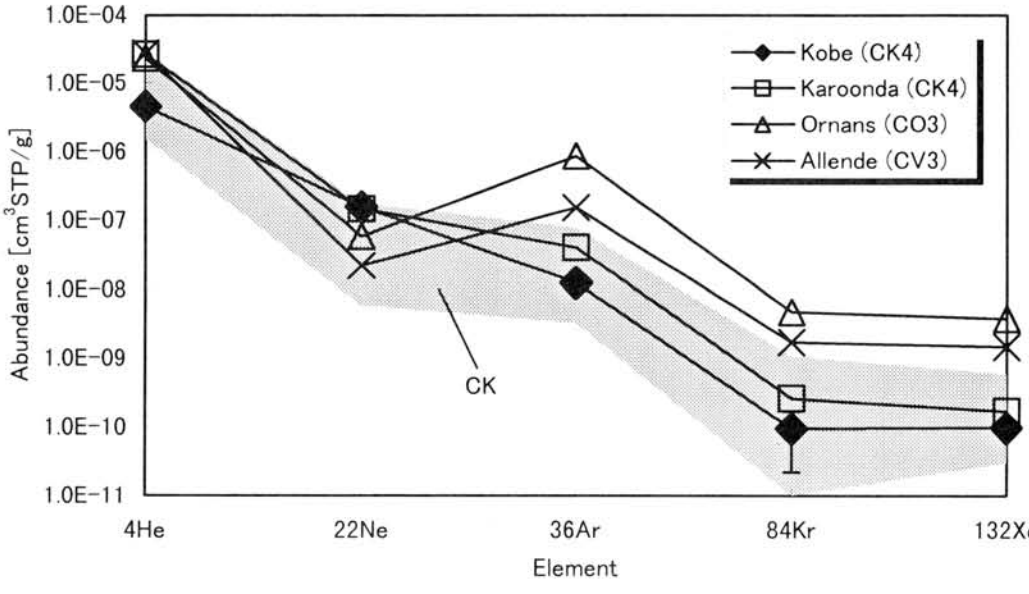

Fig. 1: Noble gas abundances in Kobe (this work). Those from Karoonda, Ornans and Allende [2] are also shown for comparison. The shaded area (labeled as CK) shows the range of the noble gas abundances previously reported for CK chondrites [2]. The results of Kobe are within the CK range.

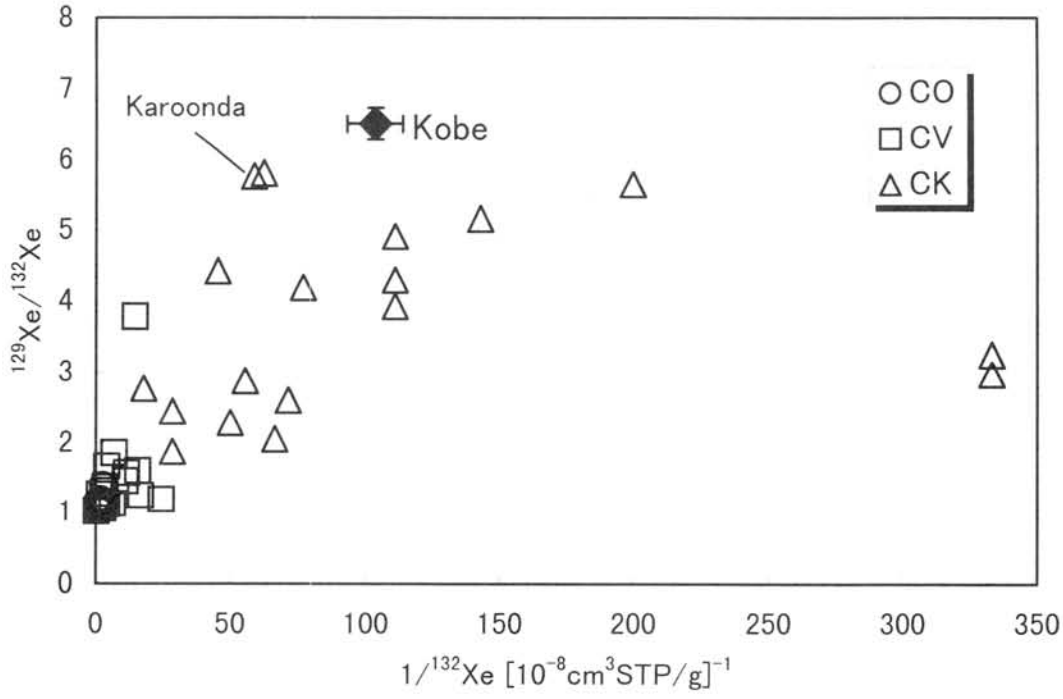

Fig. 2: A $^{129}Xe/^{132}Xe$ vs. $1/^{132}Xe$ diagram. As observed in many CK chondrites [2], the present Kobe meteorite shows a very high $^{129}Xe/^{132}Xe$ ratio.

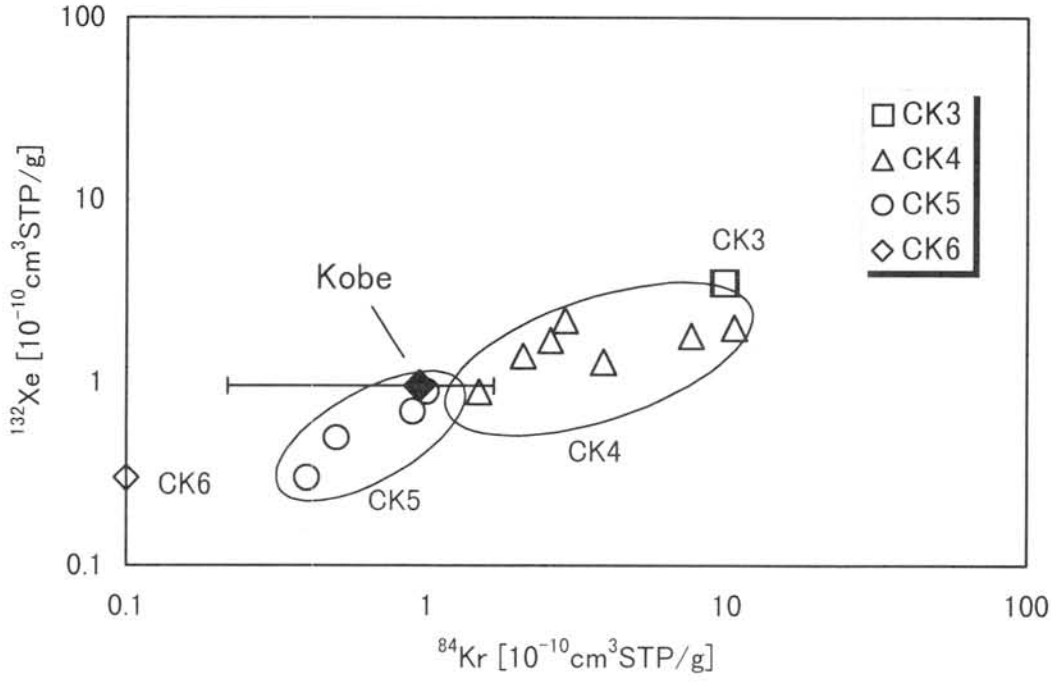

Fig. 3: A ^{132}Xe vs. ^{81}Kr diagram. Kobe is from this study and the others are from Scherer *et al.* [2].

Conceptual Design for a Receiving and Quarantine Facility for Returned Mars Samples

Gordon McKay[1], Donald Bogard[1], and Carl Agee[2]
[2]*SN, Earth Science and Solar System Exploration Division, NASA Johnson Space Center, Houston TX 77058, USA*
[1]*AC, Office of the Director, NASA Johnson Space Center, Houston TX 77058, USA*

NASA plans to return a sample from Mars via robotic spacecraft late in the current decade, possibly as soon as 2008. This will be the first sample returned from a planet other than the moon, and promises to yield scientific results at least as exciting as those from the Apollo lunar samples. Following the Apollo model, Mars samples will be distributed to scientists around the world for analysis in the world's best laboratories using sophisticated, state-of-the-art analytical techniques.

The Johnson Space Center has developed great expertise in sample handling and preservation through its long history of curating lunar samples, Antarctic meteorites, and cosmic dust particles. Thus, JSC is the logical choice for curation of the Mars samples. Accordingly, we are developing plans for a facility where the samples will be opened, examined, documented, and processed upon return to earth.

There are two major differences between the Mars samples and previous samples such as Apollo samples. First, according to the Space Studies Board of the National Academy of Sciences, samples returned from Mars must be contained and treated as though potentially hazardous until proven otherwise. Second, one of the major goals of the Mars Exploration Program, including sample return missions, is to determine if Mars has now or has ever had living organisms. These two differences place major constraints on the way in which the returned samples are handled. The first requires that the Mars sample handling facility be designed to protect the terrestrial environment and ecosystem from any potential biohazards contained in the Mars samples. The second requires that the Mars samples be scrupulously protected from contamination with terrestrial material that could be incorrectly interpreted as evidence for Martian biological activity. As explained below, these two constraints will require a new type of facility that has not previously been built.

With the above principles in mind, we have developed a general scheme for Mars sample handling that shown in Fig. 1. After collection at Mars and return to Earth, the sample will be retrieved in a manner that will biologically isolate it from the environment. The sample will then be transported to the Mars Receiving Facility. This facility will have two major units. One unit, the Preliminary Examination Laboratory (PEL) will have two major functions. First, this unit will be designed to keep the samples from being contaminated with terrestrial material (both organic and inorganic), and to provide biocontainment so that the samples do not contaminate the terrestrial environment. Second, the unit will contain the necessary equipment to examine, catalog, and classify the samples to the degree required for selecting representative samples for hazard testing. Also, this unit will have the capability to sterilize selected samples or subsamples so that they can be removed from biological containment for scientific study. The second major unit in the Receiving Facility is the Biological Examination Laboratory (BEL), where selected samples will be tested for biohazards and possibly certified as non-hazardous and thus available for distribution without sterilization. The methods for this hazard testing are yet to be defined. Because biohazard testing in the BEL may result in sample contamination or degradation, any samples transferred from the PEL to the BEL will no longer be considered "pristine", and will not be returned to the PEL. After samples are either sterilized or certified

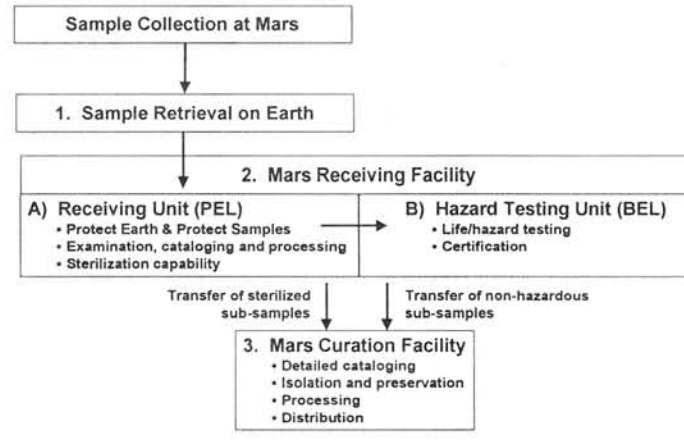

Fig. 1. Overview of Mars sample handling.

to be non-hazardous, they will be transferred to the Mars Curation Facility for detailed cataloging; long term isolation, preservation, and storage; processing; and distribution.

The requirement to keep the Mars samples free from terrestrial contamination is similar to that for Lunar samples, except that it is even more stringent. This extra stringency is a result of the scientific focus on detection of evidence for life, and the complications arising from a false positive resulting from terrestrial contamination. To satisfy this requirement, the samples must be protected from terrestrial contamination by handling in a clean environment. To protect the samples from airborne particlate contamination, the samples will be contained and handled in a clean environment that is under positive differential pressure relative to the surrounding environment (top panel, Fig. 2), as is currently the case for Lunar samples.

The requirement to keep the terrestrial environment free from contamination by the Mars samples is similar to that for a biosafety level 4 facility of the type used to contain dangerous airborne pathogens such as Ebola virus (middle panel, Fig. 2). Such a lab contains the pathogens, but because it is at a negative pressure relative to the surrounding environment, it would not protect the sample from terrestrial contamination.

Thus a new laboratory design is required. This laboratory must protect the sample from contamination by terrestrial material, in part by keeping the sample in an environment that is at positive pressure relative to the adjacent region. The laboratory must also protect the terrestrial environment from the Mars sample, by maintaining the region surrounding the sample cabinet at a negative pressure relative to outside ambient (bottom pane, Fig. 2). One consequence of the latter requirement is that the room containing the cabinet must be treated as a biologically "hot" lab. This may require that workers processing the samples wear biological isolation suits.

The time required to design, build, certify, and commission a typical BSL-4 facility is about 6 years. Because of the unique requirements for both cleanliness and biological isolation, we anticipate that the Mars receiving facility will be even more difficult to design and build. There are many challenges to overcome. We plan to enlist the aid of private companies and academic and government organizations to insure that the Mars samples are handled in a way that both preserves their scientific integrity and protects the Earth from potential hazards.

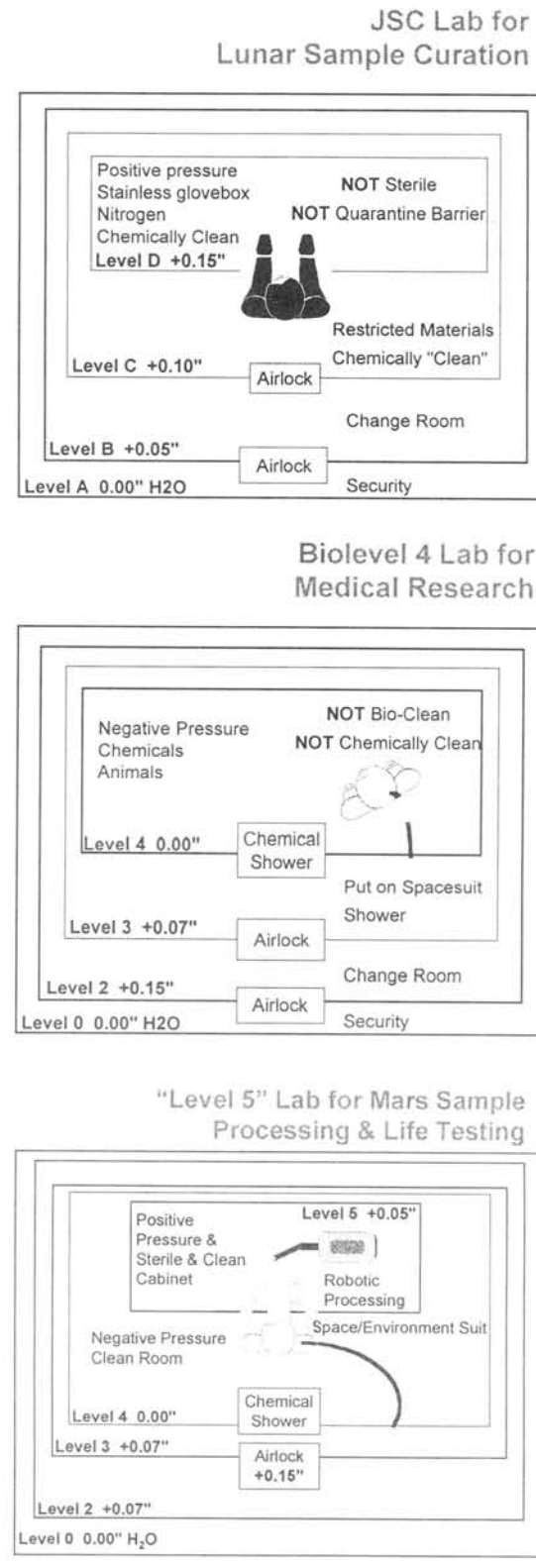

Fig. 2. Schematic diagrams of existing Lunar Sample Facility, BSL 4 facilities, and proposed Mars receiving facility. Differential pressures are given in inches of H_2O and are meant only to suggest relative pressures.

A new angrite Sahara 99555: Mineralogical comparison with Angra dos Reis, Lewis Cliff 86010, Lewis Cliff 87051, and Asuka 881371 angrites

T. Mikouchi[1,2], G. McKay[1], and L. Le[3]

[1]*Mail Code SN2 Planetary Science Branch, NASA Johnson Space Center, Houston, TX77058, USA*
[2]*Department of Earth & Planetary Science, University of Tokyo, Hongo, Bunkyo-ku, Tokyo 113-0033, JAPAN*
[3]*Lockheed Martin Eng. & Sci. Co., Mail Code C23, 2400 Nasa Road 1, Houston, TX77058, USA*

Introduction

Angrite is a small group of basaltic achondrites represented by a very old crystallization age (4.56 b.y.) and unusual mineralogy [e.g., 1-4]. Major constituent minerals are fassaitic clinopyroxene, anorthitic plagioclase and Ca-rich olivine. These unique mineral assemblages are attributed to the fact that angrites are depleted in volatile elements whereas enriched in refractory elements. In spite of these interesting characteristics, only four angrites (Angra dos Reis, Lewis Cliff 86010, Lewis Cliff 87051, Asuka 881371) were previously known and they were all small (especially, Antarctic angrites). Sahara 99555 was recently recovered from the Sahara and classified to be the 5th angrite [5]. Sahara 99555 weighs 2,710 g and is the largest angrite ever found. Therefore, the discovery of Sahara 99555 is expected to offer additional information to better understand unusual petrogeneses of this antique achondrite group. It can also allow us to refine on the chronological record of igneous activity in the very early solar system. In this abstract we present petrological and mineralogical study of Sahara 99555 and compare results with those of other angrites, especially Antarctic angrites, Lewis Cliff 87051 (LEW87051) and Asuka 881371.

Petrography

Two thin sections were prepared for this study from a 2.6 g rock chip. They were analyzed by scanning electron microscopes and electron microprobes. Sahara 99555 shows a fine-grained ophitic texture typical for a quenched magma (Fig. 1). It is mainly composed of fassaitic clinopyroxene, anorthitic plagioclase, and Ca-rich olivine (including kirschsteinite). Minor phases are titanomagnetite, troilite, and an unknown silico-phosphate. X-ray maps obtained by microprobe give the following modal abundances of minerals: 33% anorthite, 24% fassaite, 23% Mg-rich olivine, 19% Fe-rich olivine (including kirschsteinite), and 1% others. Mineral sizes are generally up to 0.5 mm though anorthites are lath-shaped often reaching 1 mm long. There is no evidence suggesting strong shock effects in Sahara 99555 that are also absent in the other angrites. The cut surface of the Sahara 99555 main mass shows millimeter-size spherical vesicles, showing a similarity to Asuka 881371 [6,7].

Fig. 1. Photomicrograph of the Sahara 99555 thin section (plane-polarized light). The section shows an ophitic texture mainly composed of lath anorthite with chemically zoned fassaite and Ca-rich olivine. Scale bar is 1 mm.

Mineral Chemistry

Olivine in Sahara 99555 is colorless and is euhedral to subhedral. They sometimes show a skeletal growth texture intergrown with anorthites and fassaites. Olivine shows extensive chemical zoning. The composition ranges from the Fo_{63} cores to extremely Fe-Ca-enriched rims. There is a compositional jump between inner Mg-rich areas and outer Ca-Fe-rich rims near the composition of fe# (atomic Fe/(Fe+Mg)) = 0.65-0.8. Mn is positively correlated with Fe and MnO is about 0.8 wt% at the rim. The FeO/MnO ratio (wt%) is 75-90 that well agrees with other angrites. Cr_2O_3 is less than 0.05 wt%. Olivine rims exhibit complex mixtures of Ca-rich fayalite and Ca-poor kirschsteinite, suggesting an exsolution relationship. The most Ca-rich kirschsteinite contains 20 wt% of CaO. Even the olivine core with the least fe# contains 1 wt% of CaO.

Fassaitic clinopyroxene is subhedral to euhedral and shows a strong pleochroism. It is bright brown in the core and is dark brown at the rim, suggesting chemical zoning. Chemical zoning is extensive in both major and minor elements. However, CaO is nearly constant at 22-23 wt%. The fe# of Sahara 99555 fassaite ranges from 0.5 to 1. Al_2O_3 is 6-9 wt% although some fassaite inclusions in olivine reach up to 18 wt% Al_2O_3. TiO_2 increases 1.5-5 wt% from core to rim as fe# increases. On the other hand Cr_2O_3 drops from 0.4 wt% in the core to nearly zero at the rim.

Plagioclase is usually intergrown with olivine of Fo_{50-40} and skeletal anorthite crystals are sometimes observed. Plagioclase is essentially Na-free (Na_2O <0.1 wt%) giving almost pure anorthite composition. Anorthite contains high amounts of FeO and MgO, each usually 1.5 wt% and 0.4 wt% or higher, respectively.

Titano-magnetite is the most abundant minor phases in Sahara 99555. It contains about 25-27 wt% of TiO_2 and 1.5-2.0 wt% of Al_2O_3. **Troilite** is also observed and some grains contain up to 2 wt% of Ni. A Ca-rich **silico-phosphate** phase (up to 45 wt% CaO and 37 wt% P_2O_5) was found in Sahara 99555. A similar phase is only known in Asuka 881371 reported by [7,8]. The silico-phosphate in Sahara 99555 appears to have a wide compositional range from a Ca-P-rich and Si-Fe-poor composition to vice versa. No merrillite was detected in the thin sections unlike other angrites.

Mineralogical Comparison with Other Angrites

The ophitic texture of Sahara 99555 is similar to those of LEW87051 and Asuka 881371, but is quite different from granular Angra dos Reis and Lewis Cliff 86010 (LEW86010) textures (Fig. 2). The situation of the modal abundances of minerals is almost same. The Sahara 99555 mineral abundances are similar to those of LEW87051 and Asuka 881371 whereas different from LEW86010 and especially Angra dos Reis (Angra dos Reis has >90 % fassaite with minor amounts of olivine). Chemical zoning patterns of olivine and fassaite are also very similar to those of LEW87051 and Asuka 881371 although they contain forsteritic olivine xenocrysts (up to Fo_{90}) that are absent in Sahara 99555. Unlike these three angrites, olivines in Angra dos Reis and LEW86010 are homogeneous (LEW86010 contains exsolution lamellae of kirschsteinite in olivine), suggesting slower cooling rates and higher degrees of diffusive homogenization. Fassaite chemistry shows similar properties. Angra dos Reis fassaite is essentially unzoned, LEW86010 fassaite moderately zoned in Fe/Mg and highly zoned in minor elements, and fassaites in LEW87051, Asuka 881371 and Sahara 99555 strongly zoned in both Fe/Mg and minor elements. In spite of the similarities among LEW87051, Asuka 881371 and Sahara 99555, Sahara 99555 has apparent differences from the other two. The cores of Sahara 99555 fassaite and olivine are more Fe-rich than those of LEW87051 and Asuka 881371. Although minor element patterns of fassaite are generally similar to LEW87051 and Asuka 881371, Cr content is lower in Sahara 99555. The complex intergrowth texture of olivine and anorthite was only seen in the Sahara 99555 angrite.

Discussion and Conclusion

Thus, Sahara 99555 is a new angrite similar to LEW87051 and Asuka 881371 in several respects. Nevertheless, Sahara 99555 has clear differences from LEW87051 and Asuka 881371 as described above. Because Sahara 99555 does not contain any xenocrysts unlike LEW87051 and Asuka 881371 [4], we believe that the bulk composition closely represents a magma composition. The presence of skeletal olivine and plagioclase crystals suggests that Sahara 99555 crystallized very quickly from the magma, probably faster than or as fast as LEW87051 and Asuka 881371 cooled. The complex intergrowth of olivine and anorthite might be achieved by rapid cooling of magma. In our preliminary report [5] we found that 50 °C/hr cooling run of the Asuka 881371 groundmass melt successfully reproduced texture, zoning patterns of olivine and fassaite, general mineral abundances, mineral sizes and mineral compositions of Sahara 99555. Thus, we conclude that Sahara 99555 cooled very quickly, presumably less than 1 m from the surface. The appropriate geological setting was crystallization in a thin lava flow. The Sahara 99555 magma was slightly more Fe-rich than those of LEW87051 and Asuka 881371 and did not contain olivine xenocrysts. We think that the Sahara 99555 magma was closely related to those of LEW87051 and Asuka 881371 and was derived from slightly evolved LEW87051 and/or Asuka 881371 magma(s). Floss *et al.* [9] reported that melt compositions calculated from LEW87051 and Asuka 881371 core fassaite REE abundances are nearly identical to those determined for Sahara 99555, but LEW86010 melt has lower REE abundances. Although LEW87051 and Asuka 881371 have different cosmic-ray exposure ages [10], suggesting that they came from different sites on the parent body, it is likely that LEW87051, Asuka 881371 and Sahara 99555 share common petrogenesis and crystallization history. In contrast, Angra dos Reis and LEW86010 have different petrogeneses.

Acknowledgement: We thank Prof. T. Tagai (The University Museum, Univ. of Tokyo) for supplying the Sahara 99555 sample. This work was partly supported by the National Academy of Sciences through an NRC associateship at NASA Johnson Space Center and the Grant-in-Aid for Encouragement of Young Scientists by the Japanese Ministry of Education, Science and Culture (No.12740297).

References: [1] Prinz M. *et al.* (1977) *Earth Planet. Sci. Lett.*, **35**, 317-330. [2] Mittlefehldt D. W. and Lindstrom M. M. (1990) *Geochim. Cosmochim. Acta*, **54**, 3209-3218. [3] Nyquist L. E. *et al.* (1994) *Meteoritics*, **29**, 872-885. [4] Mikouchi T. *et al.* (1996) *Antarct. Meteorite Res.*, **9**, 174-188. [5] Mikouchi T. *et al.* (2000) *Lunar Planet. Sci.*, **XXXI** Abst. #1970 (CD-ROM). [6] Yanai K. (1994) *Proc. NIPR Symp. on Antarct. Meteorites*, **7**, 30-41. [7] Warren P. H. and Davis A. M. (1995) *Antarct. Meteorites*, **XX**, 257-260. [8] Prinz M. and Weisberg M. K. (1995) *Antarct. Meteorites*, **XX**, 207-210. [9] Floss C. *et al.* (2000) *Meteorit. and Planet. Sci.*, **35**, Suppl. (submitted). [10] Weigel A. *et al.* (1997) *Geochim. Cosmochim. Acta*, **61**, 239-248. [11] Lugmair G. W. and Galer S. J. G. (1992) *Geochim. Cosmochim. Acta*, **56**, 1673-1694. [12] Premo W. R. and Tatsumoto M. (1995) *Antarct. Meteorites*, **XX**, 204-206.

Table 1. Five known angrites Angra dos Reis, LEW86010, LEW87051, Asuka 881371 and Sahara 99555.

	Angra dos Reis	LEW86010	LEW87051	Asuka 881371	Sahara 99555
Recovered site	Brazil	Antarctica	Antarctica	Antarctica	Sahara
Weight	1.5 kg	6.9 g	0.6 g	11.3 g	2,710 g
Texture	Granular	Granular	Porphyritic	Ophitic	Ophitic
Xenocryst	None	None	Olivine (~10%)	Olivine (~10%)	None
Olivine	Fo_{53}	Fo_{32}	Fo_{91-0}	Fo_{89-0}	Fo_{63-0}
Fassaite					
*fe#	0.28	0.25-0.45	0.4-1	0.4-1	0.5-1
Al_2O_3 (wt%)	10	6-12	5-8	6-8	6-9
TiO_2 (wt%)	2	1-3	1.5-7	1.5-4	1.5-5
Cr_2O_3 (wt%)	0.2	0.8-0.2	0.85-0	0.7-0	0.4-0
Pb-Pb age (Ma)	4558 ± 4 [11]	4558 ± 5 [11]	—	4566 ± 24 [12]	—
Sm-Nd age (Ma)		4553 ± 34 [11]	—	—	—
		4530 ± 40 [3]	—	—	—
Cosmic-ray exposure age (Ma)	55.5 [10]	17.6 [10]	≥0.2 [10]	5.4 ± 0.7 [10]	—

— : Not determined

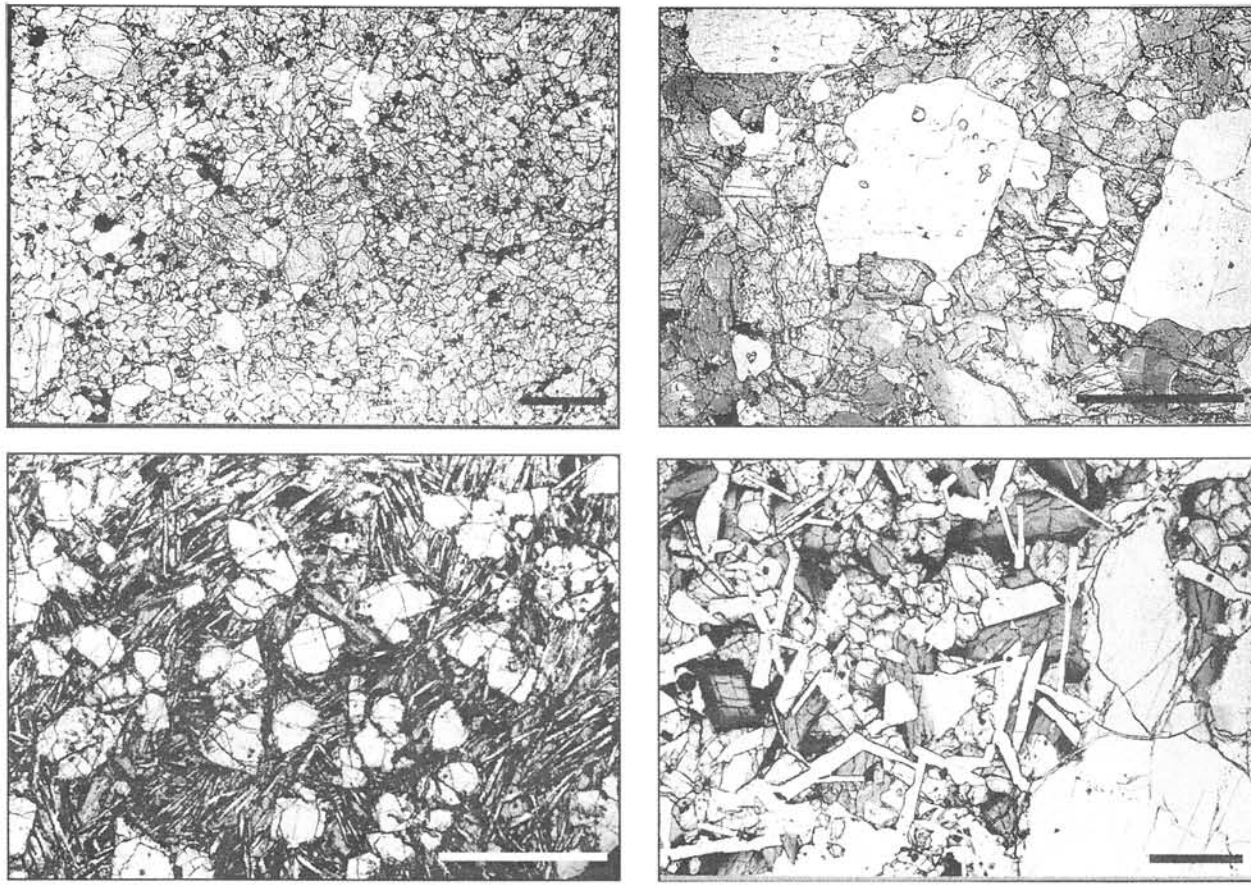

Fig. 2. Photomicrographs of previously known angrites (plane-polarized light). Upper left: Angra dos Reis. Upper right: LEW86010. Lower left: LEW87051. Lower right: Asuka 881371. Scale bars are 1 mm. Angra dos Reis shows a granular texture composed of >90% of fassaite. No plagioclase was included in the section. LEW86010 also shows a glanular texture. It is composed of 40% fåsaite, 30% anorthite, and 20% olivine. Olivine contains kirschsteinite exsolution lamellae. LEW87051 is mainly composed of porphyritic olivine and anorhite lath set in a fine-grained groundmass. Some olivine cores are proposed to be xenocrysts. Asuka 881371 shows an ophitic texture composed of euhedral to subhedral fassaite, olivine and anorthite with minor amounts of olivine xenocrysts.

An attempt to measure carbon-14 terrestrial ages of Antarctic meteorites with a Tandetron AMS at Nagoya University

Masayo Minami[1], Nobuo Takaoka[2] and Toshio Nakamura[3]

1) Department of Earth and Planetary Sciences, Graduate School of Science, Nagoya University, Chikusa, Nagoya 464-8602, Japan
2) Earth and Planetary Sciences, Faculty of Science, Kyushu University 33, Hakozaki, Fukuoka 812-8581, Japan
3) Center for Chronological Research, Nagoya University, Chikusa, Nagoya 464-8602, Japan

Introduction Terrestrial ages of Antarctic meteorites give us important information to estimate the terrestrial history of the meteorites. With the advent of AMS, the required sample mass of meteorite for measurement has been reduced as small as 0.1g. As a result, many more ^{14}C measurements have been performed intensively by the Toronto AMS group, Canada, the Arizona AMS group, USA, and so on (eg., Beukens et al., 1988; Brown et al., 1984; Jull et al., 1984). In Japan, AMS ^{14}C measurements of meteorites have been scarcely performed, to our regret. We are now at the early stage of the program for studying ^{14}C activities in meteorites, and constructing a system to extract ^{14}C from meteorites, in a similar method used by the Arizona group (Jull et al., 1989a, 1993). In this paper, we report the performance of the carbon extraction system with iron standards of known carbon content and ^{14}C activities of some Antarctic meteorites.

Samples and Experiments The iron standards used were 4.67%C cast iron supplied by LECO Corporation, 0.196%C steel (part No. JSS 030-7) and 0.049%C steel (part No. JSS 201-12) supplied by The Japan Iron and Steel Federation. Two Antarctic meteorites of Y-75102 and ALH-77294 were examined to measure ^{14}C concentrations. The terrestrial ages of the meteorites were reported to be 3+1 kyr and 10+1 kyr, respectively (Jull et al., 1984, 1989b). A sample mixed with about 2g combustion accelerator (high purity Fe, LECO corp., part No. 502-231) is combusted in a RF furnace (LECO HF-10) in the presence of purified carbon-free O_2 in a closed vacuum-tight glass line system. The meteorite samples were preheated prior to the combustion in the RF furnace in muffle furnace at 500℃ to remove organic contamination and low-temperature weathering products. The sample gases evolved are passed through MnO_2 and Pt/CuO traps, and then the CO_2 is separated in a liq.N_2 trap, by pumping out O_2 completely. The amount of $^{14}CO_2$ is determined by a pressure transducer in a certain volume and diluted with a known amount of ^{14}C-free CO_2. The total CO_2 is graphitized by reducing with hydrogen in a

Fe-powder catalyst and the produced graphite is measured of its ^{14}C concentration with a Tandetron accelerator mass spectrometer at the Center for Chronological Research, Nagoya University.

Results and Discussion The extraction efficiency of the iron standards was summarized in Table 1. The results by the wet method, which consists of dissolution of iron with with a Cu^{2+} solution and dissolution of deposited Cu in HCl, are also shown in Table 1 (Oda et al., 1999). The ^{14}C ages of the iron standards by the RF melting method agree with the known ages of corresponding samples treated by the wet method. The agreement means that the contamination by modern carbon is negligible for the melt-extraction procedure. Furthermore, this procedure gave high carbon extraction yields (85-95%) for low carbon content samples as well as high carbon content samples by the improved extraction system. The improved points are (1) decrease in O_2 flow at combustion, (2) increase in the number of liq.N_2 traps for condensing CO_2, and (3) little by little pumping out O_2 to prevent sample CO_2 gas from flowing away together with O_2.

Table 2 shows the ^{14}C concentrations and the resulting ^{14}C terrestrial ages of two Antarctic meteorites. The saturation activities of 51 dpm/kg and 47 dpm/kg were used for Y-75102 and ALH-77294, respectively. The carbon yields of the meteorites were significantly low, and the terrestrial ages were different from the reported values. The result might be caused either by imperfect combustion and conversion CO to CO_2 of the meteorites. Further studies are needed to improve analytical techniques, for instance, heating time in the RF furnace and a amount of combustion accelerator.

In the near future, we will investigate pairing of Y-74190, Y-75097, Y-75102, Y-75108 and Y-75271 by the ^{14}C terrestrial ages.

Reference

Beukens, R. P., Rucklidge, J. C. and Miura, Y. (1988) *Proc. NIPR Symp. Antarct. Meteorites* **1**, 224-230.

Brown, R. N., Andrews, H. R., Ball, G. C., Imahori, Y., Milton, J. C. D. and Fireman, E. L. (1984) *Earth Planet. Sci. Lett.* **67**, 1-8.

Jull, A. J. T., Donahue, D. J., Zabel, T. H. and Fireman, E. L. (1984) *Proc. Lunar. Planet. Sci. Conf. 15th, J. Geophys. Res.* **89**, C329-335.

Jull, A. J. T., Donahue, D. J. and Linick, T. W. (1989a) *Geochim. Cosmochim. Acta* **53**, 2095-2100.

Jull, A. J. T., Donahue, D. J. and Linick, T. W. (1989b) *Lunar. Planet. Sci.* **XX**, 488-489.

Jull, A. J. T., Donahue, D. J., Cielaszyk, E. and Wlotzka, F. (1993) *Meteoritics* **28**, 188-195.

Oda, H, Nakamura, T. and Furukawa, M. (1999) *J. Radioanalytical and Nuclear Chemistry* **239**, 561-564.

Table 1 Extraction results of iron standards

	Sample weight g	Accelerator weight g	Yield of CO_2 mgC	Extraction efficiency %	$\delta^{13}C$ ‰	^{14}C age yrBP
LECO Fe (4.67%C)						
[RF melting method]						
1	0.095	1.0	4.25	96.2	-25.9	36,260±420
2	0.091	3.0	4.07	96.2	-26.1	37,390±580
3	0.033	2.0	1.36	87.0	-26.6	-------
4*	0.073	2.0	3.23	95.4	-26.2	-------
5*	0.008	2.0	0.34	93.7	-26.4	-------
[wet method]						
6	0.159		6.15	83.0	-25.2	37,150±330
7	0.067		2.66	84.8	-25.1	36,290±330
JSS 030-7 (0.196%C)						
[RF melting method]						
1	1.012	1.0	1.78	90.2	-23.5	23,930±350
2	1.004	3.0	1.79	93.7	-24.9	27,250±260
3	1.035	2.1	1.57	77.2	-23.8	25,180±270
4	1.005	2.0	1.50	76.0	-24.2	24,570±270
5	1.008	2.1	1.56	79.0	-24.2	24,040±330
6	0.217	2.1	0.24	56.9	-26.0	-------.
7*	1.044	2.0	1.73	84.6	-24.4	-------
8*	0.233	2.0	0.40	87.7	-----	-------
[wet method]						
9	1.529		2.65	88.4	-23.0	25,980±270
10	1.530		2.59	86.4	-23.3	25,330±270
JSS 201-12 (0.049%C)						
[RF melting method]						
1	1.005	1.0	0.33	66.4	-23.7	-------
2	1.052	3.1	0.27	52.8	-27.4	-------
3*	1.034	2.0	0.45	88.5	-25.8	-------
[wet method]						
4	6.004		2.47	84.1	-25.0	20,030±190

The data by the wet method are from Oda et al. (1999).
The asterisked data were obtained by the improved extraction system.

Table 2 Terrestrial ages of two Antarctic meteorites

Sample	Weight g	Yield of CO_2 mgC (%C)	$\frac{(^{14}C/^{12}C)_{Sam}}{(^{14}C/^{12}C)_{STD}}$	^{14}C dpm/kg	Terrestrial age kyr
Y-75102	0.982	0.0234 (0.002%)	24.3±0.9	11.6±0.4	12±1
ALH-77294	0.832	0.0881 (0.011%)	1.8±0.1	3.7±0.2	21±1

NBS oxalic acid standard (RM-49)
Mesurements errors are 1 standard deviation.

INCORPORATION OF RADIOGENIC LEAD COMPONENTS INTO PLAGIOCLASE DURING SHOCK METAMORPHISM: A POSSIBLE REDISTRIBUTION MECHANISM OF VOLATILE LEAD

Keiji Misawa[1,2], Fumie Yamazaki[2], Shinobu Sawada[1,2], Toshimori Sekine[3] and Noboru Nakamura[2]
[1] Antarctic Meteorite Research Center, National Institute of Polar Research, 1-9-10, Kaga, Tokyo173-8515, Japan
[2] Department of Earth & Planetary Sciences, Kobe University, Kobe 657-8501, Japan
[3] National Institute for Research in Inorganic Materials, 1-1, Namiki, Tsukuba 305-0044, Japan

Introduction: It is well known that there were heavy bombardments of meteorites on lunar surface at around 3.9 Ga (terminal lunar cataclysm, [1]), not only resulting excavation of crustal rocks but also triggered mare basalt volcanism. Plagioclase is the main constituent of lunar crust, which considered to be produced from an early lunar differentiation, lunar magma ocean. Because of the key role of plagioclase in the U-Pb systematics of lunar rocks, it is important to understand the mobility of volatile Pb in plagioclase during shock metamorphism. Almost all the samples recovered from the Apollo and Luna missions as well as lunar meteorites experienced heavy shock-effects. With increasing shock intensity, plagioclase transforms into diaplectic glass, so called 'maskelynite', which is commonly observed in highland rocks. Excess radiogenic Pb-components were clearly observed in lunar regoliths [2], plagioclase [3-5], "rusty rock" 66095 [6], and lunar meteorite Asuka 881757 [7]. The data points of maskelynitized plagioclase and whole-rock fractions from A-881757 lie above the 3.94 Ga isochron (*i.e.*, ^{207}Pb-rich), indicating an open-system behavior owing to a disturbance in the U-Pb system.

If the Pb mobilized from older lunar rocks had contaminated with most of the lunar anorthosites, breccias, soils, and mare basalts during lunar cataclysm at ~3.9 Ga, it will affect modeling of lunar crust-mantle evolution, especially estimating lunar initial Pb isotopic compositions and U/Pb ratios. Dating results from the annealing experiments indicate that post-shock annealing plays the most important role in resetting K-Ar, Rb-Sr isotopic systems [8]. Moreover, volatile-element transformation occurred during shock events. For example, "rusty rock" 66095 contained a remarkably large amount of Pb, which was not supported *in situ* U and Th. This excess Pb was considered evolving in a source environment similar to that for KREEP [6]. Whether Pb from older lunar high-μ sources was incorporated into plagioclase due to transformation into maskelynite or adsorbed Pb was left along grain surfaces and cracks during the cooling stages after impact events or both is an issue of importance in evaluating the evolution history of lunar rocks. As an initial step we have carried out shock recovery and annealing experiments on plagioclase with samarskite in order to understand the disturbance in the U-Th-Pb systems of lunar rocks.

Experimental: Sample used for annealing experiments was same as those for shock recovery experiments [9]. Anorthite grains (ϕ > 250 μm) without inclusions were washed in distilled water and leached by 6 N HCl in an ultrasonic bath. Quartz tubes were washed by HCl and rinsed with distilled water before using. The acid-washed and dried anorthite, weighed about 120 mg, placed in a fused-quartz tube that was closed at one end. This insert was then placed in a larger quartz tube in which about 50 mg of samarskite was placed at the bottom. After evacuation to a pressure of ~1 Pa, the outer tube was sealed at top end. The apparatus was placed in the vertical furnace, and heated for 46-118 hrs at 420-1050°C. Annealing temperatures were monitored by thermocouples of Pt-Rh. After annealing, the apparatus was removed from the furnace and then quenched in a water bath. Because of vaporized Na from starting anorthite, the silica tubes heated at 1050°C were partly reacted with anorthite.

Shock recovery experiments were performed using a propellant gun (ϕ = 30 mm) at the National Institute for Research in Inorganic Materials. The projectile was a 4-mm thick stainless steel plate bedded at the front of a high-density polyethylene sabot. The target was annealed anorthite at ~750°C with samarskite for 24 hrs, encapsulated in a cylindrical container made of SUS304 stainless steel. Because the peak pressure of container depends on the initial porosity of material, the samples were pressed at 40 MPa before shock loading.

Several grains from annealed samples were embedded in epoxy resin and polished. Thin sections of shock-loaded anorthite were observed by an optical microscope. Major and minor element compositions of anorthite/glass were determined by an electron probe microanalyzer. *In situ* Pb isotopic measurements have been done using the SHRIMP II ion microprobe at the NIPR followed by the methods for zircon and feldspar analyses [5, 10]. An O_2^- primary beam of 5-7 nA was focused on a spot with a diameter of ~30 μm. Mass resolution power was 4700 at 1% peak height.

Results: *Texture and Major Element Chemistry* Optical microscopic observation revealed that anorthite shocked to 19.5 GPa are fractured. Anorthite shocked to 25.4 GPa partly shows undulatory extinction, and is partially isotropic at the original grain-boundary. Anorthite shocked to 31.5 GPa has almost transformed into diaplectic glass. In spite of these textural differences, any detectable major element fractionation among anorthite/glass was not observed by EPMA analysis.

TIMS Results Annealed samples were decomposed in a mixture of HF and HNO_3 in PFA Teflon screw-cap jars. The chemical separation procedure for Pb followed that described previously [7]. Results are shown in Fig. 1. The Pb isotopic compositions of the acid residue of anorthite, which annealed at 1050°C without samarskite, were not different from those of the starting anorthite. This indicates that the Pb isotopes of anorthite were not affected by Pb in quartz tube or surface Pb of apparatus even at high temperatures. The Pb isotopes of acid leachates and residues of anorthite annealed at 700°C or 1050°C were more radiogenic when compared with those of samarskite, indicating that radiogenic Pb was evaporated from samarskite and adsorbed on anorthite surfaces and/or incorporated into anorthite. The Pb isotopes of acid residue annealed at 420°C were less but still radiogenic compared with those of starting anorthite.

Ion Microprobe Results In Fig. 2, results of *in situ* SHRIMP measurements of annealed anorthite are shown. Radiogenic Pb was observed only at and along the cracks

near the grain surface, strongly suggests that the radiogenic components observed in acid leachates and residues of annealed anorthite (Fig. 1) were derived from surficial, adsorbed Pb. In the 19.5 GPa- and 25.4 GPa-samples, radiogenic Pb was observed only at the original grain surfaces. On the other hand, radiogenic Pb was more heterogeneously distributed in the 31.5 GPa-sample, suggesting incorporation of radiogenic components into diaplectic glass.

Discussion: Anorthite is expressed to be $CaAl_2Si_2O_8$ and the part of Ca can be occupied by divalent cations such as Sr^{2+}, Ba^{2+}, or Eu^{2+}. The stable form of Pb at the experimental conditions is considered to be almost Pb^{2+} [11], so it is not surprising that mobilized and/or volatilized Pb^{2+} from samarskite could be substituted for Ca^{2+} and incorporated into the crystal structure of anorthite. Diffusion coefficient of Pb in anorthite measured by [12] is comparable to that of Sr [13], and Pb uptake is correlated with a reduction of Ca, indicating the involvement of Pb-Ca exchange in chemical diffusion. Even if temperature exceeds 1100°C for 10 min, diffusion distance of Pb is calculated to be less than 1 μm. Results of *in situ* Pb isotopic analyses of annealed anorthite are consistent with the diffusion calculation, and indicate that radiogenic components observed in annealed anorthite are surface, adsorbed Pb.

Pb on the Moon is very radiogenic compared to that of the Earth and most meteorites. A difficulty with lunar U-Pb chronology is the absence of a known lunar initial Pb isotopic composition and initial U/Pb ratio for the bulk Moon. Thus the primordial Pb isotopic composition obtained from Cañon Diablo troilite (CDT) is used with the assumptions: 1) the Pb isotopic composition in the solar nebula was homogeneous and 2) the U/Pb ratio of the nebula was sufficiently low such that CDT represents a realistic value at the time of lunar formation.

Ferroan anorthosites (FANs) are considered to be represented primordial lunar crusts that formed by floatation of plagioclase during lunar magma ocean. Plagioclase does not contain sufficient amounts of U or Th, thus sometimes used for estimate initial Pb isotopic compositions. However, most of the FANs are characterized to severely brecciated, maskelynitized, and in soma cases melted. Especially 15415, 60015, and 62237 show young K-Ar and Rb-Sr ages along with extremely high $^{207}Pb/^{206}Pb$ values of ~1.45, and are considered to be affected by post crystallization disturbance, *i.e.*, shock metamorphism [14-17]. On the other hand, mineral separates from 60025 [18, 19] show old Pb-Pb ages with low $^{207}Pb/^{206}Pb$ values of < 0.9, which requires low-μ (between ~35 and 100) source(s) at 4.4 Ga [20]. If Pb was volatilized from early-formed, high-μ sources such as KREEP during lunar cataclysm at around 3.9 Ga, plagioclase could be a sink for radiogenic Pb.

The implication is that incorporation of radiogenic Pb components into plagioclase could be occurred during intense shock events, and that plagioclase glasses in FANs and mare basalts have been contaminated by KREEP Pb, produced from early-formed, high-μ magma sources. This component are hardly removed from anorthite/glass by conventional acid leaching steps using HBr and/or HNO_3.

References: [1] Tera F. *et al.* (1974) *EPSL* **22**, 1-21. [2] Silver L. T. (1970) *Proc. Apollo 11 LSC* 1533-1574. [3] Nunes P. D. *et al.* (1973) *PLSC* **4**, 1797-1822. [4] Tera F. & Wasserburg G. J. (1972) *EPSL* **14**, 281-304. [5] Compston W. *et al.* (1991) in *"Stable Isotope Geochemistry"* pp. 473-486. [6] Nunes P. D. & Tatsumoto M. (1973) *Science* **182**, 916-920. [7] Misawa K. *et al.* (1993) *GCA* **57**, 4687-4702. [8] Nyquist L. E. *et al.* (1991) *LPSC* **XXII**, 985-986. [9] Misawa K. *et al.* (1998) *Antarct. Meteorites* **XXIII**, 83-85. [10] Compston W. *et al.* (1984) *JGR* **89**, B525-B534. [11] Otto E. M. (1966) *J. Electronchem. Soc.* **113**, 525-527. [12] Cherniak D. J. (1995) *CMP* **120**, 358-371. [13] Cherniak D. J. & Watson E. B. (1994) *GCA* **58**, 5179-5190. [14] Tera F. *et al.* (1972) *The Apollo 15 Lunar Samples*, 396-401. [15] Tatsumoto *et al.* (1972) *The Apollo 15 Lunar Samples*, 391-395. [16] Premo R. W. *et al.* (1989) *PLPSC* **19**, 61-71. [17] Snyder G. A. *et al.* (1994) *LPSC* **XXV**, 1309-1310. [18] Hannan B. B. & Tilton G. R. (1987) *EPSL* **84**, 15-21. [19] Premo W. R. *et al.* (1999) *Interntl. Geol. Rev.* **41**, 95-128. [20] Carlson R. W. & Lugmair G. (1988) *EPSL* **90**, 119-130.

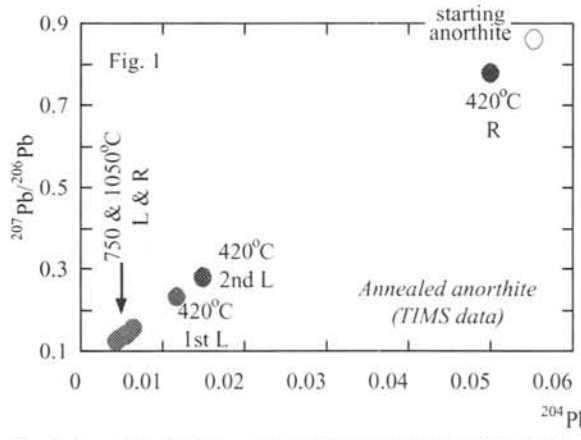

Fig. 1. Annealed anorthite was leached first in 1 N HBr and next in 7 N HNO_3 for five times each. The Pb isotopes of the anorthite (both leachates and residues) annealed at 750 or 1050°C are highly radiogenic. The Pb isotopes of the anorthite residue annealed at 420°C are still radiogenic compared with those of starting anorthite.

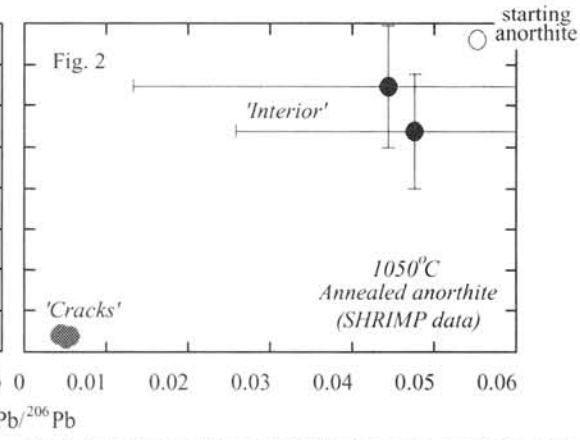

Fig. 2. Annealed anorthite at 1050°C for 46 hrs was mounted in epoxy resin and Pb isotopes were measured by using the SHRIMP II. Radiogenic Pb components were observed only at/along the cracks, suggesting that radiogenic Pb observed in Fig. 1 are surficial, adsorbed ones. Errors are 1σ for counting statistics. Large errors for 'interior' data are due to the low concentration of Pb (~0.2ppm) in the starting anorthite.

Hafnium and Tantalum as Petrogenetic Indicators for Weathered Antarctic Eucrites

David W. Mittlefehldt[1] and Marilyn M. Lindstrom[2]
[1]C23, Lockheed Martin SO, 2400 Nasa Rd. 1, Houston, TX 77058, USA
[2]SN2, NASA/Johnson Space Center, Houston, TX 77058, USA

Introduction. Eucrites are basaltic composition igneous rocks from a differentiated asteroid, quite possibly 4 Vesta. Eucrites are the most common achondrite type among observed falls, but even so, only 2 new eucrite falls have been recovered in the last 30 years. Since the time of the first antarctic expedition specifically tasked to recover meteorites from the blue ice, the 15th JARE in 1973-1975, many hundreds of eucrites have been returned by Japanese and American teams. This large collection of new eucrites has provided us new and unusual petrologic types [*e.g.* 1] which expand the range of information we can obtain from the eucrite parent body.

Basalts have compositions that are defined by the compositions of their source regions and the melting processes. Incompatible lithophile trace elements are widely used to derive models for the genesis of basalts. They partition quantitatively into the melt phase, and their concentrations can be used to estimate degrees of melting or amounts of fractional crystallization. Incompatible lithophile trace elements have been used to develop numerous models for eucrite petrogenesis [*e.g.*, 2-4]. For antarctic eucrites, however, terrestrial weathering has affected the trace element compositions of many of them [5].

We have analyzed newly reported eucrites, falls as well as finds, since 1987 as part of our effort to understand the fundamental petrologic processes that occurred on the eucrite parent body. Here we report on the geochemistry of a large suite of non-cumulate eucrites from the Japanese and American antarctic collections we have analyzed since our first report on weathering effects [5]. We discuss which incompatible lithophile trace elements appear unaffected by antarctic weathering, and thus may be used for petrogenetic interpretations.

Incompatible Trace Elements in Non-Cumulate Eucrites. We have done instrumental neutron activation analysis on a suite of non-cumulate eucrite falls and antarctic finds. We always request interior samples, and often specifically select the material we will use for analyses in an effort to avoid weathering problems. Nevertheless, our results demonstrate that the rare earth elements (REE) have often been affected by terrestrial alteration processes. Figure 1 shows an example from ALHA81001. ALHA81001 is the finest-grained eucrite known [6], and therefore sample heterogeneity should be negligible. We have analyzed two interior chips, while [6] have done duplicate analyses on a single chip. Our results show complimentary REE patterns. Split ,35 is depleted in REE^{3+} and has positive Ce and Eu anomalies. We attribute this pattern to dissolution of REE-rich phosphates with loss of the solution [5]. Europium is primarily contained in plagioclase and so is less affected by this process, while Ce becomes oxidized to Ce^{4+} and is precipitated from the solution before it can be removed. Split ,37 has been enriched in REE^{3+} by precipitation from the solution derived from elsewhere in the meteorite and has negative Ce and Eu anomalies. The sample analyzed by [6] has REE abundances between those of our samples.

Of the REE, Eu varies the least, and possibly is unaffected by the weathering process. In spite of this, Eu is not suitable for use as a petrogenetic indicator. Figure 2 shows Eu *vs.* La for eucrite falls. The Eu and La concentrations are in approximately chondritic ratios in those eucrites with the lowest trace element contents, but the more evolved, trace element-rich samples

do not have chondritic ratios of Eu to La. Europium varies less than does La in the suite, and thus is less incompatible. Because of this, Eu does not provide as clear a record of igneous fractionation.

Also shown in Figure 2 are Hf and Ta *vs.* La. Both of these elements are highly correlated with La and maintain chondritic ratios through the entire range of non-cumulate eucrites. Thus, both Hf and Ta can be used as indexes of the degree of partial melting or the amount of fractional crystallization in the eucrite suite. Figure 1 also shows the CI-normalized Hf and Ta abundances for ALHA81001. Unlike the case for the REE, Hf and Ta in all analyses of ALHA81001 show very little variation. Thus, Hf and Ta show no evidence for alteration in the terrestrial environment. Figure 3 compares Ta *vs.* Hf for eucrite falls and antarctic eucrites.

Discussion. We previously presented a model for the formation of anomalous REE patterns in antarctic eucrites by dissolution in melt-water films made acidic by equilibration with the atmosphere (formation of carbonic acid) and/or oxidation of troilite (formation of sulfuric acid) [5]. Phosphates are the major host of REE^{3+} in eucrites [*e.g.*, 7]. Only Eu, because much of it is Eu^{2+}, is contained in a major phase, plagioclase. Ion probe analyses of phosphates in eucrites generally do not contain measurements for Hf or Ta [7], so we can not determine whether phosphates are a significant host for these elements. Geochemical and mineralogical arguments suggest that phosphates are not the major host. The REE^{3+} (ionic radii 113 to 94 pm) substitute for Ca^{2+} (ionic radius 108 pm) in phosphates, and the more highly charged and smaller Hf^{4+} and Ta^{5+} (ionic radii 79 and 72 pm, respectively) will be less easily accommodated in a phosphate host. Eucrites contain zircon and baddeleyite as trace accessory phases [8], and Hf^{4+} should readily substitute for Zr^{4+} (ionic radius 80 pm) in these phases. Zircon in eucrite Y-791438 contains 1.74 wt% HfO_2 [1]. Ilmenite is a minor phase and titanite is a trace accessory phase in eucrites [8], and Nb^{5+} and Ta^{5+} (both with ionic radius of 72 pm) substitute for Ti^{4+} (ionic radius 69 pm) in these structures [*e.g.*, 9]. Based on terrestrial experience, we expect that these phases will be more resistant to alteration in the antarctic environment, and thus the Hf and Ta contents of antarctic eucrites should be much less affected than are the REE.

Summary. Hafnium and Ta are highly incompatible elements in the eucrite suite, and thus can be sensitive indicators of partial melting or fractional crystallization processes. Comparison of Hf and Ta data with REE data from eucrite falls and antarctic eucrites shows that Hf and Ta are probably unaffected by the terrestrial alteration that has changed the REE patterns of antarctic eucrites. These two elements are sited in different phases than the REE, and their host phases are much less susceptible to terrestrial alteration. The host phases for Hf and Ta, like for the REE, are minor and/or trace phases, so sample heterogeneity is a serious concern for obtaining representative compositions.

References. [1] Saiki H. *et al.* (1991) *Proc. Lunar Planet. Sci. Conf.* **21,** 341.; [2] Consolmagno G.J. and Drake M.J. (1977) *Geochim. Cosmochim. Acta* **41,** 1271; [3] Righter K. and Drake M.J. (1997) *MAPS* **32,** 929; [4] Ruzicka A. *et al.* (1997) *MAPS* **32,** 825; [5] Mittlefehldt D.W. and Lindstrom M.M. (1991) *Geochim. Cosmochim. Acta* **55,** 77; [6] Warren P.H. and Jerde E.A. (1987) *Geochim. Cosmochim. Acta* **51,** 713; [7] Hsu W. and Crozaz G. (1996) *Geochim. Cosmochim. Acta* **60,** 4571.; [8] Delaney J.S. *et al.* (1984) *Proc. 15th Lunar Planet. Sci. Conf., J. Geophys. Res. Sppl.* **89,** C251; [9] Parker R.L. and Fleischer M. (1968) *USGS Prof. Paper* **612.**

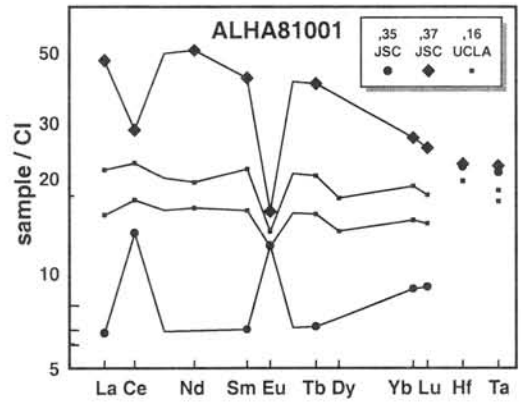

Figure 1. REE, Hf and Ta analyses on three samples of ALHA81001. JSC = our data; UCLA = data of [6].

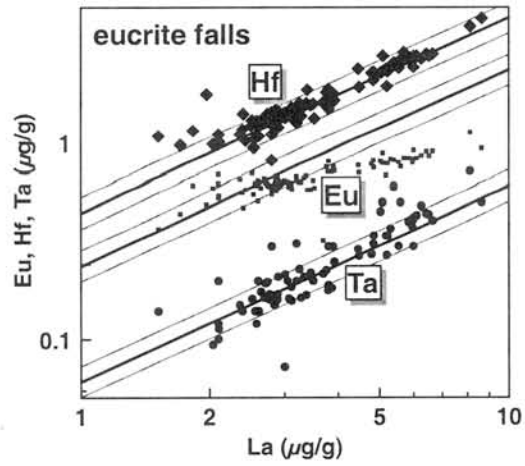

Figure 2. Eu, Hf and Ta *vs.* La for individual analyses from the literature of non-cumulate eucrites falls. Heavy lines are CI ratios; light lines are ±20% deviations from the CI ratios.

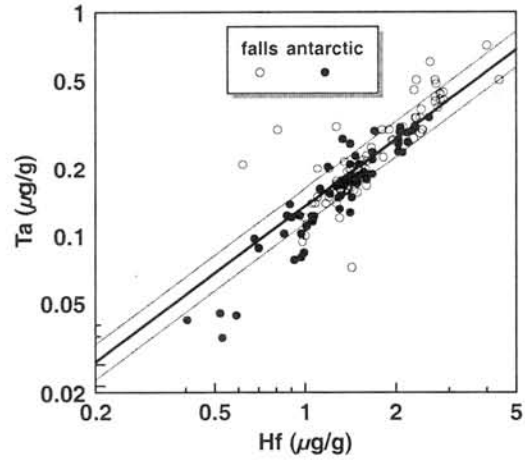

Figure 3. Ta vs. Hf for non-cumulate eucrite falls and antarctic finds. Heavy line is the CI ratio; light lines are ±20% deviations from the CI ratio. Some of the scatter for the eucrite falls may be due to poor analytical quality in older analyses.

Noble gases in Y-791192, Y-75032-type diogenites, and A-881838

Yayoi N. Miura[1] and Keisuke Nagao[2]

[1] Earthquake Research Institute, University of Tokyo, Yayoi, Bunkyo-ku, Tokyo 113-0032, Japan.
[2] Laboratory for Earthquake Chemistry, Graduate School of Science, University of Tokyo, Hongo, Bunkyo-ku, Tokyo 113-0033, Japan.

Introduction

Among Antarctic diogenites (more than eighty [1, 2]), 44 and 18 have been identified as fragments of two single falls [1]. The diogenites belonging to these groups are called Y-74013-type (or Diogenite-A) and Y-75032-type (or Diogenite-B), respectively, based on the name of their representative specimens. Takeda *et al.* [*e.g.* 3] have examined mineralogical features of Y-75032-type diogenites in detail, and reported that the diogenites are polymict breccias containing diverse fragments of diogenites, ordinary eucrites and cumulate eucrites. The meteorites of this group are also characterized by unique shock melt veins and clustered pyroxene compositions around Mg#67. In addition to the eighteen diogenites classified into the Y-75032-type [1], Y-791192, originally classified as a polymict eucrite, was considered as a member of subclass of the Y-75032-type [4]. Because Y-791192 contains more eucritic and less diogenitic components, Takeda *et al.* [4] has proposed reclassification of this achondrite as an unusual howardite or polymict cumulate eucrite with affinity to Y-75032-type diogenites. We investigate noble gas isotopic compositions of Y-791192 as well as three Y-75032-type diogenites, Y-75032, Y-791000 and Y-791199. Noble gases in another diogenite, the monomict diogenite A-881838 [1], are also reported here.

Results and discussion

Y-75032-type and Y-791192 Three diogenites, Y-75032, Y-791000 and Y-791199, have similar noble gas abundances and isotopic compositions each other. Helium and Ne in these diogenites are mostly cosmogenic. Argon is also dominant in cosmogenic component accompanying a significant amount of radiogenic ^{40}Ar. The light noble gas compositions in Y-791192 are close to those in the three Y-75032-type diogenites. The concentrations of cosmogenic ^{3}He, ^{21}Ne and ^{38}Ar as well as the obtained cosmic-ray exposure ages are summarized in Table 1. The average of the exposure age for the three diogenites is calculated to be 22 m.y., which is just on the main exposure age cluster around 22 m.y. for HED meteorites [5, 6]. The exposure ages obtained from ^{3}He, ^{21}Ne and ^{38}Ar for Y-791192 do not show a constant age, however, it can be explained by the following: Y-791192 contains more abundant eucritic and less abundant diogenitic clasts compared with the Y-75032-type diogenites [4], which leads both relatively higher production of cosmogenic ^{38}Ar and lower production of cosmogenic ^{21}Ne due to more abundant target element of Fe and less abundant target

element of Mg, respectively. This tendency is seen in the cosmogenic ^{21}Ne and ^{38}Ar concentrations for Y-791192. The Y-791192 samples for which the bulk chemical compositions were determined [1, 7, 8] are, however, thought to have been more abundant in eucritic and less abundant in diogenitic clasts. This causes overestimation of production rate of ^{38}Ar and underestimation of ^{21}Ne to the sample measured for noble gases. The shifts of the ages (T_{21} and T_{38}) tending toward opposite directions are canceled out each other, hence the average of T_{21} and T_{38} agrees with the exposure age for Y-75032-type diogenites of 22 m.y. The concentration of cosmogenic ^{3}He in Y-791192 is somewhat lower than those in Y-75032-type diogenites (Table 1). On the diagram of ^{3}He/^{21}Ne versus ^{22}Ne/^{21}Ne ratios (Fig. 1), the datum of Y-791192 plots below the typical range for diogenites [6]. This seems to be due to ^{3}He loss from plagioclase, which may be more abundant in Y-791192, from where a part of cosmogenic ^{3}He might have been lost.

On the basis of ^{81}Kr method [10], we calculated upper limits of the terrestrial ages; <0.08, <0.02, <0.08 and <0.03 m.y. for Y-75032, Y-791000, Y-791199 and Y-791192, respectively. The cosmic-ray exposure ages and the terrestrial ages studied here and also K-Ar ages, which will be shown letter, support close relation between Y-75032-type diogenites and Y-791192. We suggest that Y-791192 must be a fragment of the same fall as Y-75032-type diogenites. The term of "Y-75032-type achondrites" is suitable for representing the group of Y-75032-type diogenites, Y-791192 and the other related achondrites as suggested by [4].

The concentrations of radiogenic ^{40}Ar are 1.75, 1.12, 1.22 and 2.92 x 10^{-6} cm^{3}STP/g for Y-75032, Y-791000, Y-791199, and Y-791192, respectively. Adopting K contents of 0.033, 0.025, 0.030 and 0.025 wt. % in literature [1, 6, 8], the K–Ar ages are obtained to be 1.1, 0.9, 0.8 and 1.8 b.y., respectively. All the ages show disturbance of radiogenic ^{40}Ar. Y-75032-type achondrites commonly have shock melt veins and maskelynitized plagioclase, indicating that these achondrites experienced shock event in the history of the crustal evolution before they finally ejected from the Vesta-like body by the last large impact [3, 4]. The preservation of these signatures implies that thermal annealing did not take place after their formation. The obtained K-Ar ages indicate the time for large shock event or an upper limit of the time.

A-881838 The cosmogenic noble gases in this diogenite are summarized in Table 1. The concentrations of ^{3}He, ^{21}Ne and ^{38}Ar do not differ largely from those in the Y-75032-tpe achondrites. Since the bulk chemical compositions have not been reported, the cosmic-ray exposure ages calculated with average chemical compositions of diogenites are tentatively shown. Because mineralogical feature is different between A-881838 (monomict [1]) and Y-75032-type achondrites (polymict), they must not be paired. However, they might have been ejected from a parent body by the same impact event occurred around 22 m.y. ago.

References

[1] Yanai K. and Kojima H. (1995) *Catalogue of the Antarctic Meteorites*, 230 pp., NIPR, Tokyo. [2] Score R. and Lindstrom M. M. (1990) *Antarctic Meteorite Newsletter* 13, 1. [3] Takeda H., Saiki K. and Ishi T. (1998) *Antarctic Meteorites* 23, 148-150. [4] Takeda H., Saiki K. and Ishi T. (1999) *Antarctic Meteorites* 24, 172-174. [5] Eugster O. and Michel Th. (1995) *Geochim. Cosmochim. Acta* 59, 177-199. [6] Welten K., Lindner L., Borg K., Loeken T., Scherer P. and Schultz L. (1997) *Meteoritics Planet. Sci.* 32, 891-902. [7] Jarosewich E. (1990) *Meteoritics* 25, 323-337. [8] Mittlefehldt D. and Lindstrom M. M. (1993) *Proc. NIPR Symp. Antarct. Meteorites* 6, 268-292. [9] Schultz (1986) *Mem. Natl. Inst. Polar res. Spec. Iss.* 41, 319-327. [10] Marti (1967) *Phys. Rev. Lett.* 18, 264-266. [11] Michel Th. and Eugster (1989) private com. to L. Schultz; in Schultz and Kruse (1989) *Meteoritics* 24, 155-172.

Table 1. Concentrations of cosmogenic noble gases and comic-ray exposure ages.

	^{3}He	^{21}Ne	^{38}Ar	T_3	T_{21}	T_{38}
	10^{-9}cm^{3}STP/g			m.y.		
Y-75032	390[#]	70.4[#]	11.9[#]	23.6	22.7	22.3
Y-791000	348[$]	71.1[$]	11.2[$]	21.0	22.0	21.7
Y-791199	351[$]	64.2[$]	10.9[$]	21.3	22.1	22.1
Y-791192	276	56.5	16.0	16.8	26.7	17.6
A-881838	400	89.8	8.58	(24.0)[&]	(21.7)[&]	(26.9)[&]

The production rates of cosmogenic ^{3}He, ^{21}Ne and ^{38}Ar were calculated based on the formula presented in [6], which are functions of bulk chemical compositions and ^{22}Ne/^{21}Ne ratio as a shielding indicator. Bulk chemical compositions are referred form [1, 6, 8]. [&] The exposure age is calculated using the production rate with mean chemical compositions of diogenites [6]. [#] The average of this work and [5, 9, 11]. [$] The average of this work and [6].

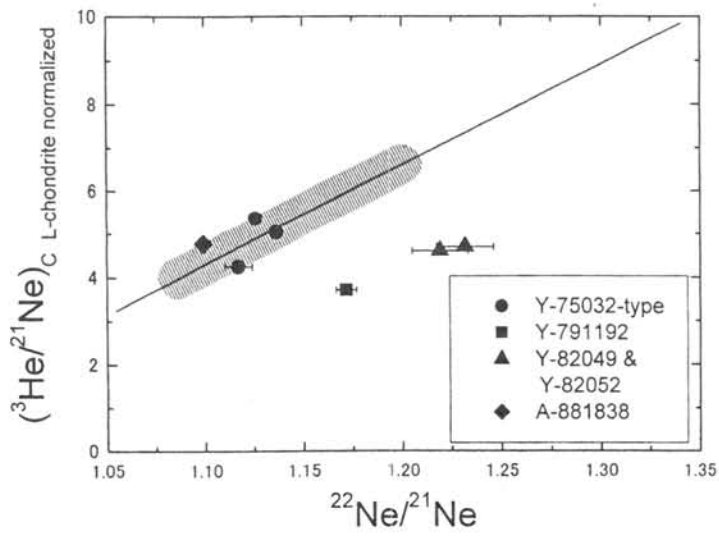

Fig. 1. Plot of ^{3}He/^{21}Ne vs. ^{22}Ne/^{21}Ne. The (^{3}He/^{21}Ne) ratio normalized to the chemical composition of L-chondrite is plotted. The correlation line for diogenites is shown, and the shaded area is the typical range for diogenites [6]. Two polymict HED achondrites also plot for comparison.

The ^{26}Al chronology of chondrules from the least equilibrated chondrites

S. Mostefaoui[1], N. T. Kita[1], S. Tachibana[2], H. Nagahara[2], S. Togashi[1], and Y. Morishita[1]
[1]Geological survey of Japan, 1-1-3 Higashi, Tsukuba 305-8567, Japan
[2]Geological Institute, University of Tokyo, Hongo, Tokyo 113-0033, Japan.

Introduction: The recent studies on the chronology of meteorites revealed that it did not take more than 10 million years (My) from the formation of CAIs and chondrules to the magmatism on the differentiated meteorite parent bodies. The usage of short-lived nuclide as a chronometer becomes important to resolve the short time difference (i.e., million years or less) between the formation of various meteoritic components. We have succeeded determining the initial $^{26}Al/^{27}Al$ ratios of ferromagnesian chondrules from both Semarkona (LL3.0) and Bishunpur (LL3.1) [1-3]. The excess ^{26}Mg from the decay of ^{26}Al (half life of 0.73 My) was detected in high Al/Mg glassy mesostasis and interstitial plagioclase in the chondrules by focusing the SIMS spot size down to 3- 5 μm [1-2]. From these studies, we found following results; (1) chondrules in both Semarkona and Bishunpur showed the initial $^{26}Al/^{27}Al$ ratios of between 5×10^{-6} and 1×10^{-5}, which correspond to the formation of these chondrules ~ 2 My younger than CAIs (the initial $^{26}Al/^{27}Al$ ratios ~ 4.5×10^{-5}). (2) The results are in the same range with two Al-rich chondrules measured by Russell et al. [4], indicating those ferromagnesian chondrules and Al-rich chondrules formed at the same time. (3) Other Al-rich chondrules from type 3.4 chondrites measured by Russell et al. [4-5] showed significantly lower initial $^{26}Al/^{27}Al$ ratios, which suggests that the Al-Mg system might be disturbed even in only moderately metamorphosed UOCs. For this reason, we should use highly unequilibrated chondrites like Semarkona and Bishunpur for the study of chondrule chronology using the ^{26}Al as a chronometer. Here we summarize the Al-Mg data from 16 chondrules from Semarkona and Bishunpur, including several new data from Bishunpur, and discuss possible relationships to their chemical and petrological characters.

SIMS Analyses: We used the Cameca IMS 1270 at the Geological Survey of Japan for isotopic analyses [1-2]. The primary ion of O_2^- was shaped to a diameter of ~5 μm. In order to avoid the high Mg ion intensity from the Ca-pyroxene inclusions, we carefully selected clean and inclusion-free areas, and observed Al and Mg ion images before each analysis. Three plagioclase standards (An95-An60) and four geological glass standards (basalt, andesite, and ryolite) are used to calibrate SIMS Al/Mg relative sensitivity. The averages of the relative sensitivity factors, defined as $F = (^{27}Al/^{24}Mg)_{SIMS}/ (^{27}Al/^{24}Mg)_{true}$, for plagioclase and glass are 1.26 and 0.88, respectively. These factors among plagioclase standards and glass standards agree within 10% from the average values.

Results and Discussion: List of the samples is shown in Table 1. Most of the chondrules are ferromagnesian chondrules. They contain either SiO_2-Al_2O_3 rich glassy mesostasis that

accompanying Ca-pyroxene microcrystallites and/or interstitial plagioclase. Many plagioclase-bearing chondrules show calcic plagioclase. Because of analytical requirement of measuring high Al/Mg area to detect ^{26}Mg excess, these samples are strongly filtered to plagioclase bearing chondrules and porphyritic chondrules with high Al/Mg glassy mesostasis, which constitute only 10% of the total chondrules. However, volume of Al-rich phase in these chondrules are between 5 % and 15%, so that they are not Al-rich chondrules. The range of molar FeO/(MgO+FeO) in olivine and pyroxene is between 0.01 and 0.3 and proportion of pyroxene phynocryst is between 20% to 100%, which is same as those of the majority of chondrules in Semarkona and Bishunpur.

The initial $^{26}Al/^{27}Al$ ratio for each chondrule was estimated by the least square fitting of the data in the ^{26}Al-^{26}Mg isochron diagram and shown in Fig. 1. These estimates obtained from low $^{27}Al/^{24}Mg$ data have a large uncertainty. Plagioclase data with low $^{27}Al/^{24}Mg$ ratios (20-30) need some cautions, because lower $^{27}Al/^{24}Mg$ ratios might be caused by micron-size pyroxene inclusions in the analyzed area. Assuming the homogeneous ^{26}Al distribution in the early solar system, the time relative to CAIs is calculated by the following equation;

$$\Delta t = \ln\left(\frac{(^{26}Al/^{27}Al)_{chondrule}}{(^{26}Al/^{27}Al)_{CAI}}\right)\times\frac{1}{\lambda_{26Al}} \qquad (1),$$

where $(^{26}Al/^{27}Al)_{CAI} = 4.5\times10^{-5}$ and $1/\lambda_{26Al} = 1.05My$. The initial $^{26}Al/^{27}Al$ ratios of 16 chondrules vary between 3×10^{-6} and 1.5×10^{-5}, corresponding to the time of formation between 1 and 2.5 My after CAIs. Compared to Semarkona data, Bishunpur data show a wider variation of the initial $^{26}Al/^{27}Al$ ratios, probably because we sampled wider variation of chondrule types for Bishunpur. There is no systematic variation of the initial $^{26}Al/^{27}Al$ ratios between Semarkona and Bishunpur, between Type I and Type II chondrules, and among the chondrules with different Al-rich phases. Previously, time difference between formation of CAIs and chondrules is estimated to be nearly 2 My [1-2, 4], while present results indicates that there are some chondrules (B1-C4, B2-C1, and B1-C56) formed as early as 1 My after CAIs. These data need re-evaluation because of low $^{27}Al/^{24}Mg$ ratios in plagioclase (B1-C4 and B2-C1) and measuring albitic plagioclase (B1-C56) which is more Na rich than the plagioclase standards (An95-An60). Yet, the relative time to CAIs varies at least 1 My among other chondrules, indicating that the duration of chondrule formation was as long as 1 My. This observation constrains the process of chondrule formation that it should occur over the time scale of 1My in the solar nebula.

Reference: [1] Kita et al. (1998) MAPS 33, A83-A84. [2] Kita et al. (1999) submitted to GCA. [3] Mostefaoui et al. (1999) MAPS A84. [4] Russell et al. (1996) Science, 273, 757-762. [5] Russell et al. (1997) LPSC 28th, 1209-1210.

Table 1. List of chondrules analyzed for the ^{26}Al-^{26}Mg study. "S" indicates Semarkona (LL3.0) and B1 and B2 indicate two thin sections of Bishunpur (LL3.1)

Chondrule type	Sample	Type	Mg#	Al-phase	$^{27}Al/^{24}Mg$	Ref
Semarkona Type I	S-CH3	IAB	97	An100	75-110	2
Bishunpur Type I	B2-C13	IB	91	An82 + Gl	17-29	
	B2-C17	IB	95	An19 +Gl	40-50	
	B2-C10	IAB	99	Gl	40	
	B2-C7	IAB	90	Gl	20-30	
Semarkona Type II	S-CH23	III	82	An100	50	2
	S-CH60	IIB	85	An34 + Gl	100-190	2
	S-CH4	IIAB	84	Gl	40-210	1
	S-CH36	IIAB	76	Gl	40-290	2
Bishunpur Type II	B1-C18	IIAB	77	An91	18-31	3
	B1-C4	IIAB	84	An90	15-37	3
	B2-C1	IIAB	81	An87	25-37	
	B1-C56	IIB	50-88	An30-An4	60-110	
	B2-C18	IIAB	78	An88 + Gl	20-170	
	B2-C12	IIAB	57-87	Gl	40-160	
	B2-C20	IIAB	82	Gl	25-50	

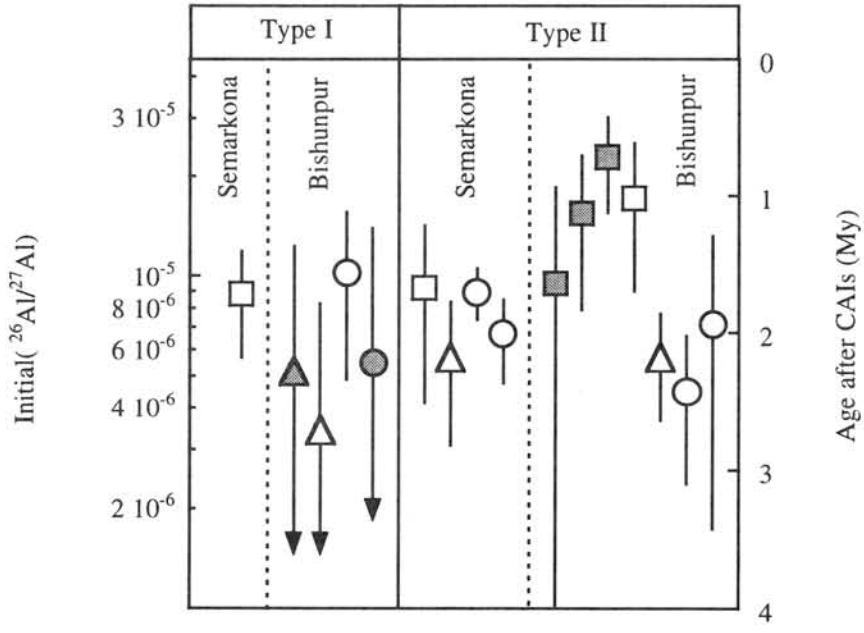

Fig.1. The initial $^{26}Al/^{27}Al$ ratios of chondrules and their formation time after CAIs. Symbols indicate the types of Al-rich phases in chondrules and their $^{27}Al/^{24}Mg$ ratios. Plagioclase (□ : $^{27}Al/^{24}Mg > 40$, ■ : $^{27}Al/^{24}Mg < 40$), Glass (○ : $^{27}Al/^{24}Mg > 40$, ● : $^{27}Al/^{24}Mg < 40$), Plagioclase and Glass (△ : $^{27}Al/^{24}Mg < 40$, ▲ : $^{27}Al/^{24}Mg > 40$)

Investigation of distribution pattern of carbonaceous matter in Kenna meteorite using laser Raman microscope

Tatsushi MURAE[1] and Yoshihiro NAKAMUTA[2]

1) Department of Earth and Planetary Sciences, Faculty of Sciences, Kyushu University, Hakozaki, Fukuoka 812-8581, Japan
2) University Museum, Kyushu University, Hakozaki, Fukuoka 812-8581, Japan

Kenna meteorite belongs to ureilites that contain significant amount of carbon. Berkley et al. showed the presence of three types of carbon polymorphs by X-ray diffraction analysis, namely graphite, diamond, and lonsdaleite (1). The carbonaceous material occurs as vein-like area interstitial to the silicate grains. Berkley et al. have reported that diamond and lonsdaleite occur as small (<1~3 μ m) anhedral to subhedral grains set in a fine granular graphite and silicate matrix (1). Nakamuta and Aoki have claimed that the C minerals may have originally crystallized as coarse-grained graphite together with olivine and pyroxene during igneous of metamorphic processes, and then part of the graphite was converted to diamond (2). This claim bases on the X-ray diffraction patterns of C-rich grains from several urelites, which contains carbonaceous matter as various mixing rate of graphite and diamond. Kenna has been suggested to be seriously shock-metamorphosed, and most of carbonaceous matter transformed to diamond.

Although the X-ray diffraction method clearly indicates the mixing state of crystalline diamond and graphite, it is difficult to obtain the information of none-crystalline carbonaceous matter and the distribution pattern of each carbon polymorph in the meteorite. We have characterized the carbonaceous matter in Kenna meteorite using laser Raman microscopic spectroscopy and examined the distribution pattern of the each carbonaceous matter.

The thin section of Kenna meteorite has been prepared using alumina powder in order to avoid contamination of diamond (2). The Raman spectra determined by JEOL JRS-2000DS microscopic spectrometer. The carbonaceous matter condensed in the grain boundaries observed as dark parts as shown in Figs. 1A and 1B. In the dark grain boundary, the shade of blackness is observed. The Raman spectra obtained at the point having mean shade of blackness as shown in the center of Fig. 1A showed the peaks at ca 1400 and 1370 cm^{-1} indicating no sign of graphite nor diamond. The Raman spectra of the darkest part in the C rich region (the center of 1B) showed a single sharp peak assigned to diamond (Fig.2B). By the observation using high magnitude objectives, we could find a bright particle that shows the Raman shifts at about 1330, 1370, and 1400 cm^{-1} with high intensity with low fluorescent back ground as shown in Figs 1C and 2C. The signal of graphite could be observed only from the limited part showing the texture as shown in Fig. 1D.

These observations are not compatible with the former indications on carbonaceous matter in ureilites. The major component of carbonaceous matter in Kenna is possibly the material such as shown in Fig 1C that gives the Raman spectra like as Fig. 2C. The identification of the material is under way including possibility of lonsdaleite. The difficulty of finding graphite may be explained by the broadening of Raman peaks by disordering of graphite plain structure and/or loss of graphite during the polishing processes. The mappings of the carbonaceous matter using individual Raman peaks in the carbon rich part in Kenna are on the way to obtain the information about the formation processes.

References:

(1) Berkley J.L. et al., G.C.A. 40 (1976) 1429-1437;
(2) Nakamuta, Y. and Aoki, Y., Meteoritics & Planetary Sciences, 35 (2000) in press.

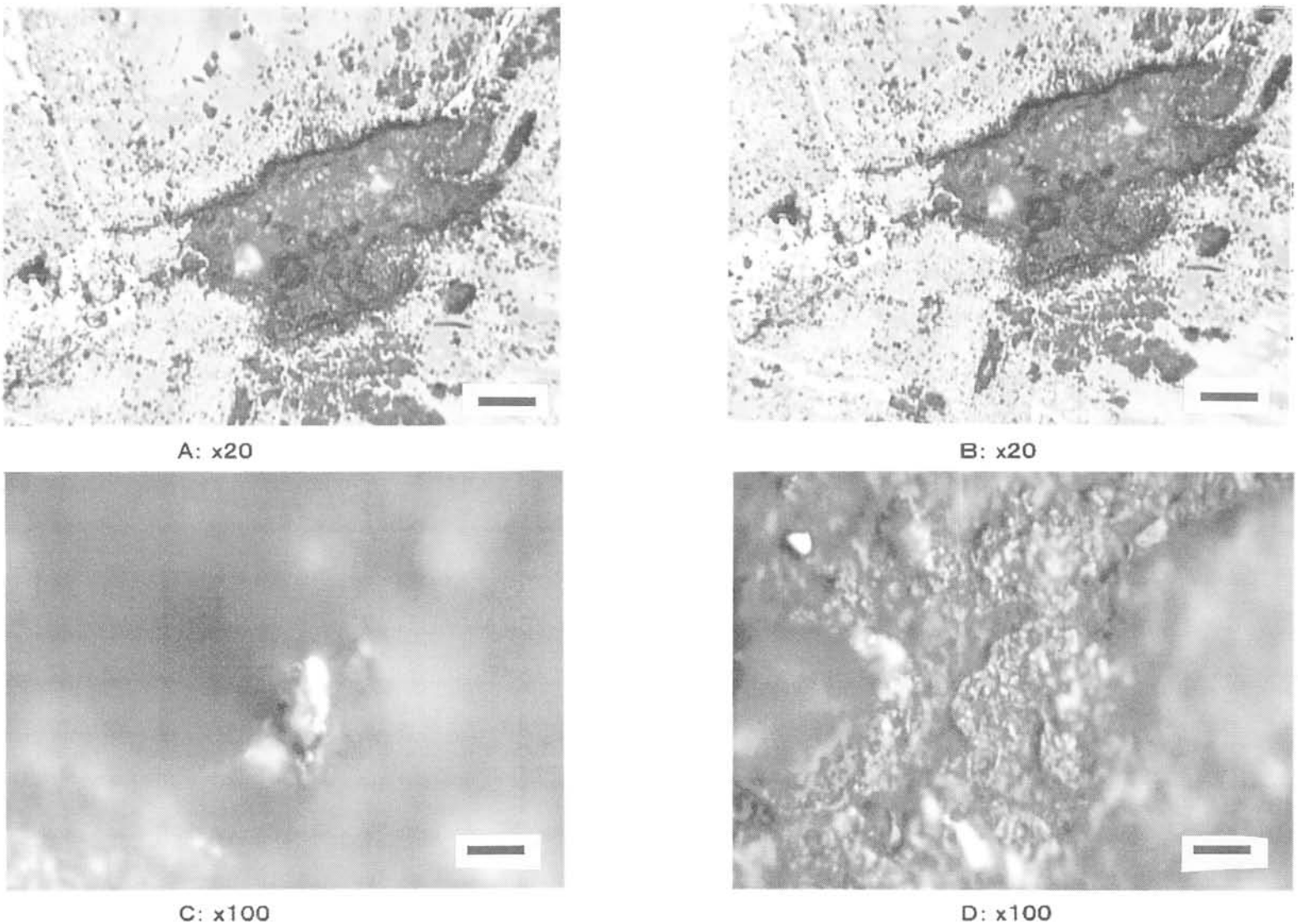

Fig. 1 Photomicrographs, A: The C rich part of Kenna meteorite, Raman spectrum A in Fig. 2 was obtained from the center showing dark brown, B: the same part as A, moved slightly to set the darkest part into the center from which the spectrum B was obtained, C: the particle that gives the most popular Raman spectra with high intensity in the C rich part, D: the part to show the Raman spectra of graphite in the C rich part. Scale bar equals to 50 μm for photos A and B, and 10 μm for photos C and D.

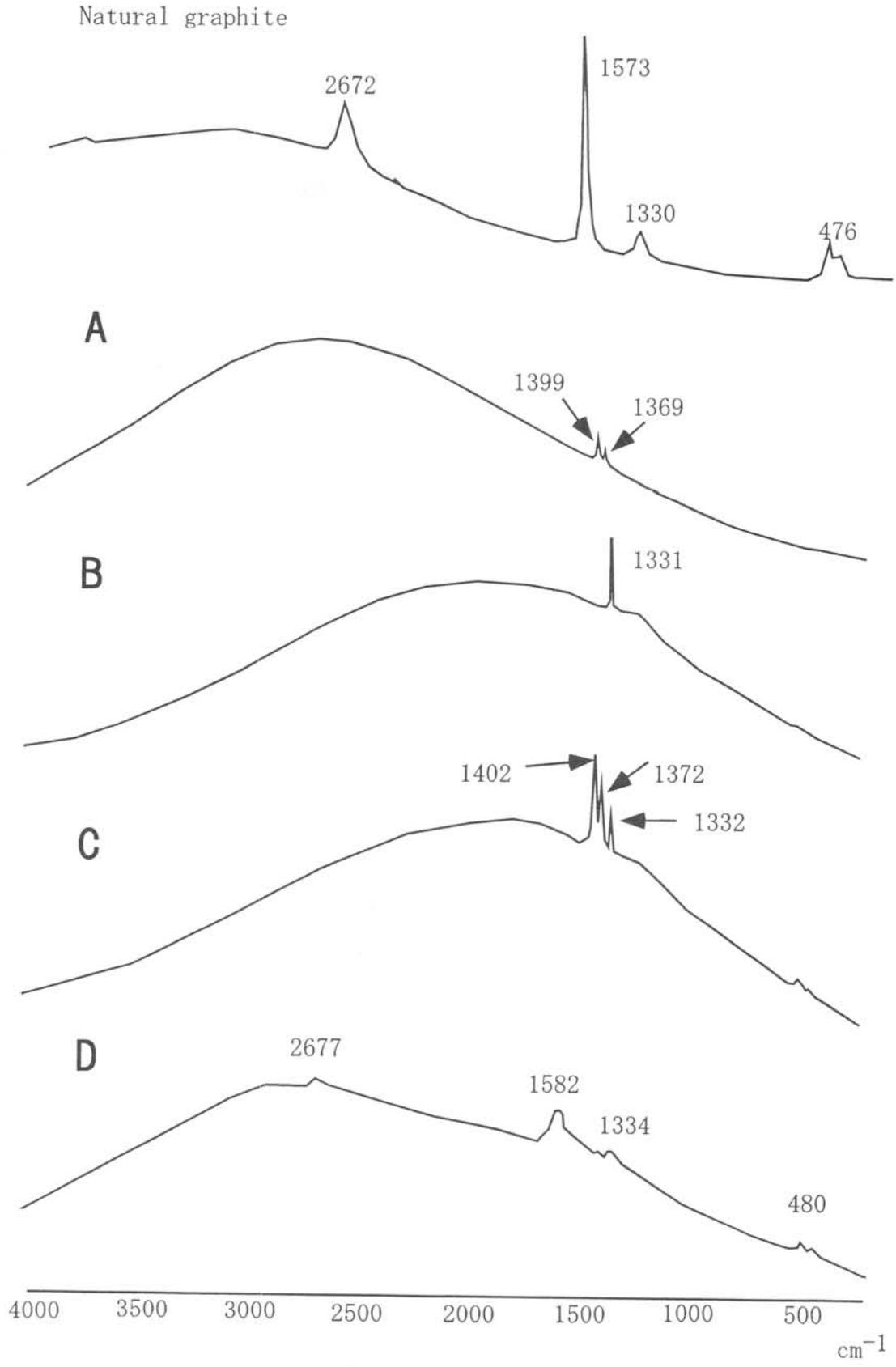

Fig. 2 Raman spectra of natural pure graphite and the spectra A, B, C and D are obtained at the central point of the photos A, B, C, and D in Fig. 1, respectively.

CHEMICAL FRACTIONATION DURING EVAPORATION IN THE PRESENCE OF AMBIENT GAS

Hiroko Nagahara and Kazuhito Ozawa
Dept. Earth Planet. Sci., Univ. Tokyo, Hongo, Tokyo 113-0033
(hiroko@eps.s.u-tokyo.ac.jp)

1. Introduction Evaporation and condensation are key processes responsible for cosmochemical fractionation. Chemical and isotopic fractionation during evaporation of condensed phases has been extensively studied in these ten years, and evaporation coefficients of major rock forming materials, such as forsterite, enstatite, Fe-metal, FeS, CAI melt, FeO melt, have been experimentally obtained. However, those data were obtained in vacuum experiments, and thus its applicability to natural processes is not necessarily clear because of the presence of nebular gas. In the present study, the effect of ambient gas on chemical fractionation during evaporation is studied experimentally, and the results are compared with theoretical consideration.

2. Experiments Evaporation experiments were carried out by using a Knudsen cell with varying size of orifice. Knudsen cell was designed to get the equilibrium vapor pressure of a substance with the weight loss through an orifice that should be small enough to keep equilibrium pressure in the capsule [1]. The equilibrium condition breaks when the orifice size is no longer small enough compared to the capsule size. In the present study, sealed platinum capsules, 3mm in diameter and about 1cm long were prepared. They are holed by 0.25 mm to 1.0 mm diameter orifices , which are located near the top of the capsule. A silicate portion of Jilin (H5) chondrite was prepared from the powdered sample (10-50 microns) by separating the magnetic portion. About 30 mg of the powder was used in each experiment. Experimental temperature was 1300°C and the duration was 40 minutes, 3 hours, and 10 hours. The sample in a capsule was put in a vacuum furnace described in [2], pre-evacuated at 500 °C for several hours to achieve high vacuum, heated to 1300°C at a rate of 30 deg/min, kept at 1300°C, and cooled to 1000 °C in 2 minutes by radiation. The change of sample weight was measured, and the chemical composition of the glass was analyzed.

3. Experimental Results Residues occupy the lower one third to half portion of the capsules and the bottom and wall are attached to the capsule, showing selective evaporation from the top surface. The weight loss ranged from about 1 to 5 mg with increasing orifice size. The residues show porphyritic texture with rectangular olivine and pyroxenes set in interstitial melt. Most olivine and pyroxenes are normally or reversely. The melt fraction is 20 - 30 vol.%, and the melt distributes almost homogeneously in all the experiments except for the very top surface. There are many pores with 30 microns to 2 mm in size. The chemical composition of the interstitial glass varies systematically as a function of the orifice size, position within a capsule, and experimental duration: they have become poorer in volatile elements (Na, K, and Si) and richer in refractory elements (Al, Ca, and Mg). The concentration of volatile elements decreases with increasing orifice size, duration, and distance from the capsule bottom (Fig. 1). The concentration of elements across a capsule from bottom to top is suggestive of diffusion-controlled evaporation.

4. Model Calculation Effects of back reaction on chemical fractionations are examined by a closed system evaporation model based on the Hertz-Knudsen equation for evaporation [3]. Evaporation of condensed phases increases the amount of metallic gas species in the ambient gas, which can cause back reaction. The back reaction suppresses chemical fractionation [3-5], in which congruent evaporation of a condensed phase proceeds in an isothermal condition. The model is generalized for evaporation from a stoichiometrically evaporating binary condensed phase. The degree of dust enrichment, the ratio of initial dust to the amount of dust required to attain gas-dust equilibrium, and the change of system volume are controlling parameters.

The calculation results show that elemental fractionation is progressively suppressed as evaporation proceeds due to the increase of the partial pressure of the species concerned in the ambient gas, of which rate is large when the chemical fractionation factor is much larger than or smaller than from unity. The fractionation is further suppressed when diffusion of the species in the condensed phase is slow.

5. Discussion The experimental results are examined in the relationship between partial pressure and evaporation rate of a species. The slope of the relationship represents the minimum value of the condensation coefficient, which is the kinetic barrier for condensation through back-reaction during evaporation. The results give the fractionation factors of 10 to 100 for Na and 2 to 20 for K between melt and gas and the condensation coefficient of 0.01 to 0.08 for Na and 0.02 to 0.14 for K. This is the first report for the chemical fractionation factor of Na and K for chondritic melt, and it enables us to evaluate the time scale of chemical fractionation or conditions to keep the chondritic composition for partially melted chondritic materials, such as conditions for chondrule formation or magma ocean of small or large planetary bodies.

6. References [1] Paule, R.C. and Margrave, J. L. (1967) in "High-Temperature Vapors (Margrave, J. L., ed.), Wiley, [2] Ozawa, K. and Nagagahara, H. (2000) *GCA* **64**, 939-955, [3] Nagahara, H. and Ozawa, K. (1996) *GCA* **60**, 1445-1459, [4] Tsuchiyama A. et al. (1999) *GCA* **63**, 2451-2466, [5] Nagahara, H. and Ozawa, K. *Chem. Geol.* (in press).

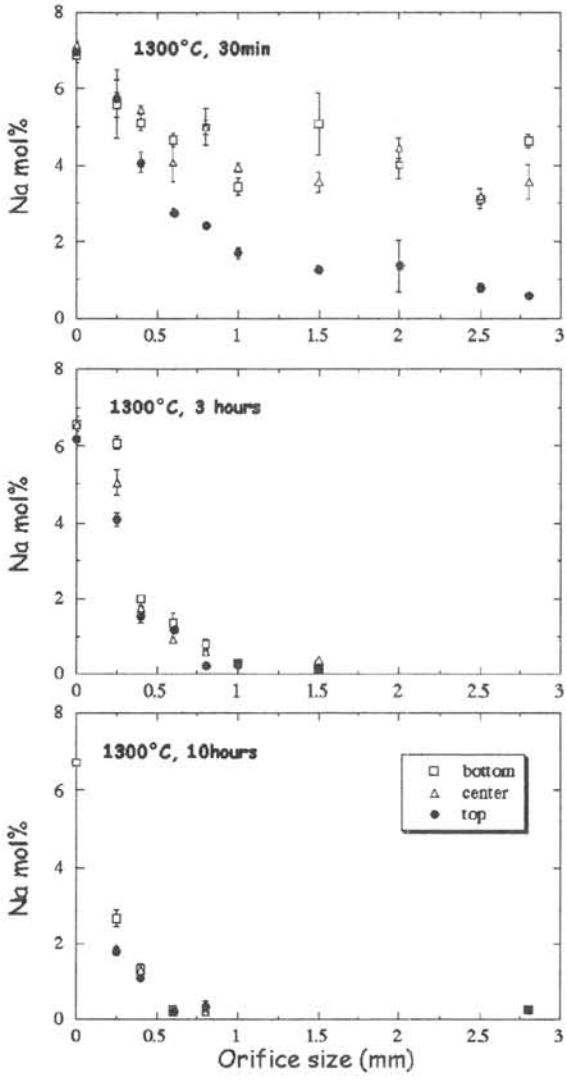

Fig. 1 Na concentration of partially molten chondritic melt in capsules with various sizes of orifice heated at 1300°C for 30min., 3 hours, and 10 hours.

Experimental Study on Interplanetary Dust Particles for the Rosetta Mission

K. Nakamura[1,8,*], W. Klöck[1], J. Romstedt[2], T. Grund[3], A. Greshake[4], W.Erfurth[5], M.Wiegand[5], H. Stenzel[5], B. Basnar[6], G. Friedbacher[6] , F.Syrowatka[7] & K.Tomeoka[8]

[1]*Institut für Geologische Wissenschaften, Universität -Halle, Domstraße 5, 06108 Halle/Saale, Germany*
[2]*Solar System Science Division ESA/ESTEC, Noordwijk, Netherlands*
[3] *Institut für Planetologie, Universität Münster, Germany*
[4]*Museum für Naturkunde, Humboldt-Universität zu Berlin, Germany*
[5]*Max-Planck-Institut für Mikrostrukturphysik, Weinberg 2, 06120 Halle/Saale, Germany*
[6]*Institut für Analytische Chemie der TU Wien, Getreidemarkt 9/151, A-1060 Wien, Austria*
[7]*Zentrum für Materialwissenschaften, Universität Halle, Germany*
[8]*Dept. of Earth & Planetary Sciences, Kobe University, Kobe, 657-8501 Japan*

Introduction: The cometary mission Rosetta proposed by ESA will be launched in the year 2003, and after its eight-year cruise the satellite will rendezvous with comet 46P/Wirtanen and follow the near-nucleus phase at a heliocentric distance of about 3.25 AU[1]. The prime scientific objective of the mission is to study its nucleus and environment in great details for a period of nearly two years. Investigating the pristine comet should shed light on the origin of comets, the relationship between comets and interstellar materials and its implications with regard to the origin of the Solar System since comets are believed to be the most primitive bodies in the solar system [2].

MIDAS – **M**icro **I**maging **D**ust **A**nalysis **S**ystem - will be one of the instruments onboard Rosetta which is dedicated to the micro-textural and statistical analysis of cometary dust particles. The MIDAS experiment is based on an atomic force microscope (AFM) combined with a dust collector expected to image individual particles with a resolution of a few nanometer [3]. In order to interpret the images obtained by the MIDAS AFM, a sophisticated database of morphologies and correlated internal textures of various materials is needed as a reference. Experiments are under way on artificial cometary analogues [4] as well as on interplanetary dust particles (IDPs) [5,6].

Samples and Experiments: IDP samples collected in the stratosphere by NASA are used for the MIDAS pre-mission experiment. IDPs have an average chemical composition similar to the bulk composition of chondrite meteorites [7], although carbon and some volatile elements are found in excess of CI-chondrite abundances [8]. There are significant differences between these tiny particles and meteorites with regard to crystallography, mineral chemistry, mineralogy and isotopic properties. Particles of one particular group are considered to be the most likely candidates for cometary dust [9].

In our study, first IDPs are carefully cleaned from the collecting medium and mounted on substrates suitable for imaging. Without conductive coating they are imaged in FE-SEM with 1-9kV acceleration voltage and/or in environmental SEM at 1.4- 2.6 Torr and 9kV, and subsequently the particles are studied by AFM. After AFM imaging the particles are coated with a thin layer of Cr, or C for high resolution FE-SEM imaging. After AFM and SEM studies, the IDPs are finally sectioned with an ultramicrotome for TEM studies. With TEM techniques interior properties of the IDPs are characterized. Over 30 individual IDPs have been examined for this study so far.

Results and Discussion:

L2006J2 is a 20 μm-size silicate sphere. The linear arrangements of magnetite crystallites are all over on the surface(Fig.1). On this kind of smooth surface IDPs, information from FE-SEM and AFM images can be easily correlated and interpreted. Octahedral shapes of magnetite crystallites are visible on the AFM amplitude image (Fig.1a).

L2005U2 is a 10x12μm size Fe-sulfide particle (Fig.2a). An interesting component of the AFM image is the feature of 120 degree angles (Fig.2b) up to 500nm size which are not evident in the FE-SEM images (Fig.2a). Fig.2c is a secondary electron image of two intergrown pyrrhotite ($Fe_{1-x}S$) grains separated from *Orgueil*, CI chondrite, which shows similar 120^{O} angles. The TEM study reveals that this particle is dominated by pyrrhotite containing a small area of carbonaceous material. Pyrrhotite is based on the troilite structure, but with ordered Fe vacancies yields a host of hexagonal to monoclinic structures, also exhibiting a variety of polytypism and twinning [10]. AFM should help to identify possible mineral compounds of IDPs. Ni-containing monosulfide suggests that this particle is of extraterrestrial origin[11].

L2006G9 is a 8x16μm size very porous chondritic IDP. Each of the tiny building blocks is clearly visible in the AFM image. The AFM images display fluffy assem-

*current mailing address: Division of System Science, Graduate School of Science and Technology, Kobe University, Kobe, 657-8501 Japan. e-mail address: keiko@shidahara1.planet.sci.kobe-u.ac.jp

blages of 10-100 nm-sized regular features which are most likely the basic building blocks of the porous IDP.

L2036H4 (37x 28μm) is one of the largest chondritic IDPs that we have studied. It shows compact smooth morphology. In AFM images euhedral platelets possibly *card house structure* [12] of layer silicates are ubiquitous.

L2006E14 is a 12x17μm size chondritic particle. E14 contains large amount of sulfides, mainly pyrrhotite and pentlandite, Ni contents up to 10 atomic %. Only a small amount of saponite is present, hosting some carbonates.

L2006I2 is a 10x17μm size chondritic IDP. A whole scan image with AFM is available since this particle has relatively smooth surface. Some euhedral platelets are visible on AFM images.

L2008E4 displays small rectangular crystallites attached to the surface and larger crystals and some fine-grained material seems to make up the interior. The morphology as well as the chemical composition of this IDP is unusual, because micrometer-sized euhedral crystals are not common in the interior of IDPs, and the particle contains high amounts of sodium and phosphorus (8 and 14 wt% respectively). The TEM study shows the presence of hexagonal and rectangular euhedral crystals varying from several hundred nanometers to several micrometers in size throughout the whole particle.

Summary: Although AFM technique are limited with height difference, AFM images reveal fine structures, especially on rather smooth surfaces. In these cases information from FE-SEM images and AFM images can be easily correlated and interpreted.

On very porous IDPs FE-SEM images and AFM images do not seem to correlate very well. There are several reasons for this problem: *1.* The imaging angle is variant at the different methods. The secondary electron detector is set 45 degree right in the FE-SEM, although AFM scans samples vertically. *2.* While electrons penetrate into the sample, the SEM image does not provide direct information of the sample surface, whereas AFM does. *3.* The resolution of FE-SEM images of uncoated samples is not high enough to identify unambiguously characteristic details seen in the AFM images, and in most cases, the imaging angle is different. *4.* Due to the porous nature and extremely rough topography of some IDPs studied, AFM images contain artifacts, which are not readily recognizable. Therefore misinterpretations of sizes and shapes of the basic building blocks as well as of specific mineral textures are possible.

However, these uncertainties should be of less importance in the case of submicronmeter size particles. Suggested building blocks of cometary interplanetary dust particles are in the size range from a few nm up to a few 100 nm. Expected particle sizes of the dust of comet Wirtanen are mainly in the submicronmeter range. Further experiments are planned to study porous particles in the appropriate size range expected on the MIDAS collectors.

TEM investigations help to characterize the particles in more details, and are indispensable to determine internal texture, grain sizes, mineralogy and porosity of the particles studied.

The unique capabilities of AFM comprise a nm scale resolution and a true three-dimensional data set. On that data the power of image processing software can be applied, and used to determine several material parameters. From the latter clues about the true nature of the dust can be deduced.

✓ Determination of grain size and volume
➪ Dust statistics

✓ Dimension and angle measurements on crystalline structures ➪ mineral identification

✓ roughness parameter on flat crystal surfaces
➪ space weathering and/or interaction with gas and liquid phases in the cometary environment

References:

[1] Schwehm G. et al. (1995) *ESA-SP-1179,* 28-30. [2]Whipple F.L. (1987) *Astron. Astrophys.*, 187, 852-858. [3] Riedler W. et al. (1998) *Adv. Space Res., 21,* 1547-1556. [4] Rotundi A. et al. (2000) *Planet Space Sci.* (in press) [5] Nakamura K. et.al.(1999) *Meteoritics & Planet. Sci., 34,* A85-86. [6] Romstedt J. et.al.(1997) *Scanning, 19,* 142-143. [7] Klöck W. & Stadermann F.J., (1994) *AIP Conf. Proc. 310,* 51-87 Amer. Inst. Phys., N.Y.. [8] Thomas K.L., et al., (1993) *Geochim. Cosmochim. Acta,* 57, 1551-1566. [9] Jeswiak D.J., et al. (2000) *LPSC**XXXI**,*1500 (CD-ROM*)*. [10] Vaughn D.J. & Craig J.R. (1978) *Mineral Chemistry of Metal Sulfides. Cambridge Univ. Press.* [11] Warren J.L. & Zolensky M.E. (1994) *AIP Conf. Proc. 310,* 245-253. Amer. Inst. Phys., N.Y.. [12] Izumi Y., et al. (1994) *Chem. Soc. of Japan 21, Microporous Crystal **12**,* Organic reaction Using Clay Catalysts113-126. [13] Greshake A. et al. (1998) *Meteoritics & Planet. Sci. **33**,* 267-290.

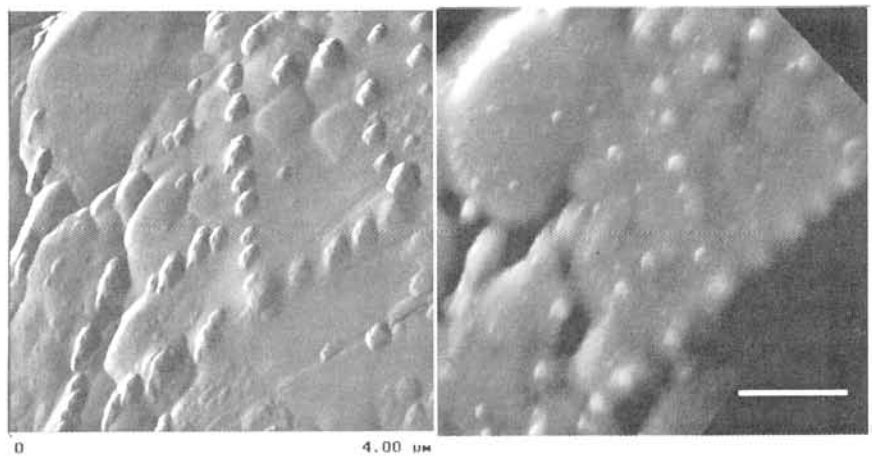

L2006J2: [Fig.1a left] AFM amplitude image of IDP *L2006J2*. Octahedral shapes of magnetite crystallites are visible. **[Fig.1b right]** FE-SEM image of the same area as Fig.1a. Scale is the same in both images 4x4µm: the scale bar equals 1 µ m. The sample was coated with carbon for FE-SEM imaging.

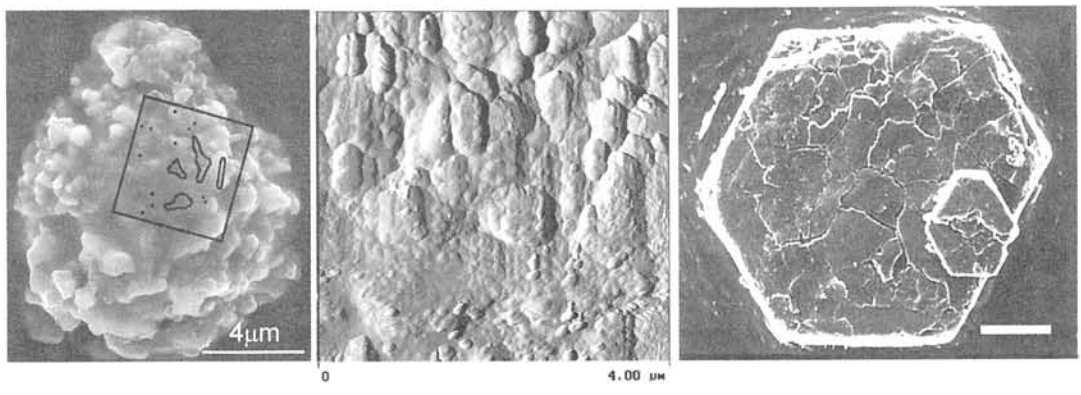

L2005U2: [Fig.2a left] FE-SEM overview of IDP L2005U2. Scale bar equals 4µm. **[Fig.2b middle]** 4x4µm AFM amplitude image of the boxed area in Fig.2a. The features of 120 degree angles (Fig.2b) up to 500nm size are ubiquitous which are not evident in the FE-SEM images. **[Fig.2c right]** Secondary electron image of two epitaxially intergrown pyrrhotite grains separated from Orgueil [13]. Scale bar equals 10µm.

THE KOBE METEORITE; CLASSIFICATION AND CONSORTIUM STUDIES

Noboru NAKAMURA[1], Hideyasu KOJIMA[2], Hiroshi HARAMURA[2], Kazushige TOMEOKA[1], Robert N. Clayton[3] & Toshiko K.. Mayeda[3] Graduate School of Science and Technology, Kobe University, Nada, Kobe 657-8501, Japan; [2]Antarctic Meteorite Research Center, National Institute of Polar Research, 9-10, Kaga, Itabashi, Tokyo 173-8515, Japan; [3]Enrico Fermi Institute, University of Chicago, Chicago, Illinois 60637, USA

Introduction The Kobe meteorite fell on 26th (local time: about 20:21) September, 1999 in Kita-ku, Kobe (the northern part of Kobe City). It has been reported that a fireball was widely observed in Kobe City and the surrounding local areas. It broke into more than 20 pieces after penetrating the roof of house of Mr. Ryoichi Hirata. The meteorite fragments recovered (totaling 136g) were delivered to the Kita Police Headquarters soon after the fall. In the next morning they were transferred to the Forensic Science Laboratory (FSL), Hyogo Prefectural Police Headquarters, where undestructive inspections and analyses were carried out under guidance of N. Nakamura. One of the largest pieces, the fragment A (65g), was promptly transferred to the Low-Level Radioactivity Laboratory, Kanazawa University, for measurements of cosmic-ray induced radioactivities. The γ-ray measurements were started from 21hrs after the fall and continued for 4 days [1]. On the other hand, two small chips (which were donated to N.N. from the finder) were examined petrographically at Kobe University and National Institute of Polar Research and the meteorite was tentatively classified as CK4 [2]. Two large fragments, Kobe C and E (total mass: about 17g) were on loan from the finder to N. N. for the consortium studies, and the remainders have been loaned by Kobe Science Museum for 6 months exhibition.

Kobe is the first observed fall of the carbonaceous chondrite in Japan and the second observed fall of the metamorphosed carbonaceous chondrite, Karoonda-type (CK-normal group) in the world. More than fifteen CK meteorites including four CK-anomalous meteorites have been reported until recent [3,4,5]. Except for a few cases, e.g. Kallemeyn et al. (1991)[3], however, the systematic examinations of CK group have been quite limited and their origins and evolution, e.g. interrelationship between CK-normal and CK-anomalous groups and relationships with CV-CO groups, and the thermal evolution of their parent bodies, have been poorly understood. Under such circumstances, the Kobe meteorite consortium have been arranged to study for a wide range of propeties of Kobe at leading laboratories in Japan and USA.

Initial processing, Petrography and Bulk chemical compositions During initial inspections of Kobe fragments A and B, chondrule-like objects, blackened clasts (or mineral fragments) and fine-grained white objects are easily observed with the naked eye on the dark broken surfaces. Two PTSs prepared from small chips (0.54g and 0.41g) were examined petrographically. Kobe contains chondrules and mineral fragments set in a translucent recrystallized matrix. Chondrules (0.2-2mm in size) are well to moderately defined. Matrix consists of abundant olivine, plagioclase and magnetite, and minor amounts of low-Ca pyroxene, pentlandite and high-Ca pyroxene. Olivine is very homogeneous, averaging Fa 31.4 (%MD=1.1), both in chondrules and matrix. Both low- and high-Ca pyroxenes are also homogeneous, averaging Fs25.8 (%MD=1.8). In contrast, plagioclase is heterogeneous,

ranging from An content of 26 to 76. Petrographically Kobe is classified as CK4 (see details in [6]).

Results of wet-chemical analyses of Kobe E, probably representative of Kobe specimen, are presented in Table 1. It is noted that abundances of major and minor elements in Kobe are substantially in agreement with those in Karoonda (CK4) and are all within the range of CK meteorites [3]. In the Zn/Mn-Al/Mn diagram, Kobe is plotted just in the CK region [7]. On the other hand, isotope dilution analyses indicate that the Kobe E has an anomalous REE pattern (indicative of vapor fractionations) which is similar to those of some type of Murchison hibonite-bearing inclusions (see details in [8]), while the bulk specimen from the different fragment (Kobe C) shows a flat REE pattern typical of CK group. The anomalous REE pattern of Kobe E suggests that Kobe contains a component (or components) carrying high-temperature nebular condensates. This is the first case of vapor-fractionated REE observed in the CK-normal group. The bulk chemical composition of Kobe is, in general, consistent with chemistry of CK group.

Table 1. Compositions (wt%) of Kobe and other CK group meteorites.

	Kobe E	Karoonda [3]	CK range [3]
SiO_2	33.36		
TiO_2	0.2		
Al_2O_3	2.91	3.14	2.95-3.14
Fe_2O_3	9.58		
FeO	18.23		
MnO	0.21	0.18	0.18-0.19
MgO	25.9	25.0	24.2-25.0
CaO	2.43	2.43	2.29-2.53
Na_2O	0.38	0.42	0.41-0.45
K_2O	0.03	0.04	0.03-0.36
H_2O (±)	0		
P_2O_5	0.25		
Cr_2O_3	0.57	0.55	0.51-0.55
(Fe,Ni,Co)S	6.41		
Total	100.47		
(total Fe)	23.63	24.00	22.10-24.40
(total Ni)	1.29	1.36	1.08-1.40
(total Co)	0.052	0.068	0.052-0.071

Oxygen isotopic compositions A duplicate analysis of oxygen isotopes was carried out for Kobe. The final analytical result is; $\delta\,^{18}O = -1.50$, $\delta\,^{17}O = -5.54$. In a three oxygen-isotope diagram, Kobe falls near the high 16-O end of the CK range and is certainly in the carbonaceous chondrite range [9]. It most closely resembles the CV chondrites, indicating a relationship with CV chondrites.

Curatorial Processing of Kobe Kobe C and Kobe E, weighing 13.6 and 3.7g, respectively, have been processed for consortium studies at Kobe University. About 50% of the surface area of Kobe C

(3.2x1.3cm in size) was covered by fusion crust which has been partially coated with white materials contaminated during penetrating the roof and ceiling boards. On the other hand, Kobe E had no fusion crust and any contaminant has been noted. No pre-treatment (such as washing with solvents) has been done for Kobe E. The 3.7g fragment was broken into several pieces using an agate mortar, and a few pieces (totaling 1.4g) was transferred to NIPR (H. Kojima), where the sample was pulverized and the major part (1.17g) was subjected to wet-chemical analyses. An aliquot (150mg) of the same powder was analyzed at Tokyo Metropolitan University (M. Ebihara) for major and trace elements by activation analyses [7] and a 66mg-aliquote was also analyzed for trace elements including REE by isotope dilution at Kobe university [8].

For processing of Kobe C, a considerable care has been directed to avoid possible contamination of house materials. Before breaking, the white materials stick to the fusion crust of Kobe C was carefully scraped off using a stainless steal knife. The inner fresh part was broken using an stainless steal needle in an agate mortar. Finally, the fragment C was chipped into 6 pieces; C-1, -2, -3,, -4,, -5 and –6. The most inner chip C-3 (12mm inside the fusion crust) was washed with clean alcohol in an ultra-sonic bath twice and crushed into coarse grains ($\Phi \leq$60mesh) but no sieving was applied. An aliquot (C-3mix-1; 0.65g) from this sample and small pieces (C-3-1; 95mg) were allocated to J. Matsuda (Osaka University) for analyze of rare gases [10]. An aliquot (C-3mix-2) of the same chip and a few pieces (C-2; 107mg) including fusion crust were sent to K. Nishiizumi (University of California) for analyses of cosmogenic nuclides Also aliquots of C-3mix were analyzed by Ebihara group and by Nakamura group. In addition to analyses of Kobe, pieces of the roof and ceiling boards were also analyzed by Ebihara group to detect any possible contamination .

The chip C-5-1 (1.14g) which includes fusion crust was initially examined by A. Tsuchiyama at Osaka University for X-ray computed topography (CT) to obtain three-dimensional structure of objects [11]. Based on CT-image obtained at Osaka University, the chip C-5-1 was cut into seven slices by T. Nakamura at Kyushu University for laser-ablation rare gas analyses (T. Nakamura; Kyushu University), the ion probe isotopic analyses of hydrogen, carbon and nitrogen by N. Sugiura (University of Tokyo), and oxygen and magnesium isotopes by H. Hiyagon (University of Tokyo). Mineralogical analysis using transmission electron microscopy by M. Kitamura (Kyoto University), analyses of organic materials by A. Shimoyama (Tsukuba University) and examinations of natural remnant magnetization by M. Funaki (NIPR) are also on going for the Kobe meteorite.

Acknowledgement-We thank Mr. Ryoichi Hirata for providing the Kobe meteorite samples for consortium studies.

References [1] Komura, K. et al. (2000), Antarctic Meteorites XXV (this volume); [2] Nakamura, N. et al. (2000), Lunar Planet Sci. 31, no.1234 (abstract); [3] Kallemeyn, G.W. et al. (1991), Geochim. Cosmochim. Acta 55, 881-892; [4] Scherer, P. & Schultz, L.(2000), Meteorit. Planet. Sci. 35, 145-153; [5] Zipfel, J. et al. (2000), Lunar Planet Sci. 31, no. 1668; [6] Tomeoka, K. et al.(2000), Antarctic Meteorites XXV (this volume); [7] Oura, Y. et al. (2000), Antarctic Meteorites XXV (this volume); [8] Hirota, Y. et al. (2000), Antarctic Meteorites XXV (this volume); [9] Clayton, N. R. & Mayeda, T. K (1999) Geochim. Cosmochim. Acta 63, 2089-2104.; [10] Matsumoto, Y. et al. (2000), Antarctic Meteorites XXV (this volume); [11] Tsuchiyama, A. et al. (2000), Antarctic Meteorites XXV (this volume).

Thermal Metamorphism of CM Carbonaceous Chondrites deduced from Phyllosilicate Decomposition and Trapped Noble Gas Abundance

Tomoki Nakamura, Fumio Kitajima, and Nobuo Takaoka

Department of Earth and Planetary Sciences, Faculty of Sciences, Kyushu University 33, Hakozaki, Fukuoka 812-8581, Japan

Many CM chondrites among Antarctic meteorite collection have experienced thermal metamorphism after aqueous alteration probably on the meteorite parent bodies [e.g., 1-10]. It is still uncertain when and how the metamorphism took place, but such heated CM chondrites are samples of hydrous asteroids formed by advanced evolution processes compared with normal CMs. In the course of metamorphism volatile elements and molecules were subjects to be lost from constituents of hydrous asteroids, thus CM chondrites are expected to retain the records of devolatilization. We have performed a combined study of CM chondrites to investigate dehydration reaction of hydrous minerals, thermal loss of trapped noble gases, and graphitization of carbonaceous macromolecular matter. In this paper, the results of mineralogical and noble-gas study are presented. The results of analysis of carbonaceous matter are reported in an another paper [11].

X-ray diffraction analysis of matrices of CM chondrites has been done using a Gandolfi camera with a monochromated synchrotron X-ray microbeam at the beam line 3A in the Photon Factory Institute of Materials Structure Science, High Energy Accelerator Research Organization. Processing technique to obtain powder diffraction data is shown in [12]. Noble gases, He to Xe, were analyzed by stepped pyrolysis using a MM5400 mass spectrometer at Kyushu University equipped with a Ta furnace and a stainless steel purification line "Jack and the Beanstalk" [13].

The results of noble gas analyses indicate that Y-793321 and A-881458 are solar-gas rich samples, while Murray, A-881334, and Y-86789 are solar-gas poor samples. Concentration of trapped ^{22}Ne (solar + Ne-A) is much higher in Y-793321 than that in A-881458, due to a large contribution of solar gases. Solar gases are usually released at low temperature because of shallow implantation depth into minerals. In fact, Ne in the low temperature steps of the two meteorites consists mostly of solar gases judging from isotopic ratios. But a release pattern of Y-793321 shows a reduction of solar-gas concentration extracted at low temperatures of 250 and 400 °C (Fig.1a). The reduction can be ascribed to loss of solar gases by heating at approximately 400 °C.

Concentrations of primordial Ne in the solar-gas poor samples decrease in the order of Murray, A-881334, and Y-86789: those of Muray are higher than those of Y-86789 by one order of magnitude. Thus it is estimated that the degree of heating increases from Murray, A-881334, and to Y-86789. When the primordial Ne is

partitioned into Ne-A2 and Ne-E, concentrations of the former decrease with the increasing degree of heating mainly due to reduction of concentrations extracted in low temperature steps, whereas those of the latter are constant among the three meteorites (Fig. 1b). This indicates that carrier phase of Ne-E is more resistant than that of Ne-A2 during the heating of CM chondrites.

X-ray diffraction analysis indicates diverse mineralogy of matrices of CM chondrites. Parts of the results are shown in Fig. 2. In principle, the degree of decomposition of phyllosilicates increases from Fig.2a to 2f. Y-791198 (Fig. 2a), Cold Vokkeveld, A-881458 (Fig. 2b), and Y-793595 (Fig. 2c) show similar diffraction patterns: very strong serpentine and magnetite, variable amounts of tochilinite and mixed layered minerals of serpentine and tochilinite, and minor amounts of calcite, olivine, and low-Ca pyroxene. The presence of serpentine, tochilinite, and mixed-layered minerals in these four samples indicates that these samples escaped significant heating. According to the T-T-T diagram developed by Akai (1992) [3] by experimental heating of Murchison, these samples experienced no heating or heating up to 300°C at most. The results are consistent with those of Akai and Tari (1997) [14]. In the TEM work of A-881458 and Y-793595 [14], 14-Å diffraction maxima were reported as a features of incipient decomposition of serpentine, but in our X-ray diffraction analyses such 14-Å diffraction was not observed (Figs. 2a-c). This is probably due to low ordering of the 14-Å phase or heterogeneous distribution of the phase in the matrix.

The reflections of serpentine, tochilinite, and mixed layered minerals disappeared and other reflections from olivine and low-Ca pyroxene are weak in the diffraction patterns of Y-793321 (Fig. 2d) and A-881334. This suggests that these samples consist mainly of amorphous material formed by break down of phyllosilicates. Secondary olivine and low-Ca pyroxene formed at the expense of phyllosilicates [e. g., 15] are rare. Therefore, these two samples were heated to 300-500°C based on the T-T-T diagram [3], which is consistent with the temperature estimated from trapped noble gas abundance. B-7904 (Fig. 2e) and Y-86789 (Fig. 2f) show completely different diffraction patterns from other samples: very strong olivine, troilite, taenite, and kamacite and weak low-Ca pyroxene. The reflections of olivine and low-Ca pyroxene are broad, suggestive small grain size of these minerals. The peak center positions of olivine (130) reflection indicate that olivine contains FeO. The broad olivine and low-Ca pyroxene reflections are characteristics of secondary silicates formed by the replacement of phyllosilicates. The presence of secondary olivine and low-Ca pyroxene in B-7904 and Y-86789 indicates that they were heated to temperature higher than 700°C based on the T-T-T diagram [3].

A noteworthy feature of strongly heated specimen B-7904 (Fig. 2e) and Y-86789 (Fig. 2f) that sets them apart from other less heated ones (Fig. 2a-d) is presence abundant kamacite and taenite. In the less heated specimen magnetite is abundant (Fig. 2a-d). This indicates that oxygen fugacity in the portions of asteroids where the

meteorites were located decreases with increasing temperatures. The lowered oxygen fugacity at high temperatures was probably realized by the coexisting carbonaceous material [11]. During and after dehydration of phyllosilicates the carbonaceous material acted as a reducing agent to facilitate dehydration reactions through the reaction, $2C+2H_2O=CO_2+CH_4$ [16], and to lower oxygen fugacity to allow formation of iron metal from iron oxide. At temperature higher than 700°C, graphitization of carbonaceous macromolecular matter proceeded in CM chondrites [11]. Therefore, thermal metamorphism experienced by B-7904 and Y-86789 occurred at oxygen fugacity below graphite stability limit [16] and IW buffer [17]. The reduced condition may explain why SiC, probable Ne-E carrier, in CM chondrites is resistant to heating like those in Enstatite chondrites [18].

Acknowledgments: We thank Dr. Tanaka and Messrs. Nozaki and Mori for supports during X-ray diffraction analysis at High Energy Accelerator Research Organization.

References:[1] Akai, J. (1988) *Geochim. Cosmochim. Acta*, **52**, 1593-1599. [2] Akai, J. (1990) *Proc. NIPR symp. Antarctic Met.*, **3**, 55-68. [3] Akai, J. (1992) *Proc. NIPR symp. Antarctic Met.*, **5**, 120-135. [4] Tomeoka, K., Kojima, H. and Yanai, K. (1989) *Proc. NIPR symp. Antarctic Met.*, **2**, 55-74. [5] Tomeoka, K. (1990) *Proc. NIPR symp. Antarctic Met.*, **3**, 40-54. [6] Paul, R. L. and Lipschutz, M. E. (1990) *Proc. NIPR symp. Antarctic Met.*, **3**, 80-95. [7] Kimura, M. and Ikeda, Y. (1992) *Proc. NIPR symp. Antarctic Met.*, **5**, 74-119. [8] Ikeda, Y., Noguchi, T. and Kimura, M. (1992) *Proc. NIPR Symp. Meteorites*, **5**, 136-154. [9] Matsuoka, K., Nakamura, T., Nakamuta, Y. and Takaoka, N (1996) *Proc. NIPR symp. Antarctic Met.*, **9**, 20-36. [10] Wang, M. S. and Lipschutz, M. E. (1998) *Meteoritics Planet. Sci.*, **33**, 1297-1302. [11] Kiatajima F., Nakamura T., Takaoka N., and Murae T. (2000) in this volume. [12] Nakamura T., Nozaki W., Noguchi T., Nakamuta Y., Tanaka M., and Takaoka N. (2000) in this volume. [13] Nakamura, T. and Takaoka, N. (1999) *Antarctic Met. Res.*,13, 311-321. [14] Akai, J. and Tari, S. (1997) *LPI Technical Report 97-02 Part I*, 1-2. [15] Brindley G. W. and Hayami R. (1965) *Mineral. Mag.* **35**, 189-195. [16] Ohmoto H. and Kerrick D. (1977) Am. J. Sci., 277, 1013-1044. [17] Ernst W. G. (1976) W. H. Freeman, San Francisco. [18] Huss G. R. and Lewis R. S. (1995): *Geochim. Cosmochim. Acta*, **59**, 115-160.

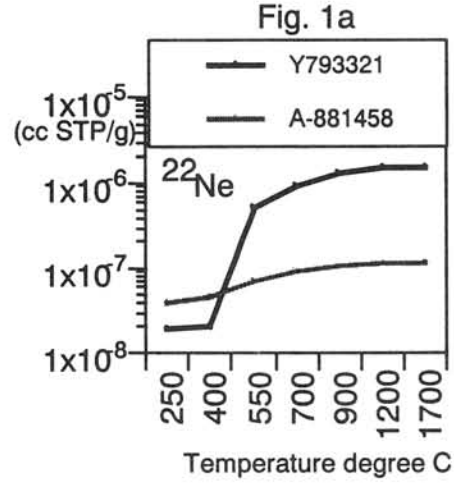

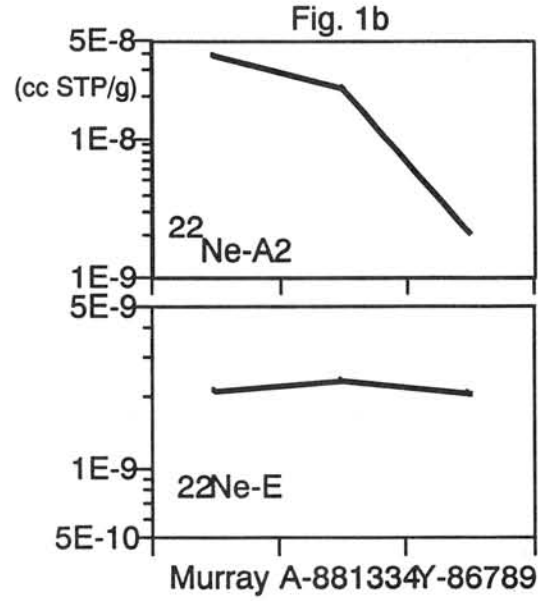

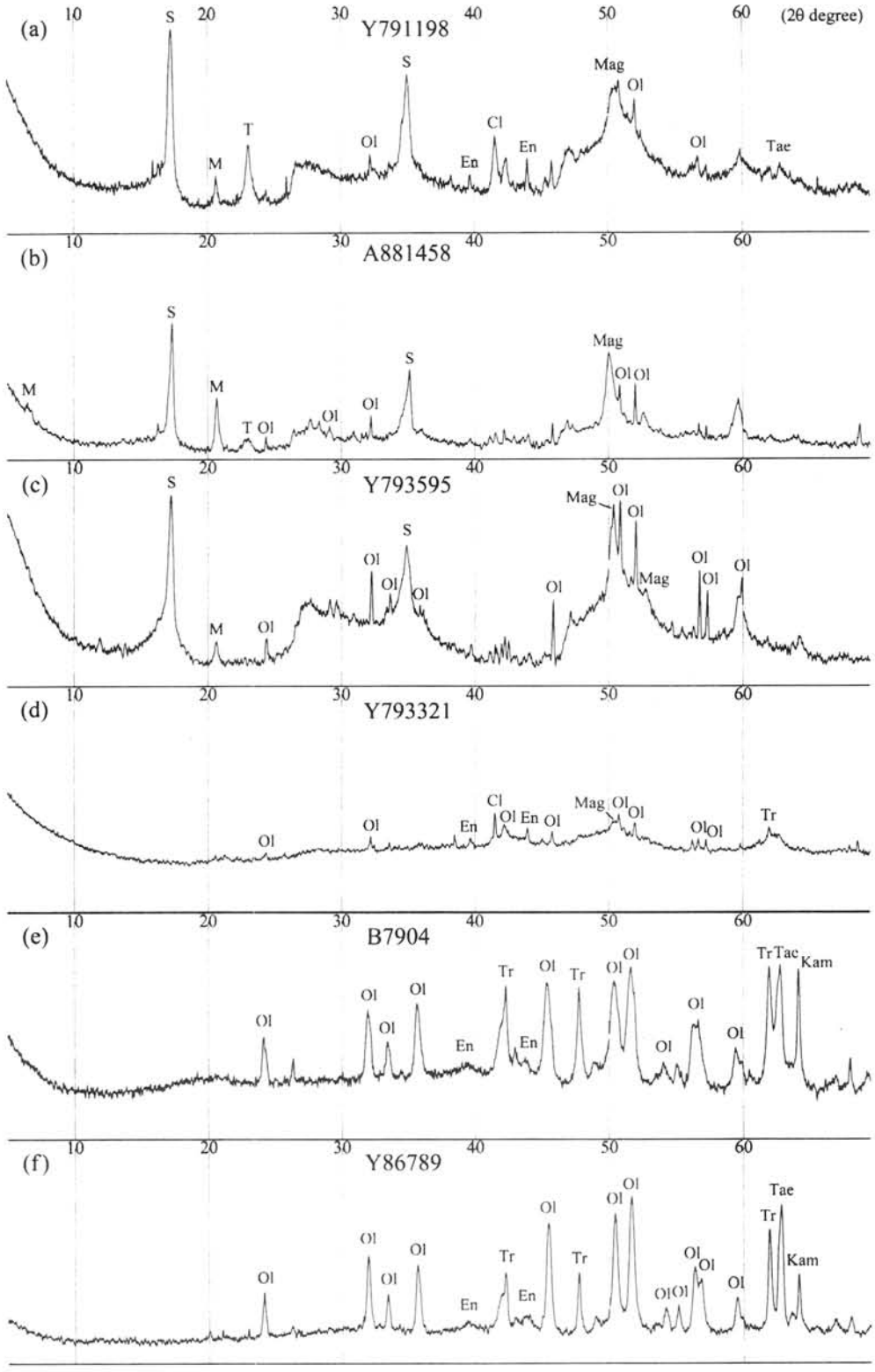

Fig.2 Powder diffraction patterns of matrices of CM chondrites.
Abbreviation: S=serpentine, M=mixed layered mineral, T=tochilinite, Ol=olivine, En=low-Ca pyroxene
Cl=calcite, Mag=magnetite, Tr=troilite, Kam=kamacite, Tae=taenite.

X-RAY DIFFRACTION ANALYSIS OF MICROMETEORITES USING SYNCHROTRON RADIATION

T. Nakamura[1], W. Nozaki[2], T. Noguchi[3], Y. Nakamuta[1], M. Tanaka[4], and N. Takaoka[1]

1. Department of Earth and Planetary Sciences, Faculty of Sciences, Kyushu University 33, Hakozaki, Fukuoka 812-8581, Japan. 2. Department of Earth and Planetary Sciences, Graduate School of Sciences, Kyushu University 33, Hakozaki, Fukuoka 812-8581, Japan. 3. Dept. of Materials and Biological Science, Ibaraki Univ., Bunkyo 2-1-1, Mito 310-8512, Ibaraki, Japan. 4. Photon Factory Institute of Materials Structure Science, High Energy Accelerator Research Organization, Tsukuba, Ibaraki 305-0801, Japan.

Antarctic micrometeorites were recovered from the Yamato meteorite ice field in 1998 [1]. These samples are now being processed for curation and studied as a consortium investigation [2]. As an initial characterization by an undestructive technique, we have performed X-ray diffraction analysis of individual micrometeorites using a Gandolfi camera with a monochromated synchrotron X-ray microbeam of 2.16Å wavelength at the beam line 3A in the Photon Factory Institute of Materials Structure Science, High Energy Accelerator Research Organization. Diffraction rings from a micrometeorite were recorded on films, taken into computer using a high-resolution scanner Canon FB1200, and converted to powder diffraction patterns using the Image Gauge software. Calculation of precise peak positions and interlayer spacing and identification of minerals were performed using a software developed by W. Nozaki and T. Nakamura.

Sixty one micrometeorites were analyzed: 25 samples recovered from Minami Yamato 3 site and 36 samples from Kuwagatayama 11 site. All samples are in a size range from 20 to 150 μm in diameter. The results of analysis indicate that 59 out of 61 samples consist entirely of anhydrous minerals (Fig. 1). These samples show similar X-ray diffraction patterns: strong reflections of olivine and magnetite and variable intensity of reflections of low-Ca pyroxene and Fe sulfides. Among 61 samples, 53, 61, 31, and 35 samples contain olivine, magnetite, low-Ca pyroxene, and Fe sulfides, respectively. Twenty five samples contain both olivine and low-Ca pyroxene, among which 16 samples contain roughly equal amounts of the two minerals. Seven samples do not contain olivine but contain low-Ca pyroxene. Magnesiowüstite (Mg, Fe)O is common in micrometeorites, especially those containing low-Ca pyroxene. This suggests a genetic relationship between magnesiwüstite and low-Ca pyroxene. Only two samples contain phyllosilicates. One of them consists of magnetite and phyllosilicate, probably smectite. The abundance of hydrous samples and the mineral assemblage of anhydrous samples are similar to those of micrometeorites recovered from the Dome Fuji Station [3].

References: [1] Yada T. and Kojima H. (2000) *Antarctic Meteorite Res.*, **13**, 9-18. [2] Terada K. *et al.* (2000) in this volume. [3] Nakamura T. *et al.* (2000) submitted.

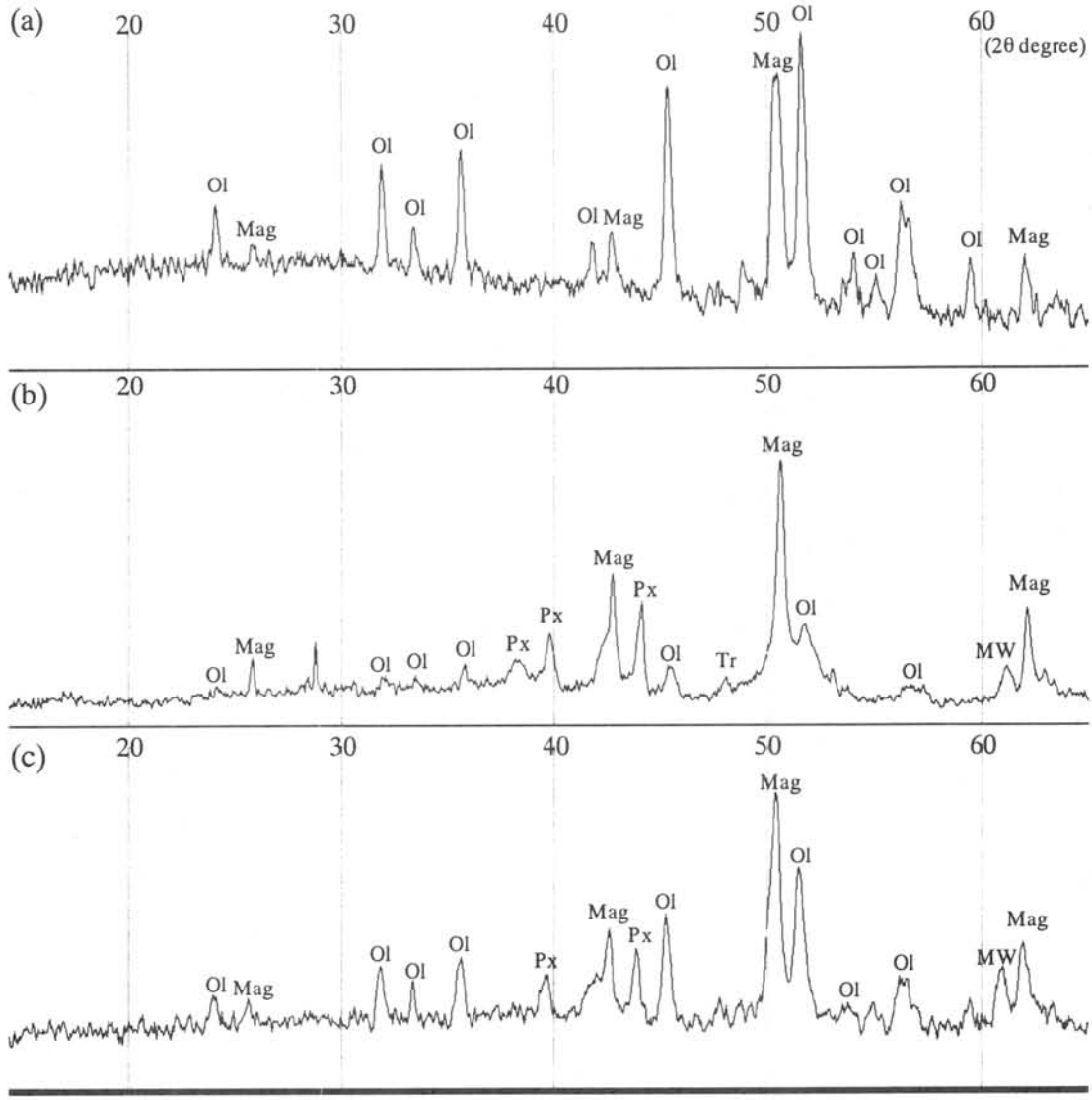

Fig.1 X-ray diffraction patterns of micrometeorites. (a) Olivine-rich, (b) pyroxene-rich, and (c) olivine-pyroxene samples. Abbreviations: Ol=olivine, Px=low-Ca pyroxene, Mag=magnetite, Tr=troilite, and MW=magnesiowüstite.

Formation Mechanism of Diamond in Ureilites

Y. Nakamuta[1)]*, and Y. Aoki[2)]

[1)] Kyushu University Museum, Kyushu University, Fukuoka 812-8581, Japan; [2)]Dept. Earth and Planetary Sciences, Faculty of Science, Kyushu University, Fukuoka 812-8581, Japan;

*Correspondence author's e-mail address: nakamuta@geo.kyushu-u.ac.jp

Introduction: Diamond was first found in ureilitic meteorites more than one hundred years ago (Kunz, 1888). The origin of diamond in ureilites has been controversial for a long time. Nakamuta and Aoki (2000) found that the basal spacing of part of the graphite coexisting with diamond is smaller compared to the normal one. The presence of the compressed graphite in ureilites gives clear evidence that the diamond formed by high-pressure conversion of graphite that crystallized during igneous or metamorphic processes. However, mechanism and P-T conditions of the conversion were not known at that time.

In this study, we found a part of a graphite crystal was converted to diamond in the Yamato-8448 ureilite. Optical and SEM observations, Raman spectroscopy, and X-ray analyses of the sample reveal the mechanism and P-T conditions of diamond formation in ureilites.

Experiments: Polished thin sections of thirteen ureilites preserved at the National Institute of Polar Research in Tokyo were observed with reflected light through an optical microscope. Carbon rich grains of 50-200 μm in size, about ten grains for each ureilite, were selected from crashed samples of each ureilite and were X-rayed by using a Gandolfi camera. Two ureilites, ALH 78019 and Y-82100, contain only graphite crystals, Y-8448 and Y-74659 contain both graphite crystals and grains composed of graphite and diamond, and other nine ureilites, Y-74123, Y-74130, Y-790981, Y-791538, ALH 77257, ALH 78262, Asuka 87031, Asuka 881931 and MET 78008, contain only grains composed of graphite and diamond.

Carbon minerals in the polished thin section, Y-8448 61-1, in which graphite crystals and grains composed of graphite and diamond occur, were further observed by a scanning electron microscope (SEM) and their Raman spectra were taken. JSM6300F of JEOL and JRS-2000SYS of JEOL were used for SEM and Raman observations, respectively. Precession photographs of a thin platy-grain composed of graphite and diamond were also taken in order to investigate the relations of crystallographic orientations between graphite and diamond crystals in a grain. A reflected light view and SEM images of carbon minerals in Y-8448 were shown in Fig. 1. X-ray powder diffraction patterns of graphite and diamond + graphite parts of a grain taken by a Gandolfi camera were also shown in Fig. 2.

Results and Discussion: The reflected-light view in Fig. 1**A** shows that a part of a graphite single crystal was converted to diamond. The part where some of graphite was converted to

diamond shows amoeboidal shape and exists at or near the grain boundary. Fig. 1**B** shows the SEM image of the graphite crystal, some of which was converted to diamond and amorphous carbon near the grain boundary. Diamond occurs as irregular-shaped particles in the region composed of diamond and graphite. Amorphous carbon occurs in contact with olivine at the grain boundary and tiny graphite crystals can be observed in it as dots, of which rims are a little brighter than their central parts and amorphous carbon. Fig. 1**C** shows a diamond grain in the region composed of diamond and graphite. The grain shows an irregular shape and looks like a sheaf of thin platy crystals. The appearance of the diamond grain reveals that cleaved graphite flakes were directly converted to diamond.

X-ray powder diffraction patterns shown in Fig. 2 suggest that kamacite coexists with diamond in the sample in which diamond occurs, but kamacite can not be observed in the sample that contains only graphite. The fact is true for almost all samples X-rayed in this study. The results strongly suggest that iron plays an important role in the conversion of graphite to diamond. Bundy et al. (1961) suggests that graphite is easily converted to diamond in the presence of certain molten metals which serve as solvent catalysts. Fig. 3 shows the P, T zone of diamond formation by catalytic transformation of graphite (Bundy et al., 1961).

Takeda (1987) suggests that ureilites underwent a two-stage cooling history: slow cooling at temperatures above 1200-1250 °C, followed by very rapid cooling, at rates possibly as high as 20 °C/hr. The second stage was probably caused by impact excavation, possibly involving extensive parent body disruption (Goodrich, 1992). The first stage temperatures, at which parent body was thought to be broken up, are also shown in Fig. 3. The diagram in Fig. 3 shows that the conditions of catalytic transformation of graphite to diamond were easily attained by a very weak shock-compression of graphite in ureilites (Stöffler et al., 1991). The relations of crystallographic orientations between graphite and diamond crystals will be also discussed based on the precession photographs of a thin platy-grain composed of graphite and diamond.

Acknowledgments: We thank H. Kojima for help in sampling of carbon grains at NIPR. SEM observations were carried out at Ceramic Research Center of Nagasaki, We thank K. Takeuchi for help in SEM observations. We also thank T. Murae for taking Raman spectra.

References: Bundy, F.P., Bovenkerk, H.P., Strong, H.M. and Wentorf, R.H. Jr. (1961) J. Chem. Phys. **35**, 383-391. Goodrichi, C.A. (1992) Meteoritics **27**, 327-352. Kunz, G.F. (1888) Science **11**, 118. Nakamuta, Y. and Aoki, Y. (2000) Meteoritics **35 No.3**, in press. Stöffler, D., Keil, K. and Scott, E.R.D. (1991) G.C.A. **55**, 3845-3867. Takeda, H. (1987) Earth Planet. Sci. Lett. **81**, 358-370.

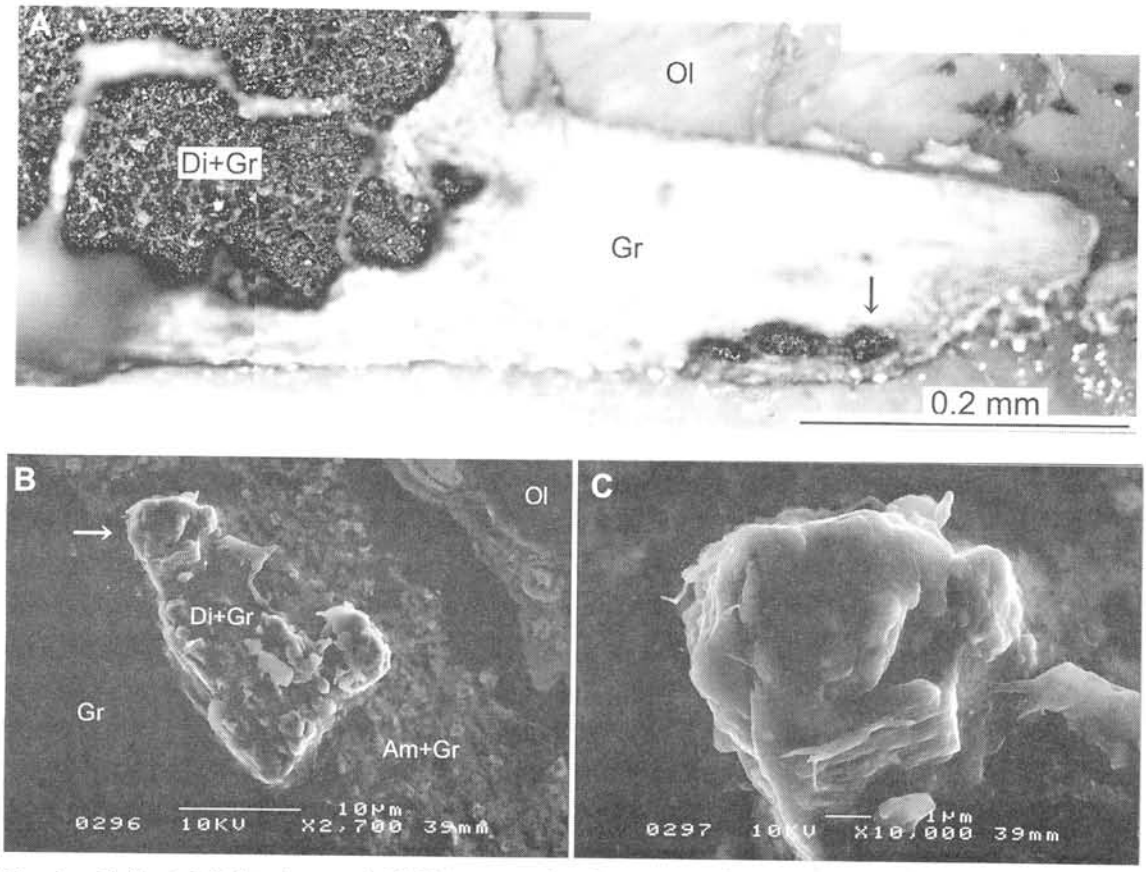

Fig. 1. Reflected-light view and SEM images of carbon minerals in Y-8448 ureilite. Minerals are graphite (Gr), diamond (Di), amorphous carbon (Am), and olivine (Ol). A: Reflected-light view of carbon minerals. A part of a graphite crystal was converted to diamond. Arrowhead shows the portion observed by SEM. The SEM images (B, C) are rotated by about 120° in the anti-clock direction. B: SEM image of the region composed of diamond and graphite. Arrowhead shows a diamond grain enlarged in C. C: Diamond grain, which shows a characteristic platy-shape.

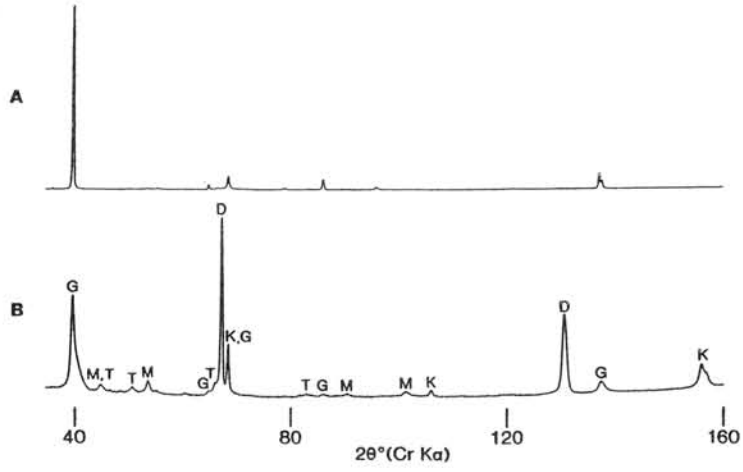

Fig. 2. X-ray powder diffraction patterns of graphite (A) and diamond + graphite (B) parts of a grain. G, D, K, M, and T: reflections from graphite, diamond, kamacite, maghemite, and troilite, respectively. Kamacite characteristically coexists with diamond.

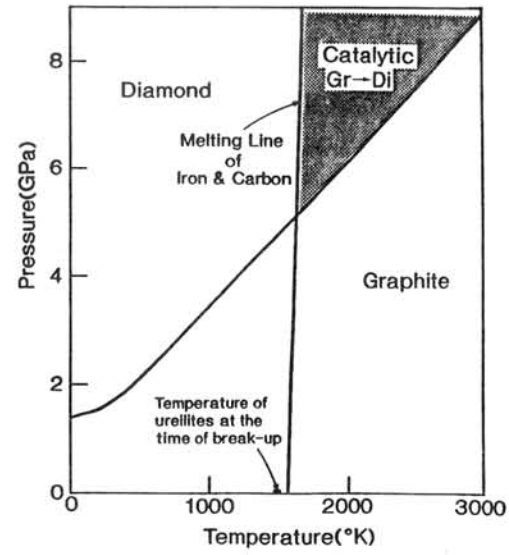

Fig. 3. P, T zone of diamond formation by catalytic transformation of graphite. The estimated temperature of ureilites at the time when ureilite parent body was broken up is also shown in the diagram.

Carbon in Iron Meteorites

Jason NEWTON and Naoji SUGIURA

Department of Earth and Planetary Science, University of Tokyo, Hongo 7-3-1, Bunkyo-ku, Tokyo 113-0033, Japan. newton@space.eps.s.u-tokyo.ac.jp

Introduction

The carbon isotopic compositions of the major components of three IAB iron meteorites (Cañon Diablo, Toluca and Deport) were measured by a combination of stepped combustion coupled with static mode mass spectrometry of the CO_2 released. Comparison of the carbon isotopic compositions between the components may impart information about their thermal histories. The following describes the $\delta^{13}C$ results for carbide and metal in these meteorites.

Although we expected to identify graphite and Fe-carbide as well as carbon in solid solution with the metal, a contaminant is associated with the low temperature steps which masks the true isotopic composition of the graphite. In future we will incorporate a low-temperature pre-combustion step in order to oxidise any organics associated with the sample or its platinum container.

All of the stepped combustion results show the following features:-

a) an increase in $\delta^{13}C$ of around 6 permil between 500 and 700°C, attributed to graphite, but masked somewhat by the contamination component, and hence omitted from the results.

b) an increased release of CO_2 between 800 and 950°C, which coincides with the combustion temperature of cohenite (Grady *et al.* 1986, Smith *et al.* 1999).

c) after a hiatus in the stepped combustion profile around 950°C, the bulk of the carbon is released, which we assume is carbon in solid solution with the metal.

d) it is evident in all experiments that there is likely to be more CO_2 released above 1300°C, but this is the limit of the furnace and the quartz combustion tube.

Results

Canyon Diablo, carbide and metal mixture

This experiment was primarily an attempt to see if the various components (carbon from metal, graphite and cohenite) could be distinguished by different temperatures of release. The

sample is a deliberate mix of components that were visible on the surface of the main Cañon Diablo sample, and we employed a coarse temperature regime of 50°C increments.

The main release of carbon occurs between 650°C and around 1000°C, peaking at 950°C and is attributed to cohenite. The isotopic profile over this temperature range is quite complicated, but the mean $\delta^{13}C$ of the cohenite is -22.6 ± 3.3 ‰, consistent with the Hoefs (1973) value of -20.6 ‰, but inconsistent with the Craig (1953) value of -17.4 ‰.

Above 1050°C, there is a smaller release of CO_2 being released from the sample attributed to carbon in solid solution with the metal. Its isotopic composition is -28.9 ± 1.5 ‰, significantly lighter than the cohenite. This does not agree with an analysis of the taenite by SIMS (Sugiura 1998), which gave a $\delta^{13}C$ value of -14.5 ± 6.0 ‰. However the SIMS data for taenite is calculated assuming an instrumental mass fractionation which is equal to that of cohenite. There is therefore a possibility that the absolute $\delta^{13}C$ values for taenite in the SIMS study are incorrect.

Canyon Diablo, metal-rich sample

This sample is metal ground from the main Cañon Diablo sample. Care was taken not to include any graphite or cohenite. This is a more detailed experiment employing 25°C increments where possible, as the primary aim was to get a picture of the isotopic profile of the carbon in the metal of Cañon Diablo.

All of the CO_2 released from the metal appears to combust above 900°C. The isotopic data between 800°C and 950°C show that there is a minor component with a $\delta^{13}C$ of -22.7 ± 0.6 ‰. This is most likely due to a small amount of cohenite.

The release of CO_2 from the metal is extremely complicated, and it is probably unwise to put too much emphasis on the variations in $\delta^{13}C$ between 950°C and 1275°C, when the experiment was stopped. However, overall the mean $\delta^{13}C$ of the carbon attributed to the metal is -28.6 ± 1.7 ‰, consistent with the previous experiment.

Toluca, metal-rich sample

This sample is metal ground from the main Toluca sample. As with the second Cañon Diablo sample, the attempt to extract a sample of pure metal was only partially successful. There is a pronounced release of carbon between 850°C and 925°C, and this is attributed to cohenite. It has a mean $\delta^{13}C$ of -23.4 ± 0.3 ‰. The carbon in the metal is released as CO_2 above 950°C, and there is expected to be some overlap in combustion between the two carbon components.

The isotopic profile for the high temperature regime is complicated, but the mean $\delta^{13}C$ of the carbon attributed to the metal is -25.2 ± 2.3 ‰, significantly lighter than earlier analyses by conventional mass spectrometry (-21.3 ‰; Deines and Wickman 1975), but in broad agreement with the SIMS investigation (-23.4 ± 5.7 ‰; Sugiura 1998).

Deport, metal-rich sample

A discrete release of carbon attributed to cohenite occurs between 800 and 950°C, with a mean $\delta^{13}C$ of -32.2 ± 0.8 ‰. After a small hiatus the carbon from the metal combusts above 975°C until the experiment is stopped at 1300°C; this has a $\delta^{13}C$ of -31.8 ± 1.4 ‰, *i.e.* is indistinguishable from that of the carbide. Although it falls within the range of the value obtained in the SIMS investigation (-26.3 ± 6.7 ‰; Sugiura 1998), it is rather light.

Discussion

Ignoring the possible presence of subcomponents of carbon, and regarding only the mean $\delta^{13}C$ of carbon released from the metallic portions of these meteorites, it is evident that in Cañon Diablo and Toluca, the carbon isotopes are fractionated between carbide and metal. The cohenite is a few permil heavier than the carbon in solid solution with the metal. In the case of Cañon Diablo the difference is about 6.2‰, and in the case of Toluca the difference is much less, about 2.2‰. In the case of Deport however, the cohenite and metal are isotopically indistinguishable with respect to carbon. This is in stark contrast to carbon isotope data on iron meteorites obtained by SIMS (Sugiura 1998), where the $\delta^{13}C$ of cohenite in IAB irons was found to be *lighter* than that of the taenite: although the absolute values for taenite in the SIMS study may be incorrect, the *relative* values for taenite should be accurate. There is therefore a need for a repeat measurement. One possibility, given that carbon from the metal is still to be fully combusted when the experiments are stopped at 1300°C, is that the lighter isotopic ratios for carbon in the metal analysed here is an experimental artifact. If the experiment causes a kinetic isotope fractionation, then the first CO_2 being released is going to be enriched in ^{12}C. This possibility needs to be thoroughly investigated.

It would be interesting to see if the fractionation of carbon isotopes between metal and cohenite is different for other IAB irons, and to interpret the cause. Therefore the analysis of carbon isotopes in different components in the other IAB irons is the immediate aim.

References

(1) Grady M.M. *et al.* (1986). *Geochim. Cosmochim. Acta* 50, 2799-2813.

(2) Smith C.L. *et al.* (1999). *Lunar Planet. Sci.* 30.

(3) Hoefs J. (1973). *Contrib. Mineral. Petrol.* 41, 277-300.

(4) Craig H. (1953). *Geochim. Cosmochim. Acta* 3, 53-93.

(5) Sugiura N. (1998). *Meteoritics Planet. Sci.* 33, 393-409.

(6) Deines P. and Wickman F.E. (1975). *Geochim. Cosmochim. Acta* 39, 547-557.

Cathodoluminescence of Forsterite and Enstatite

K. Ninagawa[1], M. Endo[1], E. Hatakeyama[1], A. Namba[1], M. Yamazaki[1] and H. Nishido[2]

[1] Department of Applied Physics, Okayama Univ. of Science, 1-1, Ridai-cho, Okayama 700-0005, Japan
[2] Research Institute of Natural Sciences, Okayama University of Science, 1201 Kawakami-son, Maniwa-gun, Okayama, 717-0602, Japan

Cathodoluminesence (CL) is the emission of light from the materials excited with an electron beam, and its appearance could be attributed to impurity, especially transition metal elements and rare earth elements, and to lattice defects in the structure. The application of the CL for geological materials is usually done to clarify calcite cementation, secondary growth of quartz and radiation damage of rock-forming minerals.

Fe-poor forsterite, Fe-poor enstatite and feldspar in meteorites have a phosphorous characteristics to exhibit the CL [1], which could be used to classify chondrules [2], to find zonation of chondrule [3] and relict olivine [4]. Fe-poor forsterite shows a variety of colors from red to purple, of which spectra indicate blue peak at 460 nm, and red one at 720-780 nm [5]. The Fe-poor enstatite in ALHA77295 (EH3) has blue peak at 480 nm and red ones at 660 and 740 nm [1], where the former is due to Mn center, the latter to Cr center. On the other hand the enstatite in EH5 E-chondrite is characterized by blue CL image, EH4, EH3 and EL3 by blue + red, and EL5 and EL6 by magenta. Aubrite has a bluish red CL image [6]. EH5 is mainly constructed of disordered orthopyroxene, and EL6 is ordered orthopyroxene respectively. Also CL colors may be reflected to the crystal structures.

We attemped to measure in detail the CL image and spectra of the forsterites and enstatites in Allende (CV), Y-8404, Y-86004 and Y-8414 (EH melt rock) by using a Luminoscope (ELM-3: American Technologies) and a CL SEM (JSM6400: Jeol and Mono CL2: Oxford Instruments). The results are as follows;

1) Forsterite and enstatite in Allende Figure 1 (a) and (c) show CL spectra of forsterite and enstatite respectively, measured with TV mode. The CL spectrum of forsterite is simillar to that of enstatite. The forsterite, however, has a peak of 630 nm different from enstatite, which has a peak of 660 nm. These peaks disappeared when measured with Spot mode (Fig. 1 (b) and (d)). These CL signal may have a short decay constant unlike the others. Infrared CL emissions were also measured to find a new CL peak. We recognized that both of the forsterite and enstatite have infrared CL emission at 900-1100 nm as shown in Fig. 2.

2) Zonation of Y-8404, Y-86004 and Y-8414 Figure 3 shows CL image of Y-86004 measured by a Luminoscope. It indicates four phases from violet at center to blue, red and black toward outer region discretely, where the black rim corresponds to fusion crust. This fact suggests that the heat arisen from atmospheric passage made such zonation in the specimen.

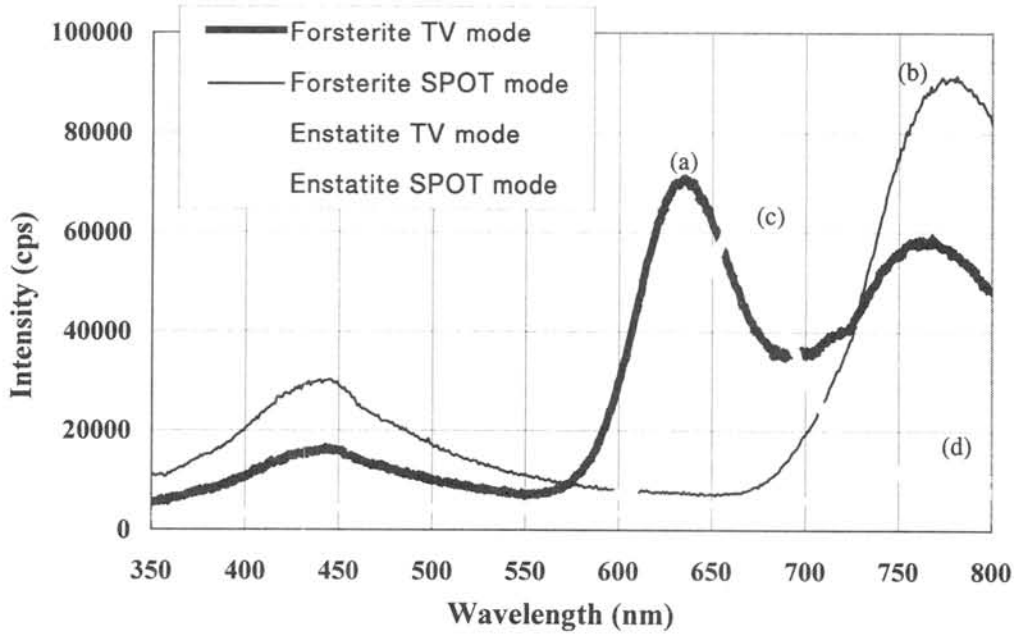

Figure 1. Visible CL from forsterite and enstatite

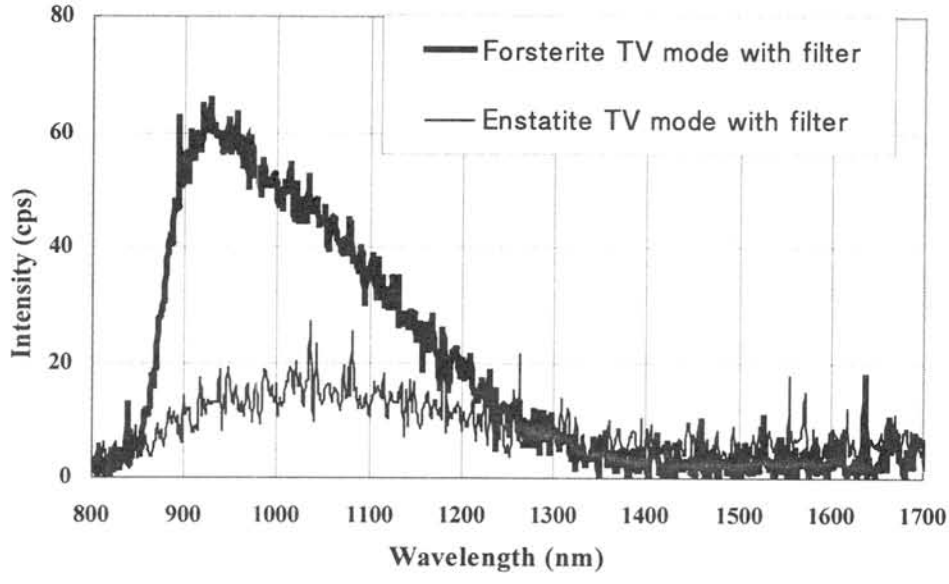

Figure 2. Infrared CL from forsterite and enstatite.

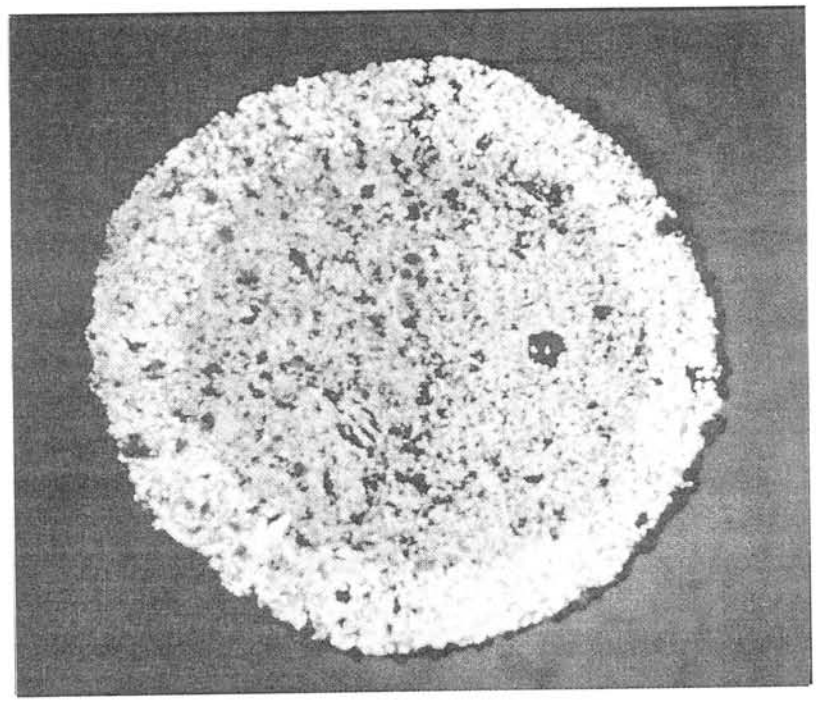

Fifure 3. CL image of Y-86004 (EH melt rock)

References: [1] Steele (1990): In Specrtoscopic characterization of minerals and their surfaces. (ed. Coyne *et al.*), pp. 150-164. *American Chemical Society*. [2] DeHart *et al.* (1992): *Geochim. Cosmochim. Acta*, **56**, 3791-3807. [3] Matsunami *et al.* (1993): *Geochim. Cosmochim. Acta*, **57**, 2101-2110. [4] Steele (1986): *Geochim. Cosmochim. Acta*, **50**, 1379-1395. [5] Steele (1986): *American Mineralogist*, **71**, 966-970. [6] Zhang *et al.* (1996): *Meteoritics & Planetary Science*, **31**, 87-96.

TEM study of Antarctic micrometeorites collected at the Yamato Mountains by 39th JARE team

○Takaaki Noguchi[1] and Tomoki Nakamura[2]
1) Dept. of Materials and Biological Sciences, Ibaraki Univ., Bunkyo 2-1-1, Mito 310-8512, Japan
2) Dept. of Earth and Planet. Sci., Kyushu Univ., Hakozaki, Fukuoka812-8581, Japan

Introduction Thirty-ninth JARE team recovered micrometeorites (MMs) from a bare ice field at the Yamato Mountains in 1998. Bulk mineralogy of 25 MMs collected at the Minami Yamato Nunatak 3 site and that of 36 ones collected at the Kuwagata Nunatak 3 site were investigated by synchrotron radiation X-ray diffraction analysis at the Photon Factory Institute of Materials Structure Science, High Energy Accelerator Research Organization (Nakamura et al., 2000). During the study, two MMs which bear abundant phyllosilicates were found. We also found a MM in which phyllosilicates were incompletely decomposed to anhydrous minerals. It was collected at the Minami Yamato Nunatak 3 site. We present mineralogy of the incompletely dehydrated MM investigated by TEM, and compare its mineralogy with that of a phyllosilicate-bearing MM collected by Maurette and his colleague.

Samples and methods Each MM was embedded in epoxy resin and microtomed by Leitz-Reihert Super Nova ultramicrotome for TEM observation. Microstructure, mineralogy, and chemical compositions of minerals of each MM were obtained by JEOL JEM-2000FX II equipped with Philips DX4 EDS. Semiquantitative analysis was based on the Cliff-Lorimer thin film approximation. Experimental k factors were determined from many mineral standards. Remainders of each embedded AMM were observed by LV-SEM, JEOL JSM-5600LV with Oxford ISIS 310 EDS in order to observe texture and analyze qualitatively of these MMs.

Results

X-ray analysis The incompletely dehydrated MM (MM1 hereafter) has strong diffraction attributed to olivine, pyroxene, and magnetite. Intensities of diffraction peaks of olivine are stronger than those of pyroxene. Weak diffraction peaks due to magnesiowüstite were also found. A weak and broad diffraction peak was observed at the position of (001) of serpentine. The (02*l*) prism diffraction of serpentine due to stacking disorder was not observed. A MM which bears abundant serpentine (MM2 hereafter) was also investigated in order to compare mineralogy. It shows a diffraction peak attributed to (02*l*) prism diffraction. Diffraction peaks due to tochilinite were not observed.

SEM observation MM1 is irregular in shape and has a porous matrix (Fig. 1a). Discontinuous thin (< 1 μm) magnetite rim was observed. Fine-grained (< 1 μm across) Fe oxides and sulfides are relatively rare and concentrated in some parts. MM2 has a compact matrix (Fig. 1b). It is composed of sub-μm sized phyllosilicate (serpentine). In the matrix, dark and bright areas are complicatedly mixed. Brighter areas have more abundant Fe than darker areas. Fe oxides and sulfides which can be resolved by SEM are very rare in the MM.

TEM observation Low magnification bright-field images of MM1 show that the matrix is composed of a porous aggregate of sub-μm sized incompletely dehydrated phyllosilicate (serpentine). Selected area electron diffraction (SAED) pattern and chemical composition indicate that the serpentine has been now decomposed almost to olivine. Such olivine crystals inherit a lamellar texture from the precursor serpentine crystal (Figs. 2a and b). Si- and Al-rich material which associated with the dehydrated serpentine was observed. Coarse (100 to 300 nm across) magnetite was found on the rim of the MM.

Low magnification bright-field images of MM2 show that the serpentine-bearing MM has a quite different texture from that of MM1. Coarse (0.1 to 1 μm across) phyllosilicate crystals were embedded in the compact matrix which is composed of very-fine grained material (Fig. 2c). SAED pattern of the coarse-grained phyllosilicate indicates that it is serpentine. EDS analysis of the coarse serpentine indicates that it is cronstedtite. On the other hand, high-resolution bright-field images, SAED patterns, and EDS analysis of the very-fine grained indicate that the crystallinity of the areas are very low and that it is much more heterogeneous in Mg/(Mg+Fe) ratios than the coarse serpentine. Anhydrous silicates such as olivine were very rare in the MM.

Discussion

Although MM1 has been almost dehydrated already, it has an incompletely dehydrated texture. Naturally and experimentally heated CM chondrites have been investigated by TEM (Akai, 1988; 1990). In them, serpentine was completely transformed to olivine or an intermediate phase between serpentine and olivine according to the degrees of heating. Compared with these data, the extent of dehydration of serpentine in MM1 is similar to that in B7904, because serpentine in B7904 is dehydrated to olivine but the olivine has lamellar-like structure. During atmospheric entry heating, matrix texture was probably changed from the texture similar to MM2 to that of MM1. MM2 is also interesting because it is a serpentine-bearing MM. Crystallinity of serpentine in this MM is higher than that of saponite in BI91/3-108 and F96CI024 saponite-bearing MMs (Klöck and Stadermann, 1994; Noguchi and Nakamura, 2000). It is interesting that texture and mineral assemblage of MM2 is different from that of CM chondrites that are the typical serpentine-rich meteorites. In the MM, coarse cronstedtite crystals were not associated with tochilinite. The abundance of Fe oxides and sulfides and that of anhydrous silicates are lower than those in CM chondrites. These data suggest that MM2 is not a fragment of CM chondrites.

References Akai (1989) GCA, 52, 1593-99; Akai (1990) Proc. NIPR Symp. Antarct. Meteorites, 3, 55-68; Klöck and Stadermann (1994) In: Analysis of Interplanetary dust, 51-87; Nakamura et al. (2000) in this volume; Noguchi and Nakamura (2000) AMR, 13.

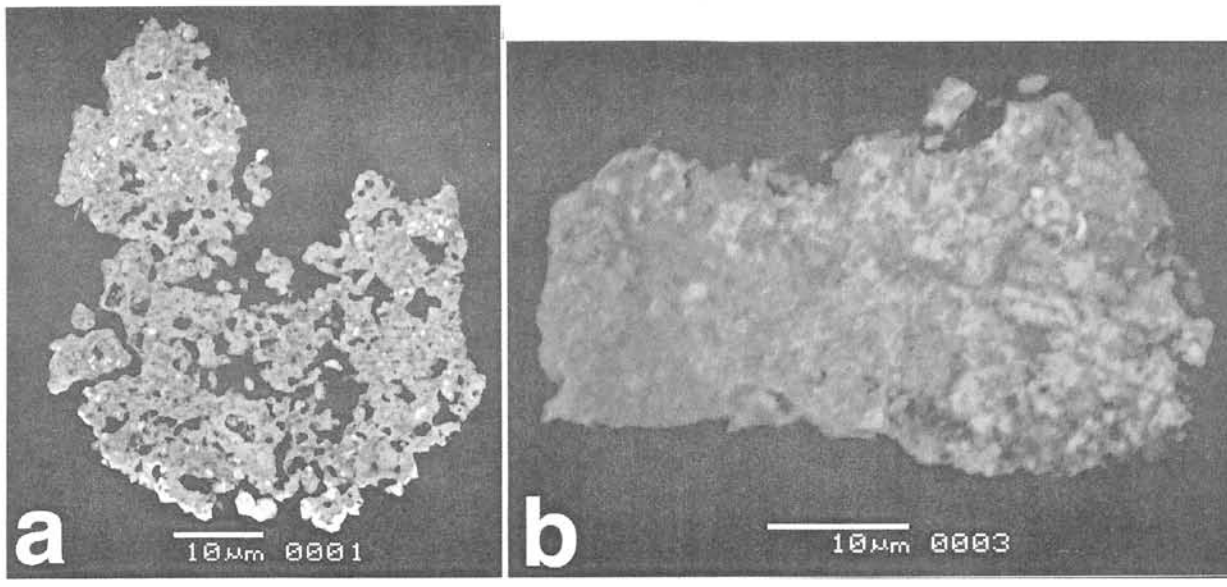

Figure 1 (a) MM1: Including incompletely dehydrated serpentine. Collected at Minami-Yamato 3 site. (b) MM2: A serpentine-bearing MM. Collected by Dr. Maurette and his colleague.

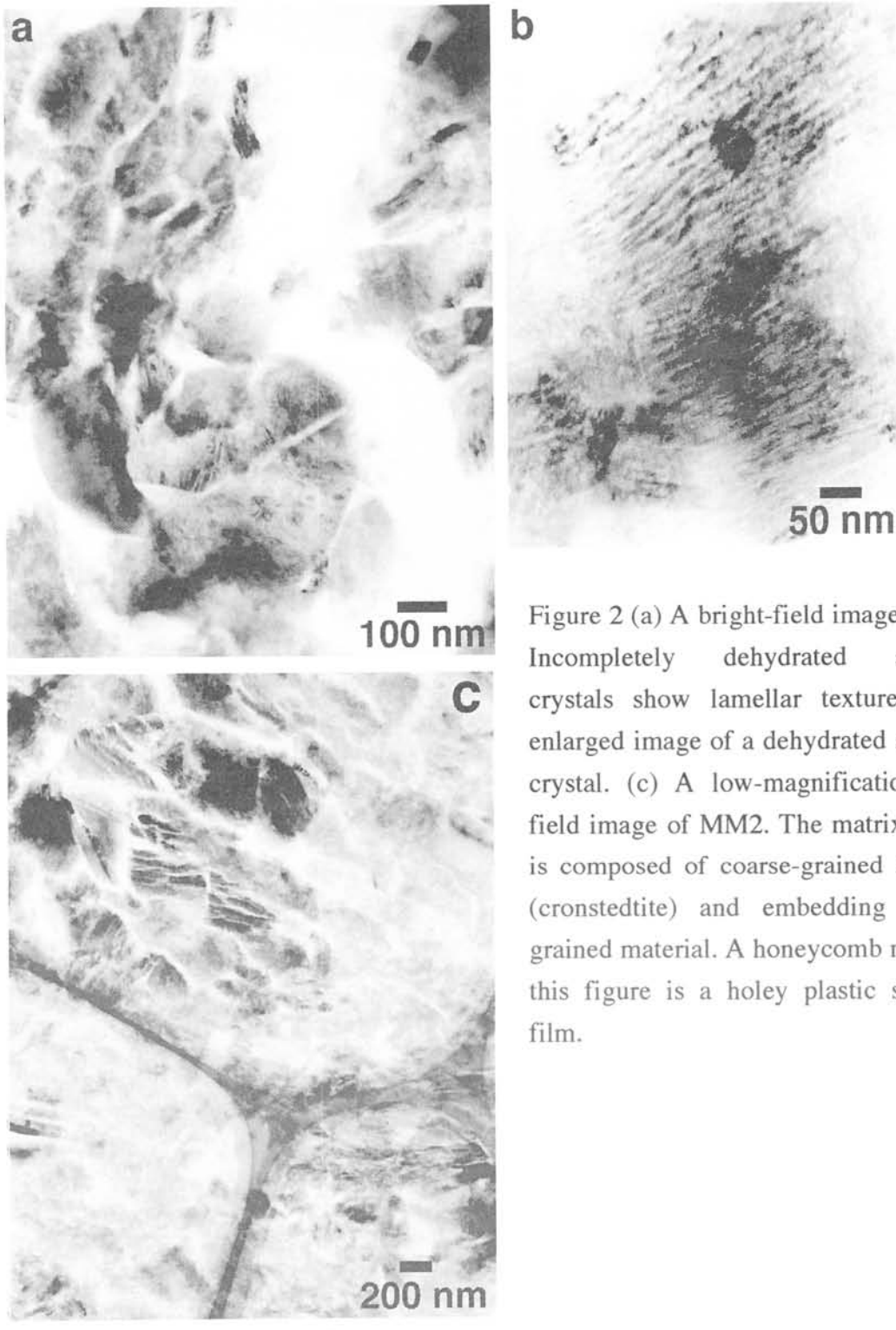

Figure 2 (a) A bright-field image of MM1. Incompletely dehydrated serpentine crystals show lamellar texture. (b) An enlarged image of a dehydrated serpentine crystal. (c) A low-magnification bright-field image of MM2. The matrix of MM2 is composed of coarse-grained serpentine (cronstedtite) and embedding very-fine grained material. A honeycomb network in this figure is a holey plastic supporting film.

Thermoluminescence Study of Japanese Antarctic Meteorites IV

M.Ohta[1], K. Ninagawa[1], S. Toyoda[1], N. Imae [2], and Kojima[2]

[1] Department of Applied Physics, Okayama Univ. of Science, 1-1, Ridai-cho, Okayama 700, Japan
[2] National Institute of Polar Research, 9-10, Kaga 1-chome, Itabashi-ku, Tokyo 173, Japan

Natural TL (thermoluminescence), the luminescence of a sample that has received no irradiation in the laboratory, reflects the thermal history of the meteorite in space and on Earth. Natural TL data thus provide insights into such topics as the orbits of meteoroids, the effects of shock heating, and the terrestrial history of meteorites. Induced TL, the response of a luminescent phosphor to a laboratory dose of radiation, reflects the mineralogy and structure of the phosphor, and provides valuable information on the metamorphic and thermal history of meteorites. The sensitivity of the induced TL is used to determine petrologic type of type 3 ordinary chondrites.

As reliable pairing approach, TL properties within large chondrites were analyzed, taking advantage of the fact that serial samples from these meteorites is known to be paired [1]. Then a set of TL pairing criteria: 1) the natural TL peak height ratios, LT/HT, should be within 20%; 2) that ratios of raw natural TL signal to induced TL signal should be within 50%; 3) the TL peak temperatures should be within 20℃ and peak widths within 10℃ was proposed. This set of TL pairing criteria is less restrictive than previously used [1].

We have measured TL of seventy-three Japanese Antarctic unequilibrated chondrites so far [2]. This time we measured TL of more thirteen Yamato meteorites and twelve Asuka meteorites. The TL data of them are listed in Table 1. In Yamato meteorites, we find three potential paring groups compared new thirteen Yamato data with those of 73 samples. Y-794007 and Y-793574 are connected to Y-790443 (H3) group, respectively. Y-86712 and Y-82059 constitute a large pairing group, Y-82055 (L3). In Asuka meteorites, we find two potential pairing groups. A-87277, A-87278 and A-87283 constitute a large pairing group, and could be paired to A-9007 (H3). However, geographical information of gathering positions is necessary for precise pairing.

The petrologic subtype of these unequilibrated chondrites were also determined from their TL sensitivity. Y-793384 (LL3), A-87319 (L3) and A-9043 (L3) was found to have very low TL sensitivity equal to petrologic type 3.0-3.1. However, microscopic observation of the thin section is necessary, because a very low TL sensitivity of Y-790787 (L3) equal to petrologic 3.0-3.1 is due to shock melt. This time, induced TL of a CO chondrite, A-87346, was also measured and found to be petrologic type 3.0-3.3. [3]

References: [1] Ninagawa *et al* . (1998): *Antarctic Meteorite Res.*, **11**, 1-17. [2] Ninagawa *et al.* (2000): *Antarctic Meteorite Res.*, **13**, in press. [3] Sears *et al.* (1991): *Proc. NIPR Symp. Antarct. Meteorites*, **4**, 319-343.

Table1 Thermoluminescence data of Okayama for twenty-five unequilibrated Japanese ordinary chondrites

Meteorite	Class	Natural TL		Induced TL				LT	Pairing	
		LT/HT	LT (10^3 counts)	TL Sensitivity (Dhajala=1)	Peak Temp. (℃)	Width (℃)	TL Subtype	/TL Sens. ($x10^3$)		
Y-82007	LL3	6.03 ± 0.05	6.9 ± 0.4	0.04 ± 0.01	169 ± 4	148 ± 1	3.2-3.3	173.3 ± 46.9		Y-82195
Y-791656	LL3			0.18 ± 0.00	85 ± 2	53 ± 1	3.5			
Y-793384	LL3			0.0008 ± 0.0011	201 ± 1	77 ± 109	3.0-3.1			
A-87225	LL3	0.24 ± 0.00	6.6 ± 0.2	0.97 ± 0.12	139 ± 1	117 ± 1	3.7-3.8	6.8 ± 0.9		
A-87250	LL3	4.18 ± 0.11	60.3 ± 4.0	0.33 ± 0.03	142 ± 4	125 ± 3	3.6	183.1 ± 20.7		
Y-8340	L3	0.04 ± 0.00	0.42 ± 0.02	0.67 ± 0.18	156 ± 7	141 ± 2	3.6-3.8	0.6 ± 0.2		
Y-74024	L3	1.17 ± 0.05	43.4 ± 0.5	0.64 ± 0.10	164 ± 6	156 ± 2	3.6-3.7	67.9 ± 11.0		
Y-8411	L3	2.89 ± 0.07	37.7 ± 2.6	0.26 ± 0.00	157 ± 10	146 ± 1	3.6	146.7 ± 10.3		
Y-86712	L3	7.97 ± 0.03	58.7 ± 2.5	0.16 ± 0.00	147 ± 17	148 ± 1	3.5	371.2 ± 16.0	○	Y-82055,Y-82095
Y-82059	L3	8.21 ± 0.35	51.2 ± 4.4	0.19 ± 0.03	150 ± 18	141 ± 2	3.5-3.6	271.8 ± 46.1	○	Y-82095,Y-793374
A-87319	L3			0.002 ± 0.001	165 ± 16	137 ± 17	3.0-3.1			
A-9043	L3		0.1 ± 0.0	0.007 ± 0.001	84 ± 3	70 ± 12	3.0-3.1	17.4 ± 3.3		
Y-793275	H3	0.08 ± 0.01	4.6 ± 1.2	0.94 ± 0.08	155 ± 2	138 ± 1	3.7-3.8	4.9 ± 1.4		
Y-794007	H3	0.76 ± 0.01	14.5 ± 0.8	0.43 ± 0.06	129 ± 1	144 ± 1	3.6-3.7	33.3 ± 5.0		Y-790443
Y-793574	H3	1.05 ± 0.16	4.3 ± 0.1	0.13 ± 0.01	137 ± 4	134 ± 1	3.5	33.0 ± 2.6		Y-794009
Y-8454	H3	2.22 ± 0.50	0.14 ± 0.01	0.13 ± 0.01	189 ± 2	150 ± 1	3.5	1.0 ± 0.1		
Y-790460	H3	3.47 ± 0.05	21.7 ± 0.4	0.19 ± 0.01	132 ± 3	132 ± 1	3.5	117.1 ± 5.9		
A-87216	H3	0.20 ± 0.01	1.4 ± 0.1	0.50 ± 0.04	147 ± 8	129 ± 1	3.6-3.7	2.8 ± 0.3		
A-87274	H3	2.73 ± 0.05	26.2 ± 3.3	0.32 ± 0.04	153 ± 1	118 ± 1	3.6	81.7 ± 13.7	◎	
A-87286	H3	3.21 ± 0.01	17.1 ± 0.5	0.23 ± 0.01	159 ± 5	119 ± 2	3.6	73.3 ± 3.2	◎	
A-87278	H3	5.72 ± 0.04	80.7 ± 9.9	0.55 ± 0.07	164 ± 1	124 ± 1	3.6-3.7	146.4 ± 25.3	●	A-9007
A-87283	H3	5.76 ± 0.13	54.3 ± 0.7	0.30 ± 0.02	157 ± 1	121 ± 1	3.6	183.0 ± 13.8	●	A-9007
A-87277	H3	6.41 ± 0.16	97.8 ± 1.5	0.58 ± 0.03	158 ± 2	124 ± 1	3.7	169.0 ± 9.3	●	
A-9046	?3		1.0 ± 0.4	0.04 ± 0.01	83 ± 3	59 ± 1	3.2-3.3	22.3 ± 9.4		
A-87346	CO3			0.02 ~ 0.09	161	119 ± 168	3.0-3.3			

Subsolar noble gas in chondrules of the enstatite chondrite Y-791790

R. Okazaki[1)], N. Takaoka[2)], T. Nakamura[2)] and K. Nagao[1)]
1) Laboratory for Earthquake Chemistry, Graduate School of Science, University of Tokyo, Hongo, Bunkyo-ku, Tokyo 113-0033, Japan
2) Department of Earth and Planetary Sciences, Faculty of Science, Kyushu University 33, Hakozaki, Fukuoka 812-8581, Japan

Introduction

Enstatite (E) chondrites contain trapped noble gases, Q-gas and *subsolar gas* (or Ar-rich gas). Subsolar gas is characterized by a high $^{36}Ar/^{132}Xe$ ratio (2800; Crabb and Anders, 1981) compared with Q-gas (60-100). The highest $^{36}Ar/^{132}Xe$ ratio determined so far is about 2800 for South Oman E chondrite (Crabb and Anders, 1981). Based on selective dissolution of constituent minerals of E chondrites (Crabb and Anders, 1981, 1982), it has been found that the subsolar gas resides in enstatite mineral. However, where the relevant mineral is located in the E chondrites and how the enstatite retains the gas are still unclear. Identification of the carrier phase of subsolar gas and its locality in E chondrites could provide useful information on the origin of this enigmatic gas and therefore on physico-chemical processes which affected the formation of minerals in a region of reducing condition in the early solar system.

In this study, we carried out laser-microprobe analysis of an unequilibrated E-chondrite, Y-791790 (Yanai and Kojima, 1995). Three slices (40-50 μm thick) were prepared, and one side of the samples was polished. After optical microscope observation and quantitative analysis by an electron microprobe analyzer, noble gas was extracted with a Nd-YAG which ranges in beam diameter 30 to 70 μm. Released noble gases were measured with a modified mass spectrometer VG 5400 (MS-II) at Laboratory for Earthquake Chemistry, University of Tokyo (*e.g.*, Nagao *et al.*, 1999).

Results and discussion

Microscopic observation revealed that chondrules in Y-791790 include porphyritic pyroxene (PP) and radial (barred?) pyroxene (RP) chondrules although the latter is rare (Fig. 1). Unlike other unequilibrated E chondrites, the matrix of Y-791790 contains euhedral pyroxene grains in opaque mineral-rich regions that are supposed to be impact-melted materials (Rubin and Scott, 1997). However, there are clear boundaries between chondrules and matrices, suggesting that chondrules have been saved from equilibration with matrices during the heating event *in the parent body* (*i.e.*, after agglomeration of chondrules and matrices).

Three components, chondrules, pyroxene grains in the matrix, and opaque nodules in the matrix, were analyzed for noble gas. A great amount of ^{36}Ar was released from PP chondrules. Concentration of ^{36}Ar, estimated from sample thickness and pit diameter, is up to 1×10^{-5} cm^3STP/g (Fig. 2) although the quantity is uneven from one chondrule to another. In addition, the noble gases released from PP chondrules are extremely enriched in ^{36}Ar compared to ^{84}Kr and ^{132}Xe (Fig. 3); $^{36}Ar/^{132}Xe$ ratio is up to 4300. As shown in Fig. 3, $^{36}Ar/^{84}Kr/^{132}Xe$ ratio of the noble gases in PP chondrules lies on an extend line passing Q-gas and subsolar gas (South Oman; Crabb and Anders, 1981).

On the other hand, concentrations of ^{36}Ar in RP chondrules, pyroxene grains in the

matrix and kamacite globules are generally lower than PP chondrules (Fig. 2). $^{36}Ar/^{132}Xe$ ratios are low relative to that of bulk samples (about 2300; Okazaki R., PhD Thesis). No measured components are enriched in subsolar gas compared to PP chondrules. In the light of ^{36}Ar content and $^{36}Ar/^{84}Kr/^{132}Xe$ ratio, subsolar gas in the E chondrite resides principally in PP chondrules.

How can PP chondrules have acquired and preserved the great amounts of subsolar gases up to 1×10^{-5} cm^3STP/g of ^{36}Ar? In order to account for the high ^{36}Ar content, two subjects must be answered. One is a trapping mechanism to explain the high ^{36}Ar content in pyroxene. A possible mechanism seems to be implantation of solar gases into chondrule precursor. Implantation meets high trapping efficiency without high Ar pressure, if solar-gas flux and surface area are sufficient. Other trapping mechanisms such as adsorption and solution require high partial pressure of Ar in the solar nebula because their trapping efficiencies (distribution coefficient) are very low.

Another is about subsistence of noble gases against heating events that have formed chondrules. For PP chondrules, heating temperature was below liquidus temperatures, so as to permit survival of nuclei (*e.g.*, Hewins, 1981). On the other hand, RP chondrules have been heated to their liquidus temperatures. This is consistent with the result that RP chondrules don't contain subsolar gases as much as PP chondrules do. In addition, chondrules must have been quenched to prevent noble-gas loss. Laboratory experiments suggest that cooling rates of 100-2000 °C/hour are expected for PP chondrules (Hewins, 1988). Diffusion coefficient of Ar in SiO_2 is about 5×10^{-8} cm^2/sec at 1500 °C (Hiyagon, 1981). If a chondrule is cooled at 2000 °C/hour between 1500 °C and 1400 °C, Ar in the chondrule will move 10 μm across. This diffusion range is too large relative to typical diameter of porphyritic pyroxene constituting PP chondrules. Thus, chondrules should have been cooled more rapidly.

References: Crabb J. and Anders E. (1981) *G.C.A.* **45**, 2443-2464; Crabb J. and Anders E. (1982) *G.C.A.* **46**, 2351-2361; Wacker J. F. and Marti K. (1983) *E.P.S.L.* **62**, 147-158; Yanai K. and Kojima H. (1995) *Catalog of the Antarctic Meteorites. Tokyo, Natl. Inst. Polar Res.*, 230p; Nagao K. *et al.* (1999) *Antarct. Meteorite Res.* **12**, 81-93; Rubin A. E. and Scott E. R. D. (1997) *G.C.A.* **61**, 425-435; Hewins R. H. (1988) *In* Meteorites and the Early Solar System (ed., J. F. Kerridge and M. S. Matthews, Univ. of Arizona), 680-696; Hiyagon H. (1981) MA Thesis, University of Tokyo.

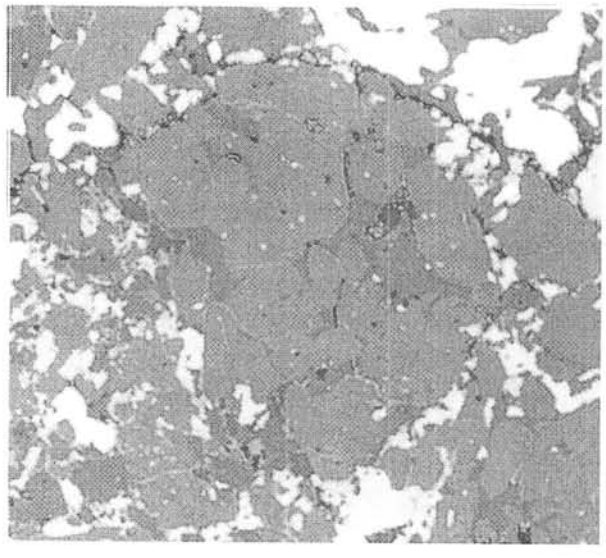

Fig. 1: Photomicrographs of a porphyritic pyroxene chondrule in Y-791790 (EH3). Apparent diameter of the chondrule is about 150 μm. Reflected light.

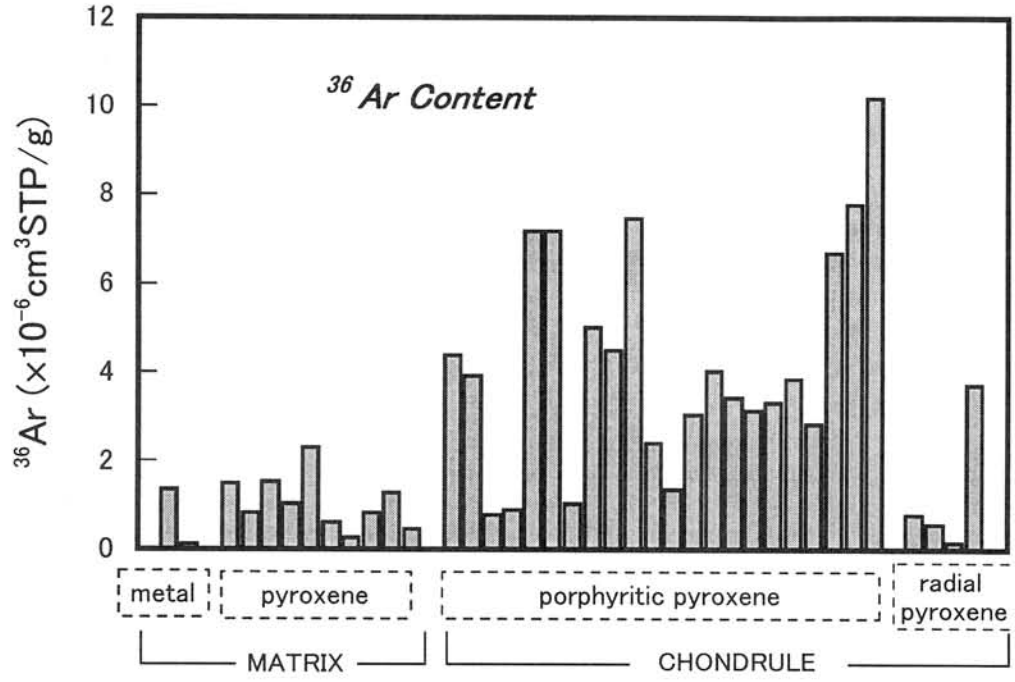

Fig. 2: Concentrations of ^{36}Ar released from each mineral component of Y-791790. Quantity of blank gas is subtracted from that of measured gas.

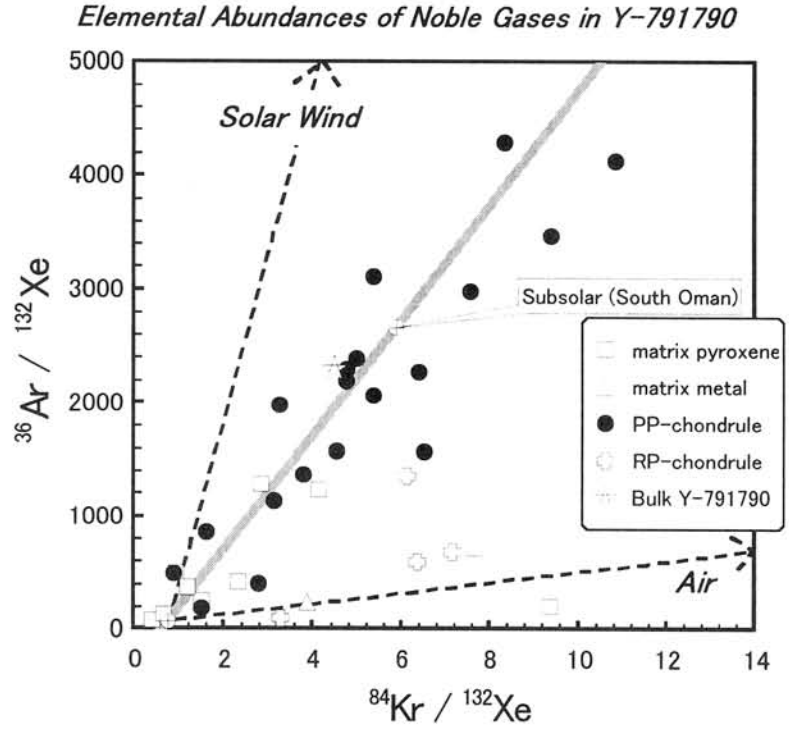

Fig. 3: Trapped $^{36}Ar/^{132}Xe$ vs. $^{84}Kr/^{132}Xe$. Noble gases released from porphyritic pyroxene chondrules are enriched in ^{36}Ar, suggesting that subsolar gas is concentrated in the chondrules.

Infrared Microspectroscopic Analyses for Meteorites and Antarctic Micrometeorites

Takahito OSAWA, Hiroyuki KAGI & Keisuke NAGAO

Laboratory for Earthquake Chemistry, Graduate School of Science, University of Tokyo, Hongo, Bunkyo-ku, Tokyo, 113-0033, Japan

Introduction

As micrometeorites are considered to be primitive materials in solar system, we can expect a preserve of organic matters and water in them. Some molecular absorption bonding can identified by absorption spectra of infrared light passing through such materials. We present results of the infrared absorption spectra for individual micrometeorites and some typical meteorites.

Experimental procedures

Both of crushed meteorites (~100 μm) and Antarctic micrometeorites were pressed between a pair of type II a diamonds and thinned in order that infrared light can go through the samples. Upper part of the diamond was removed to avoid the generation of interference fringes. Infrared spectra were recorded on a Perkin Elmer Spectra 2000 FTIR spectrometer equipped with an IR microscope. Glober light as an IR incident light source, a liquid-nitrogen-cooled HgCdTe (MCT) detector and a KBr beam splitter were used. Infrared spectra in a transmission mode were obtained through a square aperture ($60 \times 60\ \mu m^2$) with a spectral resolution of $4cm^{-1}$, and all spectra were averaged from at least 100 single scans. Dry nitrogen gas was constantly pumped into the microscope to eliminate water vapor. The justification of this diamond-press method was confirmed by the comparison to the conventional KBr pellet method.

Results

IR spectra of several meteorites measured in this study are presented in Fig. 1. Orgueil (CI) which is the most primordial chondrites with plenty water and organic matters has the highest peak of O-H stretching band in the range of 3000-3600cm^{-1} and H-O-H bending vibrations at 1640 cm^{-1}. However, no C-H or C=C band was detected in this analyses. Spectrum of Murchison (CM2) is similar to that of Orgueil but O-H peak is lower than it. Petrologic types of carbonaceous chondrites is related to a peak height of O-H stretching band. Exceptionally, Kainsaz meteorite that is classified to CO3 has obvious O-H stretching band. Allende (CV3) and Moorabie (L3) have only Si-O stretching band appeared at about 1000cm^{-1} and no OH band. Camel Donga (eucrite achondrite) has characteristic spectrum different from chondrites, especially, absorption band less than 850cm^{-1}.

IR spectra of five Antarctic micrometeorites with chondritic major element compositions and terrestrial olivine are shown in Fig. 2. All the samples were collected from

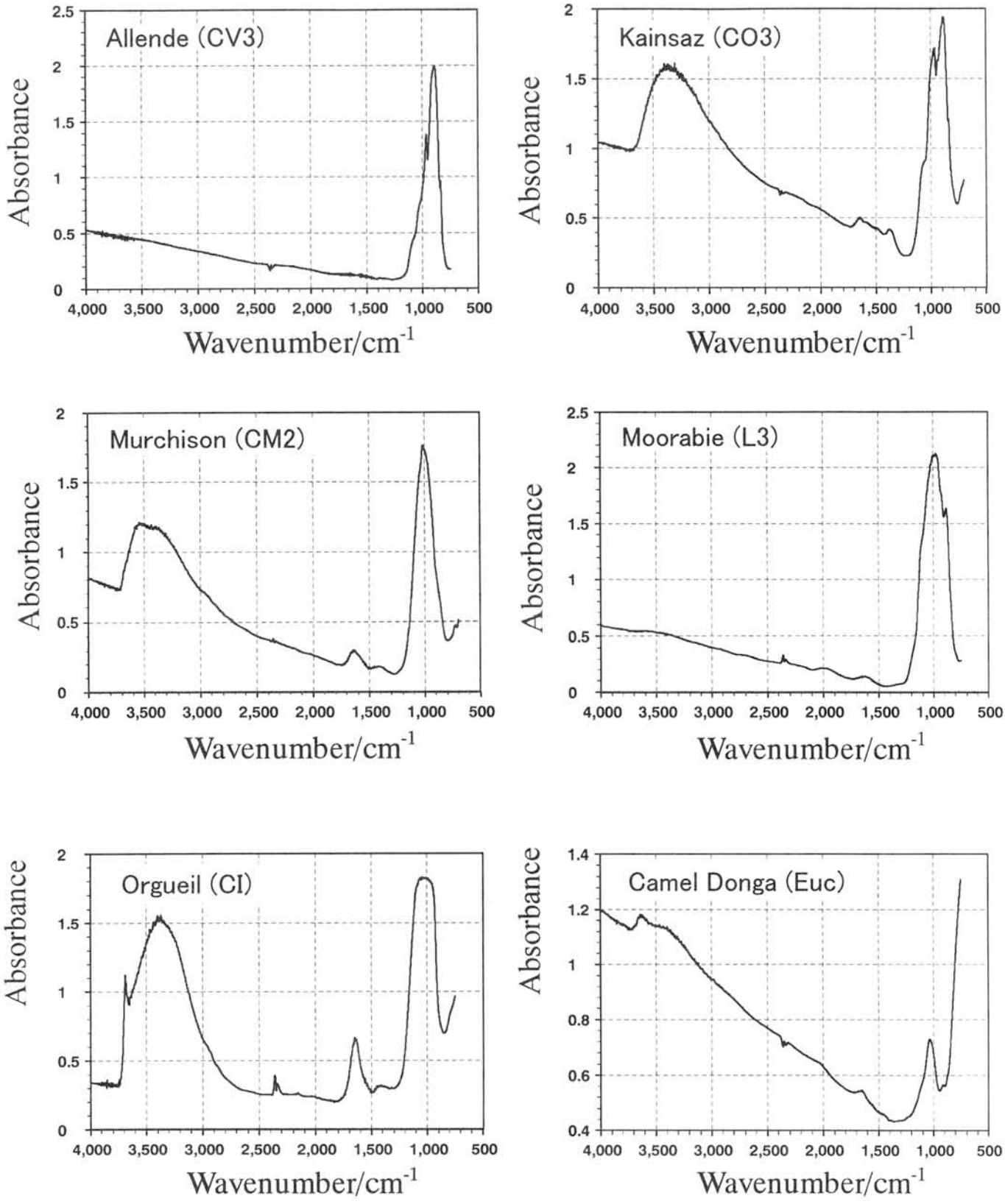

Fig. 1 Infrared absorption spectra of typical meteorites.

recent fallen snow around the Dome Fuji Station in 1997. The spectra are resemble among them, i.e., no O-H band and strong absorption bands attributable to silicate vibrations, indicating low concentration of water in them. Presumably, water was lost by heating during the atmospheric entry. Three samples, F97AC018, F97AC019 and F97BC001 have wide absorption band at 800-1100cm^{-1} which is similar to pyroxene spectrum. While, spectra of F97AC017 and F97BC002 show sharper band at 900cm^{-1} which is similar to that of olivine and Allende. Trace of organic compounds cannot be detected in these samples.

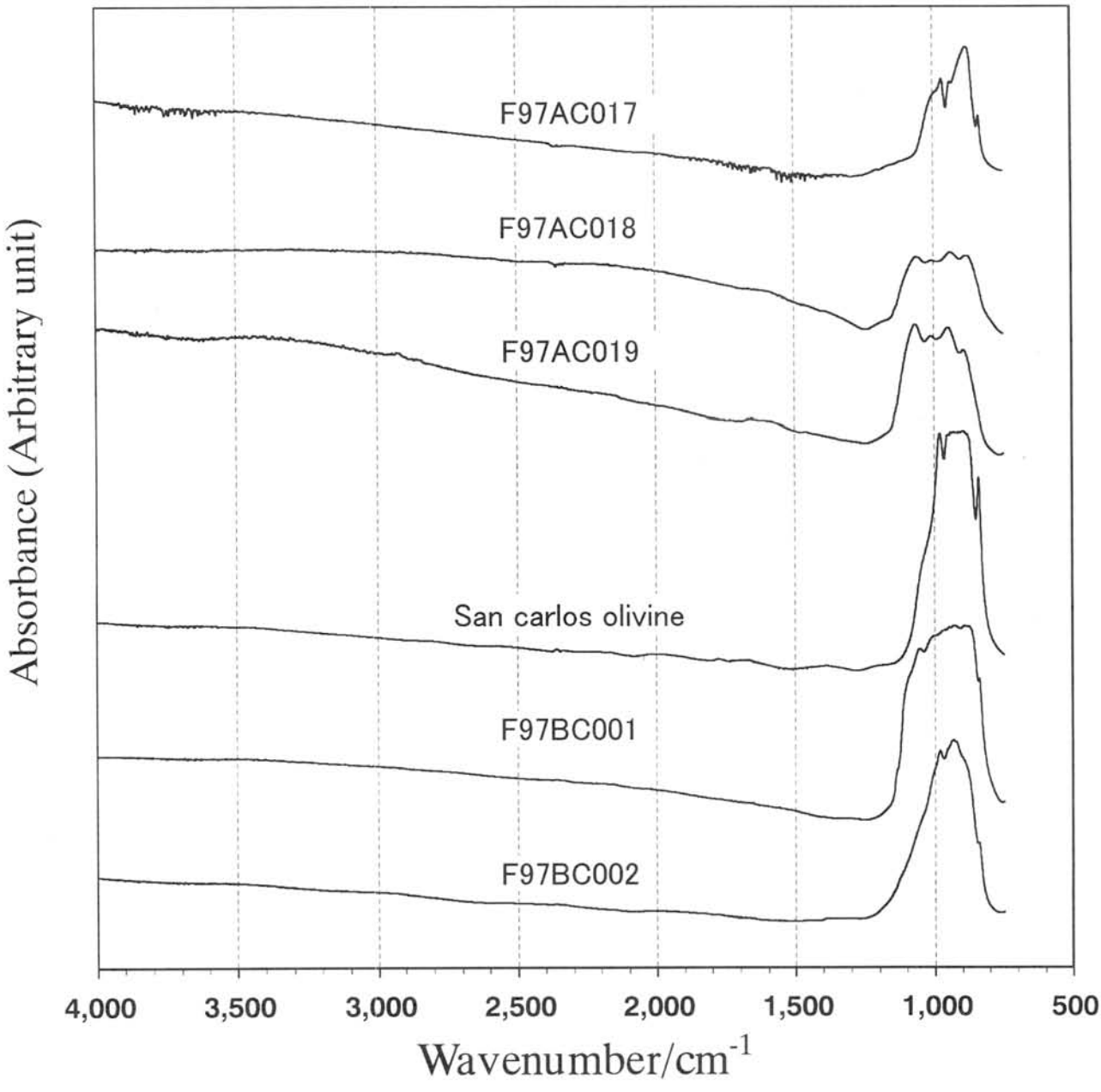

Fig. 2 Infrared absorption spectra of Antarctic micrometeorites

Chemical characteristics of Kobe and some other CK chondrites.

Y. Oura[1], M. Ebihara[1], S. Yoneda[2] and N. Nakamura[3]
[1] Graduate School of Science, Tokyo Metropolitan University, Hachioji, Tokyo 192-0397, Japan
[2] The National Science Museum, Shinjuku, Tokyo, 169-0073, Japan
[3] Graduate School of Science & Technology, Kobe University, Nada, Kobe 657-8501, Japan

The Kobe meteorite fell on 26, September, 1999 in Kita-ku, Kobe-shi, Japan. Kobe was classified as C4, and tentatively classified as CK[1]. No carbonaceous chondrite was found in Japan until Kobe fell. In this study, we analysed Kobe and two CK chondrites (Kroonda and Maralinga) for their bulk chemical compositions by three different non-destructive nuclear methods to conclude a chemical classification of Kobe.

Powdered samples (about 50 mg) were subjected to instrumental neutron activation analysis (INAA). Three successive irradiations for 100 seconds, 30 minutes, and 6 hours were performed at TRIGA II reactor, Rikkyo University. After irradiation for 100 s, irradiated samples were measured for gamma-rays one time. After irradiations for 30 m and 6 h, gamma-ray measurements were carried out several times following different cooling intervals. Another aliquots (about 100 mg) were analysed by neutron induced prompt gamma-ray analysis (PGA) using cold neutron beam at JRR-3M, Japan Atomic Energy Research Institute. After sufficient cooling, about 60 mg of the same samples used for PGA were analyzed by instrumental photon activation analysis (IPAA); samples were irradiated by bremsstrahlung with 30 MeV of end-point energy from the electron linear accelerator at Laboratory of Nuclear Science, Tohoku University for 30 min and 5 h successively. After irradiation, samples were measured for gamma-rays several times following different cooling intervals. JB-1 issued by GSJ or Allende powder by the Smithsonian Institution was used as a standard sample for determination in these three nuclear methods.

By using INAA, PGA, and IPAA methods, 33 elements were determined. INAA is commonly applied for non-destructive multielemental analysis of meteorites and its effectiveness is well acknowledged. On the contrary, PGA and IPAA are less popular as non-destructive method although both methods are highly effective for multielemental analysis. PGA and IPAA are generally of advantage in determining light elements and indeterminable elements by INAA, respectively, and, hence, can be complementary to INAA. In this study following elements were determined: Na, Mg, Al, K, Ca, Sc, Ti, V, Cr, Mn, Fe, Co, Ni, Zn, Ga, As, Se, Br, La, Sm, Eu, Yb, Lu, Os, Ir, and Au by INAA (27 elements); B, Na, Mg, Al, Si, S, Cl, K, Ca, Ti, Mn, Fe, Co, and Ni by PGA (14 elements); Na, Mg, Si, Cl, K, Ca, Ti, Cr, Mn, Fe, Co, Ni, Zn, Sr, Y, and Zr by IPAA (16 elements). The underlined elements are only determinable by each of three methods. PGA is of great advantage to non-destructive determination of Si and S in meteorite samples[2]. B, Si, and S contents in CK chondrites were obtained for the first time in this work.

CI- and Mg-normalized abundances in Kobe, Kroonda, and Maralinga were shown along with those in some CK chondrites reported by Kallemeyn et al.[3] in Fig.1(a), (b), and (c) for refractory, siderophile, and volatile elements, respectively. The abundances pattern for Kobe is generally similar to those for other CK chondrites. Kobe has slightly higher abundances of La and Sm, and lower abundance of B. It is well recognized that B is highly prone to the terrestrial contamination, which can occur even on display at the museum. Because the Kobe meteorite was analyzed in a short time after its falling, a low content of B must be indigenous for this meteorite. It seems to be significant that CI-normalized B abundance in Kobe is in the same range for Mn, Na, and K, suggesting a similar volatility for these elements. Ni, Co, Au, Se, and S abundances in Maralinga are lower than those in other CK chondrites. Of these elements, S,

Ni, and Se are strongly reduced. Considering that Maralinga is an Australian find and is a heavily weathered meteorite, the depletion of at least Ni and Co must be caused by the terrestrial weathering. In Fig.2 correlation of Zn/Mn and Al/Mn atomic ratio are compared. Kobe shown by a closed circle falls in the CK region (around 23 of Al/Mn and 0.03 to 0.07 of Zn/Mn), suggesting that Kobe is classified to CK. So, Kobe is the second observed fall of (normal) CK chondrites.

We thank Mr.Ryoichi Hirata for providing us with the Kobe meteorite.

[1] N.Nakamura et al., Lunar Planet. Sci. XXXI , #1234 (2000).
[2] Sk.A.Latif et al., J. Radioanal. Nucl. Chem. 239, 577 (1999).
[3] G.W.Kallemeyn et al., Geochim. Cosmochim. Acta 55, 881 (1991).

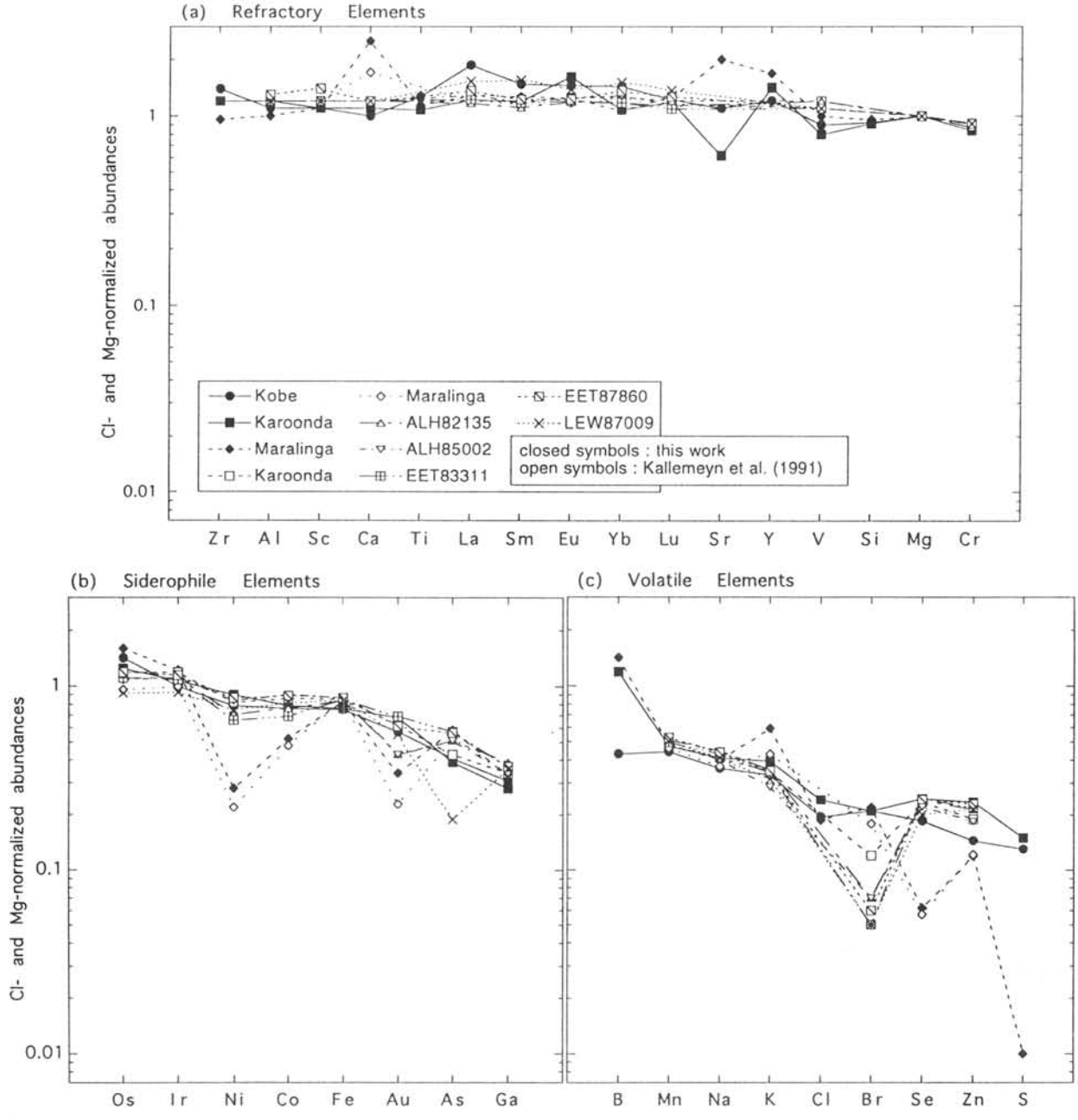

Fig.1 CI- and Mg-normalized abundance diagram of CK chondrites; (a) refractory elements, (b) siderophile elements, and (c) volatile elements. Elements are ordered in terms of decreasing nebular condensation temperature to the right.

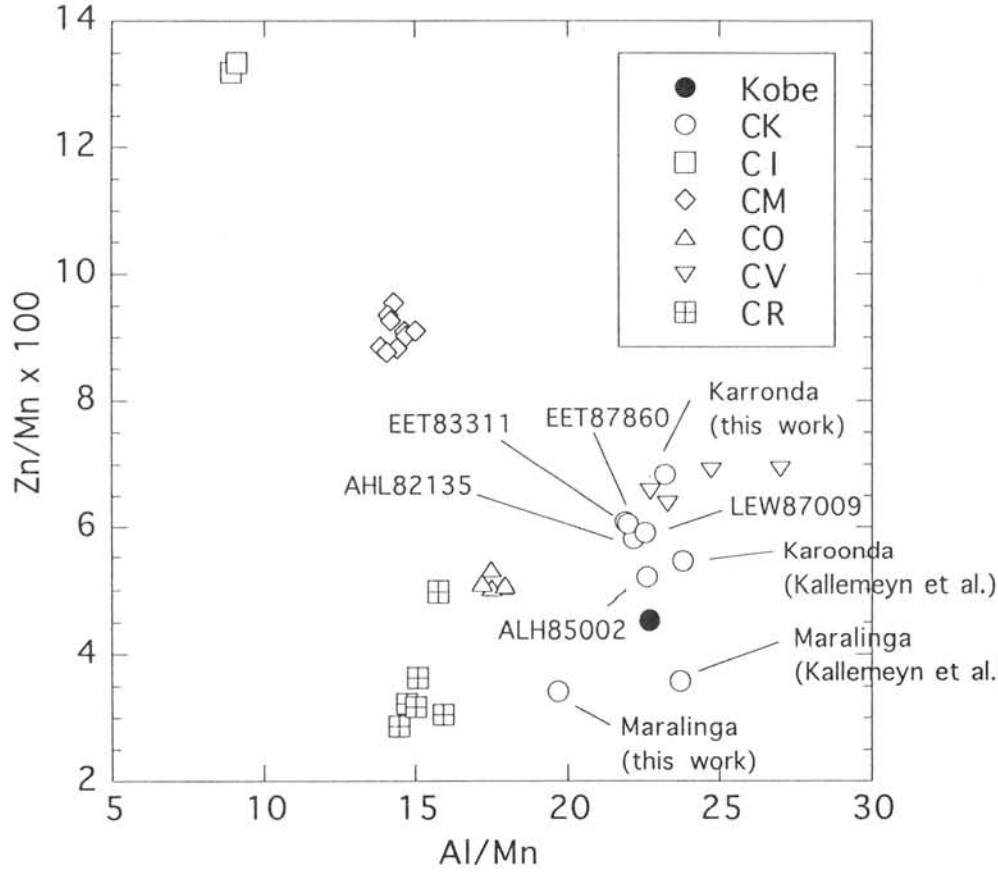

Fig.2 Correlation of Al/Mn and Zn/Mn atomic ratios for carbonaceous chondrites.

The Noble Gas Record of Enstatite Chondrites

Andrea Patzer and Ludolf Schultz

Abt. Kosmochemie, Max-Planck-Institut für Chemie, D-55020 Mainz, Germany

Introduction: Since the comprehensive noble gas analyses of enstatite chondrites by Crabb and Anders [1,2] many new specimens have been discovered, mostly in Antarctica and hot deserts. We have measured concentration and isotopic composition of all noble gases in 47 different enstatite chondrites, 33 of those are analyzed for the first time. Experimental details and complete results are given in [3]. Among these meteorites are also seven samples from the collection of the National Institute of Polar Research in Tokyo: Yamato 691, 74370, 791790, 791810, 792959, 793225, and 8404. Among these stones Y791790 and Y791810 may be paired due to their similar noble gas pattern; also Y8404 may belong to the same fall as Y8414 and Y86004 [4].

Exposure ages: The noble gases in enstatite chondrites are a mixture of different components of distinct origin. In most cases ^{4}He and ^{40}Ar is of radiogenic origin and ^{3}He, ^{21}Ne, as well as ^{38}Ar is mainly cosmogenic. From the latter isotopes cosmic-ray exposure ages are calculated with production rates derived from mean chemistry data of the respective meteorite group. Fig.1 gives a histogram of ^{21}Ne-exposure ages which are considered as the most reliable.

Most of the exposure ages range between 2 and 50 Ma which is similar to those of ordinary chondrites. The location of the parent body(ies) of E-chondrites and those of ordinary chondrites is therefore possibly similar. The shortest exposure age of about 0.065 Ma is that of Galim b [5], an enstatite pebble found together with LL specimen [6]. Galim b was most likely part of a polymict LL-chondrite. Cluster around 3, 7, and 20 Ma may represent major collisional events on the E-chondrite parent body(ies).

Solar gases: Fig.2 shows a three-isotope-plot of Ne. Five E-chondrites contain solar gases. It should be noted that all samples belong to types EL3 or EH3. In contrast, among ordinary chondrites solar noble gases are found in breccias that consist of all petrologic types. Maybe the surface of E-chondrite parent bodies are exclusively built of type 3 chondritic layers.

Trapped gases: Crabb and Anders [1,2] discovered a noble gas component in E-chondrites with elemental abundance ratios intermediate between solar and

planetary ("Q") gas. It was called subsolar (see Fig.3). This special gas pattern is found in both, EH and EL chondrites. According to our new measurements, the subsolar gas is characterized by $^{36}Ar/^{132}Xe$ = (996 ± 43) and $^{36}Ar/^{84}Kr$ = (360 ± 15) (Fig.4).

The elemental composition of the most abundant trapped gases of E-chondrites has a planetary-like pattern which is similar to "Q", the trapped gas component found in carbonaceous and ordinary chondrites. But, in addition, for EH3 chondrites with high Xe concentrations the $^{36}Ar/^{132}Xe$ ratio drops from a Q-value of 70 to about 25. This implies the presence of a new noble gas component in E-chondrites ("sub-Q", see Fig.5).

The "unequilibrated" EH3 chondrites contain with sub-Q a more fractionated component than the "metamorphosed" types 4 to 6. While there is no evidence of a strong thermal event on their parent body, this component was possibly trapped early in the history of this matter and retained essentially undisturbed.

References: [1] Crabb J, and Anders E. (1981) Geochim. Cosmochim. Acta 45, 2443-2464. [2] Crabb J, and Anders E. (1981) Geochim. Cosmochim. Acta 46, 2351-2361. [3] Patzer A. (2000) PhD-Thesis, Univ. of Mainz, Germany. [4] Okazaki R. et al. (1998) Antarctic Meteorites XXIII, 120-122. [5] Patzer A. et al. (1999) Lunar Planet. Sci. XXX, Abstr. #1145 (CD-ROM), [6] Rubin A.E. (1997) Meteorit. Planet Sci.32, 231-247.

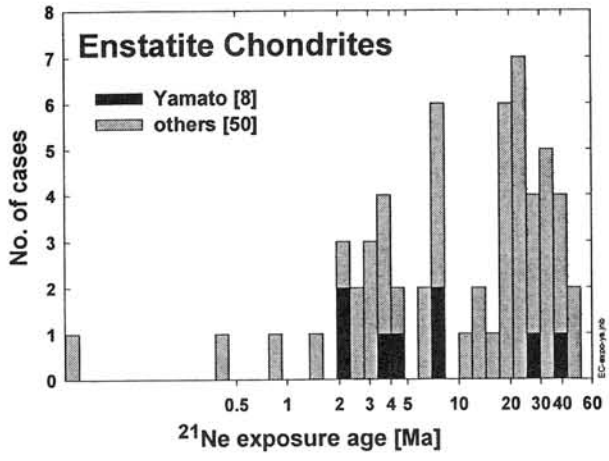

Fig.1: Cosmic-ray exposure age distribution of 58 E-chondrites (black areas indicate Yamato meteorites). The scale is logarithmic with a resolution of ±20% which is an estimate of the uncertainties.

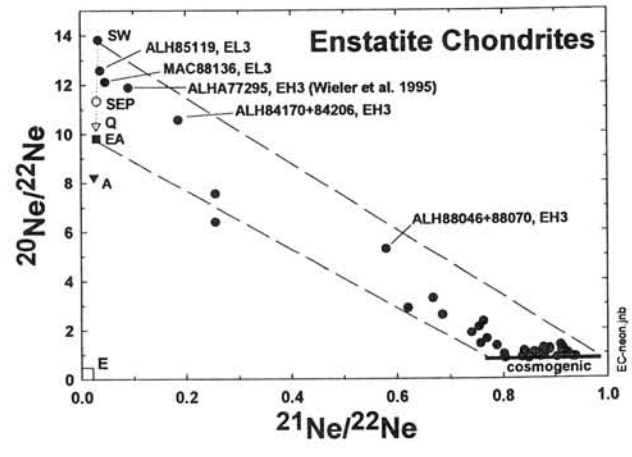

Fig.2: The Ne isotopic composition of E-chondrites. Indicated are individual components. The names of meteorites with solar gases are given.

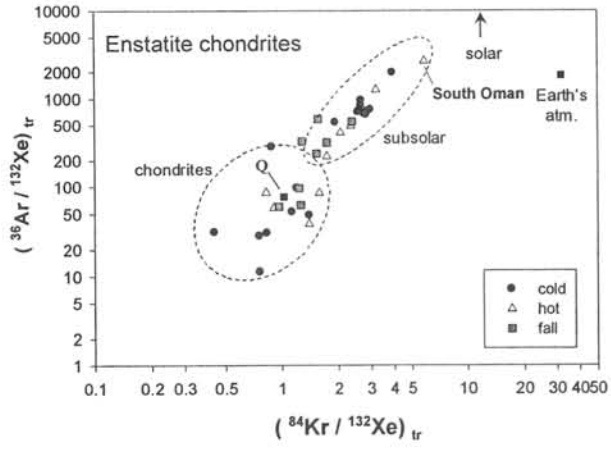

Fig.3: The plot $^{36}Ar/^{132}Xe$ vs. $^{84}Kr/^{132}Xe$ shows the fractionation of trapped gases in E-chondrites relative to solar and Q values.

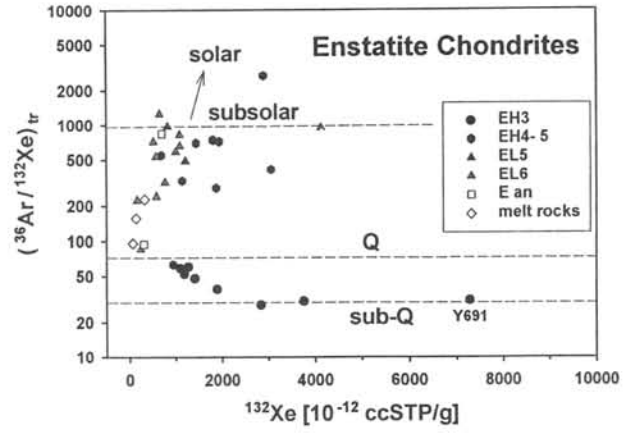

Fig.5: Ratios of $^{36}Ar/^{132}Xe$ of EH4 chondrites converge to values lower than Q ("sub-Q").

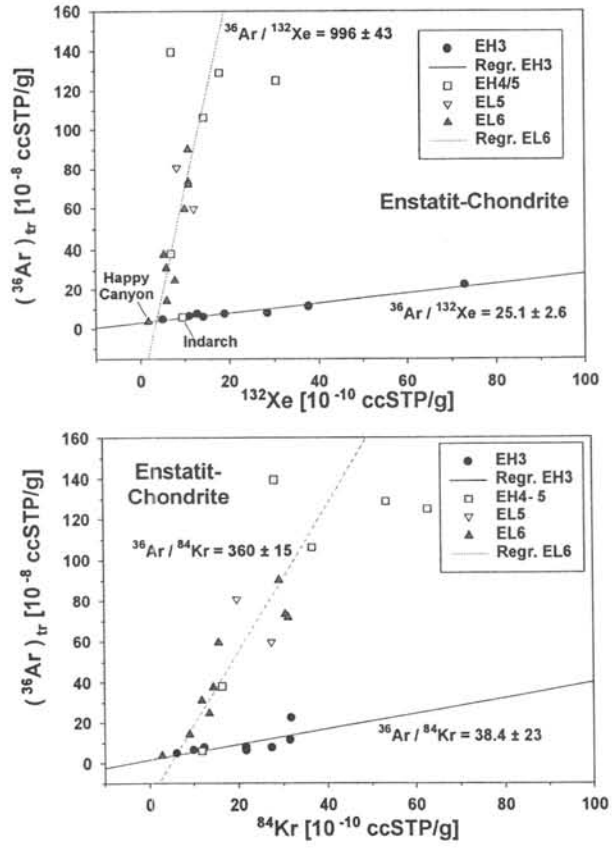

Fig.4: Concentrations of ^{36}Ar, ^{84}Kr and ^{132}Xe in E-chondrites. Subsolar and sub-Q elemental noble gas ratios are received from regression lines.

Simulation of space weathering in the laboratory: New results of olivine, pyroxene, and anorthite samples.

Sho Sasaki, Yoshimi Hamabe, Erika Kurahashi, Toshihiro Kogure

Department of Earth and Planetary Sciences, University of Tokyo
Hongo, Tokyo 113-0033, Japan

Takahiro Hiroi
Department of Geological Science, Brown University, Providence,
RI 02912, U.S.A.

The missing link between reflectance spectra of ordinary chondrites and S-type asteroids is considered to be caused by so-called "space weathering", where high-velocity impacts of interplantary dust should change the optical properties of the uppermost regolith surface of asteroids. Formation of submicron iron particles would be responsible for the reflectance changes such as reduction of spectra, reddening, and weakening of absorption bands. Such nanophase iron particles were found on the rim of lunar find soils (Keller and McKay, 1997). Recently Hapke (2000) showed theoretically that presence of nanophase iron particles on the grain surface rim should decrease and redden reflectance spectra.

At present, hyper-velocity (>10km/s) dust accelerator can hardly produce enough number of dust impacts to simulate space weathering. Using a pulse laser for heating, Moroz et al. (1996) observed the spectral change. However, the laser pulse duration was 0.5-1μs which was 1000 times of real timescale of micrometeorite (1-10μm size) impacts.

In order to simulate space weathering by impact heating of dust particles, Yamada et al. (1998, 1999) irradiated powder and pellet samples of olivine and pyroxene by a pulse laser beam (1064nm) with pulse duration 6-8 ns, which is comparable with a real dust impact. The total irradiated energy in unit area were 8 and 240 $mJmm^{-2}$, for 1 and 30mJ pulse energy, respectively. After the laser irradiation, bidirectional reflectance spectra of samples were measured; spectrum range 250 - 2600nm was recorded at every 10nm.

Yamada et al. (1999) showed decrease and reddening of reflectance spectra of olivine and pyroxene whereas scaled depth of absorption bands was not changed largely. The obtained patterns can reproduce well some olivine-rich or pyroxene-rich asteroids. Reflectance of olivine should be more easily changed than that of pyroxenes. Hiroi and Sasaki (1999, 2000) compiled asteroid reflectance data; using areas of 1μm and 2μm absorption bands, olivine-rich asteroids have more reddened spectra than pyroxene-rich asteroids.

However, microscopic process and cause of reflectance change were not clarified. What process is responsible for the optical change during laser irradiation? During pulse laser irradiation in a vacuum chamber, we observed change of the pressure gauge; evaporation should proceed on the grain surface. But it was not clear whether evaporation or recondensation should be responsible for the surface alteration. Moreover, other planet-forming minerals such as plagioclase should be studied.

In the present study, we irradiated pulse laser onto olivine, pyroxene, and anorthite pellet samples, which are formed of particles smaller than 75μm. As in the previous result (Yamada et al, 1999), we confirmed that reduction of reflectance and reddening are produced more easily in olivine samples than in pyroxene samples. Figure 1 shows olivine pellet samples before and after pulse laser irradiation. Each beam spot size is about 500μm.

Spectral decrease of pyroxene upon repetitive irradiations is nearly proportional until 2-3 times irradiations. But upon more irradiations, spectral decrease is not proportional to irradiation time. There would be some saturation effect (which can be seen on the irradiation on olivine). But heating and evaporation during irradiation should sometimes destroyed and scatter previously-altered surface materials. In fact, samples after repetitive irradiation have "altered" powders outside the laser irradiation zone. Sometimes we observed small detachment of the altered surface after more repeated (>10) irradiation. (Of course, these samples were not used in the reflectance measurements.)

For comparison, we irradiated pulse laser on the flat surface of olivine crystal. Irradiated samples were observed by TEM. Although pellet samples of olivine show significant spectral change, we observed little optical change on olivine crystal samples, although surface evaporation should proceed during the laser irradiation. No structural change on the surface was observed by TEM analyses. Upon the laser irradiation on the crystal surface, evaporated materials should go out quickly, whereas upon the irradiation on pellet samples, some fraction of evaporated materials should recondense on the surface of nearby grains. The recondensate would have different optical properties. Olivine grains from laser-irradiated pellet samples were also observed by TEM. Preliminary observation (by K. Nakamura, Kobe U.) revealed that some colored rim of irradiated olivine grains contains small (10-50nm) nanophase iron particles, which would responsible for the optical change.

We newly observed a small spectral change of anorthite pellet samples after the laser irradiation. Nearly pure anorthite from Kuttara Lake, Hokkaido, was ground into powder smaller than 75μm. Powder samples was formed into a pellet. Different from olivine and pyroxene, anorthite pellet samples are very fragile. They are sometime broken during handling and or even during the laser irradiation. Preliminary measurements of reflectance suggest that reflectance

after repeating irradiation should decrease in several per cent. (But reflectance after once irradiation shows slight increase from that of the original sample. We think this is due to the removal of surface dirty volatile materials, not due to the anothite characteristics.)

In order to discuss the change of 510nm absorption band, we performed repetitive irradiation on pellet samples of enstatite, which is from Bamble, Norway and contains 9.88wt%FeO (En85). Bidirectional reflectance was measured manually by 1nm interval between 500 and 540nm. After twice irradiation of 30mJ pulse laser scanning, 510nm band was apparently weakened. This would correspond to the change of iron oxidation state on the grain surface. This effect is also discussed by Hiroi et al. (2000) together with lunar sample data.

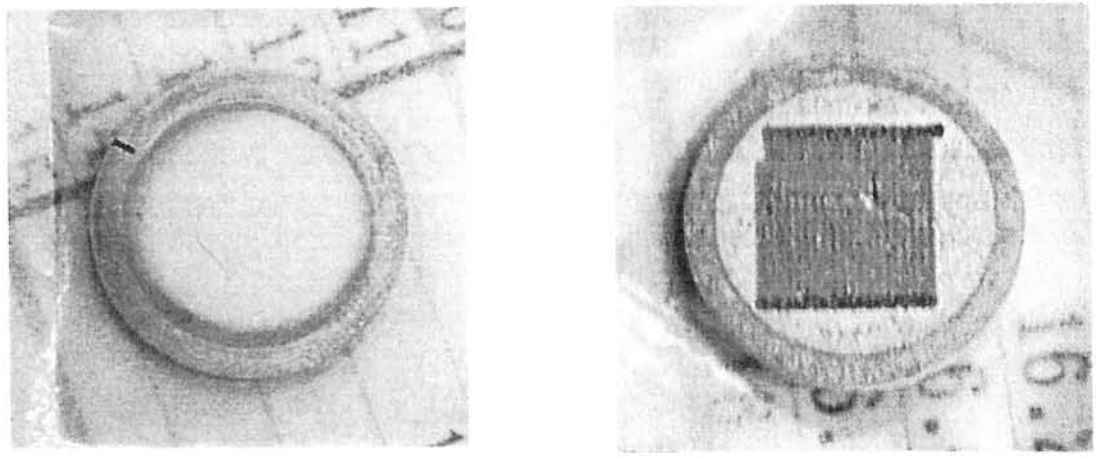

Figure 1 Olivine pellet sample before and after pulse laser (30mJ) irradiation. Size of pellet is 20mm. We use automatic X-Y stage to perform uniform scanning irradiation.

References:

Hapke, B. (2000) LPSC XXXI.
Hiroi, T. and Sasaki, S. (1999) LPSC XXX.
Hiroi, T. and Sasaki, S. (2000) submitted to MAPS
Hiroi, T. et al. (2000) This volume and WPGM abstract.
Keller, L. P. and McKay, D. S. (1997) GCA, 61, 2331-2341.
Moroz, L. V. et al. (1996) Icarus 122, 366-382.
Yamada, M. et al. (1998) Antarctic Meteoriets XXIII, pp.173-176.
Yamada, M. et al. (1999) Earth, Planets and Space 51, 1255-1265.

Cathodoluminescence and $^{40}Ar/^{39}Ar$ dating of Maskelynite in Etter

A. Sato, K. Ninagawa and H. Hyodo*
Department of Applied Physics, Okayama University of Science
*Research Institute of Natural Sciences, Okayama University of Science

We measured cathodoluminescence (CL) of an ordinary chondrite, Etter, and tried laser probe $^{40}Ar/^{39}Ar$ dating. Etter is classified to be L5 chemically and petrologically, and to be S5 in shock classification proposed by Stöffler (1991). Then Etter includes isotropization of plagioclase, a glass like phase (maskelynite).

The maskelynite is observed homogeneously under a microscope (Fig.1). However it shows inhomogeneous CL emission (Fig.2). Figure 3 is compositional mappings of the maskelynite by an electron probe micro analyzer. Sodium distributes homogeneously, but Calcium and Potassium distribute separately. CL intensity of maskelynite inversely correlated to Potassium content. Potassium is distributed in no luminescent region.

Colorless maskelynite changed to brown by irradiation of electron beam during EPMA. This was due to that the carbon courting came off from the thin section, and often observed in hydrous minerals when they lose water. This suggested that water existed in maskelynite. We tried to detect water in maskelynite by FT-IR analysis.

We also applied $^{40}Ar/^{39}Ar$ method to date the shock event producing the maskelynite in the Etter. We measured at first $^{40}Ar/^{36}Ar$ ratio on a many points of Potassium poor region in the thin section by the laser probe with 70μm spot. The ratio of $^{40}Ar/^{36}Ar$ was averaged to be 94 at low value points. We supposed that initial ratio of $^{40}Ar/^{36}Ar$ was 94. We measured $^{40}Ar/^{36}Ar$ on potassium rich region in the maskelynite, and got $^{40}Ar/^{39}Ar$ age of 5-10 billion years. L chondrite, Etter, was shocked at 5-10 billion years ago.

Reference: Stöffler D., Keil K. and Scott E.R.D. (1991): Shock metamorphism of ordinary chondrites. *Geochim. Cosmochim. Acta*, **55**, 3845-3867.

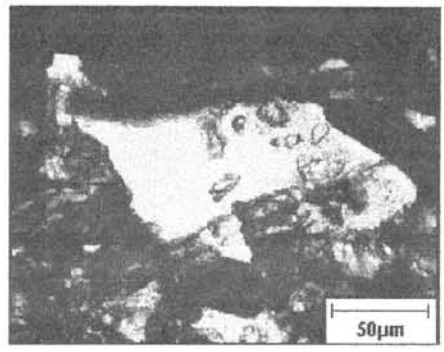

Fig.1 photomicrograph of the maskelynite

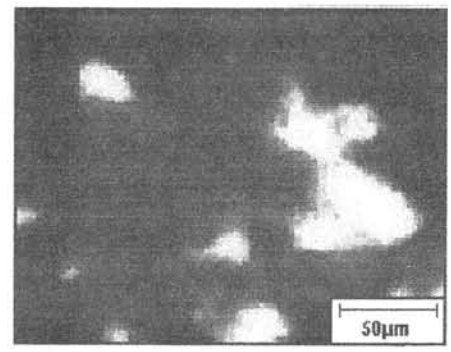

Fig.2 CL photograph of the maskelynite

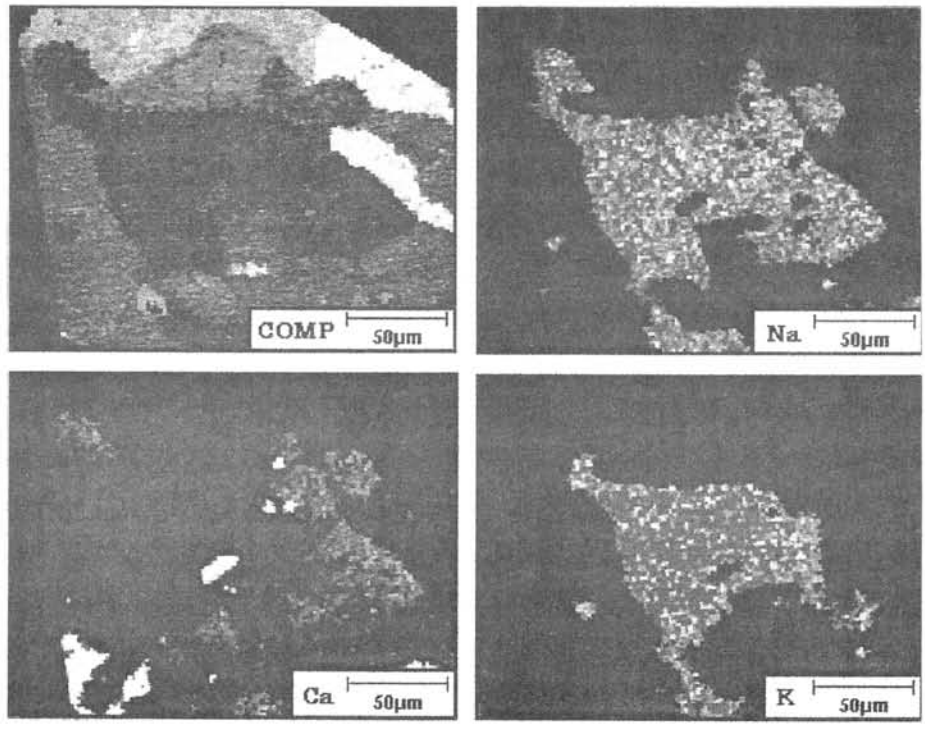

Fig.3 Compositional mappings

Measurement for Cosmogenic Mn-53 in Meteoritic Irons.

M. Setoguchi [1], M. Ebihara [1], H. Nagai [2], and M. Honda [2]
1) Dept. of Chemistry, Tokyo Metropolitan Univ., 2) Dept. of Chemistry, Nihon Univ.

A long-lived cosmogenic nuclide, Mn-53 (1), $T_{1/2}$= $3.7x10^6$y(2), has been determined in various meteoritic irons. The main target to produce Mn-53 in space is an iron atom composing most of extraterrestrial materials. For a far longer irradiation of galactic cosmic rays relative to the half-life the disintegration rate has reached to the saturation level and become equal to the production rate in the meteorites..

The determinations have been performed applying neutron activation method. When the manganese fraction separated along with or without the carrier and purified from the meteorites is irradiated in a reactor, Mn-54 , $T_{1/2}$ = 312 d, can be observed as an activated product by reactor neutrons. By this activation, due to a higher neutron capture cross-section of 80 b., the disintegration rates of Mn-53 can be enhanced to the order of 1000 depending on the reactor's capacity and time. In general, 1g meteorite contains 0.5-0.1dpmMn-53. After irradiation in a reactor we cam expect several hundred dpm Mn-54 gamma, at 835keV region, which can easily be determined with a gamma ray detector. In 1965, Millard (3) intended to estimate the life-time of Mn-53 and has initiated the method. Since 1969, by Imamura et al. (4), this method has been applied, extensively as the analytical technique in the cosmochemical studies: the data have been compiled together with other long-lived cosmogenic radio-nuclides, such as Be-10, Al-26 and Cl-36, given by Nishiizumi (5) et al. For the performances of this method, however, there are several restrictions. The first may be to search well-thermalized neutron fluxes to reduce interferences due to high energy neutrons, by Mn-55 (*n,2n*) Mn-54 . This is rather important for chondrites which contain about 0.3 %Mn but only 20-30 %Fe. For ordinary iron meteorites, however, this problem is not quite serious, because the Mn contents are lower than 1ppm and the amount of the Mn carrier can be reduced to much smaller than 0.1mg for 1g size of irons. Another factor may be in the chemical purification steps for Mn separated from meteorites. Fe should be practically absent in the sample because of a higher factor of the interference due to Fe-54 (*n,p*)Mn-54.

In this report, we describe our recent studies on the determinations of cosmogenic Mn-53 in various iron samples. Chemical procedures for preparation of sample consist of pre-irradiation steps to separate Mn fraction from meteorites. The Mn separated with the carrier is mounted on an aluminum foil holder for neutron

irradiation. According to our normal procedure, further chemical purification steps are followed after irradiation. Using an aliquot of final samples Mn recovery is determined. Historically the post-irradiation chemistry had to be introduced before a common use of a Ge detector. Recently we are developing a simplified procedure omitting the post-irradiation purification step. For this purpose, pre-irradiation chemistry must be extensive and impurities from the sample holder should also be insignificant. In fact, elimination of Ir from irons and selection of the holder free from Sc are essential (Table 1). On the other hand, because of a longer-lived activity of Mn-54, a relatively long cooling time can be helpful due to reductions of Ir-192 (74d), Sc-46 (84d) and other activities (Fig.2). In this case, a non-destructive activation analysis for the recovery of Mn can be performed conveniently without opening sample holders. Even with present techniques in the DR-1 hole of JRR3 since 1995, stony meteorites like chondrites can be examined for the Mn-53 (Fig.1). Especially for the samples of extremely low specific activities of Mn-53, such as in a deep interior of the large meteoroids, however, a highly sensitive AMS method will be applied in near future.

Reference: 1). M.Honda et al. (1961) GCA.22, 133. 2). M.Honda and M.Imamura (1971) Phys.Rev., C4,1182. 3) H.T.Millard Jr.(1965) Science 147, 503. 4). M.Imamura et al.(1969) EPSL 6. 165. 5). K. Nishiizumi (1987) Nucl. Tracks Radiat. Meas., 13, 209.

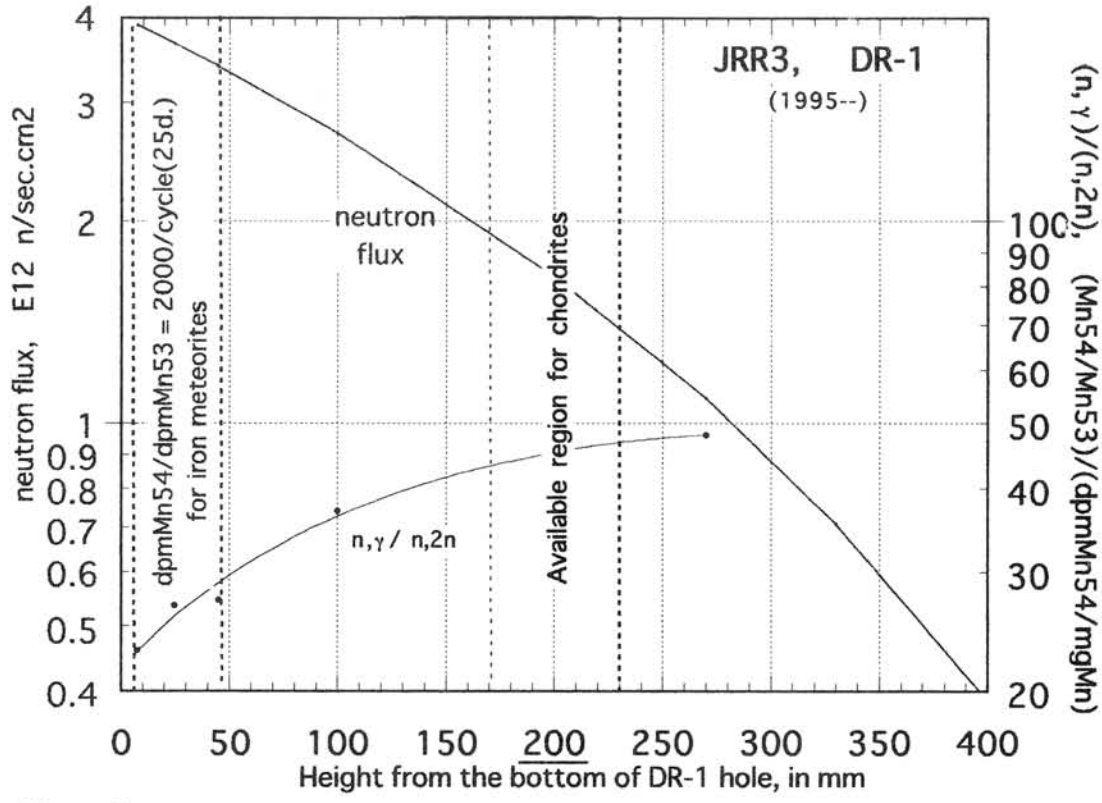

Fig. 1 JRR3 DR-1, thermal neutron flux and high energy effects

Table 1. Counting Data for Iron Meteorites and Relative Impurity Level.

Cooling for 8 months Counter: vertical Ge.								Alfoil	impurity cpm peak area---> meteoritic		Al foil impurity				Base/ch.	Al foil
sample	sample,g recover.wt*	Mn-54 cpm	±	Mn53dpm net	Mn μg	Mn,n,2n cpm	dead time %	Fe μg 1099keV	Co58 811keV	Ir192 785(s)	Ag110m 764keV	Co60 1173	Tb160 880	Sc46 889	0.5keV. 840keV	mg
Grant,sol. 1973[&]																
IIIB, 0.04ppmIr#	0.08	2.49	0.05	0.042	7.8	0.02	0.1	-0.3	-0.1	0.1	0.0	0.8	-0.18	6	0.08	Net
Henbury sol.1999[&] (193.493); IIIA, 13ppmIr	0.16	3.48	0.07	0.055	100 after chem.	0.22	0.4	1.5	17.6	53	1.47	32	1.58	85	0.74	70
Santa Apolonia,#112.36 IIIA,8ppmIr	0.54	3.13	0.18	0.049	102	0.37	1.4	2.2	0.65	206	2.6	120	2.00	141	1.6	73
Al blank	0.073	0.01	0.11	0	0.02	0	0.2	3.7	-	-	no peak	33	3.48	184	1.12	73
counter B.G.		0.003	0		0	0									0.03	

&: year of reference prepared.

#: Net contents in reference soluton were obtained by empirical subtraction of impurities in Al foil.

*: Recovery of Mn were determined by non-destructive NAA, and corrected for sample sizes.

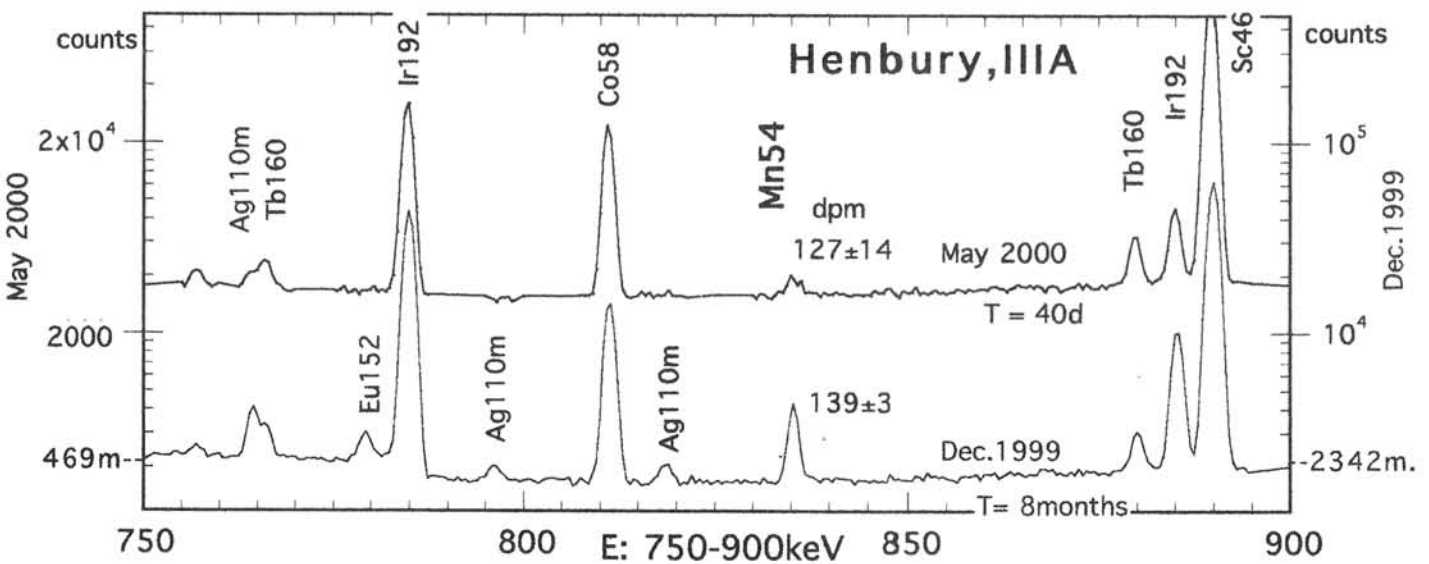

Fig.2 Gamma ray spectra of Mn fractions

Boron isotopic composition of the CAI(E-38) in Efremovka

N.Sugiura[1], Y.Shuzou[1] and A.A. Ulyanov[2]
1: Department of Earth and Planetary Science, Univ. of Tokyo
2: Geological Department, Moscow State Univ.

Introduction

Boron isotopic anomalies in meteorites were first reported by Chaussidon and Robert (1995, 1998) for chondrules. But a recent study by Hoppe et al. (2000) did not find such B isotopic anomalies. Thus, anomalies in chondrules are not well established yet. In contrast, much larger B isotopic anomalies were reported recently by McKeegan et al. (2000), for Allende CAIs. The B isotopic anomalies are well correlated with Be/B, indicating that short-lived ^{10}Be was incorporated into CAIs during crystallization. An initial ^{10}Be/^{9}Be ratio was estimated to be (9+/-1)x10^{-4}.

Because ^{10}Be is not produced by stellar nucleosynthesis, the existence of this radioisotope in the early solar system can only be due to nuclear reactions by energetic particles. It is likely that the precursor dust was irradiated by flare activity as proposed by Shu et al. (1996). McKeegan et al. (2000) showed that appropriate amounts of the other short-lived nuclides such as ^{53}Mn and ^{41}Ca (but not ^{26}Al) can be produced by the same mechanism. Therefore, it is of great importance to establish the B isotopic anomalies and the correlation with Be/B in chondritic materials. Here, we report preliminary results on B isotopic measurements of the CAI(E-38) in Efremovka.

Sample

E-38 is a coarse-grained type B1 CAI with a well developed melilite mantle. It is surrounded by a spinel rim which is rich in Fe. Three anorthite grains were examined for the Al-Mg chronology. One grain in the core showed a nearly canonical value of ^{26}Al/^{27}Al, whereas a grain near the rim showed a completely normal Mg isotopic composition. This, together with the presence of the Fe-rich spinel rim suggest that this CAI was slightly disturbed after the initial formation.

Experimental procedure

B and Be measurement conditions are similar to those used by other studies. An intense primary O^- beam of higher than 10 nA is focused on the analyzed area. Mass resolving power is about 1500. The instrumental mass fractionation of B isotope is about 0.96. Background counts of EM are corrected, although it only affects the data of the smallest count rates. The results are summarized in the table and shown in the figure.

Results

Measurements were repeated on the same grains to examine the reproducibility of the data. In the cases of melilite and anorthite, the reproducibility is faily good. In the cases of fassaite and spinel, where intrinsic B concentrations seem to be small, some of the results are dominated by contamination.

As shown in the figure, the B isotopic anomalies are well correlated with the Be/B ratios. A fassaite datum point is located above the correlation line but it is also consistent with the isochron within the one sigma error. The results suggest that ^{10}Be was alive when the CAI was formed. However, it is also possible to interpret the correlation as a mixing line.This is because the B isotopic anomalies are correlated with Si/B ratios, as far as the melilite data are concerned.

Conclusions

B isotopic anomalies are well established in CAIs. The correlation between the B anomalies and Be/B suggests the presence of live ^{10}Be, although it could also be explained as a mixing line.

References

Chaussidon and Robert (1995) Nature, 374, 337-339.
Chaussidon and Robert (1998) EPSL ,164, 577-589.
Hoppe et al. (2000) LPS, #1235.
McKeegan et al. (2000) LPS, #1999.
Shu et al. (1996) Sci., 271, 1545-1552.

Table Summary of SIMS measurements.

mineral	^{11}B (cps)	$^{10}B/^{11}B$	error (1σ)	$Be^+/^{11}B^+$	error (1σ)
melilite(1)	53.9	0.268	0.004	19.7	0.2
melilite(2)	22.3	0.267	0.006	22.4	0.4
melilite(2)	26.9	0.276	0.005	22.9	0.3
melilite(4)	7.2	0.294	0.010	98.7	2.6
fassaite(5)	84.2	0.256	0.003	1.13	0.02
melilite(4)	7.5	0.285	0.007	102.9	1.9
melilite(7)	2.1	0.359	0.017	354.2	12.6
melilite(2)	20.6	0.272	0.005	29.2	0.4
melilite(8)	4.9	0.282	0.012	48.8	1.4
spinel (15)	313.0	0.250	0.001	0.328	0.003
spinel (16)	0.41	0.265	0.030	25.2	2.1
fassaite (17)	6.2	0.252	0.007	10.6	0.2
fassaite (17)	0.12	0.348	0.070	121.2	17.8
anorthite (10)	10.3	0.272	0.006	58.8	1.0
anorthite (10)	12.3	0.273	0.005	52.7	0.6
anorthite (10)	6.0	0.272	0.007	77.3	1.3

Numbers in parentheses identify grains (the same number for the same grain).

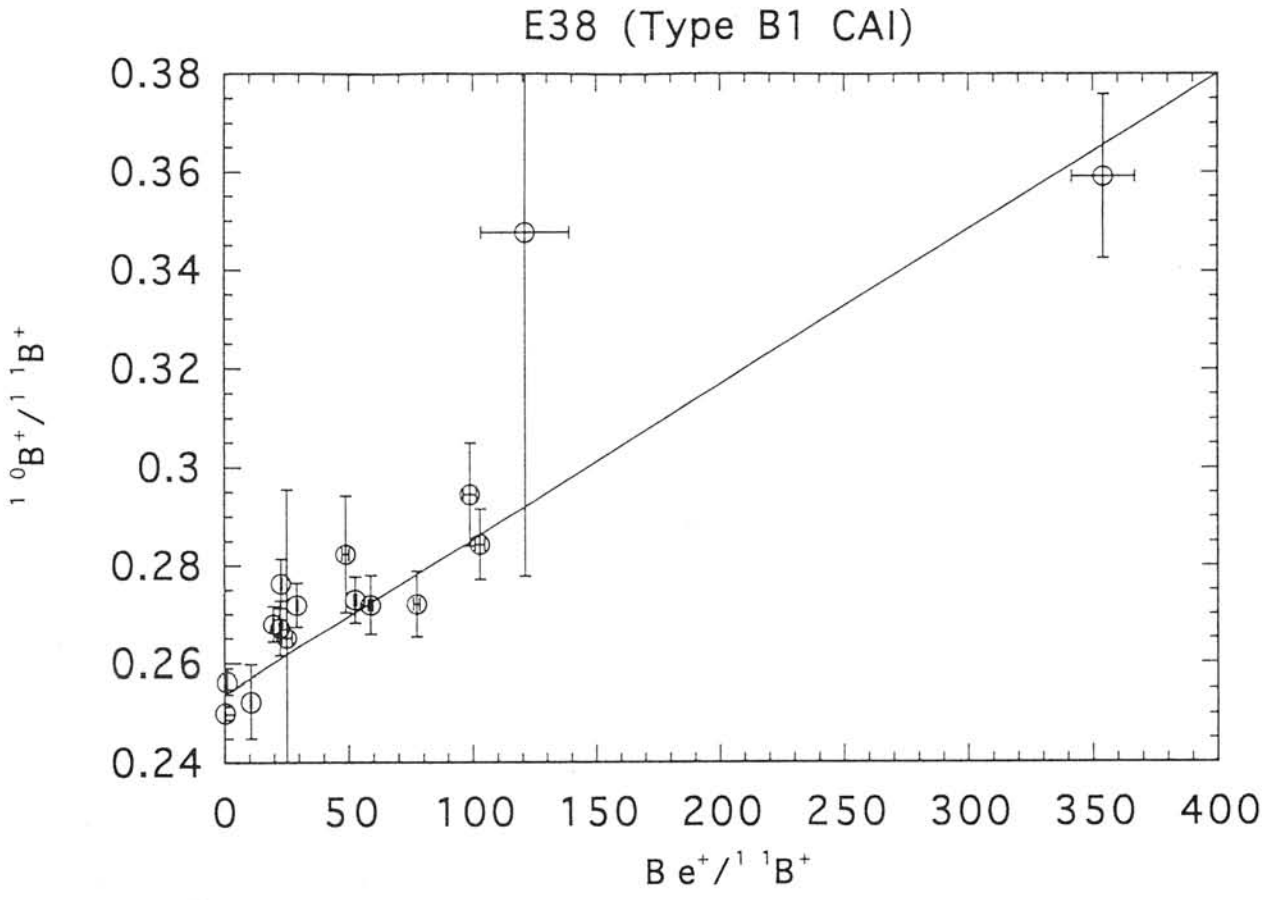
E38 (Type B1 CAI)
0.38
0.36
0.34
0.32
0.3
0.28
0.26
0.24
0
50
100
150
200
250
300
350
400
$^{10}B^+/^{11}B^+$
$Be^+/^{11}B^+$

Temperature dependence of evaporation of enstatite and its application to the evaporation behavior of enstatite in the primitive solar nebula

Shogo TACHIBANA[1], Akira TSUCHIYAMA[2], and Hiroko NAGAHARA[1]

[1]Dept. of Earth & Planet. Sci. (Bldg. No.5), Univ. of Tokyo, 7-3-1 Hongo 113-0033, Japan, [2]Dept. of Earth & Space Sci., Osaka Univ., 1-1 Machikaneyama, Toyonaka 560-0043, Japan. E-mail: tachi@sys.eps.s.u-tokyo.ac.jp

Introduction Chemical studies on chondrites have revealed that chondrites, which have been regarded as primitive meteorites containing records of early solar nebula processes, are somewhat fractionated from the solar abundance (except for CI), classified them into some dozen of chemical groups, and suggested chemical fractionation processes in the solar nebula. The abundance ratios of magnesium and silicon, both of which are the major rock-forming elements in the solar system, are different in each chemical group of chondrites. Since magnesium and silicon are different in volatility, Mg/Si ratios among chondrite chemical groups would reflect Mg/Si variations which were made during evaporation or condensation in the solar nebula. Previous studies [1, 2] have tried to explain this variation by coupling of equilibrium condensation of the solar nebula gas and extraction of condensates from the reactive system. However, equilibrium condensation models are valid only if timescale of equilibration is much shorter than timescale of thermal and/or dynamical evolution of the solar nebula. If this is not the case, knowledge of reaction kinetics helps us understand how effectively condensation and/or evaporation would proceed during the solar nebula evolution and whether or not a reaction(s) would play a key role(s) for fractionations in the nebula. We have experimentally studied kinetics of evaporation of enstatite ($MgSiO_3$), which might be an important process for Mg/Si fractionation because it evaporates incongruently forming forsterite (Mg_2SiO_4) as an evaporation residue [3]. We report our new results of temperature dependence of evaporation of enstatite and apply the results to evaluate timescale of evaporation of enstatite grains of which radii are 1 μm in the solar nebula conditions, and discuss the possibility of Mg/Si fractionation comparing with dynamical processes in the solar nebula.

Experiments Orthoenstatite single crystals were synthesized by a flux method (~1 mm x 2 mm x 3 mm) and used as starting materials in experiments. Samples were heated in vacuum furnaces, of which heating elements are tantalum or tungsten (details in [4, 5]), in vacuum (~10^{-9} bar) or hydrogen gas (hydrogen pressure of 7.2×10^{-7}, 2.0×10^{-6} or 6.1×10^{-6} bar) at 1300-1500°C with continuous evacuation. The evaporation residue formed on the surface of enstatite was identified as forsterite by EPMA analyses, X-ray diffraction and infrared spectroscopy. The thickness of the residual forsterite layer was measured by optical microscopic observation of polished thin sections of samples.

Results Enstatite evaporates incongruently forming a forsterite layer as an evaporation residue both in vacuum and hydrogen gas. The forsterite layer with several μm thickness was formed in vacuum experiments, and the thickness of the forsterite layer (X_{Fo}) increases almost linearly with time in the early stage of evaporation. X_{Fo} becomes constant as evaporation proceeds at 1400°C, while it decreases once and approaches a constant value at 1450 and 1500°C (Fig.1). The forsterite layer in hydrogen gas was too thin to observe under an optical microscope. The weight loss of samples per unit area ($\Delta W/S$) was thus used to evaluate the evaporation rate. It appears that $\Delta W/S$ has a linear correlation with time.

Disccusion (1) Evaporation kinetics Evaporation of enstatite in the early stage of evaporation, where X_{Fo} increases almost linearly with time, seems to be controlled by the surface reaction probably because the forsterite layer in the early stage is porous and gases that evaporate from the surface of enstatite can escape through the porous layer. Since residual forsterite also evaporates in the present experimental conditions, the formation rate of the forsterite layer (dX_{Fo}/dt) should be expressed by $dX_{Fo}/dt = k_{En} - k_{Fo}$, where k_{En} and k_{Fo} are the surface-reaction controlled evaporation rate constants of enstatite and forsterite, respectively. We

estimated k_{En} from X_{Fo} data in the early stage (t<55 h) using k_{Fo} which was extrapolated evaporation rates of forsterite in [6]; $k_{En}(cm\,s^{-1}) = 685(\pm1001)\exp(-362(\pm21)(kJ/mole)/RT)$, where R is the gas constant and T is the absolute temperature.

The constant thickness of the forsterite layer in the later stage of evaporation is explained by diffusion-controlled evaporation, where the formation rate of the forsterite layer is given by the diffusion-controlled evaporation rate constant of enstatite (κ_{En}) and k_{Fo} ($dX_{Fo}/dt = \kappa_{En}/2X_{Fo} - k_{Fo}$). When X_{Fo} becomes a specific thickness ($X^*_{Fo} = \kappa_{En}/2k_{Fo}$), evaporation achieves a steady state and the formation rate of forsterite (dX_{Fo}/dt) becomes zero for further evaporation. This diffusion-controlled evaporation mode appears when the porous forsterite layer becomes compact due to grain growth on the surface of enstatite. We obtained κ_{En} from the constant thickness at each temperature in the later stage of evaporation (Fig.2) using k_{Fo} in [6], $\kappa_{En}(cm^2\,s^{-1}) = 126(\pm536)\exp(-451(\pm61)(kJ/mole)/RT)$.

The depletion pattern of X_{Fo} observed at 1450 and 1500°C is explained by the change of the rate-limiting process from the surface-reaction to diffusion.

The thinner forsterite layer in hydrogen gas than in vacuum is explained by steady state evaporation in hydrogen gas ($X^*_{Fo} = \kappa_{En}/2k_{Fo}$) since κ_{En} has little dependence on hydrogen while k_{Fo} becomes larger in the presence of hydrogen [7]. The evaporation rate of enstatite should be equal to k_{Fo} in hydrogen gas if evaporation achieves the steady state in hydrogen gas. The evaporation rate of enstatite in hydrogen gas, which was obtained from the weight loss of samples, was compared with k_{Fo} in hydrogen gas [5]. The evaporation rate of enstatite in hydrogen gas was in good agreement with k_{Fo} suggesting steady state evaporation of enstatite in hydrogen gas in the present experiments.

Discussion (2) Application to evaporation of enstatite in the solar nebula Evaporation behavior of enstatite in the system Mg-Si-O-H-C-He is considered at 1400-900°C at the initial total pressure of 10^{-5} bar based on experimental evaporation kinetics of enstatite to discuss timescale of evaporation and the possibility of the Mg/Si fractionation in the nebula caused by evaporation of enstatite. A dust enrichment factor (η), which expresses the abundance ratio of enstatite grains to hydrogen atoms in the system (η=([Si]/[H])/([Si]/[H])$_{solar}$) is introduced as a parameter. It is assumed that there is no Mg-bearing and Si-bearing gas species initially in the system, but Mg and Si are present only in the condensed phase (enstatite).

Equilibrium calculations show that there are three different equilibrium states for evaporation of enstatite depending on temperature and η (Fig.2); complete evaporation (CE), partial evaporation with equilibration between residual forsterite and gas (PE/F), and partial evaporation with equilibration between enstatite, residual forsterite and gas (PE/EF). CE and PE/EF occur with small and large values of η, respectively, and PE/F occurs in the range of intermediate values of η. The Mg/Si fractionation in CE would not be expected because only a small amount of forsterite is formed by evaporation, and Mg/Si ratios in solid and gas are almost close to the original ratio of Mg/Si=1 throughout evaporation. Forsterite alone is the equilibrium condensed phase in PE/F, and the Mg/Si ratio of gas ranges from 1 to less than 0.2 at equilibrium depending on η. The Mg/Si ratio in solid at equilibrium varies from 2 to 1 as η increases, while the Mg/Si ratio in gas at equilibrium is smaller than the original ratio and constant irrespective of η in the case of PE/EF. The Mg/Si fractionation is expected in PE/F and PE/EF if solid-gas separation took place effectively.

Calculated timescales for evaporation of enstatite grains of 1 μm are also shown in Fig.2. Evaporation would be completed within several hours, a week to a few months, and a year to a few hundred years at 1400, 1100 and 900°C, respectively.

Let us compare the timescale and temperature for evaporation with early solar nebula processes and discuss the possibility of the Mg/Si fractionation. At high temperatures (1400-1300°C), evaporation in high

dust enrichment (η >several hundreds) conditions would make Mg/Si variations in solid and gas, which was caused by settlement of dust grains to the nebular midplane, as long as there were heat sources such as lightning or shock waves. At temperatures of 1200-1000°C, modest dust enrichment (several to several tens times) would be enough for the fractionation (grains do not evaporate in extreme high dust enrichment conditions). Such a degree of dust enrichment would be achieved in turbulent eddies in the active solar nebula and turbulence itself would work as a heat source (e.g., [8]) and for solid-gas separation. At low temperatures (<1000°C), dust-depleted (η<1) conditions would be needed for the fractionation and would be realized as a counterpart of the dust-enriched condition in the turbulent nebula or during dust-settlement. Coagulation of dust particles, of which timescale is hundreds years, would also work for solid-gas separation at modest to lower temperatures (<1200°C) since large dust aggregates would have a larger relative drift velocity to the Sun than gas and fine dust particles.

Acknowledgements S.T. thanks JSPS Research Fellowship for Young Scientists (J.C.).

References [1] Larimer J. W. (1979) *Icarus*, **40,** 446-454. [2] Kerridge J. F. (1979) *Proc. LPSC*, **10,** 989-996. [3] Tachibana S. et al. (1998) *22nd Antarc. Met.*, 179-181 (abst.). [4] Ozawa K. and Nagahara H. (2000). *GCA*, **64,** 939-955. [5] Tsuchiyama A. et al. (1998) *Mineral. J.*, **20,** 113-126. [6] Hashimoto A. (1990) *Nature*, **347,** 53-55. [7] Nagahara H. and Ozawa K. (1996) *GCA*, **60,** 1445-1459. [8] Bell K. R. et al. (1997) *Astron. J.*, **486,** 372-387.

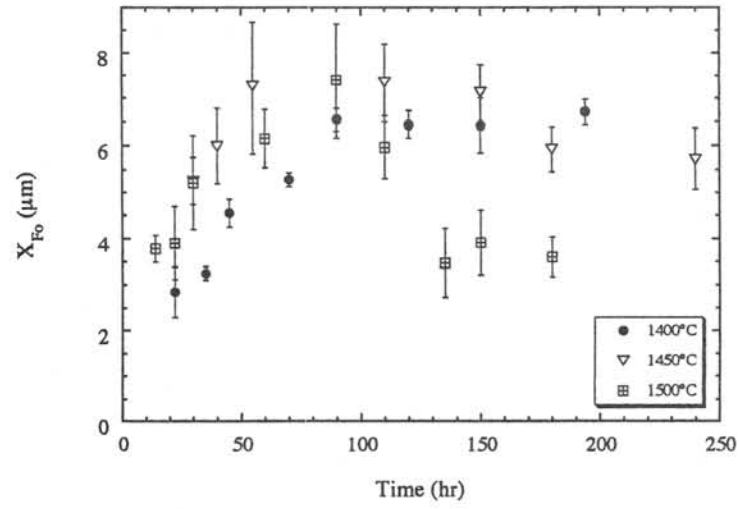

Fig.1 Change of the thickness of the residual forsterite layer (X_{Fo}) with heating duration in vacuum experiments at temperatures of 1400-1500°C.

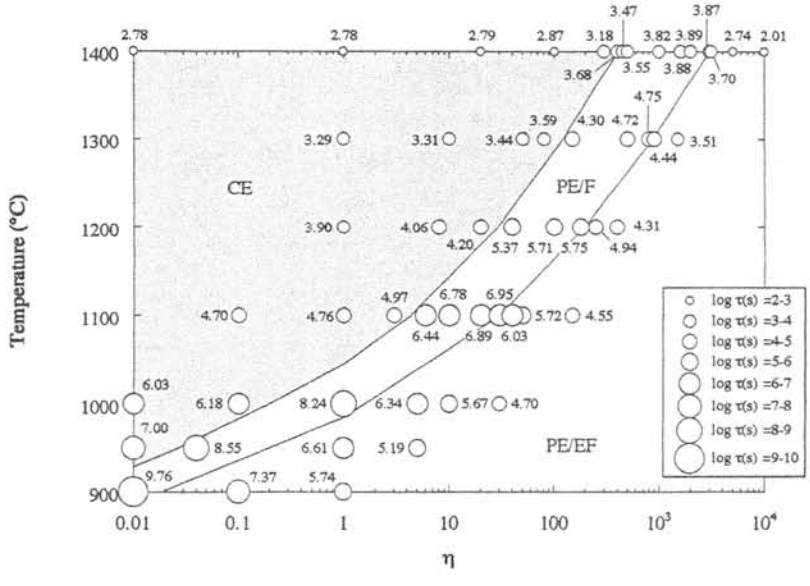

Fig.2 Three different equilibrium states of evaporation of enstatite (CE, PE/F and PE/EF; see text) and timescales for evaporation (τ) of enstatite of 1 μm.

Noble gases released by mechanical crushing of enstatite chondrites and ureilites

N. Takaoka[1], R. Okazaki[1, 2], T. Nakamura[1] and K. Nagao[2]

1. Department of Earth and Planetary Sciences, Kyushu University, Fukuoka 812-8581

2. Laboratory for Earthquake Chemistry, University of Tokyo, Tokyo 113-0033.

Introduction : Meteorites contain noble gases of various origins. Trapped gases were acquired by their host phases through adsorption, implantation, dissolution and occlusion of ambient gases in the solar system and circumstellar environments. In-situ produced noble gases originated through radioactive decays of parent nuclides and nuclear reactions of energetic particles with target nuclides in meteorites, and reside at crystal lattice points of the parent and target nuclides.

One of major goals of noble gas measurements is to find end members of noble gas component contained in samples. Besides stepped heating, mechanical crushing of meteorite samples is a useful method for this purpose from the following reason: When volatile-rich materials are heated in meteorite parent-bodies by radioactivity, gravitational energy and impact shock, volatiles such as water and carbon can generate vesicles consisting of water vapor and CO_2 gas, respectively. Appreciable amounts of noble gases can move into the vesicles this time. Noble gas itself could swell up to micro-vesicles if a large amount of gas is dissolved in the host. Sasaki et al.(1991) have reported that when SiC crystal was heated at 1400℃ for 1 hour, He atoms which originated from a (n, α) reaction on ^{10}B doped into SiC, migrated to the grain boundary and swelled up there to 3 - 30 nm bubbles. If noble gases in meteorites are expelled from silicate crystals to migrate into their grain boundary, it is expected that noble gases can be enriched in vesicles along grain boundary and within a grain. Noble gases contained therein could be released preferentially by mechanical crushing. Here we report result of noble gas analyses by crushing and heating of twelve enstatite chondrites and two ureilites. In analyses of enstatite chondrites, crushing was followed by stepped heating of the same sample without vacuum break.

Results and discussion : Noble gases released by crushing are rich in trapped gases but depleted in cosmogenic and radiogenic gases. This is the same trend as reported for Happy Canyon enstatite chondrite [1] and Y74063 acapulcoite [2]. Table 1 lists fractions of trapped ^{36}Ar and ^{132}Xe released by crushing (typically 1800 to 4200 strokes). The most prominent are the high yields of trapped Ar and Xe for Y791790 (EH3) and 793225 (EH/EL6): In particular, 31% and 24% of trapped Ar and Xe, respectively, determined in bulk sample was released by crushing Y791790, and for Kenna, 41% of trapped Xe in bulk sample. ALH78019 also released more than 20% of total trapped Ar and Xe by crushing. Among them, $^{36}Ar/^{132}Xe$ for Y791790 is 3090, the highest ratio so far reported for subsolar gas. This indicates that appreciable amounts of primordial gases are trapped at sites from which the gases can be lost easily by mechanical crushing. Micro-vesicles along grain boundary and in grains, or/and minerals of low retentivity such as graphite are candidates of trapping sites. The

present result suggests that significant amounts of trapped gases may be lost from enstatite chondrites and ureilites at sample preparation including mechanical crushing. Note that in study on trapped noble gases in ureilites, Gobel et al. (1978) have suggested other noble gas carrier in addition to carbon-rich vein material (diamond) [3]. A phase trapping noble gases that can be released by mechanical crushing may be a candidate of such carrier.

For enstatite chondrites, trapped gases reside in enstatite mineral [4]. The high yields for trapped Ar and Xe (Table 1) suggest that Y791790 trapped great amounts of primordial gases, enriched in ^{36}Ar, along boundaries and/or fractures of enstatite grains which are destructible preferentially by crushing. Because some enstatite crystals in this meteorite have many vesicle-like vacancies, micro-vesicles in enstatite grains, and mineral of low retentivity such as graphite may be candidates for carrier.

Table 1 Fractional release of trapped gases by crushing relative to total.

Crushing	Y691	Y791790	Y792959	Y793161	A77925	Y74370	Y82189	Y8414	Y86004	Y793225	H C	Ilafegh	A78019	Kenna
36Ar(%)	1	31	6.2	12	2.4	4.9	1.9	5.5	2	21	17	6.8	22	7.4
132Xe(%)	8	24	16	23	13	2.8	1.7	6.7	3.7	20	16	7.4	26	41

Great difference in isotopic ratio is found between noble gases released by crushing and by melting of enstatite chondrites (Fig.1). No correlation is found between isotope ratios and meteorite types: For example, ^{40}Ar/^{36}Ar, ^{129}Xe/^{132}Xe and ^{36}Ar/^{132}Xe are, respectively, 860 vs. 45, 1.25 vs. 1.57 and 8 vs. 60 for crush vs. melt of Y691(EH3), while 2 vs. 45, 2.62 vs. 4.23 and 3090 vs. 2300 for Y791790 (EH3). For ureilites, no significant difference is found in ^{40}Ar/^{36}Ar and ^{129}Xe/^{132}Xe, while great difference is found in ^{36}Ar/^{132}Xe (30 vs. 170) for Kenna. What are reasons for these differences is unknown yet. It is understandable that isotope ratios including cosmogenic and radiogenic gases are affected by abundances of target and parent nuclides relative to trapped gas. For the ^{36}Ar/^{132}Xe ratio of trapped gas, abundances of Q-gas [5] and subsolar gas [6] are factors affecting the ratio. Four enstatite chondrites have the ^{36}Ar/^{132}Xe ratio less than 30 for trapped gases released by crushing. ^{36}Ar/^{132}Xe ratios as low as 30 have been reported in other enstatite chondrites [7]. Such low ^{36}Ar/^{132}Xe ratio can not be explained with any noble gas component ever known. Large elemental fractionation must have taken place in mm-scale or less. A possible mechanism may depend on differences in solubility and diffusivity between Ar and Xe in silicates and associated materials. Xenon enrichment in vesicles has been proposed [8].

References : [1] Takaoka et al. (1996) LPS 27, 1303-1304. [2] Takaoka et al. (1998) Antarct. Meteorites 23, 145-147. [3] Gobel et al. (1978) JGR 83, 855-867. [4] Crabb & Anders (1982) GCA 46, 2351-2361. [5] e.g., Huss et al. GCA 60, 3311-3340. [6] Crabb & Anders (1981) GCA 45, 2443-2464. Wacker & Marti (1983) EPSL 62, 147-158. [7] Patzer & Schultz (2000) LPS 31, #1314-1315. [8] Takaoka (1994) in Noble Gas Geochem. Cosmochem. Ed. J. Matsuda, pp 23-29.

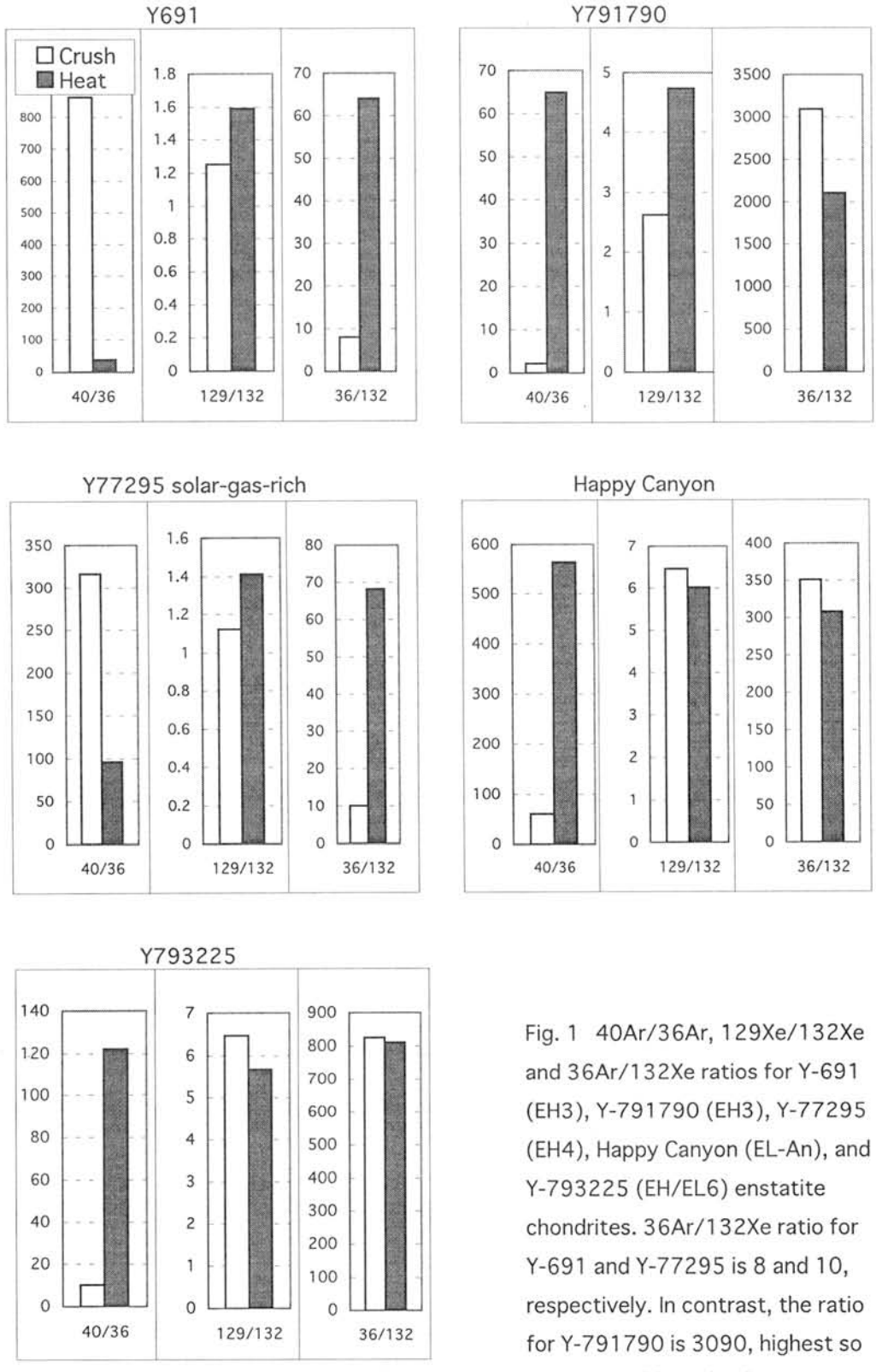

Fig. 1 40Ar/36Ar, 129Xe/132Xe and 36Ar/132Xe ratios for Y-691 (EH3), Y-791790 (EH3), Y-77295 (EH4), Happy Canyon (EL-An), and Y-793225 (EH/EL6) enstatite chondrites. 36Ar/132Xe ratio for Y-691 and Y-77295 is 8 and 10, respectively. In contrast, the ratio for Y-791790 is 3090, highest so far reported for subsolar gas.

MINERALOGY OF A NEW RECRYSTALLIZED MONOMICT EUCRITE, DAR AL GANI 647, AND THE THERMAL METAMORPHISM OF A VESTA-LIKE ASTEROID.

Hiroshi Takeda[1], Akira Yamaguchi[2] and Teruaki Ishii[3].
[1]*Research Inst., Chiba Inst. of Technology, 2-17-1 Tsudanuma, Narashino City, Chiba 275-0016,*
[2]*National Institute of Polar Research, 1-9-10 Kaga, Itabashi, Tokyo 173-8615,*
[3]*Ocean Res. Inst., Univ. of Tokyo, 1-15-1 Minamidai, Nakano-ku, Tokyo 164-0014, Japan.*

Introduction

This new meteorite was found in Libya in winter 1996/97, classified as a eucrite and reported by Wlotzka (MPI), Takeda and Kurz [1] to the Nomenclature Committee, who has given the name Dar al Gani 647. Eucrites were apparently formed on the outer crust of the HED (Howardites, Eucrites, Diogenite) parent body [2]. A notable feature of eucrites is that many of them are brecciated and metamorphosed to various degrees [3-5]. Occurrence of such breccias can be understood by astronomical evidence linking Vesta and the HED achondrites [6] and by the presence of large impact craters on Vesta observed by the Hubble Space Telescope [7]. Rare crystalline eucrites are important to estimate the time of crystallization, but most of them is a product of recrystallization [8,9]. DaG 647 has been classified as a recrystallized monomict eucrite [1]. In order to clarify this problem on the formation of such recrystallized breccias as an event taken place on a Vesta-like body, we investigated DaG 647 by mineralogical techniques.

Ibitira eucrite has been proposed to be a crystalline eucrite previously, but some investigators demonstrated that it is a product of extensive recrystallization and its age is younger than some monomict eucrites [8]. We also reported that some Antarctic crystalline eucrites were formed by recrystallization [9]. Yamaguchi *et al.* [10] reported thermal history of the EET90020 recrystallized eucrite can be explained by metamorphism and excavation by a large cratering event ca. 4.5 Ga on Vesta. Now, discovery of an andesitic material rich in Na-rich plagioclase and diopside in recrystallized chondritic materials [11], does not warrant general understanding that partial melting of chondritic source materials produces eucritic lavas. A large amount of sodium has to be lost from the surface of the Vest-like body in the early history of the body. One Antarctic eucrite had lost sodium to produce plagioclase with An 98 [9]. Studies of DaG 647 may give us some clues to understand thermal events, based on a possible geological setting of various types of HED breccias [12].

Samples and Experimental Techniques

One covered section and one polished thin section (PTS) of DaG 647 were used for this study. The sections were studied by an optical microscope, and the chemical compositions of the minerals were obtained for the PTS by electron probe microanalyzer (EPMA) JEOL 733 at Ocean Research Inst. (ORI) of Univ. of Tokyo. The data were compared with those of other recrystallized eucrites [9,10].

Results

The Major basaltic lithology of this sample shows subophitic textures with plagioclase laths, and sub-rounded smaller grains of pyroxene and plagioclase in the matrix are fused together to resemble a granoblastic crystalline texture (Fig. 1A). A part of the fusion crust is remained. The sizes of the major pyroxene crystals in crystalline parts (Fig. 1B) are larger than those of lath-shaped plagioclase crystals. Large laths of plagioclase are remained in the fine grained recrystallized areas (Fig. 1A). The boundaries between the fragmented matrices and large crystalline clasts are difficult to identify because of the apparent crystalline texture. Small pigeonite grains and ilmenite show subrounded shape (Fig. 1C). Accessory minerals include sub-rounded ilmenite and minor Ti-Cr spinel grains in the matrix, and a rare silica mineral. The mesostasis areas are also recrystallized to fine-grained granoblastic pyroxene and tear-shaped ilmenite. TiO_2 concentrations of the spinel grains vary from 12.8 to 17.3 wt. %. It seems that Ti compositions of DAG647 are in the range of those in Ibitira and EET90020. Small ranges of Ti compositions in DAG may suggest some equilibration. This is in contrast to those in Ibitira and EET which have wider ranges of chemical compositions. The pyroxene grains show fine exsolusion lamellae and thin twin bands, but "clouding" known for ordinary eucrites [14] are mostly erased and are remained only in the core of a few large crystals. The plagioclase compositions are fairly uniform (An_{85} to An_{89}, mean: An_{88}) for the lath-shaped texture. Sock texture after recrystallization has not been observed. This meteorite can best be described as a recrystallized monomict eucrite.

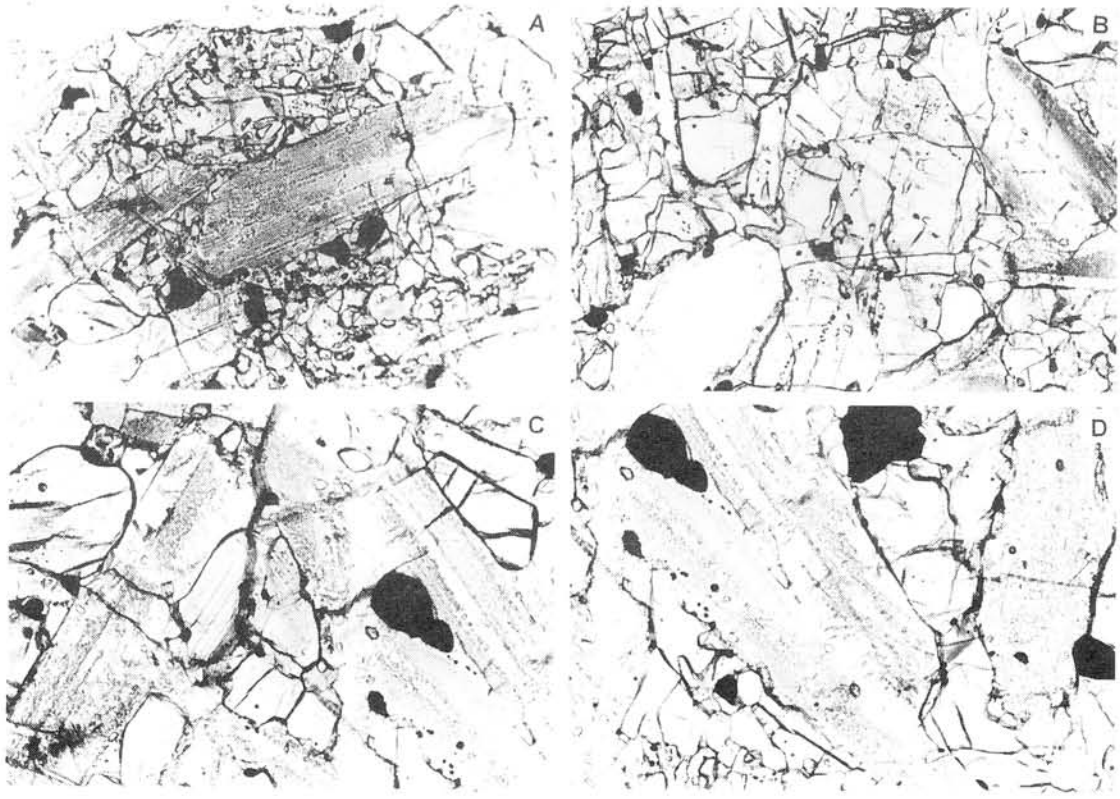

Fig. 1. Photomicrographs of the DaG 647 eucrite. Widths of A and B are 1.3 mm and those of C and D are 0.6 mm.

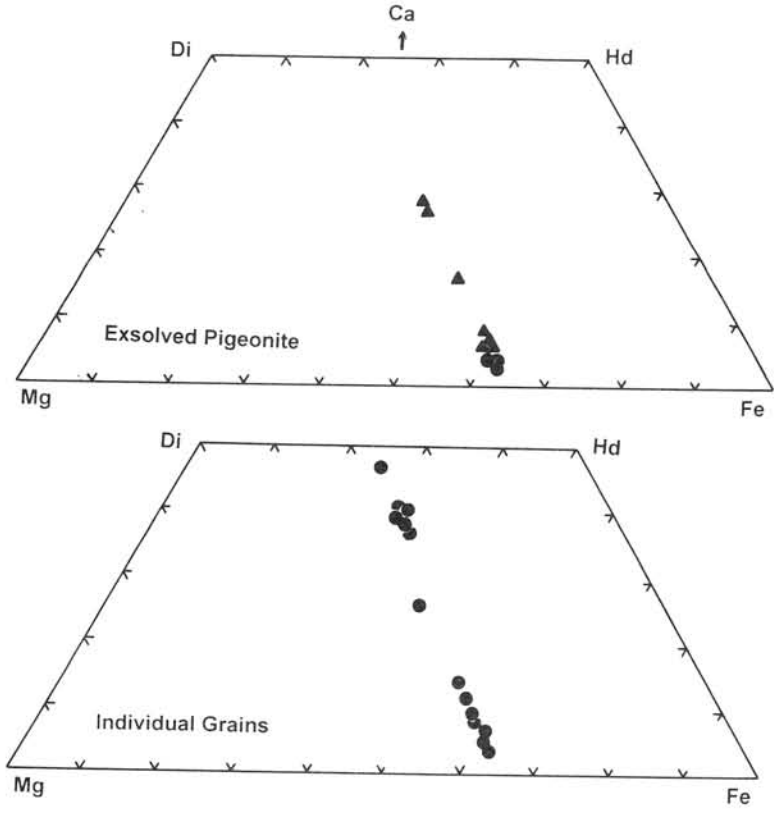

Fig. 2. Pyroxene quadrilaterals of DaG 647 eucrite. Triangles: exsolved augites. Circles: host pigeonite of the exsolved pyroxene and individual analyses of pyroxene grains.

The host low-Ca composition of pyroxene is $Ca_4Mg_{35}Fe_{61}$. The augite lamella compositions reach only as high as $Ca_{23}Mg_{33}Fe_{44}$, indicating that the lamella width is smaller than a few microns. Small individual grains of augite with $Ca_{41}Mg_{28}Fe_{31}$ are present in the matrix (Fig. 1D). The plagioclase crystals also show in part dusty clouding and transparent tiny inclusions (Fig. 1A, C, D). The features are similar to those of strongly metamorphosed eucritic breccias [5].

Discussion

DaG 647 has been classified as a recrystallized monomict eucrite [1]. Over all appearance of the covered section shows that the crystalline textures are disturbed, but the angular fragmental textures of the common monomict eucrites are not clearly observed. The observation supports an idea that fragmental texture was lost by recrystallization. The dusty pyroxenes are one of the characteristics of the monomict eucrites such as those observed in clasts of Juvinas [13]. It is generally accepted that the dusty materials (chromite and ilmenite platelets) were produced during thermal metamorphism. Preservation of a dusty core in large pyroxene crystals suggests that the DaG 647 pyroxene had dusty appearance before recrystallization. The crystallization of individual grains of augite in the matrices and the subrounded shape of pigeonites (Fig. 1C and D) indicate that recrystallization took place at fairly high temperature. The last equilibrated temperature estimated from the bulk pigeonite composition ($Ca_{7.8}Mg_{34.6}Fe_{57.6}$) is above 970 °C, and the temperature of recrystallization estimeted from the compositions of the augite-pigeonite pair is around 980 °C.

One of the unusual features of DaG 647 is the nearly uniform composition of plagioclase, in spite of the lath-shaped basaltic textures. Homogeneous plagioclase crystals have been known only for cumulate eucrites. Presence of dusty materials and tiny rounded inclusions in plagioclase crystals (Fig. 1C and D) also suggests that thermal annealing was extensive. Because diffusion of cations in plagioclase is very slow, nearly homogeneous compositions of plagioclase laths are in line with extensive, prolonged metamorphism after the formation of monomict eucrites and the previous metamorphism, which produced the dusty appearance.

In spite of the evidence of the strong recrystallizaion event, the exsolution textures of both pigeonite and augite are minor. No evidence of transformation to orthopyroxene has been observed. This observation suggests that cooling after recrystallization is fast and that the excavation may have taken place following the recrysallization. The preservation of partly dusty pigeonite and monomict textures implies recrystallization proposed in this paper took place after the metamorphism. The origin of DaG 647 is difficult to interprete by a simple model of cratering [13,14] and at least two-stage thermal events and relatively rapid cooling are required.

In conclusions, combined textural and chemical studies of the DaG 647 pyroxene revealed that this eucrite experienced a brecciation event and the global crustal metamorphism in the early history of the crustal evolution. Then, it experienced strong thermal heating and prolonged annealing followed by fast cooling. Formation of such a complex breccia may best be explained by a geological setting with repeated cratering events for a hot crust.

Acknowledgments: We acknowledge Mr. Erich H. Haiderer for providing us with the sample. This work was supported by a grant of the ORI and by a Grant-in-Aid for Scientific Research from the Japanese Ministry of Education, Science and Culture and Japan Scientific Foundation. We are indebted to Dr. Frank Wlotzka (MPI) and Matthias Kurz for information of the meteorite find and discussion in classification of the meteorites, to Mrs. M. Hatano and Mrs. M. Okamoto for their technical assistance and to Drs. L. E. Nyquist, D. D. Bogard, Prof. Yuzo Kato and Drs. R. Shinjo, H. Kojima and K. Misawa for discussion. This study was initiated at Dept. of Physics and Earth Science, Univ. of the Ryukyus.

References:

[1] WLOTZKA F., KURZ M. and TAKEDA H. (2000) Report to Nomenclature Committee. [2] TAKEDA H., MORI H., DELANEY J.S., PRINZ M., HARLOW G.E., and ISHII T. (1983) *Mem. Natl. Inst. Polar Res., Spec. Issue* **30**, 181-205. [3] TAKEDA H, and GRAHAM A. L. (1991) *Meteoritics* **26**, 129-134. [4] YAMAGUCHI A., TAYLOR G. J., and KEIL K. (1997) *J. Geophys. Res.* **102**, 13381-13386. [5] NYQUIST L. E., BOGARD D. D., TAKEDA H., BANSAL B., WIESMANN H. and SHIH C.-Y. (1997) *Geochim. Cosmochim. Acta* **61**, 2119-2138. [6] BINZEL R. and XU S. (1993) *Science* **260**, 186-191. [7] THOMAS P. C., BINZEL R. P., GAFFEY M. J., STORRS A. D., WELLS E. N. and ZELLNER B. H. (1997) *Science* **277**, 1492-1495. [8] BOGARD D. D. and GARRISON D. H. (1995) *Geochim. Cosmochim. Acta* **59**, 4317-4322. [9] TAKEDA H., ISHII T., ARAI T., and MIYAMOTO M. (1997) *Antarct. Meteorite Res.* **10**, 401-413. [10] YAMAGUCHI A., TAYLOR G. J., KEIL K., FLOSS C., CROZAZ G., NYQUIST L. E., BOGARD D. D. (2000) *in preparation.*. [11] TAKEDA H., BOGARD D. D., MITTLEFEHLDT D. W., GARRISON D. H. (2000) *Geochim. Cosmochim. Acta* **64**, 1311-1327. [12] METZLER K., BOBE K. D., PALME H., SPETTEL B. and STOFFLER D. (1995) *Planet. Space Sci.* **43**, 499-525. [13] HARLOW G. E. and KLIMENTIDIS R. (1980) *Proc. Lunar Sci. Conf. 11th*, 1131-1143. [14] YAMAGUCHI A., TAYLOR G. J., and KEIL K. (1996) *Icarus* **124**, 97-112.

A Consortium Study on Antarctic Micrometeorites Collected by the 39th Japan Antarctic Research Expedition.

Kentaro Terada[1], Hideyasu Kojima[2], Takaaki Noguchi[3], Tomoki Nakamura[4], Hajime Yano[5], Toru Yada[4], Wataru Nozaki[4], Takeshi Mori[1], Izumi Nakai[6], Miho Sasaki[6], Masato Itabashi[6], Keisuke Nagao[7], Takahito Osawa[7], Hajime Hiyagon[8], Sadahiro Mizutani[8], Toshio Murakami[9], Takaaki Fukuoka[10], Ken-ichi Nogami[11], Rie Oomori[11], and Hideo Ohashi[12]

(1) Dept. of Earth & Planetary Sciences, Hiroshima University, Higashi-Hiroshima, Hiroshima, 739-8526, Japan,
(2) National Institute of Polar Research, 1-9-10 Kaga, Itabashi, Tokyo, 173-8515, Japan,
(3) Dept. of Materials and Biological Science, Ibaraki University, Bunkyo 2-1-1, Mito, Ibaraki, 310-8512, Japan,
(4) Dept. of Earth and Planet. Sci., Fac. Of Sci., Kyushu University, Hakozaki, Fukuoka, 812-8581, Japan,
(5) Planetary Science Division, The Institute of Space and Astronautical Scince, 3-1-1 Yoshino-dai, Sagamihara, Kanagawa, 229-8510, Japan
(6) Dept. of Applied Chemistry, Science University of Tokyo, Kagarazaka, Shinjyuku, Tokyo 162-0824, Japan
(7) Laboratory for Earthquake Chemistry, University of Tokyo, Hongo, Tokyo, 113-0033, Japan
(8) Dept. of Earth and Planetary Science, University of Tokyo, Bunkyo-ku, Tokyo, 113-0033, Japan
(9) Computer Center, Gakushuin University, 1-5-1 Mejiro, Toshima-ku, Tokyo, 171-8588, Japan
(10) Dept. of Environmental Systems, Rissho University, 1700 Magechi, Kumagaya, Saitama, 360-0914, Japan
(11) Dept. of Physics, Dokkyo University School of Medicine, Mibu, Tochigi 321-0293, Japan
(12) Dept. of Ocean Sciences, Tokyo University of Fisheries, Kounan, Minato-ku, Tokyo, 108-8477, Japan

Micrometeorites are the most dominant contributor of extraterrestrial material accrettion onto the Earth. Since the first successful collection of Antarctic Micrometeorites (AMMs) was performed by EUROMET (Maurette *et al.* 1991), a number of researchers have tried to collect "non-biased" AMMs, which are free from preferential selection during the collection procedure such as magnetic separation (Maurette *et al.* 1994; Taylor *et al.* 1998). Analytical research of AMMs in Japan has become active ever since 1996 (Yano and Noguchi 1998), for the sake of establishment of curation system of fine-grained extraterrestrial materials for future works such as the JARE AMM collection project and ISAS's MUSES-C sample return mission from a near-earth asteroid. Since the discovery of more than several hundreds of AMMs in sediments at the bottom of an ice water well at the Dome Fuji Station in Antarctica in 1996-1997, consortium for the systematic AMM research in Japan has been formed (Nakamura *et al.* 1999; Noguchi *et al.* 2000a, 2000b; Nakai *et al.* 2000; Nakamura *et al.* 2000; Osawa *et al.* 2000).

From November 1998 to January 1999, the 39th Japanese Antarctic Research Expedition (JARE) performed Japan's first large-scale collection of AMMs at three different localities in Antarctica: Minami-Yamato, Kuwagata, and JARE IV East. At each locality, microparticles were collected at three, eleven, and ten sites. A total of 36 tons of bare ice at 24 different sites was melted (thus 1.5 ton of ice per location in average), and then filtered through stainless steel sieves with several mesh sizes. Fine particles were separated into four size fractions in situ (10~40 μm, 40~100 μm, 100~238 μm, >238 μm). Table 1 shows the mass of

unsorted particles, including terrestrial and artificial inclusions, in the size range of 100-238 μm, at the various collection sites. The total mass of microparticles collected in that size range amounts to more than 0.26g, about 1 % of which was found to be AMMs. All samples were kept frozen during shipping back to Japan.

Some of the important objectives during these initial investigations are (i) general characteristics of collected AMM samples as well as assessment of terrestrial and artificial contamination and (ii) better understanding of sample collection techniques and strategies from polar ice fields. The former is indispensable information obtained from this mission and can be used for flux analysis on AMMs prior to initial analyses of elemental and other properties of the individual AMMs within the consortium. The latter also provides important information to judge the best sample site and whether samples at each site were artificially biased or not. Such information has been reflected to upgrading the AMM collection activity in the 41st JARE, which is currently on-going. Due to these reasons, all the samples were divided into three different procedures; (1) Samples from 5 different locations were used for flux counting, 3 of which were also used for initial investigation within the consortium study. (2) Samples from 10 other locations are being held as "Research Samples (see below)". (3) Samples from the final 9 locations will be held for future work. (See the comment in Table 1).

In the case of (1), black irregular particles and rounded particles were handpicked under an optical stereomicroscope. These were then analyzed by scanning electron microscopes equipped with an energy dispersive spectrometer (SEM-EDS) without a conductive coating. These procedures were based on the previous studies of precipitated microparticle collected from sediments in the Dome Fuji water well (Nakamura *et al.* 1999; Noguchi *et al.* 2000). From preliminary studies of these samples, it is estimated that more than a few thousands AMMs in total were collected (Yada and Kojima 2000). More details on the influx of AMMs on each collection site will be presented by Yada *et al.* at this symposium.

We, the Japanese AMM consortium, investigated the very same 75 AMM samples by using various analytical methods (17 AMMs in the size range of 10-40 μm, 49 AMMs in the size range of 40-100 μm and 9 AMMs in the range of 100-238 μm). Mineral compositions of 61 out of 75 AMMs were investigated by a Gandolfi X-ray camera using synchrotron radiation and, moreover, 5 out of them were investigated by TEM. After major element compositions were characterized by EPMA, isotopic studies were carried out by SIMS (16 AMMs for heavy elements and 15 AMMs for Oxygen isotope analysis, respectively). 30 AMMs were used for noble gas mass spectrometry. Trace element compositions of 9 AMMs which were in the range of 100-238 μm, were characterized by INAA. These results will be presented at the symposium by other consortium members.

In regards to the "Research Samples", some of cataloged AMMs from the three locations and unbiased samples collected at ten other locations will become internationally available for qualified investigators upon research proposals to the NIPR AMM curator (Prof. H. Kojima) after this symposium. More detailed information about sample requests will be

announced during this symposium and on the Japanese AMM web site (http://dust.cc.gakushuin.ac.jp/dust/).

References

Maurette M. *et al.* (1991) Nature, **351**, 44-46

Maurette M. *et al.* (1994) Analysis of Interplanetary Dust, ed. By M. E. Zolensky *et al.* New York, American Institute of Physics, 277-289

Taylor S. *et al.* (1998) Nature, **392**, 899-903

Nakai I., *et al.* (2000), Antarctic Meteorite Res., **13**, in press

Nakamura T., *et al.* (1999), Antarctic Meteorite Res., **12**, 183-198

Nakamura T., *et al.* (2000), Antarctic Meteorite Res., **13**, in press

Noguchi T., *et al.* (2000a), Antarctic Meteorite Res., **13**, in press

Noguchi T., *et al.* (2000b), Antarctic Meteorite Res., **13**, in press

Osawa T., *et al.* (2000), Antarctic Meteorite Res., **13**, in press

Yada T, and Kojima H. (2000) Antarctic Meteorite Res., **13**, 9-18

Yano H, and Noguchi T. (1998) Antarctic Meteorite Res., **11**, 136-154

TABLE: Heating duration, estimated weight of melted ice and unbiased particles at each collection points.

Collection locations	Heating duration (hours; minutes)	Weight of ice (tons)	Weight of 100-238 Size Fraction (g)	Comments
Minami-Yamato 1	4h 45m	0.99	0.01162	Pre.
Minami-Yamato 2	5h 20m	1.11	0.00418	Req.(unbiased)
Minami-Yamato 3	4h 30m	0.94	---	Flux, Cons. Req.
Kuwagata 1	10h	2.09	0.01104	Pre.
Kuwagata 2	4h 25m	0.92	0.00209	Flux
Kuwagata 3	9h 55m	2.07	0.00519	Req.(unbiased)
Kuwagata 4	5h 25m	1.13	0.00455	Req.(unbiased)
Kuwagata 5	12h 55m	2.70	0.00545	Req.(unbiased)
Kuwagata 6	5h 55m	1.24	0.00699	Req.(unbiased)
Kuwagata 7	12h 45m	2.66	0.00763	Pre.
Kuwagata 8	6h	1.25	0.00837	Pre.
Kuwagata 9	9h 45m	2.04	0.02013	Pre.
Kuwagata 10	6h 20m	1.32	0.00676	Req.(unbiased)
Kuwagata 11	9h 15m	1.93	---	Flux, Cons. Req.
JARE IV 1	9h 45m	2.04	0.08564	Pre.
JARE IV 2	7h 15m	1.52	0.02493	Pre.
JARE IV 3	4h 40m	0.98	0.00792	Pre.
JARE IV 4	6h 20m	1.32	0.00524	Req.(unbiased)
JARE IV 5	6h 50m	1.43	0.00871	Req.
JARE IV 6	5h 15m	1.10	0.01629	Pre.
JARE IV 7	6h 30m	1.36	0.00747	Req.(unbiased)
JARE IV 8	7h	1.46	0.00331	Req.(unbiased)
JARE IV 9	5h 30m	1.15	0.00228	Flux
JARE IV 10	5h	1.04	0.00281	Flux, Cons. Req.
Total (24 sites)	171h 20m	35.79	0.25862	

Flux; for flux counting, Cons.; for Consortium, Req.; for Request Samples, Pre.; for Preservation for future works

Ion-Microprobe Analysis of Trace Elements in Antarctic Micrometeorites using SHRIMP

Kentaro Terada[1], Takeshi Mori[1], Yuji Sano[1], Takaaki Noguchi[2], Tomoki Nakamura[3], and Toru Yada[3]

(1)Dept. of Earth & Planetary Sciences, Hiroshima University, Higashi-Hiroshima 739-8526, Japan

(2)Dept. of Materials and Biological Science, Ibaraki Univ., Bunkyo 2-1-1, Mito 310-8512, Japan

(3)Dept. of Earth and Planet. Sci., Fac. of Sci., Kyushu University, Hakozaki, Fukuoka, 812-8581, Japan

Introduction

More than a few thousands of Antarctic micrometeorites (AMMs) were recovered from Antarctic bare ice at 24 different locations (300 km away from human activity), by the 39th Japanese Antarctic Research Expedition (JARE) (Yada and Kojima 2000; Terada *et al.* 2000). They are Japanese first large-scale collection of AMMs, which are considered to be the least affected by terrestrial contamination.

Prior to the 39th JARE AMMs analysis, ion-microprobe analyses of trace elements in various micrometeorites have been attempted using the SHRIMP (Sensitive High Resolution IonMicro Probe) instrument at Hiroshima University. These analyses were carried out on AMMs collected from a water tank at Dome Fuji station (Nakamura *et al.* 1999; Noguchi *et al.* 2000), cosmic spherules (CSs) and AMMs collected by EUROMET (Maurette *et al.* 1991). Preliminary results are shown in this paper, and revised results combined with the 39th JARE samples will be presented at the conference.

All of these samples were cast in epoxy resin with standard SRM610-glass and San Carlos olivine. They were polished until the inside of the grains were exposed, and also to provide a flat surface for sputtering of secondary ions. After the surface was finished using 0.25 μm diamond paste, major elements were analyzed using Electron Probe MicroAnalyser (EPMA) before SHRIMP analysis.

U-Pb systems

Based on the in-situ U/Pb dating techniques of zircons and apatites using the SHRIMP (Sano *et al.* 1999a, 1999b), we investigated the U-Pb systems of olivines in 20 AMMs collected from a water tank at Dome Fuji station and 10 CSs by EUROMET. The U concentrations of almost all of the grains are in the range of 0.01-0.10 ppm, which is consistent with previous work (bulk composition by INAA; Kurat *et al.* 1994). On the other hands, the Pb concentrations are extremely high and show widespread distribution in the range of 0.1-750 ppm, which is consistent with works done by Flynn *et al.* (1993) and Nakai *et al.* (2000) using Synchrotron X-Ray Fluorescence. Within uncertainty, isotopic ratios found for these samples are also consistent with those found in Antarctic snow and ice by Chisholm *et al.* (1995). These results would also suggest that the Pb was added during the time when the AMMs were embedded in the snow and ice, but due to experimental uncertainty it is still possible that the Pb was added during atmospheric entry and drift in the stratosphere.

Mn-Cr systems

In the field of cosmochemistry, the Mn-Cr systematic is also a useful chronometer. Recently important results have been derived from Fe-rich olivines in various Carbonaceous chondrites using SIMS (Secondary Ion Mass Spectrometer). We have tentatively performed Mn-Cr analyses on olivine in AMMs and CSs, which have Cr concentrations lower than the detection limit of EPMA (< 500 ppm). In 3 of the 16 grains analyzed, significant positive $^{53}Cr/^{52}Cr$ anomalies were found. At this point it seems that they are not correlated with $^{55}Mn/^{52}Cr$ ratio, but with the shape and texture of each grain. Irregular AMMs, with coarse-grained crystalline or scoriaceous textures, had normal Cr ratios. Four CSs measured, which had barred-olivine texture and did not contain any "voids", also did not show any significant anomalies. On the other hand, the other three spherules, which had scoriaceuos texture, showed significant anomalies (up to several percent).

These anomalies were most probably due to mass fractionation (Rayleigh-type distillation) during atmospheric entry, which has been proposed from Fe isotopic fractionations and Ni isotopic fractionations in I-type spherules collected from deep sea sediments (Xue et al, 1995; Herzog et al. 2000). Detailed results on the relationship

between micrometeorite textures and their Cr, Fe and Ni isotopic compositions, will be presented at the conference.

Acknowledgement

Our special thanks to Prof. Maurette and Dr. Engrand and Mr. Gounelle from the C.S.N.S.M for sample preparations. And also thanks to Mr. Ly for useful discussing about Pb contamination in Antarctica. This research was supported partly by grants from the Saneyoshi Scholarship Foundation and the Sumitomo Foundation.

References

Chisholm W. *et al.* (1995), Analytica Chimica Acta, **311**, 141-151.

Flynn G. J. *et al.* (1993), Antarctic Meteorite Res., **6**, 304-324

Herzog G. F. *et al.* (2000), G.C.A., **63**, 1443-1457.

Kurat G. *et al.* (1994), G.C.A., **58**, 3879-3904.

Maurette M. *et al.* (1991) Nature, **351**, 44-46

Nakai I. *et al.* (2000), Antarctic Meteorite Res., **13**, in press

Nakamura T. *et al.* (1999), Antarctic Meteorite Res., **12**, 183-198

Noguchi T., *et al.* (2000), Antarctic Meteorite Res., **13**, in press

Sano Y.*et al.* (1999a), G.C.A., **63**, 899-905.

Sano Y.*et al.*(1999b), Chemical Geology, **153**, 249-258.

Terada K. *et al.* (2000), in this volume

Xue S. *et al.* (1995), G.C.A., **59**, 4975-4981.

Yada T. and Kojima H. (2000) Antarctic Meteorite Res., **13**, 9-18

THE KOBE METEORITE: PETROGRAPHY AND MINERALOGY

K. Tomeoka[1], T. Kojima[1], H. Kojima[2] and N. Nakamura[1]

[1] Department of Earth and Planetary Sciences, Faculty of Science, Kobe University, Nada, Kobe 657-8501, Japan

[2] National Institute of Polar Research, 9-10 Kaga 1-chome, Itabashi, Tokyo 173-8515, Japan

INTRODUCTION

The Kobe meteorite fell at 8:23 p.m. on 26 September 1999 in a northern residential area of Kobe city, Japan. It penetrated the roof of the house of Mr. R. Hirata and broke into over 20 pieces. The total mass of recovered stones is 136 g. They are now in the possession of Mr. Hirata. Two pieces (17g in total mass) were loaned from the finder to N. Nakamura for consortium studies (Nakamura et al., 2000). A small fragment, ~8 mm in largest dimension, was provided to us for petrographic and mineralogical study. We report here the results of petrographic and mineralogical study of Kobe. Our study indicates that Kobe can be classified as a CK4 carbonaceous chondrite; it is the first carbonaceous chondrite known to fall in Japan.

SAMPLES AND METHODS

Two polished thin sections (44.3 mm^2 total area) were made from the meteorite fragment. They were studied using an optical microscope, a scanning electron microscope (JEOL JSM-5800) equipped with an energy-dispersive X-ray spectrometer (EDS), and an electron probe microanalyzer (JEOL JXA-8900) equipped with wavelength-dispersive X-ray spectrometers (WDS).

PETROGRAPHY AND MINERALOGY

General petrography

Kobe contains well to moderately defined chondrules and mineral fragments set in a semi-translucent recrystallized matrix. Chondrules constitutes about 35.0 vol% of the meteorite; they are commonly fragmented and blurred to various degrees. Modal analysis (15.7 mm^2 surface area) indicates that Kobe contains (in vol%): 73.0 % olivine, 5.4% low-Ca pyroxene, 3.0% high-Ca pyroxene, 13.0% plagioclase, 4.2% magnetite, 1.8% Fe-Ni sulfides, and 0.3% phosphates. A striking feature is the pronounced blackening of the matrix and chondrules. Many olivine grains exhibit moderate to strong wavy extinction, but no olivine grains show planar fractures, which indicates Kobe to be shock stage S2. No Ca- and Al-rich inclusions have been found in the thin sections.

Chondrules

Chondrules are mostly porphyritic olivine type; other minor textural types include porphyritic olivine-pyroxene, granular olivine and barred olivine. Chondrules range in apparent diameter from 200 to 2000 μm and average 750 μm. The range and the average of chondrule size are consistent with those of CK chondrites (Kallemeyn et al., 1991). Mesostases are mostly occupied by plagioclase; no isotropic glass occurs. Mesostases of some chondrules are partly occupied by vesicular olivine containing tiny inclusions of magnetite and pentlandite that is described below. Pyroxene is rare; most is homogeneous low-Ca pyroxene. Magnetite occurs as rounded to irregularly shaped inclusions (50-300 μm in diameter) commonly together with pentlandite blebs (5-20 μm). Apart from these relatively coarse-grained magnetite and

pentlandite, extremely small particles (<0.2 μm) of magnetite and pentlandite occur along grain boundaries of olivine, which probably causes chondrule olivines to appear semi-translucent in transmitted light. Neither fine-grained nor coarse-grained rims have been observed surrounding chondrules.

Matrix

Matrix consists mostly of olivine (typically 5-50 μm in diameter), plagioclase, magnetite and minor amounts of low-Ca pyroxene, pentlandite, diopside, chlorapatite and apatite (roughly in the order of abundance). Olivine in matrix occurs in two types. One forms relatively coarsely crystallized, anhedral pure crystals. The other fills interstices of the anhedral olivine crystals and contains numerous tiny vesicles (<1-5 μm in diameter) and spherical particles (<1-5 μm) of magnetite and pentlandite as well as anhedral grains (1-10 μm) of plagioclase, low-Ca pyroxene, diopside and chlorapatite. These two types of olivine are intermixed on scales of 10-50 μm throughout matrix. It is evident that the tiny inclusions of magnetite and pentlandite and vesicles in the olivines cause optical blackening of the matrix. Similar texture is also observed in the matrix of the Yamato-82104 CK5 chondrite (unpublished data). Plagioclase occurs as irregularly shaped grains throughout matrix and tends to be abundant in the peripheries of chondrules and chondrule fragments. Like the vesicular olivine, plagioclase commonly contains tiny particles (<1-5 μm) of magnetite and pentlandite as well as anhedral grains (1-20 μm) of olivine, diopside, low-Ca pyroxene and spinel.

Opaque phases

Magnetite is the most abundant opaque phase in both chondrules and matrix. Relatively large magnetite grains (>50 μm in diameter) contain exsolution lamellae of ilmenite and spinel that are typically 1-3 μm wide. These two kinds of lamellae are distinct in orientation. Spinel and ilmenite lamellae in magnetite are apparently common in CK chondrites (Geiger and Bischoff, 1990; Keller et al., 1992; Nakamura et al., 1993). Closer examination of these magnetite grains reveals extremely narrow (<0.2 μm wide) lamellae to occur at high densities in addition to the 1-to-3-μm wide lamellae. Although these lamellae are too narrow to be identified by microbeam analysis, they are probably spinel, because most of them are in parallel with the wider spinel lamellae. Rounded grains of chlorapatite (<1-10 μm in diameter) are also commonly dispersed in magnetite. Pentlandite occurs typically as fine-grained aggregates together with magnetite. Minor amounts of Fe sulfide, probably troilite, occur as 1-to-3 μm-size grains in intimate association with pentlandite. Micrometer-size refractory metal-rich particles were found in a magnetite-sulfide-rich olivine aggregate; they occur in association with magnetite and Fe-(Ni) sulfides. Elements detected in EDS and WDS spectra of the particles include Os, Ru, Pt and S. No Fe-rich metallic phases have been found in the thin sections.

Mineral compositions

Olivine is very homogeneous, averaging Fa31.1 (s_{Fa}=0.6). There are no appreciable differences in olivine composition between chondrules and matrix. The mean Fa content is virtually identical to the mean Fa content (Fa31.1) of the CK chondrite group reported by Kallemeyn et al. (1991). Olivine contains significant amounts of Ni (0.3-0.5 wt% NiO) and Mn (0.1-0.2 wt% MnO) and trace amounts of Ca (<0.03 CaO wt%), which is also common to olivines in several CK chondrites (Geiger and Bischoff, 1989; Nakamura et al., 1993).

Both low-Ca pyroxene and high-Ca pyroxene occur, but augite is rare. Like the olivine, low-Ca pyroxene is very homogeneous, averaging Fs25.9 (s_{Fs}=0.7). The mean Fs

content is closely similar to that of low-Ca pyroxene in the Yamato-82104 CK5 chondrite (Fs25.8; Nakamura et al., 1993). High-Ca pyroxene is also homogeneous and mostly Fe-poor (Fs8.9-11.3). In contrast, plagioclase is heterogeneous, ranging from An26.6 to An76.1, averaging An55.5 (s_{An}=15.9).

Magnetite contains considerable Cr (3.8-4.6 wt% Cr_2O_3) and Al (0.7-2.3 wt% Al_2O_3) and appreciable Ni (0.2-0.3 wt% NiO) and Ti (0.2-0.4 wt% TiO_2); part of these minor components may be contributed from the extremely narrow lamellae described above.

DISCUSSION

Classification

Mineralogical and petrographic characteristics of Kobe can be summarized as follows: (1) relatively large chondrule sizes (750 μm in average diameter) with considerable variations (200-2000 μm), (2) compositionally very homogenous, Fe-rich olivine (Fa31.1 on average) and low-Ca pyroxene (Fs25.9), (3) high-Ni contents (0.33-0.72 wt% NiO) and low-Ca contents (<0.1 wt% CaO) of olivine, (4) abundant plagioclase with large grain-to-grain compositional variations, (5) abundant magnetite containing ilmenite and spinel lamellae, (6) pronounced silicate blackening due to the dispersion of tiny magnetite and pentlandite particles as well as numerous vesicles, (7) the presence of refractory metal-rich particles, (8) extremely rare CAIs and metals. All these features are in common with most CK chondrites (e.g., Rubin et al., 1988; Geiger and Bischoff, 1989; Kallemeyn et al., 1991; Keller et al., 1992; Nakamura et al., 1993). Kobe apparently has a higher abundance of chondrules (~35 vol%) than typical CK4-5 chondrites (10-15 vol%; Kallemeyn et al., 1991). However, there appears to be considerable differences in chondrule abundance among the reported CK chondrites. The Ningqiang CK3 chondrite has a higher abundance of chondrules (~22 vol% excluding 13.7 vol% aggregational inclusions) than typical CK4-5 chondrites (Rubin et al., 1988). The Maralinga CK4 chondrite has a much higher abundance of chondrules (~50 vol.%) (Keller et al., 1992). Thus, there may be some uncertainty or range in chondrule abundance in CK chondrites. Chondrules in Kobe are well to moderately defined and matrix olivines have typical grain sizes of 5 to 50 μm, which is consistent with petrologic type 4 (Kallemeyn et al., 1991). In conclusion, we believe that a CK4 classification for Kobe is most appropriate.

Acknowledgment— We thank Mr. R. Hirata for providing the meteorite sample.

REFERENCES

Geiger, T. and Bischoff, A. (1989) Meteoritics 24, 269-270 (abstr.)

Kallemeyn, G.W., Rubin, A.E. and Wasson, J.T. (1991) Geochim. Cosmochim. Acta 55, 881-892.

Keller, L.P., Clark, J.C., Lewis, C.F. and Moore, C.B. (1992) Meteoritics 27, 87-91.

Nakamura, N., Ebihara, M., Hirota, Y., Oura, Y., Kojima, H., Tomeoka, K., Kojima, T., Komura, K., Clayton, R.N., Mayeda, T.K. and Wang, D. (2000) Lunar Planet. Sci. 31, 1234 (abstr.).

Nakamura, T., Tomeoka, K. and Takeda, H. (1993) Proc. NIPR Symp. Antarct. Meteorites 6, 171-185.

Rubin, A.E., Wang, D., Kallemeyn, G.W. and Wasson, J.T. (1988) Meteoritics 23, 12-23.

Petrology of ALH-77252: An L3-6 Polymict Chondritic Breccia

T. Tomiyama[1], A. Yamaguchi[1,2] and K. Misawa[1,2]

[1] *Department of Polar Science, School of Mathematical and Physical Science, Graduate University for Advanced Studies, 1-9-10 Kaga, Itabashi, Tokyo 173-8515, Japan.* [2] *National Institute Polar Research, 1-9-10 Kaga, Itabashi, Tokyo, 173-8515, Japan.*

Introduction:

Binns [1] and Scott et al. [2] described chondritic breccias, which contain fragments having distinctive metamorphic grades within one specimen, and suggested that they might constitute the majority of ordinary chondrites. Although it is uncertain how constituents of chondritic regolith breccias are genetically related, they occurred together on their parent bodies. If these rocks preserve a record of pre-brecciation metamorphic events, they will give us remarkable information on the thermal history of ordinary chondrite parent bodies. We therefore have started a survey of chondritic breccias. In order to constrain the thermal history of chondrite parent bodies, as a first step, we have carried out petrologic studies of ALH-77252, a polymict L-chondritic regolith breccia.

Samples and Experimental Methods:

ALH-77252 was classified as an L3/L6 [3], L3 [4, 5], or L4/L6 [6] chondrite, and suggested to be paired with ALH-77215, -77216, and -77217. The high concentration of solar-wind implanted noble gases indicates that ALH-77252 is a regolith breccia [5, 7]. ALH-77215 contains isolated inclusions of graphite-magnetite [8]. The acid residue fraction of ALH-77252 shows a heavy REE-enriched pattern with a large positive Eu anomaly, indicating the nature of equilibrated chondrites [9].

Three polished thin-sections (PTS 84-1, 91-1, 91-2) of ALH-77252 were studied microscopically in transmitted and reflected light, and further examined with a scanning electron microscope (JEOL JSM-5900LV), to resolve the fine-grained textures. Chemical compositions of constituent phases were determined by using an electron probe microanalyzer (JEOL JXA-8800M), with an acceleration voltage of 15kV and a beam current of 12nA.

Results:

ALH-77252 is composed of angular chondritic clasts (<3.5 mm in size) and chondrules in clastic matrix up to 20μm in size. The clastic matrix shows a darker appearance under the transmitted light because of the presence of abundant fine-grained Fe-sulfides. The petrologic classification [10, 11] of individual clast was possible only for two equilibrated clasts (#101 and #201) and one unequilibrated clast #202. Other clasts were too small to define the petrologic types. We measured chemical compositions of constituent phases of small clasts as well. The followings are petrological descriptions of large clasts, which include shock stages [12].

Clast #101: (3.25×2.5mm in size, type-5, S3) The clast contains two barred olivine (BO) chondrules, one radial pyroxene (RP) chondrule, and one porphyritic olivine-pyroxene (POP) chondrule with olivine or pyroxene having a constant Fe/(Fe+Mg) ratio (Fa=22.1-24.7, Fs=18.4-21.1). Intramatrix materials (~15μm in size) are recrystallized. Chondrule-matrix boundaries are less clear. Barred olivine chondrules contain abundant chromite. Undulatory extinction and weak planar fractures were observed in olivine grains. **Clast #201:** (3.5×2.3mm in size, type-6, S3) Two BO chondrules, one PR chondrule, and one POP chondrule were identified in the clast, but they are all fragmental. Compositions of olivine and low-Ca pyroxene are homogeneous, with having a constant Fe/(Fe+Mg) ratio (Fa=22.1-23.9, Fs=18.0-20.1). Inferred typical grain-size of clastic intramatrix is 10μm. Undulatory extinction and planar fractures are visible in olivine grains. **Clast #202:** (3.0×2.8mm in size, type-3, S4) The clast contains one POP, two PP, three RP, three POP, and one BO chondrules. Intramatrix materials among chondrules are almost absent. Olivine in the clast has Fa 21.7-22.6, while low-Ca pyroxene grains have inhomogeneous ferrosilite concentrations, Fs 10.7-23.6. Undulatory extinction, planar fractures, and mosaic textures were observed in some olivine grains.

The majority of clasts and matrix materials are equilibrated, having homogenized Fe/(Fe+Mg) ratios in olivine and pyroxene compositions (Fa=21-25, Fs=17-22). On the other hand, some minor clasts, isolated chondrules, and the rimming materials have olivine and/or low-Ca pyroxene with aberrant chemical compositions (Fa=0.3-43.6, Fs=1.6-36.4). Most of unequilibrated clasts and chondrules which consist of unequilibrated olivine/pyroxene show Mg-Fe zoning near the grain boundaries, and some of them have clear glass materials.

Unequilibrated olivine grains are mainly found in the isolated chondrules and rimming materials but rarer than unequilibrated low-Ca pyroxenes. Some unequilibrated clasts have both equilibrated olivines and unequilibrated low-Ca pyroxenes.

The backscattered electron images of unequilibrated chondrule and mineral fragment are shown in Fig. 1. Isolated POP chondrule #209 (Fig. 1a) consists of coarse-grained olivine (Fa=4.5-7.2) and fine-grained (<30μm) pyroxene grains, surrounded by discrete Fe-rich, fine-grained olivine aggregates. One olivine grain contains a large glassy inclusion (Na_2O=6.8, MgO=1.3, SiO_2=63.7, Al_2O_3=25.0, FeO=2.3, TiO_2=1.1, Cr_2O_3=0.7wt%). Olivine and pyroxene grains show Fe-Mg zoning. Low-Ca orthopyroxene fragment #115 (Fig. 1b) shows very weak Fe-Mg zoning. Opaque inclusions of metallic iron are visible along the planar fractures. Iron-rich rimming olivine-aggregates are strongly zoned and opaque under transmitted light.

The CaO, Cr_2O_3 and TiO_2 compositions are different between equilibrated low-Ca pyroxenes and unequilibrated ones (Fig. 2a-c). The minor element contents of equilibrated low-Ca pyroxenes (Fs=17-22) have the range; CaO: 0.1-2.9wt% (0.81wt% in average), Cr_2O_3: 0.0-0.7wt% (0.15wt%) and TiO_2: 0.0-0.7wt% (0.18wt%). On the other hand, the minor element contents of unequilibrated low-Ca pyroxenes (Fs=2-36) have the range; CaO: 0.1-2.3wt% (0.36wt%), Cr_2O_3: 0.2-1.1wt% (0.43wt%) and TiO_2: 0.0-0.1wt% (0.03wt%). These features of minor elements of low-Ca pyroxenes in ALH-77252 are quite similar to those observed in Weston (H3-7 regolith breccia) [13].

Discussion:

The wide range of fayalite composition of olivines and the presence of clear glass materials suggest that ALH-77252 did not suffer from thermal metamorphism after final lithification.

Because the diffusion rate of Fe^{2+} in olivine is higher than that in pyroxene [14], olivines equilibrate more rapidly than low-Ca pyroxenes [e.g., 15,16,17]. Weak thermal metamorphism may result in the presence of clasts which have both equilibrated olivines and unequilibrated pyroxenes. Furthermore, the rare occurrence of unequilibrated olivines indicates that most unequilibrated pyroxenes suffered from weak thermal metamorphism before final lithification.

The feature of minor element compositions reveals two distinct metamorphic sequences of equilibrated and unequilibrated low-Ca pyroxenes. If both equilibrated and unequilibrated low-Ca pyroxenes were derived from similar initial materials, low-Ca pyroxenes drastically changed their minor element compositions during thermal metamorphism. If it is the case, the majority of low-Ca pyroxenes were increased in Ca and Ti contents and decreased in Cr content by severe thermal metamorphism. The weak thermal metamorphism could only affect on Ca content of unequilibrated low-Ca pyroxenes. Otherwise, if initial materials are different, the conditions of crystallization may have varied between unequilibrated and equilibrated low-Ca pyroxenes. Most low-Ca pyroxenes we observed are inferred to have been constituents of chondrules before brecciation. Thus, their compositions may reflect the properties of chondrule formation, such as melt composition, redox condition and cooling rate. Since Ti is immobile elements in low-Ca pyroxene, it may be difficult that Ti diffuses into pyroxenes during thermal metamorphism. Therefore, we suggest that the latter case is rather favorable.

References:

[1]Binns, R. A. (1967) EPSL, **2**, 299-317. [2]Scott, E. R. D. et al. (1985) JGR, **90**, D137-D148. [3]Yanai, K. (1983) Tent. Catalog. Victoria Land Meteor., NIPR, Tokyo. [4]Yanai, K. and Kojima, H. (1995) Catalog. Antarct. Meteor., NIPR, Tokyo. [5]Scott, E. R. D. (1984) Smithon Contrib. Earth Sci., **26**, 73-94. [6]King, T. V. V. et al. (1980) Smithon. Contrib. Earth Sci., **23**, 12-44. [7]Nautial, C. M. et al. (1984) LPSC, **15**, 587-588. [8]Scott, E. R. D. et al. (1981) EPSL, **56**, 19-31. [9]Ebihara, M. (1989) Proc. NIPR Symp. Antarct. Meteor., **2**, 279-287 [10]Van Schmus, W. R. and Wood, J. A. (1967) GCA, **31**, 747-765. [11]Dodd, R. T. (1981) Meteorites, Cambridge Univ. Press, pp. 23-28. [12]Stöffler, D. et al. (1991) GCA, **55**, 3845-3867 [13]Noonan, A. F. and Nelen A. (1976) Meteoritics, **11**, 111-130. [14]Brady, J. B. (1995) Min. Phys. and Crystallography., pp. 269-290. [15]Dodd, R. T. et al. (1967) GCA, **31**, 921-951. [16]Tsuchiyama, A. et al. (1988) Proc. NIPR Symp Antarct. Meteor., **1**, 173-184. [17]McCoy, T. J. et al. (1991) GCA, **55**, 601-609.

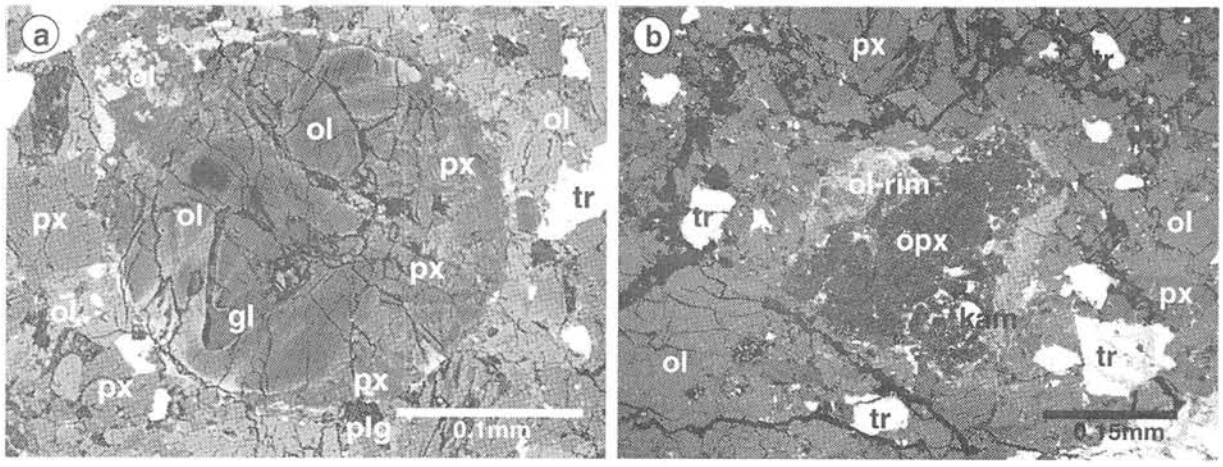

Fig. 1: The backscattered electron images of the textures of unequilibrated materials. **a:** An isolated POP chondrule #209 with discrete iron-rich olivine rim. Olivine and pyroxene grains show Fe-Mg zoning. One olivine grain contains a large glassy inclusion. **b:** An orthopyroxene fragment #115. Fine-grained metallic irons are observed along the planar fractures. Iron-rich rimming olivines are strongly zoned. (ol: olivine, px: pyroxene, tr: troilite, kam: kamasite, plg: plagioclase)

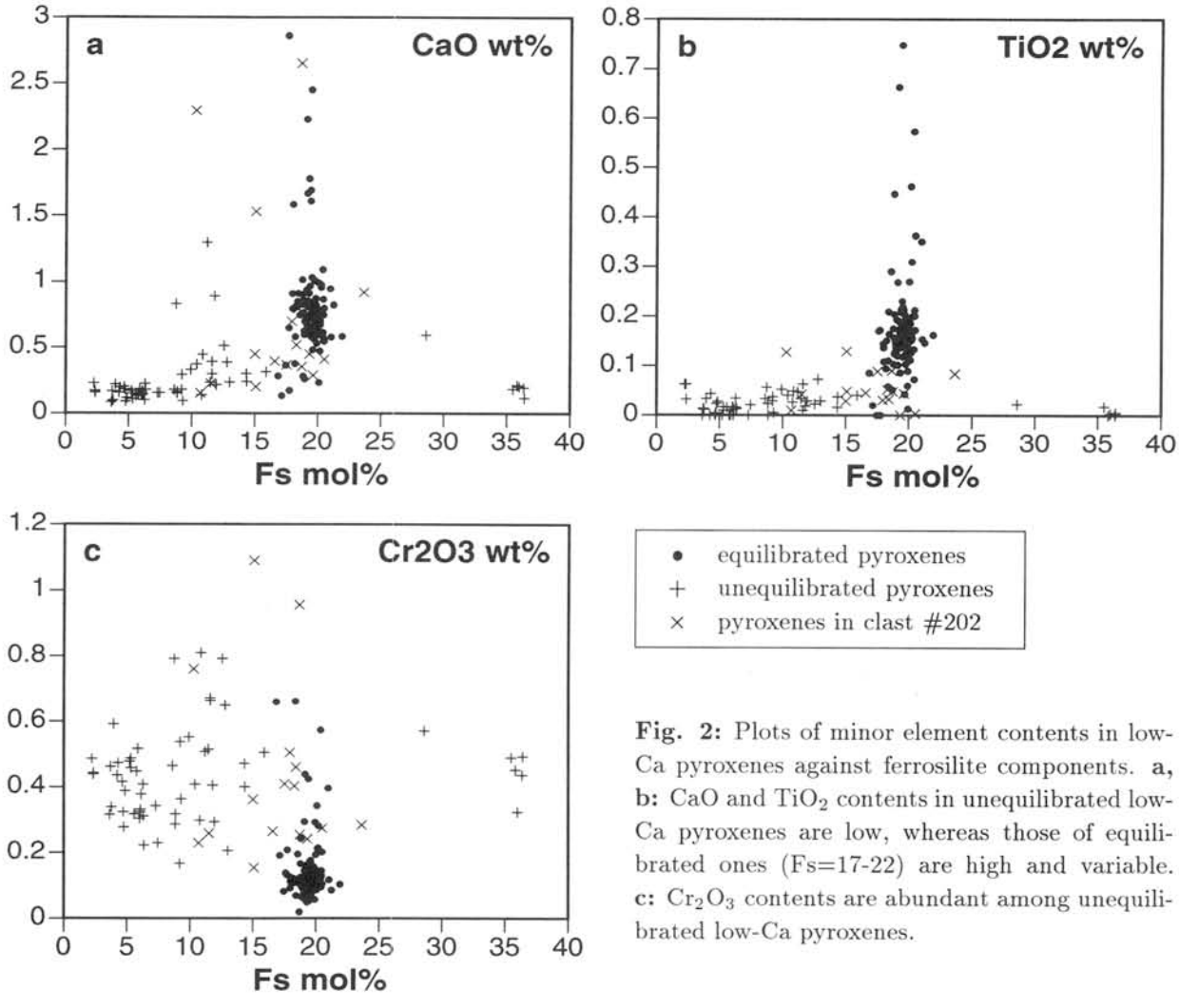

Fig. 2: Plots of minor element contents in low-Ca pyroxenes against ferrosilite components. **a, b:** CaO and TiO_2 contents in unequilibrated low-Ca pyroxenes are low, whereas those of equilibrated ones (Fs=17-22) are high and variable. **c:** Cr_2O_3 contents are abundant among unequilibrated low-Ca pyroxenes.

Three-dimensional structures of chondrules observed by an XTM (X-ray tomographic microscope) at SPring-8: high speed spinning chondrules.

TSUCHIYAMA Akira[1]*, KAWABATA Toshiharu[1], UESUGI Kentaro[2], NAKANO Tsukasa[3], SUZUKI Yoshio[2], YAGI Naoto[2], UMETANI Keiji[2], and SHIRONO Shinichi[4]

*1) Department of Earth and Space Science, Osaka University, 1-1 Machikaneyama-cho, Toyonaka 560-0043, JAPAN, *akira@ess.sci.osaka-u.ac.jp, 2) [4]Japan Synchrotron Radiation Research Institute, Mikazuki, 679-5198 JAPAN, 3) Geological Information Center, Geological Survey of Japan, Tshukuba, 305-8567 JAPAN, 4) Department of Earth and Planetary Sciences, Kobe University, Kobe, 657-8501, JAPAN..*

Introduction

X-ray computed tomography (CT) can give textural information without breaking samples, and provide three-dimensional structures by successive imaging. This method has been applied to meteorites and many studies have been done by using industrial X-ray CT scanner for commercial use (*e.g.*, [1-3]). However, as polychromatic X-ray beams are used in these scanners, some artifacts, such as beam hardening, are inevitable in the CT images and the contrasts (CT values) cannot correspond quantitatively to the X-ray linear attenuation coefficients of objects. Lately, we have developed a new X-ray CT system (XTM: X-ray tomographic microscope) in Spring-8 of synchrotron radiation (SR) facility in Japan [4]. In this XTM, monochromatic X-ray beam can be available. Furthermore, a highly collimated SR beam can make a high resolution three-dimensional image.

Kawabata *et al.* [3] reported a three-dimensional structure of a chondrule obtained by an industrial X-ray CT scanner. They proposed a possibility that the chondrule was spinning during their formation based on the fact that the chondrule is oblate in its external shape and voids are concentrated near the minor axis of the oblate chondrule. In the present study, three-dimensional structures of chondrules including barred olivine chondrules were examined by the XTM [4] with higher resolution to discuss the possibility of spinning of chondrules.

Experiments and image analysis

Sixteen chondrules (1.0-1.7 mm in diameter) removed from the Allende meteorite (CV3) were examined by the XTM. Fourteen chondrules have porphyritic texture, and the other two chondrules have barred olivine texture. Monochromatic beams of 18-25 keV were used, and cross-sectional images were reconstructed with a convolution back projection method from 300-360 projections taken by sample rotation. The images have CT values of 16-bit gray scale, which correspond directly to the X-ray attenuation coefficients of objects and have voxels of 6μm x 6μm x 6μm in size. Successive images of about 180-280 slices were taken to reconstruct the three-dimensional structures. Specific algorithms were developed in the present study to analyze the three-dimensional structures; (1) analyzing the external shapes of chondrules, and (2) extracting the constituents of the chondrules, such as voids. Some

chondrules were thin sectioned to examine the CT images by an optical microscope and an SEM.

Results

Voids were recognized at least in fourteen chondrules (<0.001 - 0.9 vol.%). Many chondrules have craters on their surface. Two chondrules seem to be compound chondrules. The surfaces of the barred olivine chondrules are smooth, while those of porphyritic chondrules are rough or smooth. The external shapes of some chondrules are irregular due to imperfect recovery of the chondrules during their separation. The rest of chondrules (four to six including the two barred olivine chondrules) are approximately oblate with the aspect ratios of 0.70-0.94 (Fe-rich fine rim has been removed by the image analysis). Although deviation of chondrule shapes from a sphere is generally accepted, this is the first time that three-dimensional shapes were described quantitatively.

One barred olivine chondrule (BO-1) consists of a parallel set of thin olivine plates throughout the whole chondrule (Fig.1b). The other barred olivine chondrule (BO-2) has three or more sets of olivine plates. The olivine plates in BO-1 are nearly perpendicular to the minor axis of the oblate chondrule (Fig.1). In BO-2, the minor axis is nearly perpendicular to one set of parallel olivine plates, which occupies the largest volume of the chondrule.

Voids are not clearly concentrated near the minor axes of the oblate chondrules as observed in the previous study [3]. However, the voids have tendency to concentrate near the minor axes. Even in BO-1, many voids are not present near the outside part of the chondrule although voids are not concentrated near the minor axis (Fig.1a).

Discussion

The oblate shapes of the chondrules are caused either by (1) spinning of molten chondrules in a space or (2) deformation by shock loading or gravitational compaction after accumulation as a chondrite. The concentration of voids along the minor axis [3] strongly suggest the origin of (1); light voids were moved towards the spinning axis by centrifugation. The presence of phenocrysts or olivine plates prevented the voids moving towards the axis. If this is the case, voids should be present while the chondrule was molten. Boiling of volatiles may form voids.

Olivine plates in the barred olivine chondrules nearly perpendicular to the minor axis may be also related to spinning of chondrules. To check the three-dimensional feature of barred olivine chondrules, we examined about forty barred olivine chondrules in thin sections. If the chondrules are oblate and the olivine plates are perpendicular to the minor axes, the directions of olivine bars must be always parallel to the major axes of ellipsoidal chondrules in the two-dimensional sections. The angles between the bar directions and the major axes, ϕ, were plotted against the aspect ratio of the chondrules in Figure 2. For chondrules with multiple-bars, the direction of bars having the largest area in each chondrule was selected. About 90% of the chondrules have $\phi<20^{\circ}$, which are consistent with the three-dimensional structures obtained by the CT study. Interestingly, the rest of about 10% have $\phi>60^{\circ}$, and no chondrules with $\phi=20$-60° were observed except for chondrules deformed by shock loading.

The present results suggest that most chondrules were spinning during their formation. If this is the

case, we can estimate the spinning rates by considering the balance between the surface tension of droplet chondrules and centrifugal force by spinning. The shape of a rotating droplet is determined by angular velocity of rotation, equatorial radius of the droplets, bulk density, and interfacial surface tension [5]. If we used the surface tension of basalts [6], the spinning rates of the oblate chondrules are estimated to be about 100-300 rpm. Such spinning rates may put some constraints on chondrule formation process, such as rotation by planetesimal collision or rotation of dust-balls in a turbulent nebula.

The authors thank Ms. C. Sakaguchi of Okayama University and Dr. T. Noguchi provided some chondrule samples and Mr. R. Shigeyoshi for EPMA analyses of some samples.

References: [1] Arnold *et al.* (1982) *Science*, **219**, 383-384. [2] Kondo *et al.* (1997) *Antarct. Meteor. Res.*, **10**, 437-447. [3] Kawabata *et al.* (1999) *Antarctic Meteor.*, ***XXIV***, 64-66. [4] Uesugi *et al.* (1999) *Proc. SPIE*, **3772**, 214-221. [5] Chandrasekhar (1965) *Proc. Roy. Soc. London*, Ser.A, **286**, 1-26. [6] Murase and McBirney (1973) *Geol. Soc. Am.*

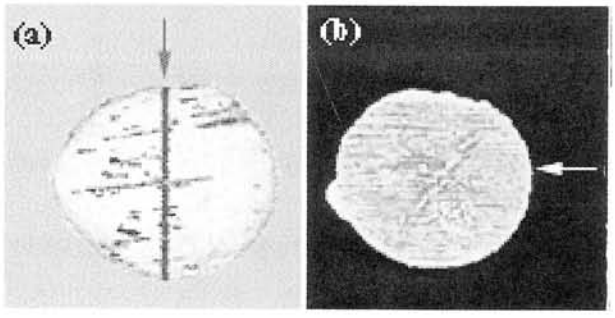

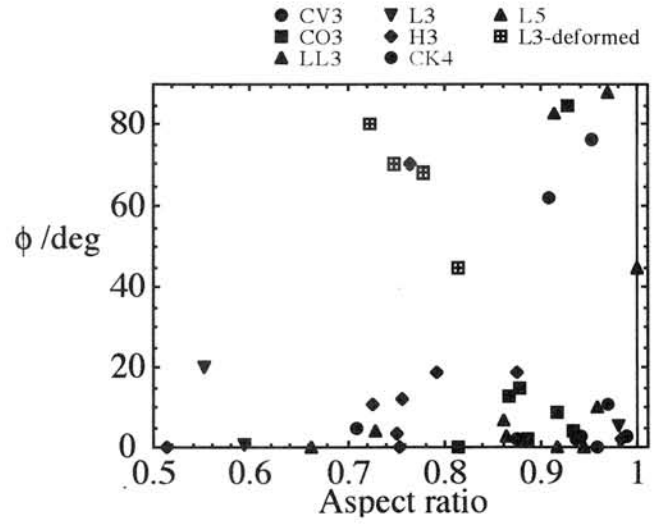

Figure 1 (left). Three-dimensional structure of barred olivine chondrule (BO-1). (a) Side view of the oblate chondrule. An arrow shows the minor axis. Voids present between olivine plates are also shown. (b) A sliced CT image along the minor axis viewed from a different direction from (a). An arrow shows the direction of olivine bars. The major axis of this chondrule is 1.12 mm.

Figure 2 (right). The angle between the direction of olivine bars and the major axis, ϕ, plotted against the aspect ratio of barred olivine chondrules. L3-deformed shows chondrules in a deformed L3 chondrite by shock loading.

Possibility of three-dimensional description for meteorites by X-ray CT method: Kobe meteorite as an example.

TSUCHIYAMA Akira[1]*, NAKAMURA Tomoki[2], and NAKAMURA Noboru[3]

*1) Department of Earth and Space Science, Osaka University, Toyonaka 560-0043, JAPAN, *akira@ess.sci.osaka-u.ac.jp, 2) Department of Earth and Planetary Sciences, Kyushu University, 33 Hakozaki, Fukuoka 812-8581, JAPAN, 3) Department of Earth and Planetary Sciences, Kobe University, Nada Kobe 657-8501, JAPAN.*

Introduction

X-ray computed tomography (CT) is a non-destructive method for obtaining a three-dimensional structure of an object by stacking successive cross-sectional images. In an X-ray CT image, the contrast is expressed as a two-dimensional distribution of CT values, which are related to the X-ray linear attenuation coefficients. We can discriminate between constituents (or phases) in an object by using the CT values. Although this method has been developed for medical diagnosis, this has broad applicability to material sciences. Meteorites and related materials were also examined by X-ray CT method (*e.g.*,[1-4]).

This method has potential to describe meteorites three-dimensionally as an initial stage of examining the meteorites, especially for important but rare samples. In the present study, a three-dimensional structure of Kobe meteorite was obtained by an industrial X-ray CT scanner.

Experiments

The Kobe meteorite fell in September 1999 in the northern part of Kobe, Japan. This meteorite was classified as CK4 by mineralogical and geochemical studies [5]. One of the fragments of the meteorite (about 13 g) was broken into pieces for various analyses. The piece C-5-1 (1.144 g and about 7-9 mm in size) was imaged by a micro focus X-ray CT scanner, ELESCAN NX-NCP-C80-I(4) (Nittetsu Elex Co.) at Osaka University. The piece was mounted in Si powder (99.999%) to reduce artifacts of CT images, such as beam hardening. The sample was wrapped with kitchen foil before the mounting to avoid contamination from the Si powder.

The CT scanner belongs to the third generation type. This has a micro focus X-ray tube (6x8 μm) with a W target and a CCD camera (54x72 mm and 480x640 pixels) as an X-ray detector. The accelerating voltage for the X-ray tube was 65 kV and the X-ray tube current was 40 μA. 450 projections were obtained by each 0.4 degree with 15-bit contrast. Cross-sectional images were reconstructed from the projections by a filtered back projection method. Each reconstructed image has 512x512 pixels. The magnification was 4.44, and thus the pixel size

and slice width became 31.6 μm x 31.6 μm and 25.3 μm, respectively. A three-dimensional structure was obtained from successive 378 slices. It took about 10 hrs for taking the projections and another 10 hrs for the back projection.

After the imaging, the piece C-5-1 was mounted in glycol phthalate and cut physically into seven plates with the width of about 1 mm. Two thin sections were made from one of the plate (P-4) to examined the CT images by optical and electron microscopes. Other plates were used for other analyses by micro laser and SIMS at other laboratories in the consortium studies.

Results and discussion

A three-dimensional image of C-5-1 is shown in Figure 1. In the X-ray CT images (*e.g.*, Fig.2a), we can distinguish opaque minerals (pentlandite and magnetite), ferromagnesian silicates (olivine and pyroxene) and plagioclase. It is hard to discriminate between pentlandite and magnetite because they usually exist within olivine grains and grain boundaries as small grains. Olivine and pyroxene cannot be discriminated too because of their small difference of the linear attenuation coefficients between them (Table 1).

Although the silicate minerals are recrystallized and homogenized, many chondrules and some inclusions can be recognized. As the directions of the thin sections are different from those of the CT slices, it is not easy to examine the CT images by the thin sections under microscopes at present. In Figure 2, a porphyritic chondrule in a thin section under an optical microscope is recognized in a CT image. This chondrule was observed on the surface of the sample before the imaging. Fusion crust cannot be recognized in the CT image. Some chondrules are easily recognized in a CT image by surrounding opaque minerals (chondrules B and C in Fig. 2). We are now developing image analysis method for three-dimensional structures. X-ray CT method becomes important in the initial stage of examining meteorites if such image analysis will be available.

We are indebted to Mr. R. Hirata for providing N.N. with the Kobe meteorite specimens for the consortium studies.

Table 1. The X-ray linear attenuation coefficients (cm^{-1}) of major minerals at different photon energies, E, calculated from the chemical compositions and assumed densities.

E /keV	olivine	plagioclase	opx	cpx	magnetite	pentlandite
50	2.37	0.941	1.80	1.67	7.54	8.68
55	1.92	0.812	1.48	1.39	5.86	6.73
60	1.61	0.723	1.27	1.19	4.71	5.37
65	1.39	0.656	1.11	1.05	3.89	4.41

Figure 1. Three-dimensional structure of the Kobe meteorite C-5-1 (7-9 mm in size). Objects with bright, gray and dark contrasts are opaque minerals (pentlandite and magnetite), ferromagnesian silicates (olivine and pyroxene) and plagioclase, respectively.

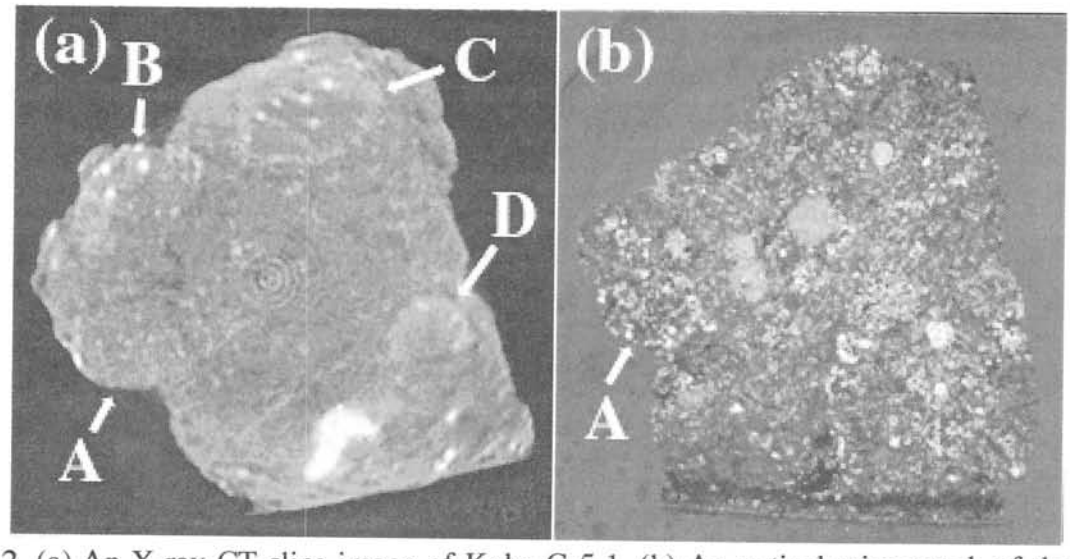

Figure 2. (a) An X-ray CT slice image of Kobe C-5-1. (b) An optical micrograph of the same sample (cross-polarized light). The width of the photo is 8.7 mm. At least four chondrules (A-D) are recognized in the CT image. The chondrule A is seen in the thin section. The other chondrules are not clearly seen in the thin section because the direction of the CT image is different from that of the thin section. Fusion crust at the bottom of the sample cannot be recognized in the CT image.

References: [1] Arnold *et al.* (1982) *Science*, **219**, 383-384. [2] Kondo *et al.* (1997) *Antarct. Meteor. Res.*, **10**, 437-447. [3] Uesugi *et al.* (1999) *Proc. SPIE*, **3772**, 214-221. [4] Tsuchiyama *et al.* (2000) *LPS.*, **XXXI**, 1566. [5] Nakamura *et al.* (2000) *LPS.*, **XXXI**, 1234.

Crystallization of Cosmic Materials in Microgravity

○ K. Tsukamoto[1], H. Kobatake[1], K. Nagashima[1], H. Satoh[2], H. Yurimoto[3]

[1] Fac. Science, Tohoku University [2] Geological Survey of Japan [3] Tokyo Institute of Technology

e-mail: ktsuka@mail.cc.tohoku.ac.jp

When the phenomena at the formation stage of early solar nebra are imagined, there are many interesting topics which we have to investigate in the light of nucleation and growth of crystals. The formations of cosmic dusts after the explosion of super-nova are the result of nucleation and aggregation of crystals from the vapour phae. The chondrules are probably resulted from the melting and crystallization in melt phases. To reveal the thermal history and the rate of formation of these cosmic materials in the history, it seems very important to understand the crystallization process based on the experimental results.

However experiments for this approach are not so easy as can be supposed from the facts that (1) crystallization takes place at high temperature, (2) fine particles nucleates in extremely low vapor pressure, (3) crystallization of chondrules are so rapid, and (4) natural cosmic materials are formed in open space without a crucible or a holder.

In order to solve the problems (1) and (3), we already developed a method employing a high speed TV system to visualize the crystallization process of chondrules successfully using aero-acoustic levitation method. The problem (2) are more serious. If we want to analyze the nucleation of the ultra-fine particles, real-time dynamic light scattering (RDLS), which are capable of resolving the particles with a few nm in diameter, would be suitable in a well-defined temperature and vapor pressure near the melt/gas interface. The configuration of the optical observation system is shown in Fig.1.

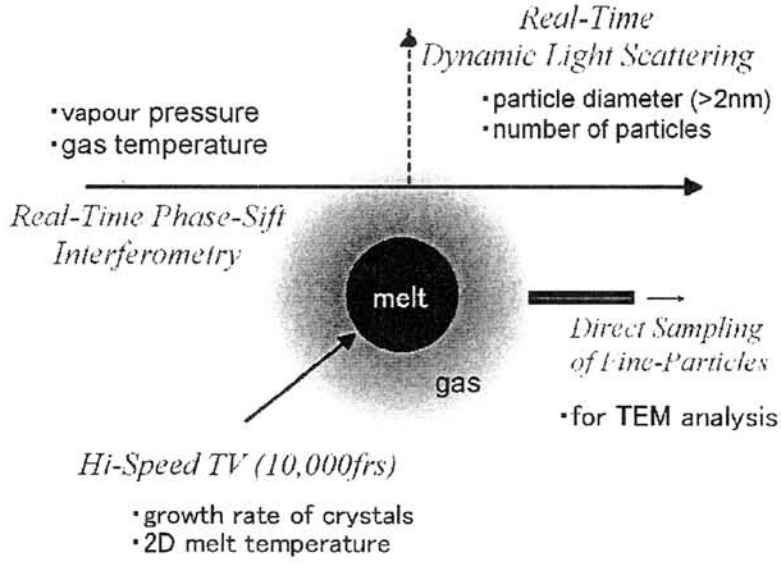

Fig.1 Concept of Optical Configuration.

As reported in the previous symposium, the coupling effect of thermal and mass transport in the melt sphere plays an important role for the formation of the chondrule texture, from which we concluded that the cooling rate of the melt are not responsible for the texture but that the degree of supercooling (typically ~800 degC) at which nucleation starts is responsible.

Although the experiment was done during levitation using aero-acoustic levitation method, in which the rapid transfer of heat from the

melt to the holder or to the crucible could be suppressed completely, there still remained gravity which lead to the air convection around the melt and complex convection in the melt. We therefore tried to do similar experiment in microgravity using an airplane (GII) during the parabolic flight.

Enstatie, CAI, meririte, anorthite, and forsterite glasses were used for this experiment, in which the glass was melted by CO2 laser (100W) followed by rapid cooling. In our former experiment, pyrometer using 1.4um wavelength was employed to measure the temperature. However such long wavelength is not suitable to image the crystallization process precisely. We therefore image the process using visible light by high speed TV (10,000 frs), the image of which was then transformed to the temperature distribution on the melt surface by calculating the radiation power. Fig.1 is such an example to show the crystallization process under normal gravity initiated from the Pt holder located at the bottom in the figure. One can clearly see the recalescence in Fig.3, which shows the thermal history of the melt.

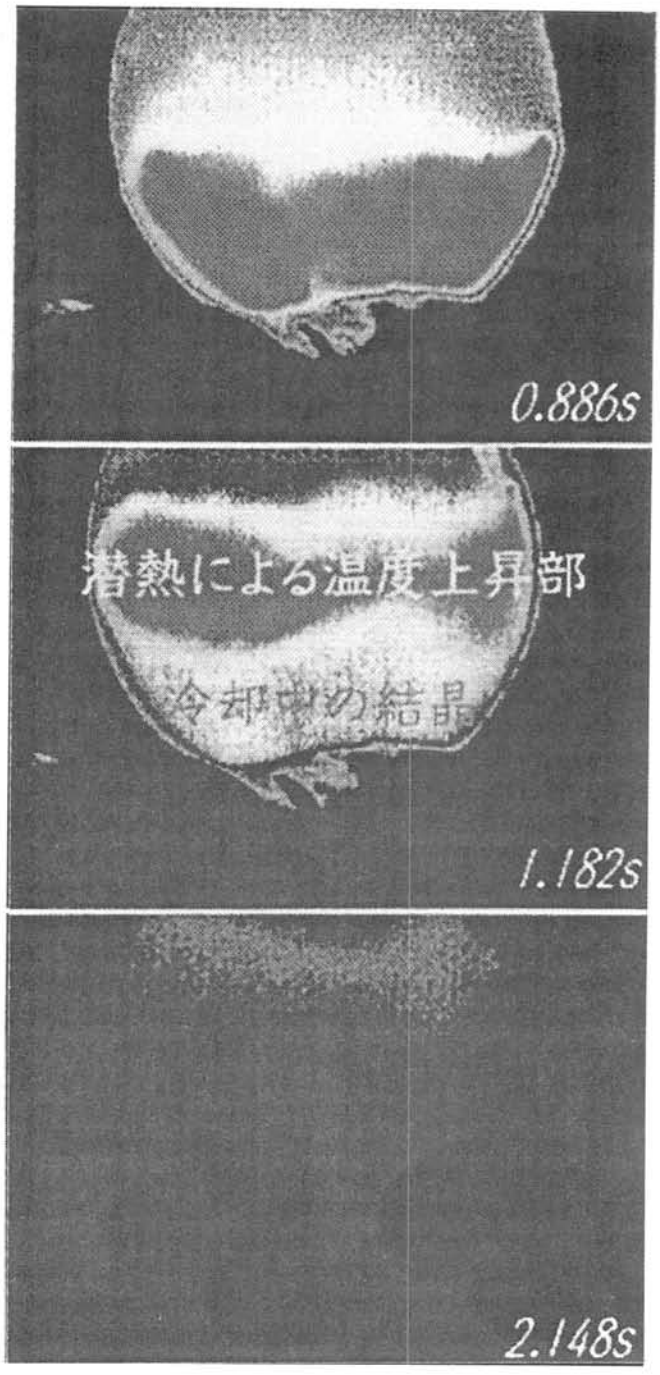

Fig.2 Successive Thermal Images, En, normal g.

When the same experiment was done in microgravity, crystallization can hardly be seen and thus glass formation was dominant, which is shown in Fig.4. No recalescence was also seen in the thermal history, Fig.5.

The difference is attributed to the fact that nucleation was delayed in microgravity and thus due to the rapid temperature drop, the melt temperature rapidly approached to the glass transition temperature. Whereas, nucleation was easy under normal gravity, and thus the recalescence process started far beyond the glass transition temperature.

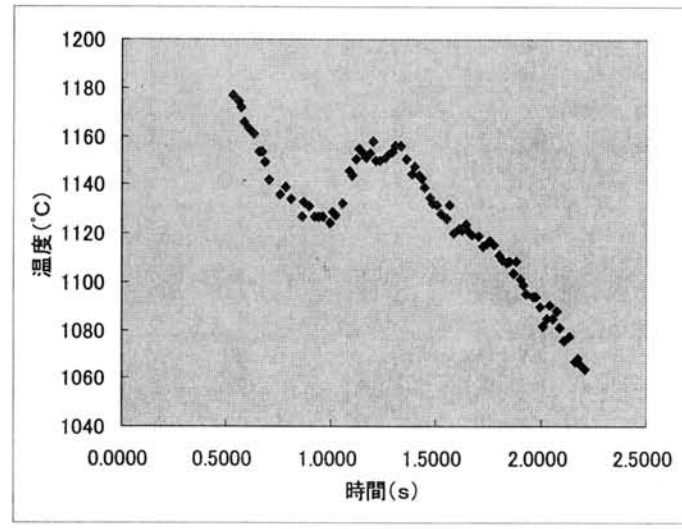

Fig. 3 Thermal history of En melt in gravity.

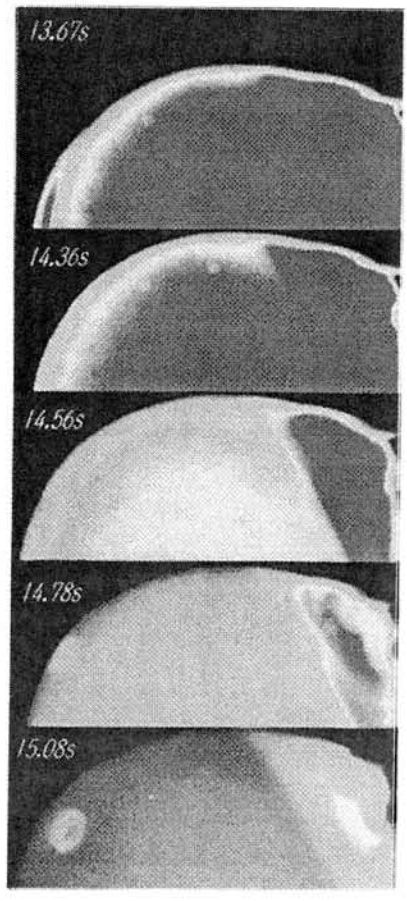

Fig.4 Successive Thermal Images, En, μg.

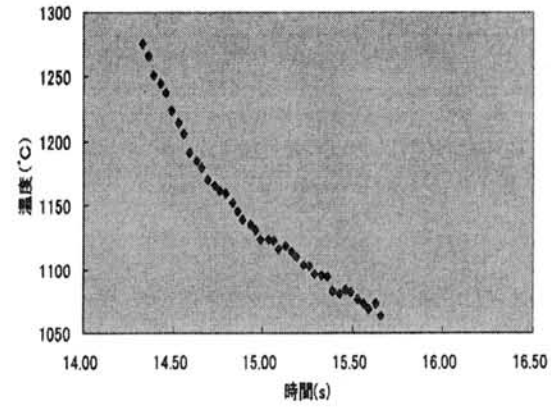

Fig.5 Thermal history of En melt in microgravity.

COMPARISON OF JAPANESE ANTARCTIC AND CARPATHIAN BASIN HUNGARIAN SNOUTED SPHERULES

K. Török [1], Sz. Bérczi [1,2], B. Lukács [3],

[1]Dept. Petrology/Geochemistry, Eötvös University, H-1088 Múzeum krt. 4/a, Budapest, Hungary
[2]Dept. G. Technology, Eötvös University, H-1117 Pázmány P. s. 1/a, Budapest, Hungary,
[3]Central Research Inst. Physics, RMKI, H-1525 Budapest. 114. POB. 49., Hungary,

ABSTRACT We compared the glassy, frequently occurring snouted spherules from Carpathian Basin (Hungary, Roumania, Slovakia) and the snouted spherules reported from Antarctica. We defined the "Pannon B" homogeneous spherule group (probably common origin) from the Carpathian Basin. We identified 2 other groups, genetically different, but analogous: one of them also of Carpathian Basin. The result of comparison of Pannon-B and Antarctica snouted spherules: they may have common origin, probably noncosmic.

INTRODUCTION

In the last 5 years several dozen spherule layers were identified in the Carpathian basin. Locality and geologic times were determined by drill cores [1-3]. But no real model about the origin of these spherules has been suggested because of their controversial character [2-3]. The main controversy is: several spherule layers (very different drill-core ages) contain apparently identical spherules [2]. We have found a far away counterpart (similar shape and composition) spherules from Antarctica, Dome Fuji [5-6]), for comparing all data, performing statistical analyses, to solve "mystery" of their origin. Our preliminary result are: 1) chemical compositions of Carpathian Basin (CB) and Dome Fuji (DF) spherules are sufficiently different not to be in direct genetic connection, 2) but they both deviate into the same direction from "usual" spherule types. The projection of their main components onto cement industry material maps help to explain a probable origin.

THE CLASSIFICATION OF SPHERULES

Snouted spherules (belonging to Paraspherulites in classification of [4]) are "produced from terrestrial matter in terrestrial environment". Spherules of great extinction zones belong to Euspherulites: "formed when crossing the atmosphere downward". (Atmosphere crossing does *not* imply that Euspherulites would consist of extraterrestrial matter; in an impact most spherules come from the target local surface. But for Euspherulites the impactor is extraterrestrial. The 3 types of Euspherulites are: a) Meteoritic dust, b) mostly impactor, c) mostly target spherules. Each of them have "markers": chemistry, size, colour, shape for identification.)

CARPATHIAN BASIN (CB) & DOME FUJI (DF) SPHERULES

Two spherule types occur frequently in Hungary [1, 3, 7-9]. Both: size range is ca. 0.2 mm, first found in NW Hungary. We call them **Pannon A and B**. Holotypes were suggested: For Pannon A: Magyarpolány Mp-42 (drill-core [10]). For Pannon B: Bakonyjákó-528 (drill-core [11], nearby localities). (Magyarpolány Mp-42 also contains Pannon B', [12] without chemical analDifferences between the two types: **Pannon A** is *magnetic*; spherical, some contains a void in center (some show blasting up), colour is black(ish), mainly iron oxide. (Further we do not discuss Pannon A.) **Pannon B's**, are *nonmagnetic*, glassy, translucent, average is light yellow. Shape: characteristic feature is the snout(s): long tendrils from droplets [12]. Dome Fuji spherules are similar to Pannon B-s, for appearance [5]. (size is ca. 0.2 mm, yellow, also snouted [13]). Fig.1 shows Pannon B spherules from **B**akonyjákó, **A**szófõ & **V**érhalom-1, (shortly BAV).

MEASUREMENTS

23 BAV spherules (3 localities, 4 (?) (drill core) ages ([36, 2]) were measured [14]. (AMRAY 1830I electron microscope, with an EDS detector PV 9800, 15 kV, beam current 2nA, measurm. time 100 s. Standard samples: kaersutite, diopside, chalcopirite, synthetic Ba-glass.) All were glassy, Pannon B type spherules.

PANNON B SPHERULES AND THEIR RELATIVES

We defined Pannon B spherules by **holotype, locality, age, diagnosis**, and **description** [14] as follows. *Pannon B (nonmagnetic, glassy) spherules*: **Holotype**: The spherules of the drilling core of borehole Bakonyjákó-528 [11], chemistry [14-15, 2, 16-18]). **Locality and age**: Bakonyjákó-528, Bakony Mts. Hungary. (Age of drill-core: Santonian/Campanian.). **Diagnosis**: Homogeneous spherule group. Differs from most glassy spherules by the high Ca content (CaO, SiO_2), differs from other high Ca spherule types as: more Mg, and more Ba, as in Nagylózs group [14] and as in Dome Fuji group [5]. **Description**: ***Pannon B: nonmagnetic, glassy spherules. Diameter: cca. 0.2 mm or upwards, shape:rounded, teardrop or elongated, with curved appendices ("snouts"). Colour: colourless, yellowish, sometimes light brown. Chemistry:*** Na_2O ***0.42±0.04 %,*** MgO ***8.8±0.4 %,*** Al_2O_3 ***9.3±0.8 %,*** K_2O ***0.67±0.07 %,*** CaO ***37±2 %,*** BaO ***2.6±0.2 %,*** FeO ***0.2±0.1 %.*** (for chemistry ± ranges denote 1 sigma stat.). This composition is strange. An impact spherule would be similar to either the impactor or the target area ([20]; (processes [21]). The chemical analyses were on Bakonyjákó-528

spherules, (2 groups: a) at 58.5 m., in marl, b) 80.5 m. in Csehbánya Formation [11], at Magyarpolány [12]), (mixture of marl, pebbles, sand and silt: difficult to compose above target composition, especially for high Ba), but such a high Ca/Si ratio is also unusual in spherules: even the Ca-rich fraction of Senzeilles (F/F) Ca/Si is only 0.75, while here is almost 1.5. If the spherules are from impactor, then their composition is quite alien from meteorites, perhaps with exception of Angra dos Reis [22], even Angra dos Reis contains substantial FeO (cca. 10 %) and less CaO; high Ba is example.

Other Pannon B sites: 1) Aszófô, [8], 2) Vérhalom-1, [15], [2-3], 3) Sopron-89, [8], [23-24], 4) "Budapest", [8], [23-24], *Sites with spherules of similar appearance but without measured compositions:* I) Városmajor-1, [11], II) Balatonarács[3], III) Nekézseny[25], IV) Recsk-136, [3], *Analogous but distinguishable species*: **Nagylózs-1** [26-27], *Pannon B relatives in the Carpathian Basin: 1).* Piatra Craiului Mtn.(Királyerdő) E.Carp. Basin (Roumania) [23], [28], 2) Northern Slovakia [29], *Analogon from Antarctica:* They are certainly recent; found in containers for melting snow for freshwater [5], [13]. **Dome Fuji spherules** [5] satisfy the Pannon B definitions - "sister taxa" -, but differ in composition, so same source is excluded. Chemistry data fall for both in narrow range, (except Ba), overall compositions show similar peculiarities. Averages, mean deviations: Na_2O 0.20±0.01 %, MgO 6.0±0.9 %, Al_2O_3 15.2±0.5 %, K_2O 0.33±0.03 %, CaO 38.1±1.7 %, BaO 0.08±0.01 %, FeO 0.32±0.03 %.

THE STATISTICAL ANALYSIS OF SOME DATA

From the data of [14] we determined averages, mean deviations, which were correlated [30]. SiO_2 strongly *anti*correlated with the other major components. Any theory for the type of correlation would need a definite idea about the formation processes of Pannon B, unavailable in this stage. We may assume distributions are not far from normal (sample sizes are small to verify this)[31].).

Results. 1) The two Bakonyjákó-528 samples (two layers in drill-core) cannot be distinguished. 2) The maximal Chi-square of any site from the average is 10.67 for degree of freedom 7, so the sites are not distinguishable. 3) "Budapest", Sopron-89 spherules are undistinguishable, Nagylózs-1-s differ significantly.

AN ANTARCTIC PANNON B (OR B'): DOME FUJI

Dome Fuji spherules in narrow chemistry distribution and glassy nature are similar. (Recent analysis on 5 spherules [38]). Statistically all three differ significantly (Nagylózs-1 is middle between Pannon B and Dome Fuji.) Ca is for all three is identical. Pannon B/Nagylózs-1 are similar in Na and Al too, Dome Fuji is poorer in Na but richer in Al. Nagylózs-1/Dome Fuji are very similar in Mg, contrast to Pannon B. (Ba in Pannon B-s is very high, in Nagylózs-1 some fifth, high too, Dome Fuji Ba is "normal".)

DISCUSSION ABOUT ORIGIN

We draw crude conclusions. Problem is the *great chemical homogeneity of Pannon B spherules*, their "recurrent in time" (from drill-core ages:4 drill-core ages: Miocene, Santonian, Campanian, Anisian, Norian.) Their chemistry is "improbable", high Ba content point to a very special formation process.

Kákay-Szabó [23-24] suggested lunar origin. The composition is not lunar, no explanation on the lacking of Pannon B-s outside Hungary. She is right: all such spherules may have common origin. We now shortly follow the scenarios how to generate them. **Are they impact of extraterrestrial origin?** Then, impact was not planetwide; (from size of Hungary we guess: projectile was smaller than Ries Crater former, so <1 km.) Only Angra dos Reis is superficially similar, (if compared: Pannon B is very poor in Fe and very rich in Ba: no probability of such a strange large meteorite.). **Are they spherules of the target?** The target could not have been so homogeneous at 4 places separated by 200 km, during 150 Myears. We do know that including layers are different; but Nagylózs site is in the neighbourhood with distinguishable spherule composition. Extraterrestrial origin does not explain the facts. Then there remains a ***completely* terrestrial origin**. No complete theory of terrestrial formation of spherules is yet. But how could a mechanism produce same strange spherule compositions (lack of Fe; abundance of Ba) in the far past at a variety of sites *and* times. **We conclude: Explanation is easier if either times, or locations (preferably both) were artifacts.** (*not* arguing for this; we need something more positive than the lack of explanations [2]. To this one important idea was suggested by **Dome Fuji spherules.** ***They are clearly recent; and the main problem was recurrence.*** If Pannon B's are recent too, then there would be easy to find a source. **CEMENTS?:** Apart from Ba Pannon B,/Nagylózs/-Dome-Fuji group chemistry is compatible with cement powders. High Si and Ca content with moderate Mg and Al, (Fe removed) is characteristic for cements. Projection of Pannon B and related spherules to the SiO_2 - CaO (+MgO) - Al_2O_3 system. [38-39] show this similarity, especially to blast furnace slag cements. Cement powder is abundant in the atmosphere, and its occurrence is probable even above Antarctica. But how recent cement powder could invade drill cores, (no Aszófô: it is surface exposure) stored for long times. Contamination from *laboratory* ceiling [8] was suggested, verification was unsuccessful. Aszófô spherule compositions significantly differ from laboratory ceiling in Gif-sur-Yvette [8]. Aszófô spherules were measured in Hungary in 1996 [2, 15], with essentially the same results as [8]. So the existence of Pannon B as a homogeneous spherule group is established. The problem of origin can be solved in the future.

ACKNOWLEDGEMENTS: OTKA T/026660 support, discussions with Miono Sh., Miura Y., Szederkényi T., Tazawa Y., Cs. Detre, Gy. Don and P. Solt are acknowledged.

REFERENCES: [1] Detre., & al. Int. Meeting Spherules/Global Events, KFKI-1996-05, [2] Török & al., 1997: Proc. of TISS 1, ed. Miura, p. 30, [3] Dosztály, & al. 1997 Proc. Impact/Extraterr. Spherules: (ed. Raukas), Tallinn, [4] Bérczi., & al. in Detre, & al. (eds.) Proc. Int. Meeting, KFKI-1996-05, p.113, [5] Fukuoka & al., 1999 *Antarctic Meteorites* **XXIV**, 24 [6] Fukuoka & al., PIECE 99 (ed. Miura), p. 29, [7] Marini & al. Proc. 1998. Ann. Meeting IGCP 384. p. 63, [8] Marini & al. Proc. 1998. Ann. Meeting TECOS [9] Szõõr. & al. 1996: Annal. R. Eötvös, Sect. Geophys. & Meteorol. **XII**, 79, [10] Szarka 1996 in Detre., & al. (eds), p. 83, [11] Dávid, & al. 1996: in Detre & al. (eds), p. 127, [12] Bodrogi & al. 1996: in Detre & al. (eds), p. 73, [13] Fukuoka 1999: Lecture, NIPR Symp., Tokyo, June 3, [14] Bérczi et al. KFKI-1999-09/C, [15] Török & al. 1997: Lect. Debrecen Conf. Spherules/Global Events, [16] Bérczi & al. Proc. 1998. Ann. Meeting IGCP 384 p. 6, [17] Bérczi & al. 1998 Ant. Meteorites **XXIII**, 11 [18] Bérczi & al. PIECE 99 (ed. Miura), p. 5, [19] Bérczi Sz. & al. PIECE 99 (ed. Miura), p. 9, [20] Fáy & al. PIECE 99 (ed. Miura), p. 25, [21] Miura 1995 Shock Waves ...(ed. Takayama), Springer, Vol. 1, 1073, [22] Yanai et al 1995 Catalog of Ant. Meteorites. NIPR, Tokyo, [23] Kákay-Szabó 1996 Chem. Erde **56**, 449, [24] Kákay-Szabó 1997 Acta Mineral.-Petrol. **XXXVIII**, S105, [25] Siegl-Farkas 1996: in Detre & al. (eds), p. 143, [26] Borbély-Kiss & al. 1995 Ant. Meteorites **XX**, 16, [27] Rózsa & al. 1995: Ant. Meteorites **XX**, 211, [28] Rajta & al. 1996 in Detre & al. (eds), p. 99, [29] Jakabská 1996 in Detre & al. (eds), p. 35, [30] Lukács KFKI-1998-02, [31] Jánossy 1965 Theory of Evaluation ...Clarendon, Oxford, [32] Siegl-Farkas Proc. 1998. Ann. Meeting IGCP 384, 90, [33] Miono & al. 1993 Nucl. Inst. & Methods/Phys. Res. **B75**, 435, [34] Miono 1998 Proc. 1998. Ann. Meeting IGCP 384, p. 15, [35] Miono & al, 1998 LPSC **XXIX**, #1029, [36] Detre & al. 1998 Proc. Ann. Meeting of IGCP 384, 29, [37] Terada & al. 1999 Ant. Meteorites **XXIV**, 175, [38] Bérczi et al. KFKI-1999-09, [38] Varga & al.: *Kémiai Technológia*, Budapest, 1953

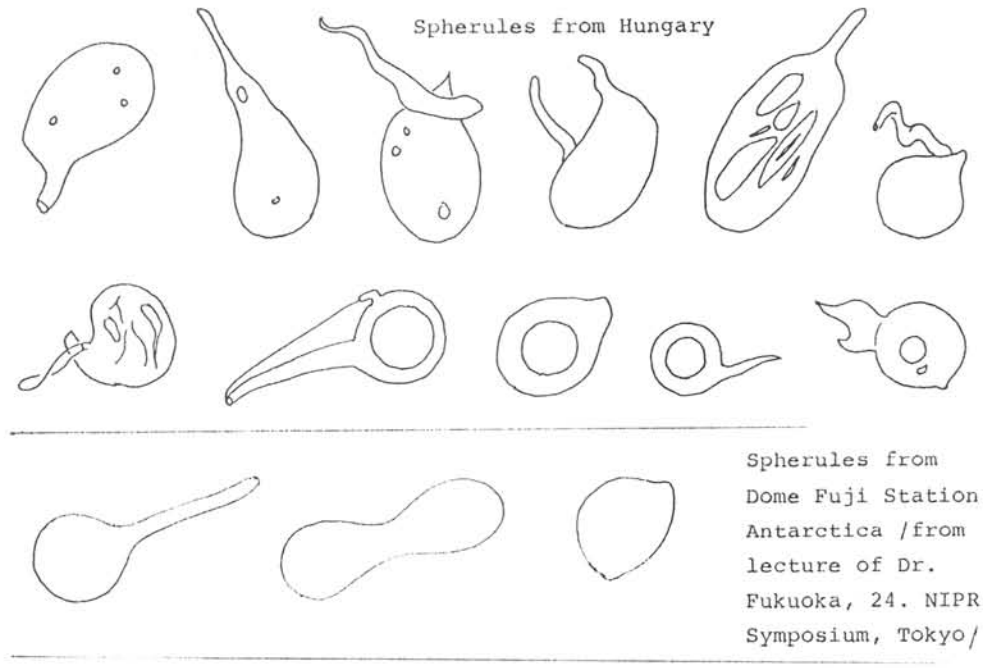

Fig. 1. Snout-tailed spherules from Hungary and from Antarctica.

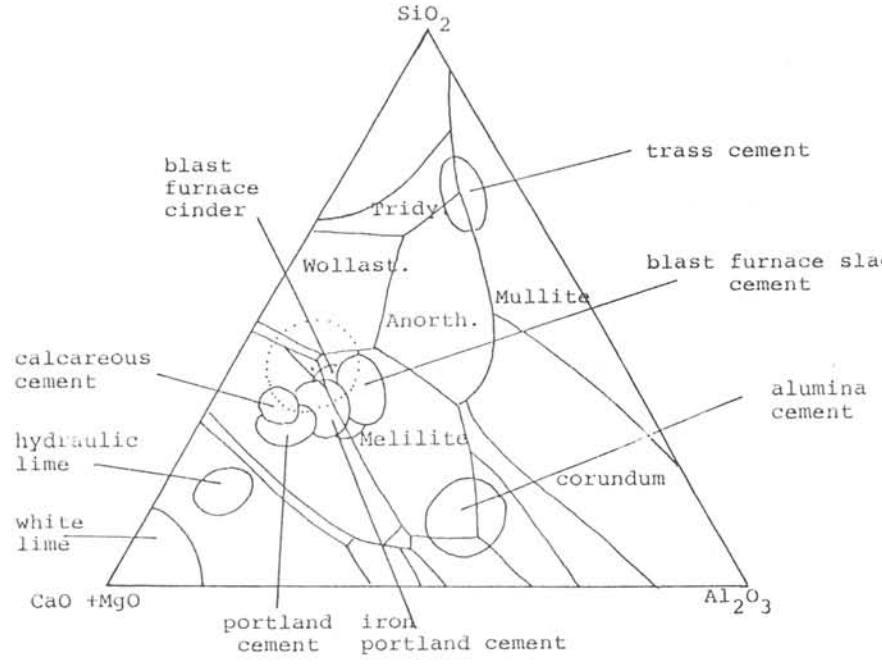

Fig. 2. Ternary system of SiO_2-Al_2O_3-CaO +MgO with compositional regions of cements and the region of snout-tailed spherules from Hungary and from Dome Fuji Station, Antarctica. /Antarctic data from Fukuoka et al. 1999, 24th Symposium on Antarctic Meteorites, NIPR, Tokyo, 25./

NATURAL $NaAlSi_3O_8$–HOLLANDITE IN THE SHOCK MELT VEINS OF SUIZHOU L6 CHONDRITE

XIE Xiande, CHEN Ming and Wang Deqiang

Guangzhou Institute of Geochemistry, Academia Sinica, Guangzhou 510640, China

Introduction

Hollandite is a structure –type after the mineral $BaMn_8O_{16}$ whose structure is constructed of edge-sharing octahedra that form a four-sided eight-membered channel that is capable of containing a low-valence large-radius cation [1]. As early as in 1967, Ringwood and his co-workers transformed sanidine into the hollandite structure with Al and Si randomly occupying the octahedral sites at 12 GPa and 900℃ [2]. This was the first oxide structure identified with both Al and Si displaying sixfold coordination and only the second after stishovite [1].Liu reported the synthesis of $NaAlSi_3O_8$ hollandite at 21 to 24 GPa in 1978 [3]. The crystal structure of the $KAlSi_3O_8$ phase was determined by Yamada et al. in 1984 [4]. It is found that alumino-silicate hollandite is capable of containing many large low valence cations at elevated temperatures and pressures [2].

First natural $NaAlSi_3O_8$ –hollandite was reported by Gillet P., Chen M. and co-authors only one month ago [5]. This high-pressure polymorph of plagioclase was found in the shock melt veins of a Chinese meteorite – Sixiangkou L6 chondrite, and occurs as intergrowths of $NaAlSi_3O_8$ –hollandite + albitic glass. Most of the observed glass + hollandite intergrowths are surrounded by ringwoodite grains or the liquidus majorite-$pyrope_{SS}$ + magnesiowüstite, and in some rare cases, jadeitic pyroxene have also been found [5].

During our recent micro-mineralogical studies on the shock melt veins of another Chinese meteorite – Suizhou L6 chondrite, we also found $NaAlSi_3O_8$ –hollandite grains in the corse-grained assemblage of the veins, and they are surrounded by the fine-grained liquidus phases. The results of our preliminary study on two (coarse- and fine-grained) high-pressure mineral assemblages in shock melt veins of Suizhou has been reported in this abstract volume [6]. In this paper we report the results of our study on the newly found $NaAlSi_3O_8$ –hollandite in Suizhou shock melt veins.

Methods

A Suizhou meteorite sample that contains two black very thin melt veins was chosen for our study. The vein width is ranging from 0.03 to 0.09 mm. This sample was made into a polished thin section and was investigated with following techniques for identifying and characterizing minerals: a MPV-SP optical microscope (OM) and a scanning electron microscope(SEM) with a Link ISIS X-ray energy dispersive spectrometer (EDX) in the Guangzhou Institute of Geochemistry, Academia Sinica, a SX-51 electron mocroprobe (EPMA) in the Institute of Geology, Academia Sinica, Beijing, and a RM-1000 laser Raman microscope (LRM) in the Beijing Institute of Non-ferrous Metals.

Results

1. Occurrence of $NaAlSi_3O_8$–hollandite in Suizhou melt veins

$NaAlSi_3O_8$ –hollandite occurs as one of the main constituents of the corse-grained high-pressure mineral assemblage in the veins of Suizhou. The dark-coloured and rounded grains of $NaAlSi_3O_8$ – hollandite are smooth and unfractured. The grain size is ranging from 8 to 25 μm in diameter. Among the other high-pressure polymorphs in the corse-grained assemblage of the veins are ringwoodite and majorite [Fig.1]. These minerals are surrounded by the fine-grained liquidus majorite-$pyrope_{SS}$ + magnesiowüstite.

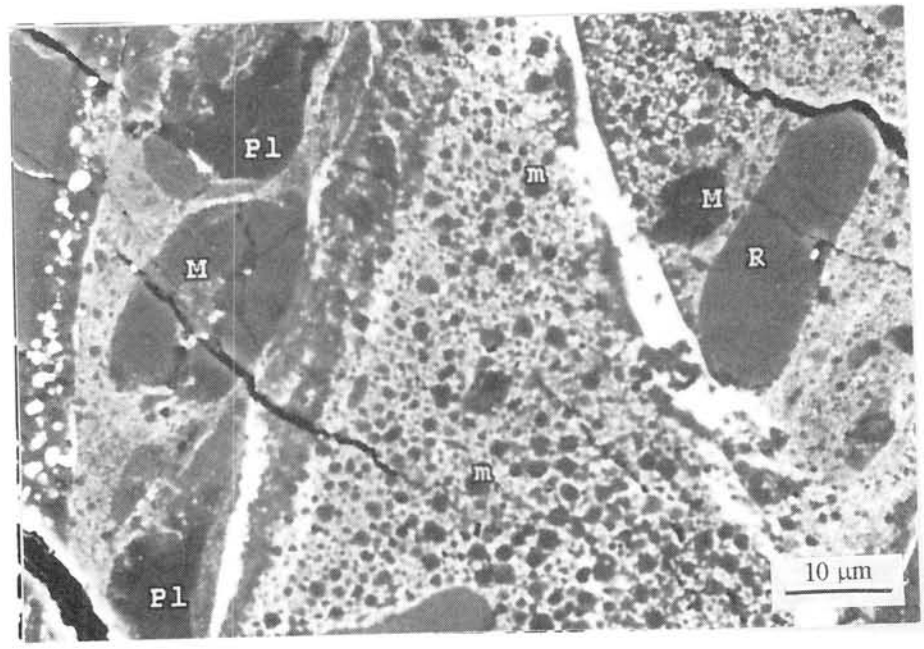

Figure 1. Back-scattered electron imege of a shock melt vein in Suizhou (Pl—$NaAlSi_3O_8$–hollandite, R—Ringwoodite, M—Majorite, m—Majorite-$Pyrope_{ss}$)

2. Chemical composition of $NaAlSi_3O_8$–hollandite in Suizhou melt veins

The chemical composition of $NaAlSi_3O_8$–hollandite in shock melt veins of Suizhou was determined by EDX and EPMA methods. The results of both analyses are very close with each other. Table 1 shows the average chemical composition of $NaAlSi_3O_8$–hollandite in the veins of Suizhou and that of plagioclase outside the Suizhou veins. For comparison, the chemical compositions of $NaAlSi_3O_8$–hollandite and plagioclase in Sixiangkou meteorite [5] are also listed in

Table 1. Average chemical composition for $NaAlSi_3O_8$–hollandite in Suizhou and Sixiangkou melt veins (in wt.%)

Mineral	SiO_2	TiO_2	Al_2O_3	FeO	MnO	MgO	CaO	Na_2O	K_2O	Cr_2O_3	Totals
Suizhou Hollandite(4)	65.275	0.042	21.362	1.080	0.023	0.622	2.216	9.137	0.902	0.008	100.016
Suizhou Plagioclase(3)	65.764	0.043	21.733	0.414	0.017	0.004	2.209	8.867	1.311	0.027	100.659
Sixiangkou Hollandite	65.21		21.65	0.75		0.34	2.20	9.24	1.46		99.85
Sixiangkou Plagioclase	65.01		21.00	0.29		0.03	2.08	9.61	0..98		99.00

The number in parentheses is the number of analyses,.

this table. All values of Suizhou minerals in the Talbe 1 were determined by EPMA in weight %. From this table we can see that $NaAlSi_3O_8$–hollandite in shock melt veins of Suizhou has almost the same chemical composition as that of plagioclase (oligoclase) outside the veins. However, $NaAlSi_3O_8$–hollandite in Suizhou veins has slightly higher FeO, MgO and Na_2O contents and lower K_2O content than those of plagioclase outside the veins.

3. Raman spectroscopic study of Suizhou $NaAlSi_3O_8$–hollandite

The Raman spectroscopic study of $NaAlSi_3O_8$–hollandite in Suizhou melt veins shows that this

high-pressure polymorph of plagioclase is a single crystalline phase [Fig.2]. The intense peak at 765 cm^{-1} is assigned to the Si-O stretching vibrations in the SiO_6 octahedra. The Raman spectra of other high-pressure minerals, which are surrounding the $NaAlSi_3O_8$–hollandite grains in Suizhou melt veins, indicate that these minerals are corse-grained ringwoodite, majorite and liquidus majorite-$pyorope_{SS}$ [Fig.2].

Discussion

The hollandite high-pressure polymorph of plagioclase has been identified in shock-induced very thin melt veins of Suizhou chondrite. The occurrence of $NaAlSi_3O_8$–hollandite in Suizhou melt veins together with ringwoodite, majorite and liquidus majorite–$pyrope_{ss}$+ magnesiowüstite constains the pressure and temperature in melt veins to be 20 to 24 GPa and 2050℃ to 2300℃ [6].

The chemical composition of Suizhou hollandite is very similar to that of Sixiangkou hollandite [5], and the Raman spectra of Suizhou hollandite can be compared with that of K-rich feldspars (in M'bale L6 chondrite)experimentally transformed at 22 GPa and 1500 K into $KAlSi_3O_8$ - hollandite, and partly with that of $NaAlSi_3O_8$–hollandite in Sixiangkou melt veins [5].The Raman data of Sixiangkou hollandite show that the crystalline hollandite is interwoven with glass of similar composition [5]. The lack of the broad intense peak at 490 to 500 cm^{-1} and the less intense broad peak near 1100 cm^{-1} for the Suizhou hollandite [Fig.2] indicates that no silicate glassy phase , such as albitic glass, was incorporated with Suizhou hollandite.

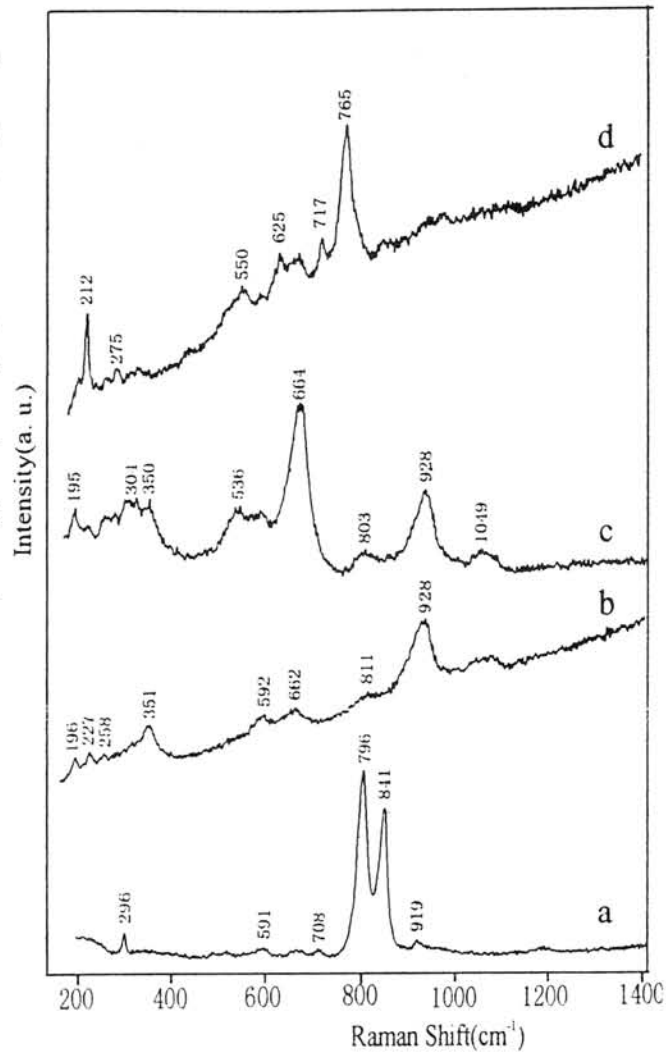

Figure 2. Raman spectra of high-pressure phases in Suizhou melt veins (a — Ringwoodite, b — Majorite, c — Mj-Py_{SS}, d — $NaAlSi_3O_8$ -hollandite)

The discoveries of hollandites in natural materials are of important significance in understanding of the Earth's mantle geochemistry, because the large four-sided tunnels in the structure of this high-pressure phase might host important elements like Na, K, Rb, and Sr and carry them from Earth's surface down into the deep mantle during the subduction process.

Acknowledgements This research is supported by National Natural Science Foundation of China, Grant No. 49825106 and 49672098. Special thanks are extended to Senior engineer Pu Yumei of Ranishaw Beijing office for her assistance in micro-Raman analyses, and to Dr. Han Xuling for her help in EPM analyses.

References [1] Prewitt C. & Downs R. (1998) Review in Mineralogy, 37: 287-317, [2] Ringwood A. et al. (1967) Acta Cryst., 23: 1093-1095, [3] Yamada H. et al. (1984) Mineral J.(Japan) 12: 29-34, [4] Liu L. (1978) EPSL, 37: 438-444, [5] Gillet P. et al. (2000) Science, 287: 1633-1637. [6] Xie X. et al. (2000) in this abstract volume.

TWO HIGH-PRESSURE MINERAL ASSEMBLAGES IN SHOCK MELT VEINS OF SUIZHOU L6 CHONDRITE

XIE Xiande[1], CHEN Ming[1,2], El GORESY A.[2] and GILLET P.[3]

1. Guangzhou Instiurte of Geochemistry, Academia Sinica, Guangzhou, 510640 China
2. Max-Planck-Institut für Chemie,55128 Mainz, Germany
3. Laboratory of Earth Sciences, Ecole Normale Superieure de Lyon, France

Introduction

The Suizhou L6 chondrite is a weakly to moderately shocked stone meteorite, fell on April 15, 1986 in Dayanpo, 12.5 km in the southeast of the Suizhou city,Hubei Province, China. The chondritic mass has light-grey colour, and consists of olivine, low Ca-pyroxene, plagioclase, FeNi metal, troilite, whitlockite, chromite and ilmenite, and it was classified as an ordinary chondrite of L6 type [1]. Only a few thin melt veins (0.02 to 0.09 mm in width) were found in this chondrite. According to previous investigators, silicate minerals in the veins were only brecciated by shock, no high-pressure minerals were found in the veins[1]. Our recent preliminary studies on the shock melt veins of Suizhou chondrite have revealed two high-pressure mineral assemblages in the veins of Suizhou, namely the coarse-grained mineral assemblage of ringwoodite + majorite, and the fine-grained mineral assemblage of majorite–pyrope $_{ss}$ + magnesiowüstite. These two assemblages constitute 70% to 80% of the veins by volume. The other constituents of the veins are coarse-grained "maskelynite" and chromite and fine-grained metal-troilite eutectic intergrowths. In this paper we report the results of our preliminary study on the two high-pressure mineral assemblages in Suizhou melt veins.

Methods

A polished thin section was made from a Suizhou fragment which contains two black melt veins of 0.03 to 0.09 mm in width[Fig.1]. The following techniques were used for our study on shock melt veins: a MPV-SP optical microscope and a scanning electron microscope (SEM) with a Link ISIS 300 X-ray energy dispersive spectrometer (EDX) in the Guangzhou Institute of Geochemistry, China, a field emission scanning electron microscope (FESEM) in the Max-Planck-Institut für Chemie, Mainz, Germany, and a XY Dilor multi-channel micro-Raman spectrometer (LRM) in the Ecole Normale Superieure de Lyon, France.

Results

1. Coarse-grained high-pressure mineral assemblage

Ringwoodite The polycrystalline grains of ringwoodite (10 to 30 μ m in length) in Suizhou shock veins are smooth and unfractered. SEM, FESEM and LRM investigations showed that these grains are single -phase ringwoodite (γ -phase of olivine)[Fig.2]. A micro-Raman spectrum obtained from a 30 μ m-long grain of ringwoodite shows two Raman peaks at 838 and 788 cm^{-1} which are characteristic for this high-pressure mineral phase[Fig3]. Our EDX analyses revealed that these ringwoodite grains have the same chemical composition as the olivine outside the melt veins. It is clear that these ringwoodite grains must have formed directly from olivine through isochemical solid state phase transformation and no additional elements were incorporated with these grains from the surrounding matrix melt. The rounded shape of both ends of the long ringwoodite grains indicates that these grains had experienced local melting caused by the heat of the surrounding shock-produced hot matrix melt after the ringwoodite was formed.

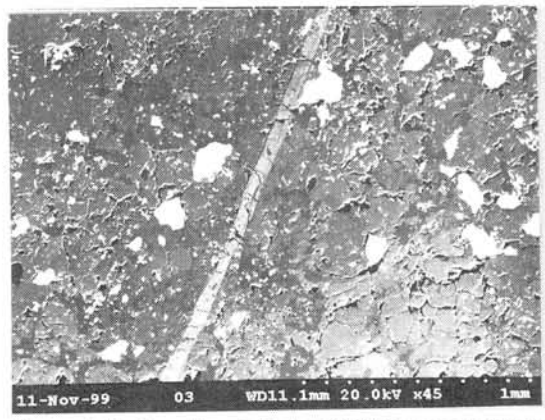

Figure 1. Back scattered electron(BSE) image showing a shock melt vein (0.05 – 0.07mm in width) in the Suizhou meteorite.

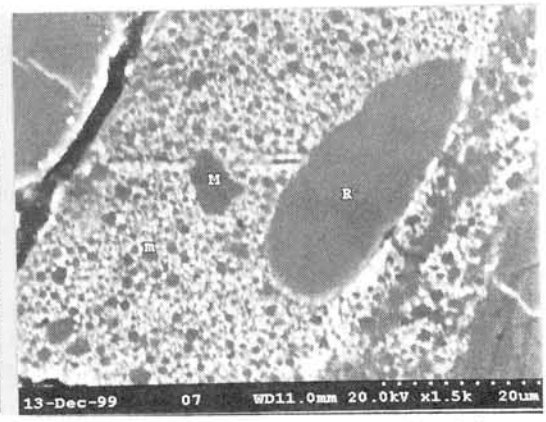

Figure 2. BSE image showing corse – grianed ringwoodite (R) and majorite (M) in fine-grained matrix of a melt vein in Suizhou.

Majorite Majorite, the high-pressure polymorph of pyroxene, occurs in the shock melt veins of Suizhou in the form of individual subeuhedral polycrystalline grains. The grain size is ranging from 8 to 30 μ m in diameter.These grains are also smooth and unfractered, and have dark-grey colour under the SEM. Our EDX analyses show that majorite in Suizhou melt veins has the same chemical composition as the low-Ca pyroxene outside the veins. No additional elements were incorporated with these corse majorite grains from the surrounding matrix melt.

2. Fine-grained high-pressure mineral assemblage

Majorite–pyrope $_{ss}$ The matrix majorite garnet occurs as tiny idiomorphic crystals ranging from 0.03 to 2 μ m in diameter (Fig.4). Our Raman spectroscopic study on a 2 μ m-sized crystal of such matrix garnet shows three peaks at 926, 638 and 586 cm^{-1}, that are characteristic for liquidus majorite garnet (Fig.5). The presence of the broad band at the range of 420 to 650 cm^{-1} indicates the existence of a quench silicate melt phase incorporated with majorite garnet. This matrix garnet is richer in Al_2O_3, CaO, Na_2O and Cr_2O_3 in comparison with that of pyroxene outside the veins. The rather high content of Al_2O_3 (up to 3.51 wt %) indicates that the matrix garnet is constituted not only of majorite composition, but also of pyrope composition.It is evident that this matrix garnet exists in the form of majorite –pyrope solid solution (Mj.-$Py._{ss}$).

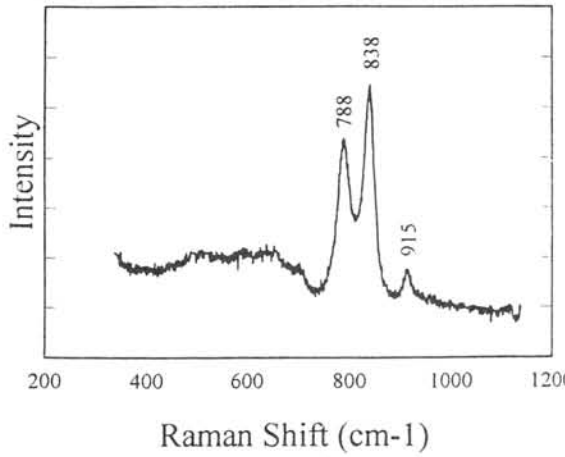

Figure 3. Raman spectrum of a 30 μ m–long ringwoodite grain in Suizhou vein.

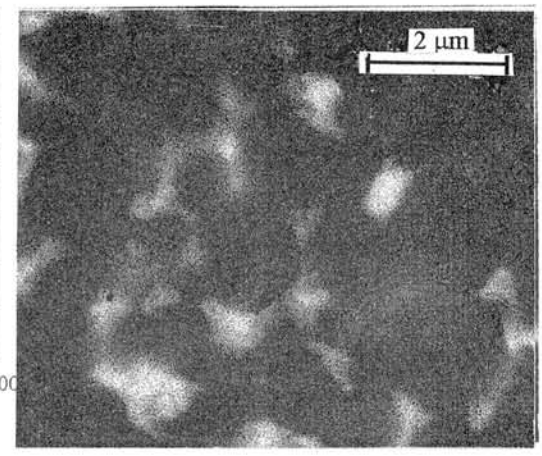

Figure 4. BSE image of the fine-grained majorite garnet (black), magnesiowüstite (grey) and FeNi-FeS blebs (white).

Magnesiowüstite The fine-grained magnesiowüstite in the shock vein matrix was identified by its grey colour and its textural relations with matrix garnet crystals (Fig. 4). It constitutes less than 8 % of the veins by volume. Our SEM and FESEM observations show that matrix magnesiowüstite grains occur in the interstitial chennels between euhehedral crystalls of micro- crystalls of garnet . Most of them are irregularly shaped, some are in the shape of cresent moon surroundimg the crystals of majorite garnet.These magnesiowüstite grains are too small (<0.5 μ m) to be analysed by EDX.

Discussion

Two lithologies of high-pressure polymorphs have been found in some shock melt veins of Sixiangkou type L6 chondrites[2].The shock veins in this type chondrites have the width ranging from 0.1 to 10 mm. For the coarse-grained minerals in the veins, the grain size can reach to 300 μ m in diameter, and the diameter of the fine-grained minerals in the vein matrix can also reach to 5 μ m[2]. The black melt veins in Suizhou are extremely narrow, only 0.02 to 0.09 mm in width, and the concentration of melt veins in Suizhou is very low. The grain sizes for both corse- and fine-grained minerals in the Suizhou melt veins are much smaller in comparison with those in melt veins of Sixiangkou and other L6 chondrites. The discovery of two high-pressure polymorphs in Suizhou shock melt veins not only provides a new member of Sixiangkou type melt veins, but also gives us very important informations concerning the mechanism of formation of two mineral assemblages under very high pressure and temperature regime in the very thin shock melt veins of L6 chondrites. On the basis of static high-pressure experiments[3, 4],the presence of ringwoodite and lack of wadsleyite in coarse-grained assemblage constrains the pressure in Suizhou melt veins to be greater than 20 GPa, the majorite garnet + magnesiowüstite assemblage in the fine-grained matrix of Suizhou crystallized from shock-induced silicate melt at 2050℃ to 2300℃ and 20 GPa to 24 GPa. It is evident that inspite of the very small width of the shock melt veins, the high pressure (up to 24 GPa) and high temperature (up to 2300℃) regime did exist in these thin melt veins.

The presence of two high-pressure mineral assemblages in the thin shock melt veins also indicates that regardless of the small width of shock melt veins in Suizhou, the duration of shock - induced high - pressure regime in the veins of the chondrite parent body should be long enough for the phase transformation of coarse - grained minerals in solid state and then for crystallization of fine-grained high-pressure matrix minerals from the shock-induced silicate melt.

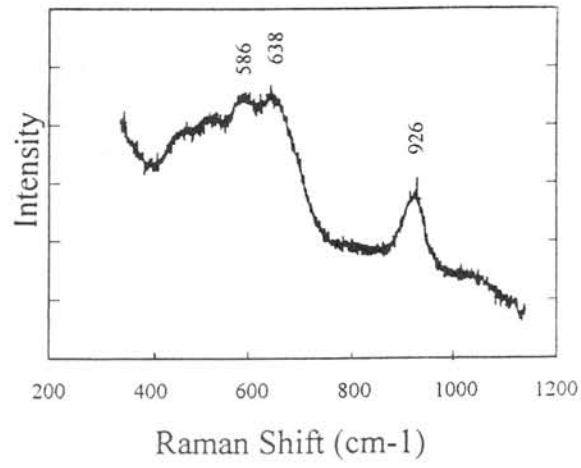

Figure 5. Raman spectrum of a fine-grained majorite-pyrope garnet.

Acknowledgements This research is supported by National Natural Science Foundation of China (Grant No. 49825106 and 49672098) and partly supported by the Max – Planck - Institut für Chemie, Mainz, Germany. Special thanks are extended to Dr. Wang Deqiang of Guangzhou and to Mr. Huth J. of Mainz for technical assistance in SEM and FESEM analyses.

References [1] Wang R. & Li Z. (1990) Comprehensive Studies on the Suizhou Meteorite, Publishing House of the China University of Geology, Wuhan, 12-19. [2] Chen M. et al.,(1996) Science, **271:** 1570-1573. [3] Ito E. & Takahashi E.(1989), J.Geophys. Res.,**94:** 10637. [4] Zhang J. & Herzberg C.(1994) J. Geophys. Res., **99:** 17729.

Evaluation of the accretion rate of cosmic dust on the Earth in the last glacial period based on the concentration of micrometeorites in bare ice around Yamato Mts.

°Toru Yada[1], Tomoki Nakamura[1], Takaaki Noguchi[2], Hajime Yano[3], Kentaro Terada[4], Hideyasu Kojima[5], Rie Ohmori[6], Takahito Osawa[7], Sadahiro Mizutani[8], Takeshi Mori[4], Noriko Matsumoto[2], Junya Kamata[2], Masato Itabashi[9] and Takehiko Setoyanagi[9]

[1] Dept. Earth & Planet. Sci., Grad. School Sci., Kyushu University, Hakozaki Fukuoka 812-8581, Japan, [2] Dept. of Materials and Biological Science, Ibaraki University, Bunkyo 2-1-1, Mito, Ibaraki, 310-8512, Japan, [3] Planet. Sci. Div., The Institute of Space and Astronautical Science, 3-1-1 Yoshinodai, Sagamihara, Kanagawa, 229-8510, Japan, [4] Dept. of Earth & Planetary Sciences, Hiroshima University, Higashi-Hiroshima, Hiroshima, 739-8526, Japan, [5] National Institute of Polar Research, 1-9-10 Kaga, Itabashi, Tokyo, 173-8515, Japan, [6] Dept. of Physics, Dokkyo University, School of Medicine, Mibu, Tochigi 321-0293, Japan, [7] Laboratory for Earthquake Chemistry, University of Tokyo, Hongo, Bunkyo-ku, Tokyo 113-0033, Japan, [8] Dept. of Earth and Planet. Physics, University of Tokyo, Hongo, Bunkyo-ku, Tokyo 113-0033, Japan, [9] Dept. of Applied Chemistry, Science University of Tokyo, Kagurazaka, Shinjuku, Tokyo 162-0824, Japan

Introduction: Interplanetary dust particles are one of major constituents of the Solar System. Constantly supplied by comets and asteroids, they are lost from interplanetary space due to Poynting-Robertson drag and solar radiation pressure [1]. Therefore, micrometeoroids in interplanetary space are refreshed in several ten thousand years in the 1 AU region [2], and that is, their influx on the Earth, both for total mass accretion and major composition depending upon their parent bodies would most possibly change by one epoch to another. Influx of the interplanetary dust to the Earth today is estimated as 40000±20000 ton/year based on the frequency of hypervelocity impact of these meteoroids which formed micro-craters on the space-facing end of an low Earth orbit satellite, LDEF [3]. Their mass accretion rates were also estimated by extraterrestrial matters found on the Earth's surface. Based on Os isotope ratio of deep-sea sediments, the mean value of the last 80 million years was estimated as 37000±13000 ton/year [4]. Taylor et al. [5] calculated the flux between AD 1000 to AD 1500 as 2700±1400 ton/year by counting cosmic spherules found from sediments of water well at the U.S. South Pole Station.

Now we are going to utilize a new collection of Antarctic micrometeorites (AMMs) to estimate a new value of a mass accretion rate of the cosmic dust on the Earth.

Samples: AMMs used in this study were collected from bare ice around the Yamato Mts. during austral summer of 1998 [6]. Some of us (T.Y. and H.K.) had melted the bare ice and filtered the melted water to capture microparticles contained in the melted ice. Among 24

collection points, five points are selected for counting all AMMs in each collection. Two points out of the five are from JARE IV Nunataks area, the most northern area of the collection's points. Other two points are from Kuwagata Nunatak area, about 50 km south-southwest from the JARE IV Nunataks area. The last point is from South of Minami-Yamato Nunataks area, about 30 km south from the Kuwagata Nunatak area [6]. Collected microparticles that might include AMMs had been divided into four size fraction such as 10~40 μm, 40~100 μm, 100~238 μm and >238 μm by sieving the samples with four different grid sizes. We investigated into the latter three size fractions except 10~40 μm size fraction, because this size fraction has only small contribution for the accretion rate of mass, and besides, we are afraid that AMMs in this size could not reflect all AMMs contained in the melted water; all the melted ice water in the 1998 expedition might not have been able to be fully filtered at the collection points, which means that we could not filter all the small particles such as to be blown up by convection current in the melted water.

Methods: We handpicked rounded particles or blackish irregular particles within the whole collection of microparticles scattered on small petri dishes under an optical stereo microscope. Then we analyzed those particles by a scanning electron microscope (SEM) equipped with energy dispersive spectrometer (EDS) without conductive coating to reveal their qualitative chemical composition. We distinguished AMMs from terrestrial particles based on these EDS spectra data. In the case of spherules, those with chondritic composition and Fe-oxide containing no other intense peaks except Ni were classified as extraterrestrial origin. In the case of irregular-shaped particles, those of chondritic composition were selected as extraterrestrial origin. We also judged microparticles in which compositions were slightly different from chondritic characteristics, due to some elemental anomalies such as Fe enrichment, Mg depletion and minor inclusion of Na and/or K, as extraterrestrial origin because the particles should show the trace of alterations during atmospheric entry and long duration in the ice especially in their surface layers which composition we could analyze non-destructively in this study by the EDS.

Results and summaries: From Kuwagata Nunatak 2 (K02), we found 262 AMMs from three size fraction of particles. An average of their mean diameters is 90 μm, and their size distribution is shown in Fig. 1(a). From JARE IV Nunataks 9 (J09), we found 80 AMMs in the same size fraction of K02. An average of their mean diameters is 98 μm and their size

distribution is shown in Fig. 1(b). We are on the way to evaluate the total masses of the AMMs in each collection.

Machida et al. analyzed CO_2 content of an ice core drilled near by the Kuwagata Nunatak area and the value is 200 to 230 ppmv from 100 m depth to the surface [7]. This suggests that bare ice containing AMMs, around the Kuwagata Nunatak is supposed to have accumulated in the last glacial period, which is older than ten thousand years. And three collection areas are thought be different each other in their ages. With snow accumulation rates of the past and accurate masses of AMMs in each collection point, we could estimate the accretion rates of the cosmic dust on the Earth of three different ages.

Acknowledgement: We are very grateful to Prof. Yoshiyuki Fujii of NIPR for giving us useful advice about glaciology.

References: [1] Flynn (1989) Icarus, 77, 287-310. [2] Flynn (1996) Astron. Soc. Pacific Conf. Series, 104, 171-175. [3] Love and Brownlee (1993) Science, 262, 550-553. [4] Peucker-Ehrenbrink (1996), GCA, 60, 3187-3196. [5] Taylor et al. (1998), Nature, 329, 889-903. [6] Yada and Kojima (2000), Antarct. Meteorite Res., 13, 9-18. [7] Machida et al. (1996), Proc. NIPR Symp. Polar Meteorol. Glaciol., 10, 55-65.

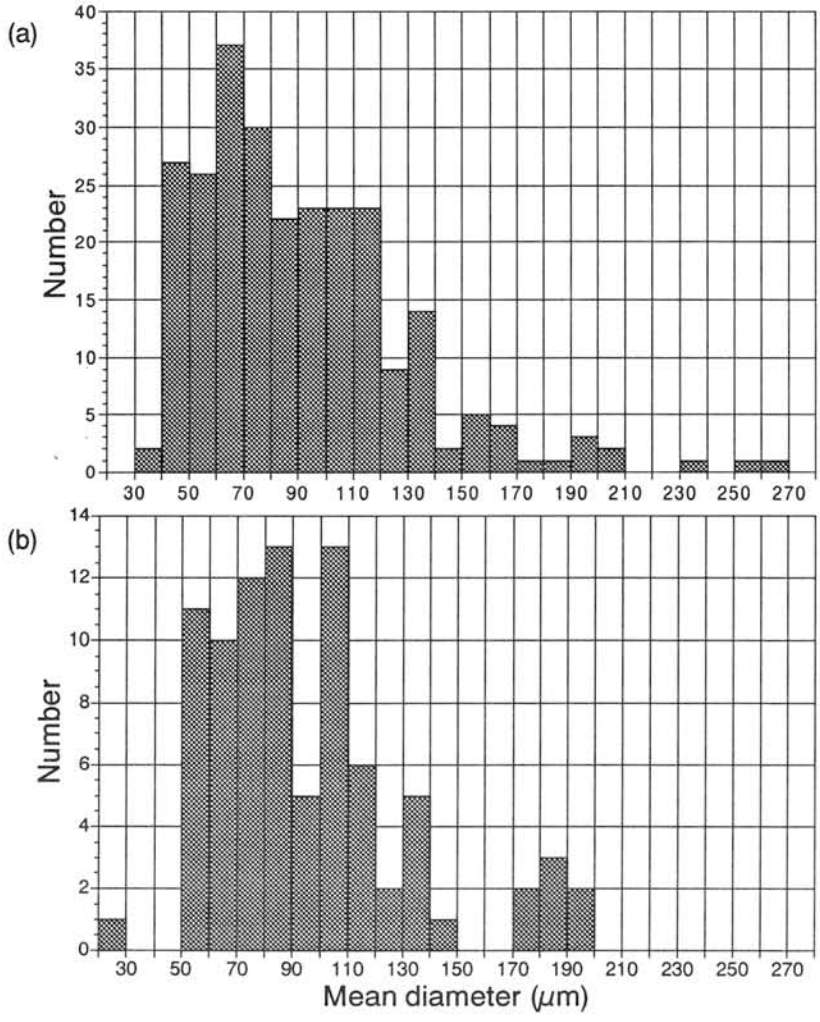

Fig. 1 Size distributions of mean diameters of AMMs from bare ice of Yamato Mts.
(a) Kuwagata Nunatak 2.
(b) JARE IV Nunataks 9.

Quantitative estimation of shock pressure experienced by ordinary chondrites with an X-ray powder diffraction method

S. Yamada[1)], Y. Nakamuta[2)]*, and Y. Aoki[3)]

[1)]NTT Docomo Chugoku; [2)]Kyushu University Museum, Kyushu University, Fukuoka 812-8581, Japan; [3)]Dept. Earth and Planetary Sciences, Faculty of Science, Kyushu University, Fukuoka 812-8581, Japan; *Correspondence author's e-mail address: nakamuta@geo.kyushu-u.ac.jp

Introduction: Shock metamorphism is pervasively recognized in meteorites, and it is an important subject to estimate the degree of shock experienced by each meteorite. Stöffler et al. (1991) classified meteorites based on the degree of shock that was recorded as shock textures on olivine. However, the classification of Stöffler et al. (1991) is qualitative one.

Uchizono et al. (1999) experimentally suggested that the crystal lattice of olivine has been strained by shock-compression and the apparent strain estimated by an X-ray diffraction method increases with the increase of the pressure loaded. In this study, we determined apparent strains of olivine crystals in ordinary chondrites by an X-ray powder diffraction method and estimated shock pressures experienced by each meteorite.

Experimental method: We analyzed six ordinary chondrites, which are listed in Table 1 together with the results of this study. The polished thin sections of the six meteorites were observed under a microscope with a polarized light. Chemical compositions of olivines were analyzed by an EPMA equipped with a wavelength dispersive spectrometer. Olivine grains of about 50μm in size, being confirmed to be homogeneous in their chemical compositions by EPMA, were taken out of the polished thin sections. Their X-ray powder diffraction patterns were obtained by a Gandolfi camera. The position and the integral breadth of each X-ray reflection were precisely determined by applying a profile-fitting technique with a pseudo-Voigt type shape function. Apparent strains of olivine crystals were determined by the method shown by Williamson and Hall (1953).

Results and discussion: An example of the X-ray diffraction pattern of an olivine grain (50 μm in size) is shown in Fig. 1. As shown in Fig. 1, a clear X-ray diffraction pattern can be obtained even from a very small crystal by using a Gandolfi camera.

The X-ray line broadening can be related to the apparent strain in a crystal by the equation, $\beta_s = 4e\tan\theta$, where e and β_s are the apparent strain and the broadening due to the strain respectively and θ is the half of the angle between incident and diffraction beams (Wilson, 1962). The measured integral breadth by using a Gandolfi camera is also affected by the size of an X-rayed grain and crystals in the grain. The resultant integral breadth β can be approximately expressed as $\beta = 4e\tan\theta + \beta_0$, where β_0 is the line broadening due to the size

effects (Uchizono et al., 1999). Fig. 2 shows the plot of β vs. $\tan\theta$ for olivine grains from the Bruderheim (assigned to S4 shock stage) and the Great Bend (S1 shock stage) chondrites. The olivine from the Bruderheim chondrite (S4) is plotted on the diagram along the line having a greater slope than that for the olivine from the Great Bend chondrite (S1). The results suggest that the former is strained more than the latter and that the apparent strain measured by an X-ray method corresponds well to the shock stage determined by the method of Stöffler et al. (1991).

For each meteorite, the apparent strains of four to six olivine grains were determined. The maximum value of the apparent strains for each meteorite is shown in Fig. 3 as a thin solid line parallel to the shock pressure-axis. The lengths of the lines show the ranges of shock pressures that are estimated for the shock stages to which each meteorite is assigned (Stöffler et al., 1991). Uchizono et al. (1999) showed experimentally that the apparent strain of a olivine single crystal increases with the increase of shock pressure experienced by it. By assuming a linear relation between the apparent strain and shock pressure as shown by Uchizono et al. (1999), we can draw two lines on the diagram of Fig. 3, which restrict the shock pressure experienced by each meteorite. The line drawn through solid circles in Fig. 3 shows the linear relation between the apparent strain and shock pressure that has the maximum slope among the lines showing the linear relation and restricts the shock pressure at the lower-pressure side for each meteorite. The other line drawn through solid squares has the minimum slope and restricts the shock pressure at the higher-pressure side. The thick solid lines drawn for each meteorite in Fig. 3 show the shock pressure ranges restricted by the maximum and minimum slope lines. The shock pressures estimated for each meteorite like this are also summarized in Table 1.

Fig. 4 shows the plot of the apparent strain vs. shock pressure for all olivine grains analyzed in this study. The values of shock pressure for each meteorite in Fig. 4 are those shown in Table 1. The thin solid lines in the diagram were drawn through the minimum and maximum values of each meteorite. The minimum values of apparent strains for each meteorite also increase with the increase of shock pressure in the range above 10 GPa. The results and the ranges of the apparent strains for each meteorite suggest that olivine crystals were compressed under the pressure range of about 10 GPa in each meteorite.

References:

Stöffler, D., Keil, K. and Scott, E.R.D. (1991) G.C.A. **55**, 3845-3867; Uchizono, A., Shinno, I., Nakamuta, Y., Nakamura, T. and Sekine T. (1999) Mineral. J. **21**, 15-23; Williamson, G.K. and Hall, W.H. (1953) Acta Metall. **1**, 22-31; Wilson, A.J.C. (1962) *X-ray Optics*, John Wiley & Sons Inc., New York.

Table 1. Meteorites used in this study and their estimated shock pressure.

Meteorites	Chemical Group	Shock Stage*	Estimated Shock Pressure (GPa)
Great Bend	H6	S1	2.8 ± 0.2
Y-790752	LL6	S2	5.5 ± 0.5
Mulga(north)	H6	S2	9.2 ± 0.8
Dhurmsala	LL6	S3	13.2 ± 1.2
Ohuma	L5	S3	18.2 ± 1.8
Bruderheim	L6	S4	22.2 ± 2.2

*: estimated with referring to Stöffler et al. (1991).

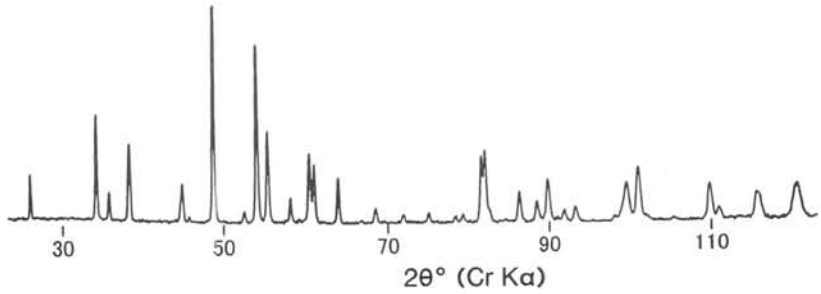

Fig. 1. X-ray diffraction pattern of an olivine grain (50 μm) taken by a Gandolfi camera.

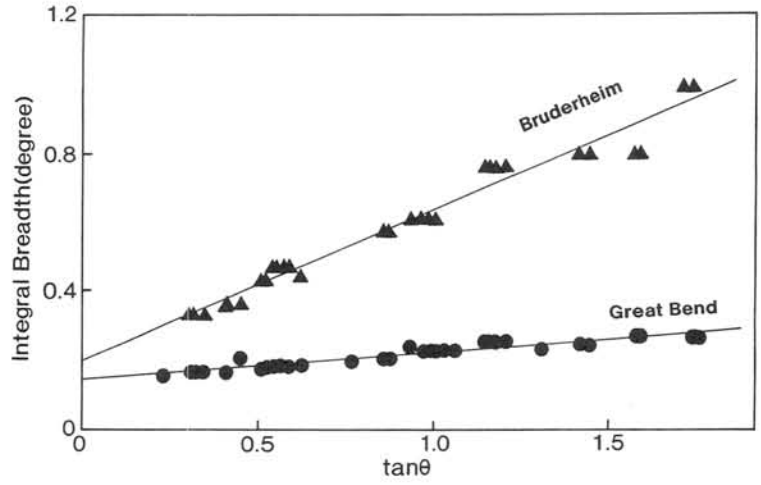

Fig. 2. Plot of integral breadth vs. tanθ for olivin grains from Bruderheim (S4) and Great Bend (S1) chondrites.

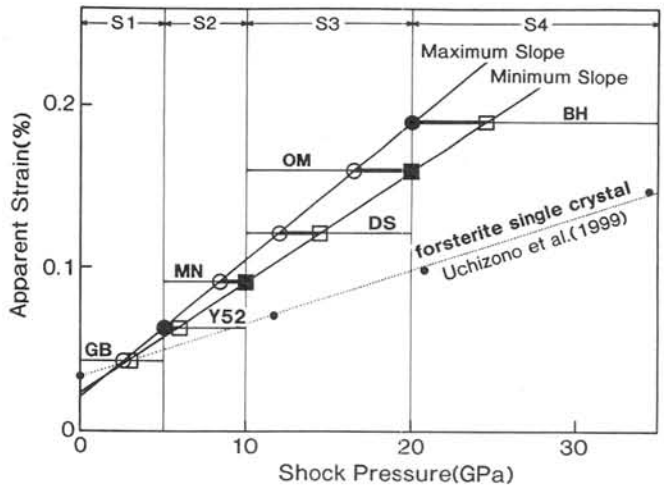

Fig. 3. Relation between the maximum value of the apparent strain for each meteorite and shock pressure. GB: Great Bend; Y52: Y-790752; MN: Mulga(north); DS: Dhurmsala; OM: Ohuma; BH: Bruderheim.

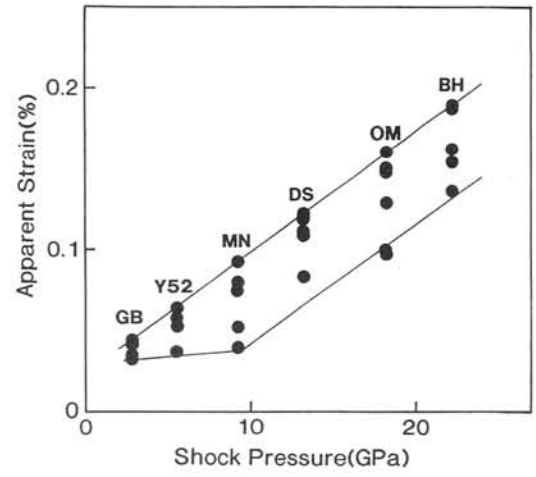

Fig. 4. Plot of apparent strain vs. shock pressure for all olivin grains analyzed in this study.

Hot shock experiments of a basaltic eucrite: Implication for impact processes on early hot crust.

Akira Yamaguchi[1], Toshimori Sekine[2], and Hiroshi Mori[3]

[1]Antarctic Meteorite Research Center, National Institute of Polar Research, Tokyo 173-8515
[2]National Institute for Research in Inorganic Materials, Ibaraki 305-0044.
[3]Faculty of Science, Ehime University, Ehime 790-8577.

Impact event is one of the most important geologic processes in the geological evolution of asteroids and planets. It is plausible that impact events significantly interacted early metamorphic and volcanic events. Recent studies of strongly metamorphosed eucrites showed that impacts occurred when the parent body was still hot ~4.5 Ga [e.g., 1]. Shock metamorphism at high initial temperatures results different shock effects from those at room temperatures [e.g., 2,3]. For example, Schmitt [3] suggested that higher initial temperature results on the larger volume of impact melts. To better understand impact processes on hot early crust of the basaltic achondrite parent bodies, we performed shock-recovery experiments of preheated (up to 863°C) basaltic eucrites.

We performed shock-recovery experiments using a single stage propellant gun at the National Institute for Research in Inorganic Material. A starting eucrite with the bulk chemical composition of Juvinas was synthesized using a lamp-image floating-zone furnace. The sample disks of the synthesized eucrite mounted in stainless container were externally heated up to 863°C The sample chamber was evacuated to 100-200Pa prior to impact. The shock recovered samples were cut along the shock propagation axis. We examined the samples except for extreme edges of the recovered disks (which are complexly deformed), using optical and scanning electron microscope, and electron probe microanalyzer. The detailed experimental procedures were described in Sekine et al. [4].

Shock textures of the samples impacted at <26 GPa preheated at < ~600°C and the samples shocked to <84 GPa at room temperature (about 20°C) were briefly described in Yamaguchi et al. [5]. Shock effects of minerals observed under optical microscope are similar to those observed in the previous studies [e.g., 6,7,8]; but the pressure of the crystal-glass transition seems to be lower when the ambient temperature is higher. In the sample shocked at <40-50 GPa, shock melts are typically formed along microfaults as a desequilibrium shock effect [8]. In the sample shocked at 84 GPa at room temperature, there are ubiquitous monomineralic melts and polymineralic melts, suggesting almost total melting without significant mixing. The sample shocked at 13.1GPa preheated at 849°C (Fig. 1) is highly brecciated, and is textually similar to the sample shocked at <20-30 GPa at room temperatures. However, at high magnification, the clastic matrix seems to be slightly welded due to high post-shock temperature. Shock melts are rarely observed in the sample.

The sample shocked at 22.8 GPa preheated at 863°C is brecciated and deformed, but some portions roughly keep the original igneous texture (Fig. 2a). Plagioclase is totally converted into glass phase and has smooth surface. In contrast to the sample shocked at 13.1 GPa at 849°C (Fig. 1), the sample contains ubiquitous melts with vugs (several tens μm in size). The shock melts seem to have been formed *in situ* because plagioclase (glass) laths extend into the shock melts in some cases (Fig. 2b). The textural settings of these melts are different from the melts observed in normal shock melts (e.g., shock melts along microfaults). The chemical compositions of the melt are relatively homogeneous and are extremely enrich in Ti and Fe compared to the bulk rock of Juvinas (Table 1). This is in contrast to the fact that shock melts are generally polymineralic and monomineralic [e.g., 5,8] and they occur along microfaults and/or melt pockets where stress is highly concentrated (see above).

The increase of the post-shock bulk temperature of solid basalt shocked at ~20 GPa is about <200°C [e.g., 8]. Thus, post-shock temperature of the sample shocked at 22.8 GPa preheated at 863°C is likely to be >1000°C, close to the solidus (~1000-1100°C). Thus, the post-shock temperature was high enough to cause partial melting of the rock. In contrast, the post-shock temperature of the sample shocked at 13.1 GPa at 849°C did not exceed the solidus temperature of the rock. The results suggest that moderate shock metamorphism at hot crust can produce significant amount of shock melts that are chemically similar to partial melts.

In the asteroid-sized bodies, shock is unlike heat source for global melting and metamorphism [9]. However, recent studies [e.g., 1] showed that some eucrites (e.g., Ibitira and EET90020) experienced partial melting due to shock accompanied by melting of mesostasis (low-temperature assemblages), the possible cause of the disturbance of various radiometric ages. The pre-shock temperature was estimated be about 800-900°C. The results of the experiments are consistent with the fact moderate shock metamorphism (~20 GPa) can cause partial melting when the ambient temperature is high. Unfortunately, we did not controlled the oxygen fugacity of the rocks during shock. Therefore, the chemical compositions of melts may be slightly different from the conditions of shock metamorphism of natural eucrites. In conclusion, shock heating cannot be a direct heat source for partial melting in a asteroid sized bodies [9], but the results of our experiments suggest that partial melting can take place only when the ambient temperature is high and is close to the solidus temperature of rocks.

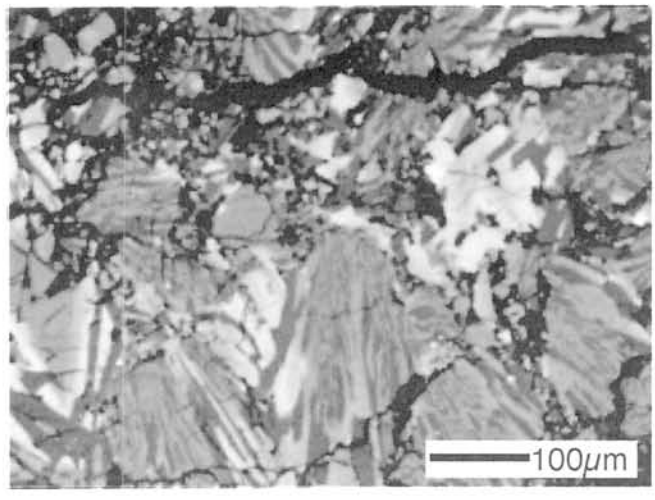

Fig. 1. Backscattered electron image (BEI) of the sample shocked at 13.1 GPa preheated at 849°C. It is brecciated and shock melts are are rarely observed. Light grey: pyroxene; dark grey: plagioclase; and black: cracks filled with epoxy.

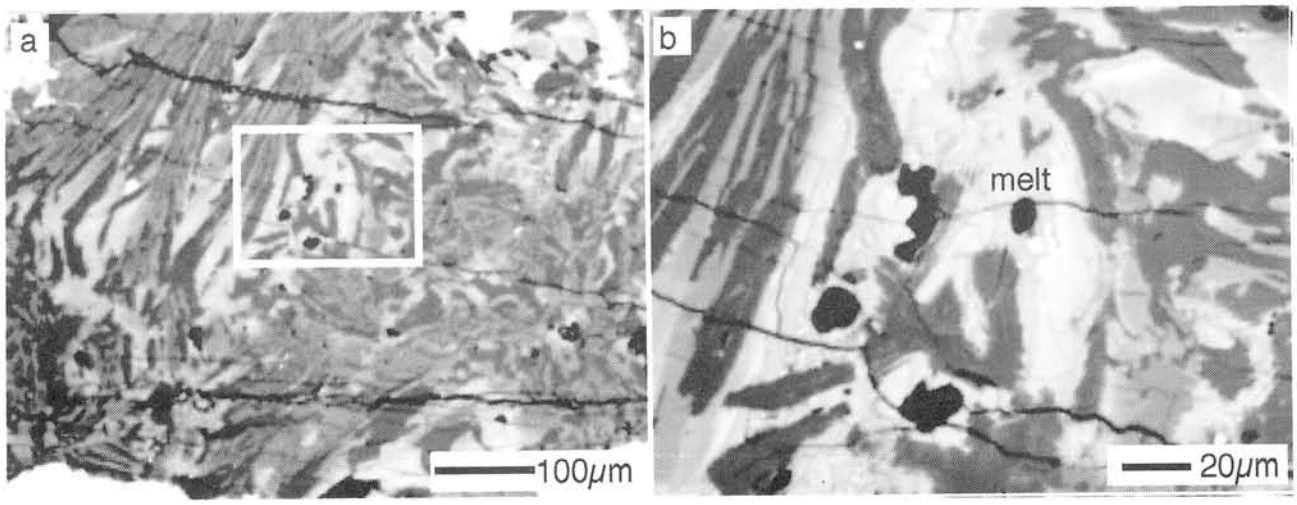

Fig. 2. (a) BEI of the sample shocked at 22.8 GPa preheated at 863°C. It roughly keeps original igneous texture. (b) Enlarged view of the portion of melts. Plagioclase lath (dark grey) extends into melts (medium grey, middle), suggesting that the melts formed *in situ*.

Table 1. Chemical compositions (wt%) of shock melts (Fig. 2b) in the sample recovered from 22.8 GPa preheated at 607°C.

	impact melts* 22.6 GPa, 607°C		Bulk composition of starting material
SiO_2	48.8	*(0.93)*	49.3
Al_2O_3	8.25	*(0.93)*	12.6
Na_2O	0.26	*(0.06)*	10.3
CaO	10.2	*(0.28)*	6.83
FeO	28.5	*(1.13)*	18.5
MgO	0.33	*(0.11)*	0.42
MnO	0.65	*(0.04)*	0.68
Cr_2O_3	0.02	*(0.02)*	0.30
TiO_2	2.14	*(0.53)*	0.53
Total	99.0		

*Average of 11 analyses.
Figures in parentheses give 1σ of analyses.

References:

[1] Yamaguchi A. et al. (1997) *MAPS* 32, A144-A155. [2] Langenhorst F. and Deutsch A. (1991) *Meteoritics* 26, 361. [3] Schmitt R.T. (2000) *MAPS* 35, in press. [4] Sekine T. et al. (1987) *J. Mat. Sci.* 22, 3615-3619. [5] Yamaguchi A. et al. (2000) *LPS* XXXI, CD-ROM. [6] Kieffer S. W. et al. *Proc. Lunar Sci. Conf.* 7, 1391-1412. [7] Schaal R. B. and Hörz F. (1977) *Proc. Lunar Sci. Conf.* 8, 1697-1729. [8] Stöffler D. et al. (1988) Meteorite and Early Solar System, 165-202. [9] Keil K. et al. (1997) *MAPS* 32, 349-363.

Aqueous Fluid-Inclusions in Chondrites

Michael E. Zolensky [1], Robert J. Bodnar [2], Mary S. Bell [3], Joel Saylor [4] and Hiroshi Takeda[5]

[1]SN2 NASA Johnson Space Center, Houston, TX 77058, USA
[2]Department of Geological Sciences, Virginia Tech., Blacksburg, VA 24061,USA
[3]Lockheed Martin, Houston, TX, 77058
[4]Dept. of Geological Sciences, Case Western Reserve University, Cleveland, OH 44106, USA
[5]Chiba Institute of Technology, 2-17-1 Tsudanuma, Narashino City, Chiba 275, Japan

Introduction: Over the past three decades we have become increasingly aware of the fundamental importance of water, and aqueous alteration, on primitive solar-system bodies [1]. Nevertheless, we are still lacking fundamental information such as the location and timing of the aqueous alteration, and the nature of the aqueous fluid itself. A major impediment to our understanding of aqueous alteration has been the complete absence of direct samples of aqueous fluids in meteorites. Here we describe aqueous fluid inclusions present in blue/purple halite and sylvite found within the matrix of two ordinary chondrite falls, Monahans (1998) (H5) and Zag (H3-6); both meteorites are gas-rich regolith breccias [2&3]. We also report new discoveries of aqueous fluid inclusions in Ca-carbonates within two CI1 chondrites, Orgueil and Ivuna.

Fluid Inclusions: Fluid inclusions are micro-samples of fluid that are trapped at the crystal/fluid interface during growth (primary inclusions), or some later time along a healed fracture in the mineral (secondary inclusions). Both primary and secondary fluid inclusions are found in meteorites, although the latter predominate. The presence of secondary inclusions indicates that aqueous fluids were locally present following halite and carbonate deposition, suggesting that aqueous activity could have been episodic on the H and CI parent asteroids.

Monahans: We have completed preliminary study of the Monahans (1998) inclusions; these range up to 15 micrometers in longest dimension. At room temperature, approximately 25% of the inclusions contain bubbles that are in constant motion, proving that the inclusions contain a low-viscosity liquid and "vapor". During cooling under the microscope, the inclusions solidified (froze) at -45 to -50°C. When the frozen inclusions are heated, first melting is observed at about -35 to -40°C, indicating that the inclusions likely contain divalent cations such as Fe^{2+}, Ca^{2+} or Mg^{2+}, in addition to Na^{+} and K^{+}; given the environment of formation, dissolved Fe and Ca are the most likely dissolved species. The presence of water in the Monahans (1998) inclusions was confirmed by Raman microprobe analysis. Raman spectra of inclusions show a significant peak at approximately 3400 cm^{-1}, diagnostic of aqueous salt solutions.

The rarity of vapor bubbles in fluid inclusions in Monahans (1998) and Zag halite suggests a low formation temperature (probably less than 50°C). The bubbles that are present are small, and probably resulted from freeze-stretching of the inclusions during space exposure. The vapor bubbles represent the water vapor in equilibrium with liquid water at room temperature and, as such, are essentially a poor vacuum with a pressure of about 0.03 bars. No gases, such as CO_2, N_2, or CH_4, were detected during Raman analysis of the inclusions.

Zag: This far we have been unsuccessful in obtaining quality Raman spectra of the fluid inclusions in Zag. However, we will be re-measuring the samples in a new instrument this summer, and believe that this attempt will be successful. We have observed S in the precipitated residues of a broken Zag inclusion, during SEM examination. This observation proves that other salts besides Na- and K-chlorides are present within the inclusions.

Orgueil and Ivuna: We report for the first time aqueous fluid inclusions within Ca-carbonates in the CI1 chondrites Orgueil and Ivuna (see figure 1). As with Zag, we intend to characterize the fluids within these tiny (<10um) inclusions this summer. Results will be reported at the meeting. We have also begun to survey a new CI fall from Canada, which contains abundant Ca-Mg-Fe carbonates. We will report on this new meteorite at the meeting.

Implications of the Halite and Fluid Inclusions in Chondrites: It is possible that halite is commonly present in chondrites, but has been overlooked, resulting in considerable errors in bulk Cl determinations for chondrites. It is also possible that a considerable fraction of the ubiquitous sulfate/halide efflorescence noted on Antarctic meteorites is derived from dissolution and reprecipitation of indigenous halite (and sulfides), rather than from components introduced from the ice as is commonly assumed.

Based upon the evidence, we can construct the following basic chronology of events for both Monahans (1998) and Zag: (1) asteroid accretion, (2) different degrees of fluid-assisted metamorphism of chondritic materials within the asteroid, (3) impact gardening to produce a regolith, and impact deposition of different materials into the regolith, (4) deposition of the halite into the regolith, (5) impact welding of regolith materials and chondritic fragments, (6) impact launching of the meteoroid from the surface.

The halite may have been deposited from indigenous briny asteroidal water trickling through the regolith, or by a water-bearing meteoroid impacting the surface. Measurement of the oxygen- and hydrogen-isotopic composition of the fluid should answer this question, and shed new light on the source of water. Measurement of the fluid composition within the inclusions will permit more realistic modeling of asteroid alteration. Apparently, water was more common on asteroids than is generally realized, and thus chondrite metamorphism paths should be reconsidered. It should also be possible to date more precisely the halite/sylvite by the $^{39}Ar/^{40}Ar$ laser ablation technique, increasing our understanding of the timing of asteroidal alteration.

The discovery of previously unrecognized fluid inclusions in well-studied CI carbonates opens the possibility that inclusions will be found in many meteorites, if properly examined.

Acknowledgements: We thank Edwin Thompson for first noting and providing the Zag halite, and the citizens of Monahans, Texas, for providing some of their meteorite.

References: [1] Zolensky and McSween (1988) In *Meteorites and the Early Solar System* (J. Kerridge and M. Matthews, Eds., U. A. Press, pp. 114-143; [2] Zolensky et al. (1999) *Science*, **285**, 1377-1379; [3] *Meteoritical Bulletin* **83**, July 1999.

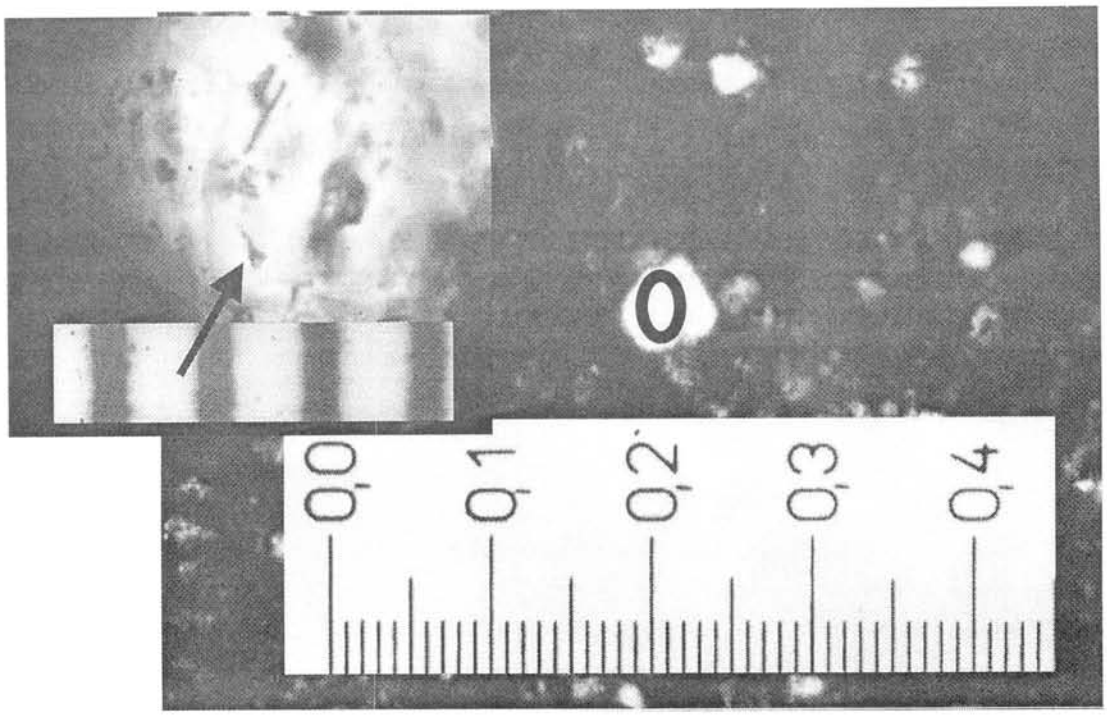

Figure 1 Aqueous fluid inclusions in carbonate grains in (above) Orgueil and (below) Ivuna. Circles indicates the positions of the inclusions, and insets show magnified views of the inclusions with the vapor bubbles (arrowed).

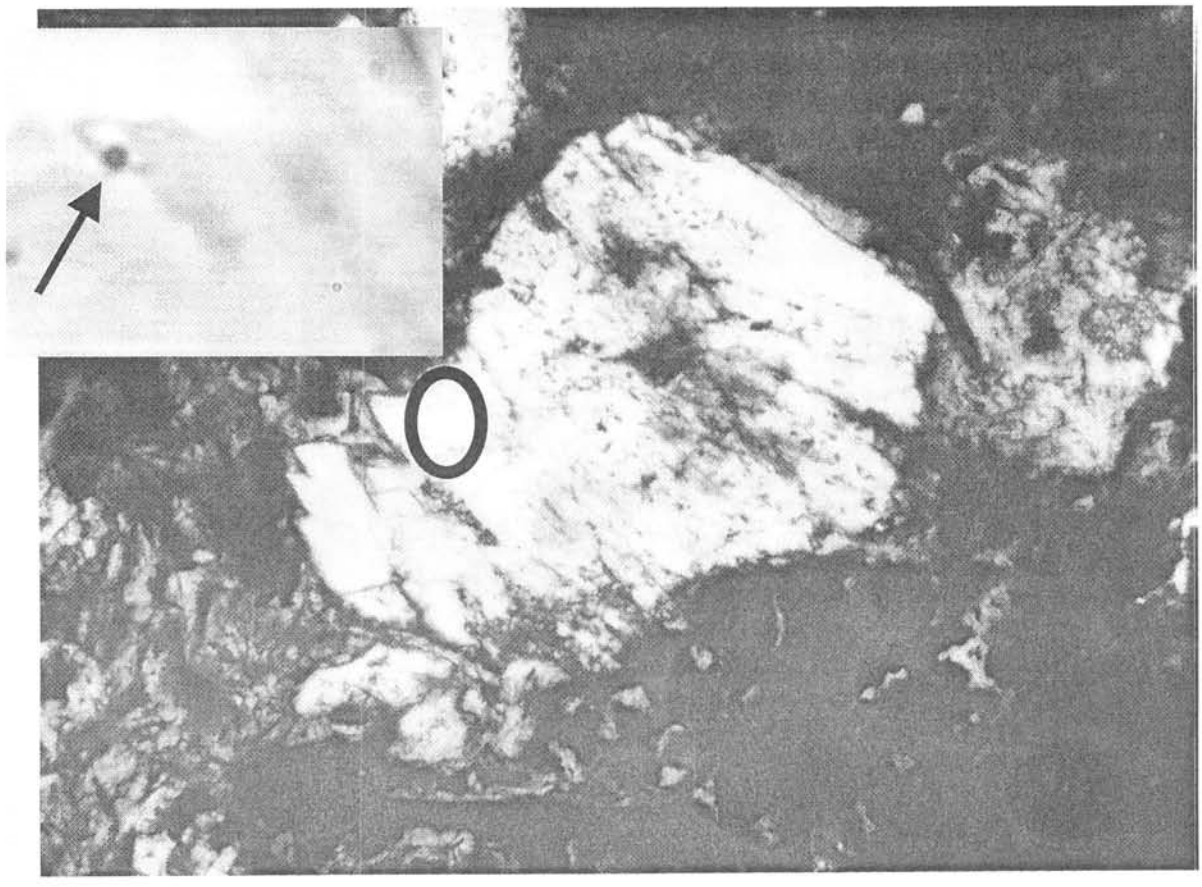

AUTHOR INDEX